CHARACTERISATION AND MODELLING OF PHOTOVOLTAIC CELLS AND MODULES UNDER PARTIAL SHADING

A thesis submitted to Cardiff University in the candidature for the degree of

Doctor of Philosophy

By

Abdulhamid M Mahmud Atia

School of Engineering

Cardiff University

March 2023

Abstract

Partial shading in photovoltaic (PV) systems is an inevitable issue that significantly deteriorates their performance. This thesis presents a detailed experimental and theoretical study on the characterisation of solar cells and PV modules under partial shading. The primary focus of this research was to improve accuracy of modelling partially shaded PV modules without the need to include the avalanche breakdown term in the model. The research started by designing an equivalent circuit parameters extraction technique for solar cells and modules, which was used in the investigations of this study. The technique is based on adding a simple iterative process to an analytical method from the literature to optimise the selection of points used to calculate the slopes on current-voltage (I-V) curves. This resulted in an accurate technique with a mean absolute percentage error (MAPE) between calculated and experimental data of less than 2% for all I-V curves presented in this thesis. In addition, the technique showed a good repeatability of the parameters using the experimental set-up of this research. The relative standard deviations (RSDs) of the parameters extracted from four I-V curves measured in sequence were less than ±3%.

This technique was then used in investigating the variations of a mono-crystalline (mono-Si) solar cell parameters with shading. In addition, the effect of partial shading on the parameters was compared with that of reducing the irradiance uniformly on the cell area, where both effects were found to be nearly identical. The MAPE between I-V curves of partial shading and those of reducing the irradiance did not exceed 1% in two investigated cases. This investigation has confirmed that it is reasonably correct to enter opaque partial shading impact in PV models as a parameter that corresponds to reducing the irradiance uniformly over the whole cell area. Then, the variations of the equivalent circuit parameters with shading were entered in models for a single cell and a PV module to assess whether considering those variations will lead to any improvement in modelling accuracy. The results revealed that the single cell model did not exhibit an appreciable improvement in accuracy. By contrast, the PV module model showed a noticeable improvement at a region on the I-V and power-voltage (P-V) characteristics at which the shaded cell is working in the reverse bias. The parameter responsible for this improvement in accuracy was identified from a systematic study and found to be the shunt resistance (R_{sh}). Hence, it has been proposed to account for the variations with shading of only the photo-generated current (I_{ph}) and R_{sh} when modelling partially shaded PV modules. The great advantage of this approach is that it provides an accurate modelling of the reverse bias region without the need to include the avalanche breakdown term in the model.

Subsequently, this research focused on the response of a mono-Si PV module when individual solar cells were partially shaded. It was found that there is a correlation between the shape of I-V characteristics under partial shading and broken contact fingers of solar cells. Different experiments, including electroluminescence (EL) imaging, were carried-out to validate this correlation. The correlation reported in this thesis has proved the feasibility of a concept of detecting broken contact fingers in PV modules from measurements of I-V curves with individual cell partial shading under day light.

Dedication

I dedicate this thesis to the greatest woman in my life, my mother, and

to the soul of my father, may Allah have mercy upon him.

Acknowledgements

In approaching the end of my PhD, first and foremost, all praises are due to Allah Almighty the Most Merciful and Most Gracious for giving me the ability and strength to complete this research.

I would like to express my sincere thanks to my supervisors Dr. Fatih Anayi and Prof. Gao Min for their help and support throughout this research. Without their kind patience and guidance, it would have not been possible to complete this research and produce this thesis. I also acknowledge the support from Dr. Zhe Li, who was with our research group during the first few months of my PhD.

Many thanks to the staff in the School of Engineering, Cardiff University, particularly staff in the Research Office, Finance Office and IT Service Desk. My sincere gratitude also goes to Mr. Andrew Rankmore, Mr. Malcolm Seaborne, Miss Amie Parnell and all other mechanical workshop staff for their assistance during the experimental set-up design. I am also equally grateful to Mr. Denley Slade, Mr. Samuel Moeller and Mr. David Billings in the Electrical Workshop for their technical support during preparations of shading objects and printed circuit boards for solar cells.

I would not have reached this stage without the prayers of my parents. Encouragement and support of my father has given me the strength to continue until the end and face all the challenges. Although he is no longer with us, I am glad to reach this stage and achieve what he wanted me to be. The continues motivation and prayer of my mother has been a great guidance that paved my way to reach this level of study and turn this dream into reality.

I would like to thank my wife for her motivation, patience, and support. I am also extremely grateful to my beloved children. Despite the challenging times during this study, their joy has been a great motivation to continue. Many thanks to my brothers and sisters for always being there for me.

I would like to express my sincere gratitude to the Ministry of Education in Libya, represented in the Cultural Attaché in London, for the sponsorship of this PhD study.

Many thanks go to my previous and current colleagues in the Thermoelectric and Photovoltaic research group at Cardiff University. Special thanks to Mr. Ali Bahr for his help in carrying-out measurements for the performance testing of the solar simulator and for useful discussions throughout my research.

Contents

List of Figures

List of Tables

List of Abbreviations and Symbols

Abbreviations:

3D	Three dimensional
ABC	Artificial bee colony
AM	Air mass
AM 1.5G	Air mass 1.5 global irradiance spectrum
APE	Absolute percentage error
a-Si	Amorphous silicon
ASTM	American Society for Testing and Materials
CAD	Computer aided design
CCD	Charge-coupled device
CdTe	Cadmium Telluride
CIGS	Copper Indium Gallium Selenide
CIS	Copper Indium Selenide
CO2	Carbon dioxide
Crystalline-Si	Crystalline silicon
DC	Direct current
DC	Direct current
DCB	Direct copper bonded
DE	Differential evolution
DSLR	Digital single-lens reflex
EL	Electroluminescence
EVA	Ethyl-Vinyl-Acetate
GA	Generic algorithm
GaAs	Gallium Arsenide
GMPP	Global maximum power point
GPIB	General purpose interface bus
IEA	International Energy Agency
IEC	International Electrotechnical Commission
IR	Infrared

ISO	Camera sensitivity
I-V	Current-voltage
LMPP	Local maximum power point
MAPE	Mean absolute percentage error
Mono-Si	Mono-crystalline silicon
MPP	Maximum power point
MPPT	Maximum power point tracking
MVO	Multi-verse optimiser
NREL	National Renewable Energy Laboratory
n-type	Negative material side of the p-n junction
PCB	Printed circuit board
PL	Photoluminescence
PLA	Polylactic acid
p-n junction	Interface of positive and negative materials
Poly-Si	Poly-crystalline silicon
PS	Pattern search
PSO	Particle swarm optimisation
p-type	Positive material side of the p-n junction
PV	Photovoltaic
P-V	Power-voltage
RAM	Random access memory
RMSE	Root Mean Square Error
RSD	Relative standard deviation of the population
SA	Simulated annealing
SD	Standard deviation of the population
STC	Standard test conditions
STL	Stereolithography
TLBO	Teaching-learning-based optimisation
TSB	Test script builder
USB	Universal serial bus
UV	Ultraviolet

Symbols:

V	Volt
µV	Microvolt
A	Amp
mA	Milliampere
µA	Microampere
nA	Nanoampere
W	Watt
mW	Milliwatt
GW	Gigawatt
Ω	Ohm
kΩ	kiloohm
m	Metre
cm	Centimetre
mm	Millimetre
µA	Micrometre
nm	Nanometre
C	Coulomb
°C	Degree Celsius
W/m^2	Watt per square metre
Hz	Hertz
J/K	Joule per kelvin
W/(m.K)	Watt per metre-kelvin
eV	Electron volt
V	Output voltage
I	Output current
R_s	Series resistance
R_{sh}	Shunt resistance
n	Ideality factor
I_s	Reverse saturation current
I_{ph}	Photo-generated current
V_{th}	Thermal voltage
k	Boltzmann constant

q	Electron charge
I_d	Equivalent circuit diode current
I_{sh}	Current through the shunt resistance
V_d	Equivalent circuit diode voltage
N_s	Number of cells connected in series
n_1	Ideality factor of the first diode
I_{s1}	Reverse saturation current of the first diode
n_2	Ideality factor of the second diode
I_{s2}	Reverse saturation current of the second diode
P_{max}	Maximum power
V_{mp}	Voltage at the maximum power point
I_{mp}	Current at the maximum power point
FF	Fill factor
A_a	Active area of solar cells (excluding busbar)
R_{ch}	Characteristics resistance at the maximum power point
V_{oc}	Open circuit voltage
$V_{oc,ref}$	Open circuit voltage under standard test conditions
K_{Voc}	Temperature coefficient of the open circuit voltage
I_{sc}	Short circuit current
$I_{sc,ref}$	Short circuit current under standard test conditions
K_{Isc}	Temperature coefficient of the short circuit current
T	Solar cell temperature in kelvin
T_{ref}	Solar cell temperature at standard test conditions (25 °C)
G	Irradiance in W/m^2
G_{ref}	Irradiance at standard test conditions (1000 W/m^2)
$R_{s,ref}$	Series resistance under standard test conditions
$R_{s,nsh}$	Series resistance under no shading condition
$R_{sh,ref}$	Shunt resistance under standard test conditions
$R_{sh,nsh}$	Shunt resistance under no shading condition
n_{nsh}	Ideality factor under no shading condition
$I_{s,ref}$	Reverse saturation current under standard test conditions
$I_{s,nsh}$	Reverse saturation current under no shading condition

$I_{ph,ref}$	Photo-generated current under standard test conditions
$I_{ph,nsh}$	Photo-generated current under no shading condition
E_g	Bandgap energy
$E_{g,ref}$	Bandgap energy under standard test conditions
R_{s0}	Approximate initial value of the series resistance
R_{sh0}	Approximate initial value of the shunt resistance
$P_{max,e}$	Experimental maximum power
$P_{max,c}$	Calculated maximum power
$R_{sh,min}$	Minimum shunt resistance
$\mathrm{M(V)}$	Avalanche breakdown term
V_b	Breakdown voltage
m_a	Avalanche breakdown exponent
a	Avalanche breakdown current fraction
k_f	The fraction of the unshaded sub-cells inside a solar cell
G_{max}	Maximum irradiance
G_{min}	Minimum irradiance
S_N	Spatial non-uniformity
x_0	x coordinate of the open circuit point used in linear interpolation
y_0	y coordinate of the open circuit point used in linear interpolation
x_1	x coordinate of the upper point used in linear interpolation
y_1	y coordinate of the upper point used in linear interpolation
x_2	x coordinate of the lower point used in linear interpolation
y_2	y coordinate of the lower point used in linear interpolation
$\bar{x}$	Mean value
x_i	i_{th} point of data samples' population
V_1	Voltage of point-1 (0 Volt)
I_1	Current of point-1 (short circuit current)
V_2	Voltage of point-2
I_2	Current of point-2
V_3	Voltage of point-3
I_3	Current of point-3
V_4	Voltage of point-4 (open circuit voltage)

I_4	Current of point-4 (0 Ampere)
$I_{i,exp}$	Experimental current of the i_{th} point on an I-V curve
$I_{i,cal}$	Calculated current of the i_{th} point on an I-V curve
N	Number of data points on an I-V curve or number of data samples
α	Shading factor
A_{sh}	Shaded area of solar cells
R^2	Coefficient of determination
c	Number of solar cells in each cell-string within a PV module
s	Number of cell-strings in a PV module
V_{cell}	Voltage of each solar cell in a PV module
$I_{ph,cell}$	Photo-generated current of each solar cell in a PV module
V_{st}	Voltage of each cell-string in a PV module
$I_{ph,st}$	Photo-generated current of each cell-string in a PV module
V_D	Forward voltage drop of the bypass diode
V_{mo}	Voltage of a PV module

List of Publications

1. **Published work:**

   a) Journal article:

   - **A. Atia**, F. Anayi, and M. Gao, "Influence of shading on solar cell parameters and modelling accuracy improvement of PV modules with reverse biased solar cells," *Energies (Basel)*, vol. 15, no. 23, pp. 1–19, Nov. 2022, doi: 10.3390/en15239067. **(Published work is presented in Chapter 5).**

   b) Conference papers:

   - **A. Atia**, F. Anayi, and G. Min, "Comparing shading with irradiance reduction effects on solar cells electrical parameters," in *2021 56th International Universities Power Engineering Conference (UPEC)*, Aug. 2021, pp. 1–5. doi: 10.1109/UPEC50034.2021.9548160. **(Published work is presented in Chapter 5).**

   - **A. Atia**, F. Anayi, and G. Min, "Improving accuracy of solar cells parameters extraction by minimum root mean square error," in *2020 55th International Universities Power Engineering Conference (UPEC)*, Sep. 2020, pp. 1–6. doi: 10.1109/UPEC49904.2020.9209780. **(Published work is presented in Chapter 4).**

2. **Work has been submitted for journal publication:**

   - Correlation between broken contact fingers and I-V characteristics of partially shaded PV modules. **(Work is presented in Chapter 6).**

Chapter 1: Introduction

1.1. Background to Renewable Energy and Photovoltaics

Over the past few decades, the worldwide energy demand has increased rapidly mainly due to the continuous increase in population and the standard of living. Despite the harmful impact of fossil fuels, namely oil, gas, and coal, they are still the major contributors to the produced energy [1]. Greenhouse effect and carbon dioxide (CO2) gas emissions constitute a major concern about the proceeded use of fossil fuels in the future. In addition, the limited expected lifetime of fossil fuels and the resulted high cost add another reason for human to look for sustainable, unlimited, and inexhaustible energy resources. Renewable energy resources include hydro power, wind energy, biomass, tidal power, wave power, geothermal power and solar energy [1], [2].

Solar energy is the primary energy supply for nearly all sources of renewable energy. Wind energy develops from wind movement, which is mostly created because of solar radiation. Hydro power is realised from the fact of water condensation due to sun energy and then it rains down. Biomass growth is conditioned by photosynthesis, which is mainly caused by sunlight. In addition, solar radiation is directly used for heat energy generation by thermal collectors, for electricity generation from heat by solar thermal power stations and for electricity generation by photovoltaic (PV) systems [1].

In order to meet the accelerated electricity demand, electricity generation has been increasing significantly. According to a recent report from the International Energy Agency (IEA) [3], renewables are soon expected to have the largest growth in the electricity sector. In a five-year-period from 2022 to 2027, it is projected that renewable energy electricity capacity will grow by almost 85% compared to the previous five years. This implies that renewables are expected to contribute by about 40% to the total global generated electricity in 2027. China, Europe, United States, and India are expected to be the main contributors to this five-year projected expansion. Furthermore, nearly 60% of this expansion is anticipated to come from PV systems alone [3].

PV systems convert sunlight into electricity in an environmental-friendly way without any emissions. Over the past few decades, the use of PV technology as an alternative

electricity generator to fossil fuels has increased rapidly. Started from powering only space satellites in the 1950s, nowadays, the applications of PV technology vary from off-grid applications to small grid-connected applications, and even to utility scale applications [1]. The large utility scale installations of PV have become the preferred option in many countries when adding a new electricity capacity due to the high cost of gas [3]. According to the Trends in Photovoltaic Applications 2022 report from IEA [4], the global cumulative installed PV capacity increased from 71 GW in 2011 to about 945.4 GW by the end of 2021. In 2021 alone, a minimum capacity of about 173.5 GW was added. Figure 1.1 depicts the evolution of PV cumulative installed capacity from 2011 to 2021 [4]. The total cumulative capacity includes installations of countries registered with the IEA as well as installations of other countries. An up-ward trend in the global installed PV capacity is clear from Figure 1.1 demonstrating the great interest in using PV technology.

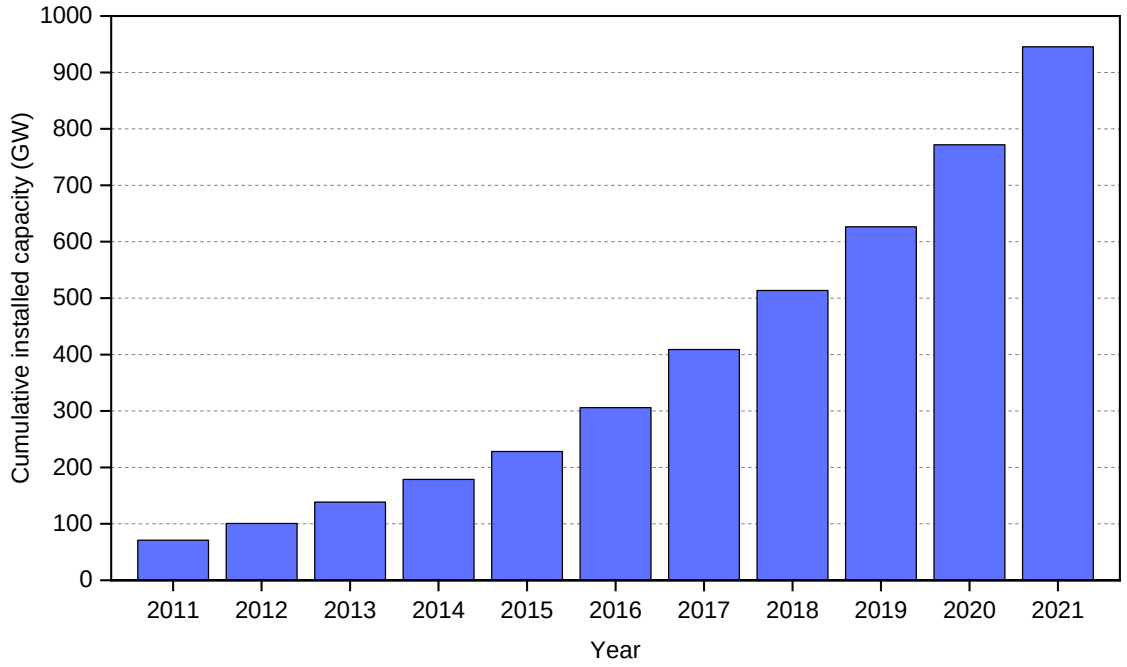

Figure 1.1. The growth in PV cumulative capacity from 2011 to 2021 (Adapted from [4]).

1.2. Research Motivation

PV systems have many advantages that make them a great candidate for the future sustainable electrical energy source. First, PV technology does not require any kind of fuel and it needs only sunlight, which is available everywhere in the globe. Second, as the installed capacity has increased over the years, the cost has decreased due to the

reduced manufacturing cost [1]. Third, the modularity feature of PV systems makes them suitable for applications ranging from milliwatt to megawatt range [2]. Despite, all these advantages, there are issues that face PV systems and are difficult to avoid, such as partial shading and broken solar cells' contact fingers.

Partial shading occurs when light reaching a PV generator is blocked or reduced by nearby objects, such as clouds, buildings, trees, chimneys and so on [1], [2], especially when the PV generators are installed in an urban environment [5]. Partial shading can also result from the structure of the PV system itself, such as shading from nearby PV arrays [1], [5], sun trackers or power overhead lines [6]. Partial shading significantly deteriorates the performance of PV systems as it causes a large amount of power loss. The degree of shading impact depends on various factors: such as the PV system size, configuration, and shading scenario [7]. It was shown experimentally in [7] that shading only half of a single solar cell in a commercial crystalline silicon (crystalline-Si) PV module, that has 60 cells connected in series, causes a power loss of about 31%. Furthermore, partial shading causes the shaded solar cells to be reverse biased and act as a load dissipating power instead of producing it [2]. Consequently, the shaded cells may heat up significantly and cause hot spots. If the PV system is not properly protected, hot spots may destroy the shaded cell and even the entire PV module [1], [8]. In addition, partial shading in PV systems may also make it difficult for maximum power point tracking (MPPT) techniques to find the maximum power point (MPP) due to the appearance of more than one MPP in the output power-voltage (P-V) characteristics of the system [5].

The large impact of this phenomenon on the performance of PV systems makes it necessary to study its influence in a great detail. Modelling and characterisation of PV systems under partial shading is essential to understand their electrical response, which is required in installation site planning, study their energy yield [5] and evaluation of different MPPT techniques [9]. Modelling of partial shading impact is also useful in proposing new solutions, such as MPPT techniques [10] and hot spots detection techniques [11]. Although partial shading modelling and analysis has been a major field of research since the 1980s [12], there are still topics that are open to further research and investigations, which include but not limited to improvement of modelling accuracy and

critical analysis of the current-voltage (I-V) characteristics of partially shaded PV modules for possible detection of solar cells faults.

As a single solar cell constitutes the basic building block in any PV system [1], the most accurate and informative modelling starts from the cell level [5]. However, it has been found from the literature that when accurate modelling of partially shaded PV systems is desired, an avalanche breakdown term is usually added to the model equation, thereby requiring the determination of more parameters, and adding more complexity. Thus, investigating possible improvements in modelling accuracy of solar cells and modules starting from the single cell stage without adding the avalanche breakdown term is the primary focus of this research. Detailed systematic investigations on the variations of solar cells equivalent circuit parameters with shading are essential in this work to identify which parameter variation would improve modelling accuracy.

Broken solar cell contact fingers is another issue, which is caused by cell breakage or creation of cracks that interrupt the contact fingers [13]. Broken contact fingers and cracks are difficult to avoid as they could develop during solar cells soldering [14], and lamination induced stress [15], PV modules handling and transportation [16]. They may also appear during the lifetime of PV modules because of temperature cycling, wind and snow loads [17]. In addition, in a study carried-out from PV installations in [17], it was shown that 4.1% of the total examined solar cells suffer at least from one crack.

In [13], the authors compared the occurrence of different types of cracks by mechanical load tests according to the IEC 61215 standards [18]. The results revealed that 50% of the occurred cracks are parallel to the cells' busbar, which is the type that leads to broken contact fingers. In addition, broken contact fingers make parts of a solar cell electrically disconnected and hence causing high power loss and hot spots [19]. Thus, detecting them in an early stage could save power and cost. In this research, observations of the I-V characteristics of PV modules when individual cells are partially shaded has signified the feasibility of usefully using partial shading to detect solar cells' broken contact fingers. Thereby eliminating the need for complex imaging techniques when it is required to detect them under day light. This research focused on this type of cell damage as it is the only type of cracking that causes significant power loss [19].

All experimental investigations, modelling and analysis in this research are dedicated to mono-crystalline silicon (mono-Si) PV technology as it has dominated the PV market in the last few years due to its high efficiency compared with the poly-crystalline (poly-Si) counterpart [4]. This is, however, except for only one amorphous silicon (a-Si) PV module used in Chapter 4 for validation of a developed equivalent circuit parameters extraction technique.

1.3. Aim and Objectives

The main aim of this research is to improve modelling accuracy of PV modules under partial shading when starting from a single solar cell model. This has been accomplished by detailed systematic characterisation of solar cells under partial shading and considering their parameters variations with shading when modelling solar cells and modules. In addition, this project aims to find a correlation between the I-V characteristics of PV modules under single cell partial shading and broken contact fingers of solar cells, and thus proving the feasibility of a concept for detection of broken contact fingers from I-V curve measurements under day light. The main objectives of this research are thus summarised in the following:

- Develop a complete solar cells and modules characterisation experimental set-up and calibration of the light source that is used to simulate sun light.
- Prepare and test solar cells and modules samples that are used in the experimental investigations of this research.
- Develop an accurate equivalent circuit parameters extraction technique for solar cells. This technique is to be used for other investigations in this research that require the determination of those parameters.
- Experimentally investigate partial shading effect on solar cells equivalent circuit parameters and performance parameters and develop equations that describe the variations of equivalent circuit parameters with shading.
- Compare the influences of partial shading and irradiance reduction on solar cells equivalent circuit parameters and performance parameters.
- Build a mathematical model for solar cells and PV modules under partial shading in MATLAB using a procedure from the literature, but taking into account the variations of single cell equivalent circuit parameters with shading.

- Investigate any possible improvements in modelling accuracy of solar cells and modules gained by taking into account the variations of single cell equivalent circuit parameters with shading in the models.
- Optimise the PV module model accuracy by taking into account the variation of every parameter with shading separately. Then, determine the parameter that needs to be considered variable with shading in the model for accurate modelling.
- Investigate the I-V characteristics' behaviour of PV modules when individual cells are partially shaded. Subsequently, correlate an obtained I-V characteristics' convex shape with broken contact fingers using microscopic imaging.
- Validate the correlation between broken contact fingers and the I-V characteristics of the PV module under partial shading by investigating a single cell's behaviour with broken contact fingers, by electroluminescence (EL) imaging and by using another PV module assembled in the laboratory.

1.4. Thesis Contributions

The work reported in this thesis has made the following contributions to knowledge:

- Developing a procedure to select suitable points on I-V curves used to calculate the slopes for analytical calculation of equivalent circuit parameters of solar cells.
- Experimentally investigating the influence of partial shading on the equivalent circuit parameters and main performance parameters of solar cells.
- Experimentally comparing the effects of partial shading and the corresponding irradiance reduction on solar cells' equivalent circuit parameters and main performance parameters. This work has confirmed that it is acceptable to incorporate partial shading in a model of solar cells as its corresponding irradiance reduction value.
- Incorporating the variations of single cell equivalent circuit parameters with shading in the models of a single cell and a PV module. Subsequently assessing modelling accuracy improvement of the single cell and the PV module when considering the variations of the parameters and identifying which parameter leads to accuracy improvement.
- Experimentally investigating and validating the correlation between broken contact fingers and the I-V characteristics of a PV module under single cell partial shading. This work has confirmed that a solar cell with broken contact fingers can

be identified through I-V characteristics of a PV module under partial shading of this cell. As a result, this work has demonstrated the possibility of detecting broken contact fingers from I-V characteristics of PV modules under day light.

1.5. Thesis Structure

This thesis has been written to comprehensively illustrate the work carried-out in this research project, which covers detailed experimental and theoretical investigations on solar cells and modules working under partial shading conditions. The outline of this thesis is divided into several chapters as follows:

Chapter 1: This chapter provides a brief background to renewable energy and PV technology alongside with their contribution to the worldwide electricity demand and the evolution of the installed PV capacity over the past few years. Moreover, the main motivation of this research alongside with its aim, objectives and contributions are presented.

Chapter 2: This chapter gives a comprehensive literature review about the research topic. It starts by a general background to solar energy and solar cells principle of operation followed by PV systems typical configurations and different solar cells' technologies. Subsequently, different models of PV systems are presented alongside with the output characteristics and the effect of irradiance and temperature variations. After that, the equivalent circuit parameters are explained with a literature survey of their extraction techniques focusing on their advantages and disadvantages. Then, partial shading impacts are presented in addition to its modelling techniques in the literature highlighting their main limitations. Finally, broken contact fingers of solar cells are discussed, again with a brief literature survey of the current detection techniques.

Chapter 3: This chapter presents the experimental techniques used in this research. A detailed description of laboratory equipment and their calibration is given. In addition, solar cells, modules and their test rig preparations are explained in detail. Testing and repeatability error analysis of laboratory equipment is also discussed. Fabrication of Three Dimensional (3D) printed shading objects is presented followed by thermal and EL imaging set-up illustrations.

Chapter 4: In this chapter, the developed equivalent circuit parameters extraction technique is illustrated. This technique is based on adding a simple iterative process to an existing analytical method, thereby making it more accurate. Experimental validation of the technique's accuracy is presented using two types of PV technology. A comparison with other methods from the literature is also presented followed by assessing the technique's repeatability and capability of detecting variations in parameters caused by different experimental conditions.

Chapter 5: This chapter provides an experimental investigation of the shading effect on solar cells' equivalent circuit parameters and performance parameters. Shading effect is then compared with irradiance reduction effect on all parameters. Models are then presented for partially shaded solar cells and modules, accounting for the single cell equivalent circuit parameters variations with shading. The PV module model accuracy optimisation is subsequently presented, which involves individually including each parameter variation with shading in the model. Finally, the parameter that mostly improve the model accuracy when it changes with shading is identified alongside with experimental validations.

Chapter 6: This part of the thesis deals with observations made from I-V curves of PV modules when individual cells are shaded. A correlation between partial shading characteristics of PV modules and broken contact fingers is then presented followed by validations using single cell investigations, thermal imaging, EL imaging and another PV module.

Chapter 7: This last chapter privides conclusions drawn from this reseach and summurises all key findings. It also presents future research recommendations to further explore the research topics.

Chapter 2: Literature Review

2.1. Introduction

Our world has become alerted about the environmental impact of emissions resulting from energy generation using fossil fuels. Using renewable energy resources has been a promising solution for a few decades. Energy from the sun is unlimited and available to use everywhere in the world [1]. The sun is a huge fusion reactor that generates a massive amount of heat energy. The amount of solar energy received by the earth in one hour is enough to meet its energy demand for a year [20]. Furthermore, the total amount of energy continuously radiated by the sun is as high as 3.845×10^{26} W [1], [2]. As explained in Section 1.1, harvesting sun light by photovoltaics for electricity generation has evolved rapidly. This also can be noticed from the diversity and large quantity of published research in the literature dealing with different aspects of this technology.

This chapter provides an overview of PV technology starting by its history, solar cells operation and technologies. Then, solar cells characteristics and modelling are discussed with a focus on the equivalent circuit parameters and their calculation techniques. Subsequently, modelling of PV systems under partial shading is covered in a great detail highlighting the main limitations in the available modelling methods. After that, broken contact fingers of solar cells are discussed focusing on their effect and a brief overview of their detection techniques. Finally, a summary section is provided, which highlights the shortcomings and research gaps in the reviewed literature that will be explored and investigated in this research.

2.2. Photovoltaics History

The term photovoltaic effect refers to the process of converting photons of light into electricity. This effect was initially discovered by the French physicist Edmond Becquerel in 1839. Later in 1877, the photovoltaic effect in a solid substance, which is selenium, was observed and examined by William Adams and Richard Day. Then, in 1883, Charles Edgar Fritts developed the first solar cells that looked similar to today's cells by covering a thin wafer of selenium with a thin gold layer. These cells showed an efficiency of less than 1% [1], [21].

The first high-efficiency modern solar cell was invented in 1954 at the Bell Laboratories in the USA by Chapin, Fuller and Pearson. These scientists produced a doped silicon solar cell that showed an efficiency of 6% based on the fundamental theory of the p-n junction presented by William B. Shockley. After this invention, solar cells were first used in a practical application in 1958, where they were utilised in space satellite applications [1], [21]. The use of photovoltaics in terrestrial applications started to gain interest in the 1970s. It was further increased and came into practice in the 1980s and 1990s [1]. Since then, there has been a sharp upward trend in installing new PV capacity [1], [4].

2.3. Solar Cells Principle of Operation

Most of the commercially available PV systems use crystalline silicon (crystalline-Si) solar cells. A silicon solar cell is basically a mono-crystalline (mono-Si) or a poly-crystalline (poly-Si) silicon p-n junction [1], [2], [20]. The p-type semi-conductor is created by doping silicon with Boron and it is called the base, whereas the n-type semi-conductor is created by doping silicon with Phosphorus and it is called the emitter. When the p and n-type semi-conductors meet by a specific manufacturing process, the p-n junction is formed. Subsequently, anti-reflective coating is applied to the front surface of the cell and finally, electrical contacts are provided for both front and rear sides to establish the silicon solar cell [1] as shown in Figure 2.1.

The front contacts are basically small strips made of silver or aluminium, which are called contact fingers [1], [2]. They collect the generated current and deliver it to the main current collector (busbar). The back contact is usually made of a flat sheet of aluminium with soldering surfaces made of silver to enable soldering the connection terminals to the cell. When a load is connected to the solar cell, the generated current will flow out of it [1]. Figure 2.1. shows the structure of a p-n junction solar cell connected to a load.

The principle of operation of a solar cell is also depicted in Figure 2.1. When there is an incident light on the solar cell, every photon that is absorbed by the cell causes the creation of an electron-hole pair. Subsequently, the generated electron-hole pairs are separated because of the electric field in the so-called space charge region and forced to travel to the contacts causing the electric current to flow. The electrons travel to the front contacts through the emitter. Whereas the holes travel to the back contact through the base [1], [20].

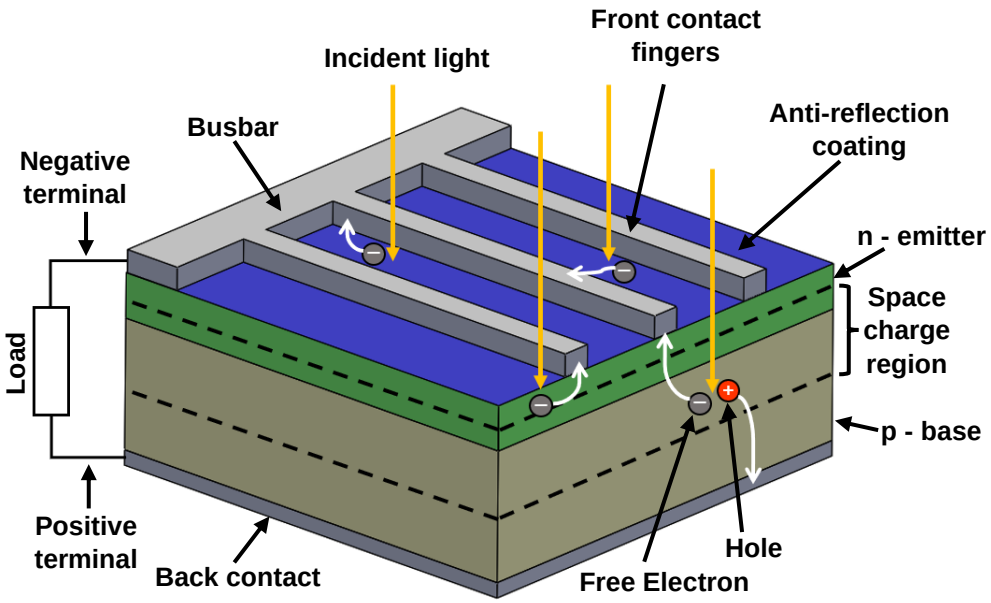

Figure 2.1. The p-n junction solar cell and its operation. (Adapted from [1]).

2.4. Photovoltaic Cell, Module and Array

A single solar cell produces a very low amount of power, which is generally not enough for most of the practical applications. Therefore, to provide a useful amount of power, solar cells can be connected in series or parallel to create a PV module [20]. In the serially connected solar cells, the output current equals to the current produced by a single cell. The output voltage in this case equals to the sum of the voltages of the cells. The output current of the parallel connected solar cells, on the other hand, equals to the sum of all the cells' currents, whereas the total output voltage equals to the voltage of one cell. Typical PV modules consist of solar cells connected in series to give a high amount of voltage. However, the module output current in this case equals to the current produced by an individual cell [2]. In crystalline-Si PV modules, the integration of solar cells into PV modules usually involves encapsulation of the cells between two layers of an adhesive plastic called Ethyl-Vinyl-Acetate (EVA). A front glass sheet and a back foil sheet are then placed before inserting the whole assembly in an aluminium frame to create the complete rigid PV module [1].

PV modules can be also connected in series or parallel configurations to create a PV array. Similar to the connection of solar cells, the PV modules may be connected in series to increase the voltage and in parallel to increase the current. A series-parallel configuration array is also possible to raise both the current and voltage [1]. Figure 2.2 shows a typical

PV array consists of series-parallel connected PV modules, where each module consists of a number of series-connected solar cells.

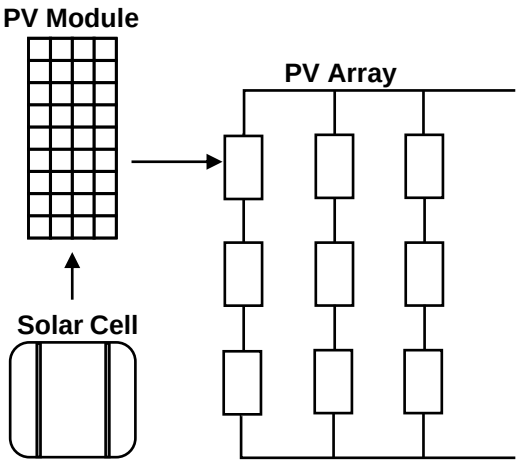

Figure 2.2. Solar cell, module, and array configurations. (Drawn from illustrations in [1], [20]).

2.5. Solar Cells Technologies

Solar cells technologies can be classified into three main categories based on the material involved in their production [22]:

- Silicon based solar cells.
- Non- silicon based solar cells.
- New solar cells concepts.

These categories are depicted in Figure 2.3 as a tree illustrating the different types of solar cells under each category that will be explained in the subsequent sub-sections. The evolution of best cell efficiency since 1976 according to the National Renewable Energy Laboratory (NREL) [23] is given in Figure 2.4. As shown, there is an up-ward trend in the efficiency of various technologies. Mono-Si solar cells for instance, had efficiencies of only 13.9% in 1977. With the developments over the years, they reached 26% in 2019 [23].

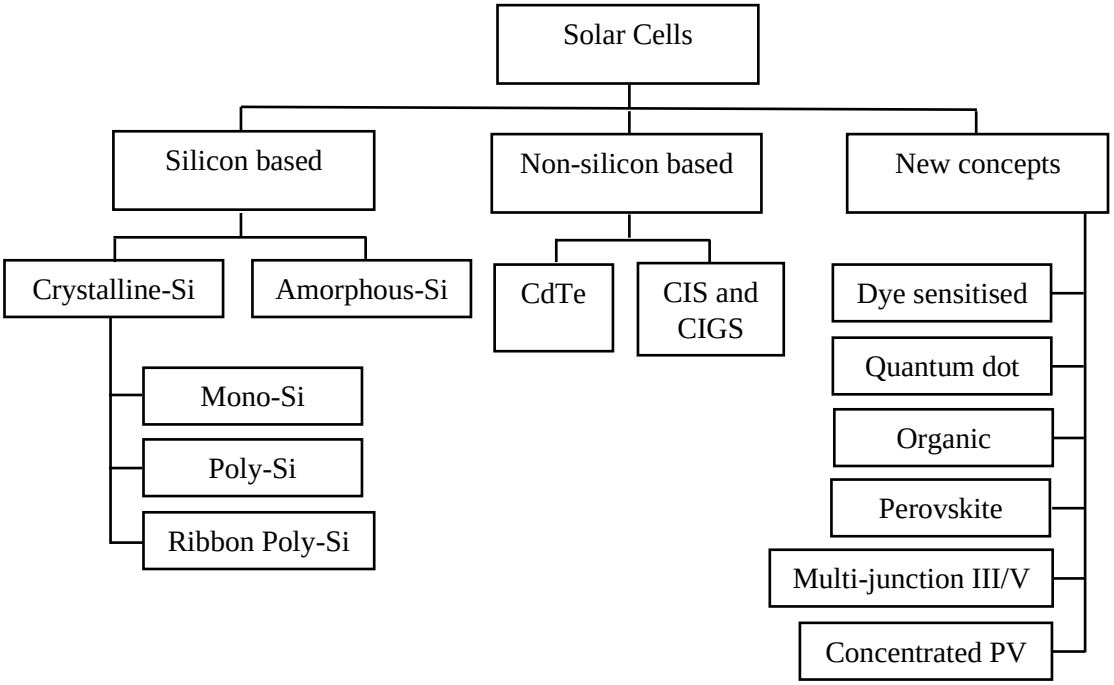

Figure 2.3. Types of solar cells technologies. (Adapted from [22], [24] with the addition of multi-junction III/V solar cells in the new concept category).

2.5.1. Silicon Based Solar Cells

Silicon solar cells represent the main technology in the PV market worldwide [4]. This category of solar cells consists of mono-crystalline, poly-crystalline, ribbon poly-crystalline and the thin film form of silicon, which is amorphous solar cells [22]. The first mentioned three types are also referred to as the first-generation solar cells [24].

2.5.1.1. Mono-crystalline Solar Cells

This type of solar cells (mono-Si) is made from single crystal using a process called Czochralski. The mono-crystalline ingot is formed by melting poly-silicon, which is made from quartz sand. Then, a seed crystal is immersed into the melt. The silicon fluid is then attached to the seed crystal and crystallised by slowly rotating the seed crystal out of the melt. The process of manufacturing these solar cells requires more energy compared to poly-crystalline silicon solar cells [1], [20]. Yet, they offer higher efficiency, which reached a value of 26% recorded in 2019 according to NREL [23].

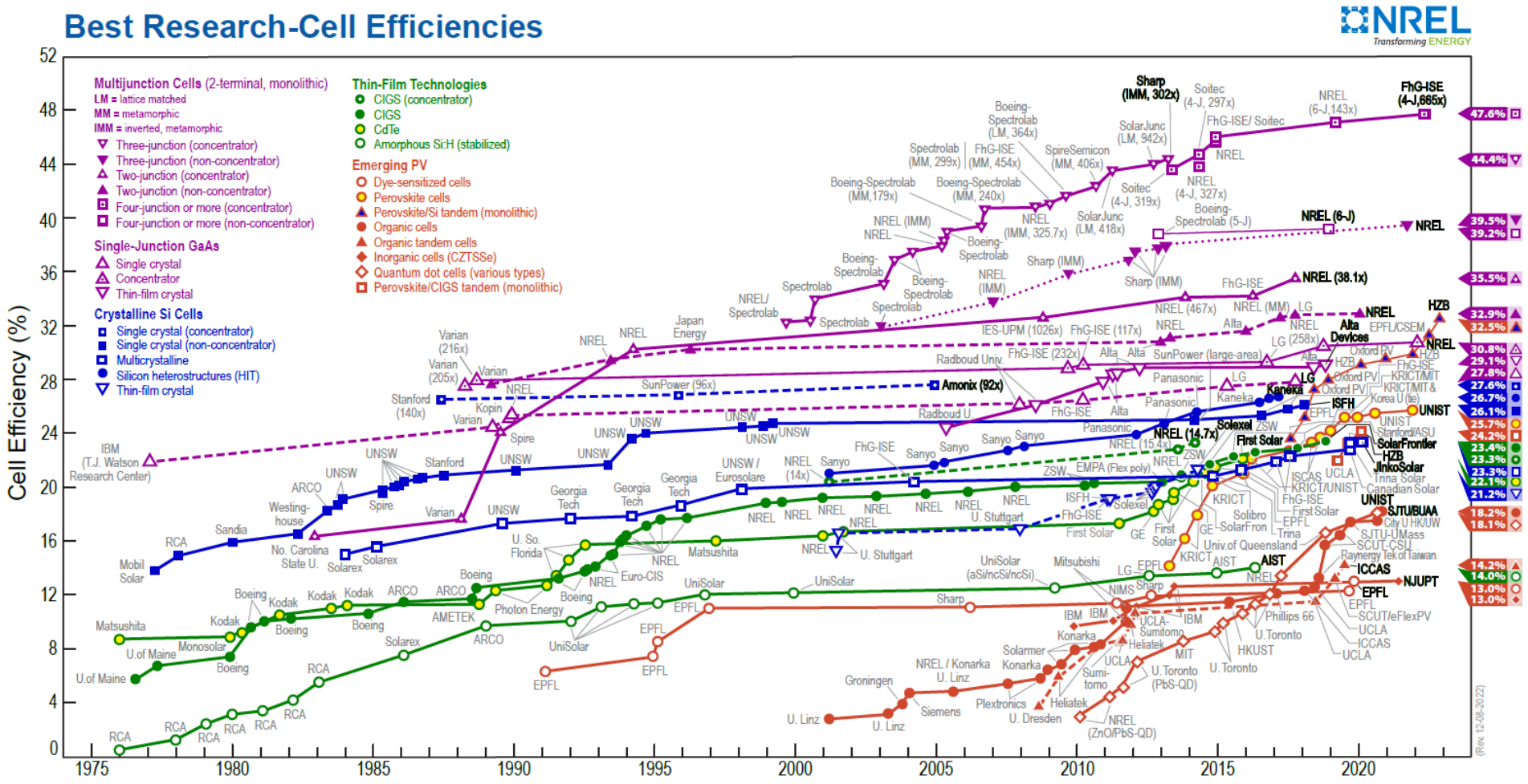

Figure 2.4. Efficiency evolution of different solar cell technologies [23].

2.5.1.2. Poly-crystalline Solar Cells

Poly-crystalline (poly-Si) or multi-crystalline solar cells have a much simpler manufacturing process than mono-Si at the cost of lower efficiency [20]. In this process, poly-silicon is placed into a crucible made from graphite and then it is heated and melted. Subsequently, the crucible is cooled from the bottom causing the formation of small mono-crystals. Finally, when the whole melt is crystallised, the block is cut into small cubes forming the poly-crystalline ingots. The efficiency of these solar cells is usually 2 – 3% lower than that of mono-Si solar cells [1].

2.5.1.3. Ribbon poly-crystalline Solar Cells

This type of silicon wafers is produced by extracting the wafers directly from the melt of poly-silicon resulting in a thin sheets [1]. This process has the advantage of preventing cutting losses [22]. However, the extracting speed of the sheet is very low in order to get a high quality crystal [1].

2.5.1.4. Amorphous Solar Cells

This is the thin film form of silicon solar cells and they are produced by depositing silicon by vapour deposition into a substrate material, such as glass. The main advantage of these solar cells over mono-Si and poly-Si cells is that they are much thinner, which significantly lowers the manufacturing effort and cost [2]. Nevertheless, their efficiency is still significantly lower than that of crystalline-Si solar cells with a maximum value of about 12% [23].

2.5.2. Non-silicon Based Solar Cells

This category includes thin film technologies which are not based on silicon in their production and it is called the second-generation solar cells [24]. They include Cadmium Telluride (CdTe), Copper Indium Selenide (CIS) and Copper Indium Gallium Selenide (CIGS) Solar Cells.

2.5.2.1. Cadmium Telluride Solar Cells

The main advantage of the CdTe material is its bandgap of 1.45 eV, which is suitable for PV applications [25], [26]. In addition, another advantage is its ability to be deposited by different techniques resulting in a thin film with high quality. The conventional way of

depositing this material is vacuum evaporation by heating the CdTe to a high temperature and then its vapour is deposited on a relatively colder substrate placed in a vacuum vessel [25]. To date, the maximum reported efficiency of these solar cells is around 22% [23]. However, tellurium is a scarce material and its worldwide availability is limited [1].

2.5.2.2. Copper Indium Selenide Solar Cells

CIS and CIGS are two different structures of this type of thin film solar cells with the latter includes gallium. The CIGS solar cells have many advantages over the CIS, such as an improved open circuit voltage. The elements of CIGS absorber are deposited at different stages at a high temperature on a substrate [27]. The maximum reported efficiency of CIGS solar cells to date is about 23.4% [23], which is considered the highest efficiency among all thin film technologies. Yet, the scarcity of indium and its high cost constitutes their main drawback [27].

2.5.3. New Solar Cell Concepts

There are new solar cell concepts that constitute the candidates for future solar cells and are currently under research and investigations. They are also called the third-generation solar cells [24]. The Dye Sensitised Solar Cells, which were introduced in the beginning of 1990s, have an in-expensive and simple fabrication process [28] and hence have attracted significant attention. Besides, they have reached an efficiency record of 13% [23]. Their main drawback, however, is the low stability of natural dyes used in their fabrication [29]. Similar solar cell concept is the Quantum Dot Solar Cells, which harness quantum dot instead of the dye and they also have a low stability [30]. These cells recorded an efficiency of 18.1% [23].

Another new concept is the Organic Solar Cells, which use polymer in their structure [1], [31]. They have an easy and low-cost fabrication process [31], but they exhibit low stability [24]. An efficiency value of 13.5% has been achieved from tandem organic cells. Whereas other various types of organic cells have recorded an efficiency of 18.2% [23]. Perovskite Solar Cells have also gained significant interest in the recent years. They have many merits, such as a low fabrication cost and a good light absorption [32], [33]. Their efficiency has been rapidly increased over the past decade reaching a record of 25.7% in 2021 [23]. Nevertheless, the main challenges associated with those solar cells are stability, degradation and toxicity of material [24].

Besides the new solar cell concepts mentioned above, Multi-junction III/V semi-conductor stacked cells have attracted a great attention as very efficient devices to use in some applications, for instance, in concentrator cells or space applications. In these devices, several materials with different bandgaps are stacked to effectively utilise the sun spectrum and achieve a high efficiency, but with a complex production. Expensive materials, such as Gallium Arsenide (GaAs) is commonly used [1]. The single junction GaAs solar cells with a thin film crystal recorded a maximum efficiency of 29.1% under non-concentration. Whereas the triple junction stacked cells of different materials have reached an efficiency of 39.46% under non-concentration [23]. Concentrated PV systems is to make use of lenses or mirrors to concentrate sun light then reflect it to the solar cell in order to improve efficiency and reduce cells' production cost. Parabolic mirrors and Fresnel lenses are the two main concepts used for this purpose [1].

2.6. Solar Cell Modelling

Accurate and reliable modelling of PV systems is required in various PV applications. A PV device (also called a PV generator), which could be a solar cell, PV module or an array, is represented by an electrical equivalent circuit model in order to produce its output characteristics [34]. Additionally, a single solar cell equivalent circuit model can be easily adapted to model PV modules and arrays [35]. There are various equivalent circuit models of a solar cell reported and studied in the literature with different degrees of accuracy and complexity. These models are shown in Figure 2.5 and are briefly discussed in the following sub-sections.

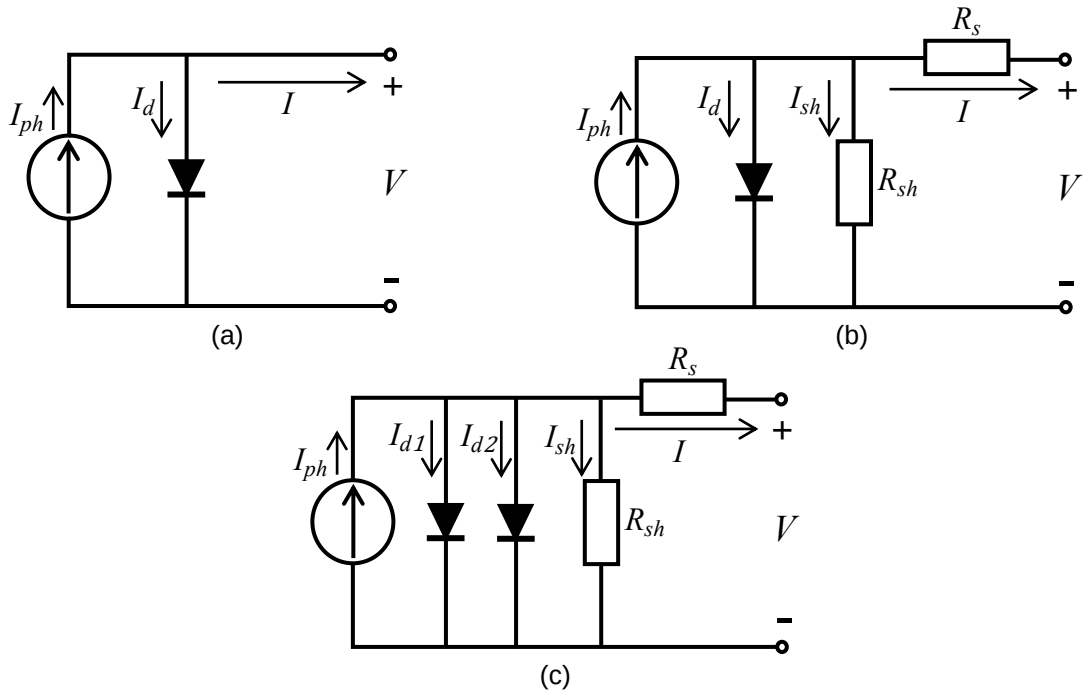

Figure 2.5. Solar cell equivalent circuit models: (a) simplified model, (b) five-parameter model and (c) double-diode model. (Adapted from [2]).

2.6.1. Simplified PV Model

The simplified model represents the solar cell by a current source, which represents the photo-generated current (I_{ph}), connected in parallel with a p-n junction diode as depicted in Figure 2.5 (a). The current through the diode (I_d) is given by the Shockley diode equation. The solar cell output current as a function of voltage is then obtained as [1], [20], [36]–[38]:

$$I = I_{ph} - I_d = I_{ph} - I_s\left(exp\left(\frac{V}{V_{th}.n}\right) - 1\right) \tag{2.1}$$

where I is the output current, V is the output voltage, I_s is the reverse saturation current of the diode, n is the ideality factor of the diode and V_{th} is the thermal voltage calculated from [1], [2], [20], [38]:

$$V_{th} = \frac{kT}{q} \tag{2.2}$$

where T is the cell temperature in Kelvin, k is Boltzmann constant ($1.3806488 \times 10^{-23}$ J/K) and q is the electron charge ($1.60217657 \times 10^{-19}$ C). Solving Equation (2.1) yields the I-V characteristics of an ideal solar cell. Although this model is simple as it depends

on an explicit equation, it provides only an approximate representation of the real solar cells' behaviour. The reason is that it does not account for the losses that occur in real solar cells because of the parasitic series and shunt resistances [1], [2], [36].

2.6.2. Five-Parameter PV Model

The five-parameter model shown in Figure 2.5 (b) takes into account the effects of the parasitic series and shunt resistances, which are neglected in the simplified model. These resistances have a negative impact on the fill factor of solar cells [1], [38]. Therefore, the five-parameter PV model represents the behaviour of solar cells more accurately, and thus it is the most commonly used model by researchers as it provides an acceptable level of accuracy with simplicity [37]. The I-V characteristics of a solar cell are obtained using the five-parameter model by the following equation [1], [2], [35], [38]:

$$I = I_{ph} - I_s \left(exp\left(\frac{IR_s+V}{V_{th}.n}\right) - 1 \right) - \frac{IR_s+V}{R_{sh}} \tag{2.3}$$

where the last term in the equation describes the current through the shunt resistance (I_{sh}). R_s and R_{sh} are the series and shunt resistances, respectively. The term $IR_s + V$ represents the voltage across the diode (V_d). The five parameters that need to be known in order to solve this model equation are R_s, R_{sh}, n, I_s and I_{ph}.

It is important to mention that not only a solar cell can be modelled by Equation (2.3), but a PV module can also be modelled by adapting the model to include the number of cells connected in series [35], [37], [39], [40]:

$$I = I_{ph} - I_s \left(exp\left(\frac{IR_s+V}{N_s.V_{th}.n}\right) - 1 \right) - \frac{IR_s+V}{R_{sh}} \tag{2.4}$$

where N_s is the number of series-connected cells. Note that R_s and R_{sh} in Equation (2.4) are for a PV module and not a single cell. If the values are given for a single cell, then they are also multiplied by the number of series-connected cells in the module. Furthermore, I_{ph} and I_s of a module are the same as those for a single cell because of the series connection [35]. Series connection of cells is mostly adopted in PV modules to raise the voltage [2] as previously mentioned in Section 2.4.

The equation of the five-parameter model contains the current at both sides and hence it can only be solved using numerical methods, such as the Newton Raphson method [2], [37].

2.6.3. Four-Parameter PV Model

The shunt resistance is sometimes neglected in the five-parameter model shown in Figure 2.5 (b) by assuming that it is infinite for the sake of simplicity. This results in the four-parameter model given by [39], [41]:

$$I = I_{ph} - I_s \left(exp\left(\frac{IR_s+V}{V_{th}.n}\right) - 1 \right) \tag{2.5}$$

This model is simpler than the five-parameter model. Nevertheless, it has been proved experimentally in [39] that it is less accurate in modelling PV modules.

2.6.4. Double and Triple Diode PV Models

The double-diode model illustrated in Figure 2.5 (c) adds another diode in parallel to the single diode five-parameter model to account for recombination in the space charge region of solar cells resulting in the following equation [1], [2], [9], [42]:

$$I = I_{ph} - I_{s1} \left(exp\left(\frac{IR_s+V}{V_{th}n_1}\right) - 1 \right) - I_{s2} \left(exp\left(\frac{IR_s+V}{V_{th}n_2}\right) - 1 \right) - \frac{IR_s+V}{R_{sh}} \tag{2.6}$$

where I_{s1} and n_1 are respectively the reverse saturation current and diode ideality factor of the first diode. Whereas I_{s2} and n_2 represent the reverse saturation current and diode ideality factor of the second diode, respectively. This model is more accurate than the five-parameter model at low irradiance levels [9], [42]. However, it increases the number of parameters required to solve its equation to seven (due to the addition of I_{s2} and n_2) [9], [36], [42], which adds more complexity, although an ideality factors of 1 and 2 are usually assumed respectively for n_1 and n_2 for simplicity [1], [2].

A triple-diode model was also proposed in [43] to consider other physical phenomenon within mono-crystalline solar cells. However, both the double and triple-diode models are not commonly used due their high complexity and high computational cost [44]. Hence, the remaining sections of this chapter and the work discussed in the subsequent

chapters will focus on the five-parameter model as it is adequate for describing real solar cells [1].

2.6.5. Solar Cell Characteristics and Effect of Irradiance and Temperature

The behaviour of a PV device is illustrated by its I-V and P-V characteristics, which are highly non-linear. For a typical mono-Si solar cell with an active area of 0.78 cm² (1 cm x 0.78 cm), the I-V and P-V characteristics are depicted in Figure 2.6. These characteristics represent the solar cell behaviour at standard test conditions (STC) and were obtained experimentally and shown here for the purpose of illustration. Details of the experimental set-up and solar cell preparation will be covered in Chapter 3. STC in PV systems refers to the meteorological conditions at which the information in the data sheet is provided. These conditions are an irradiance of 1000 W/m^2, a PV device temperature of 25 °C and air mass (AM) 1.5 spectrum [34]. Three important points are labelled in Figure 2.6, namely, short circuit current (I_{sc}), open circuit voltage (V_{oc}) and maximum power point (MPP).

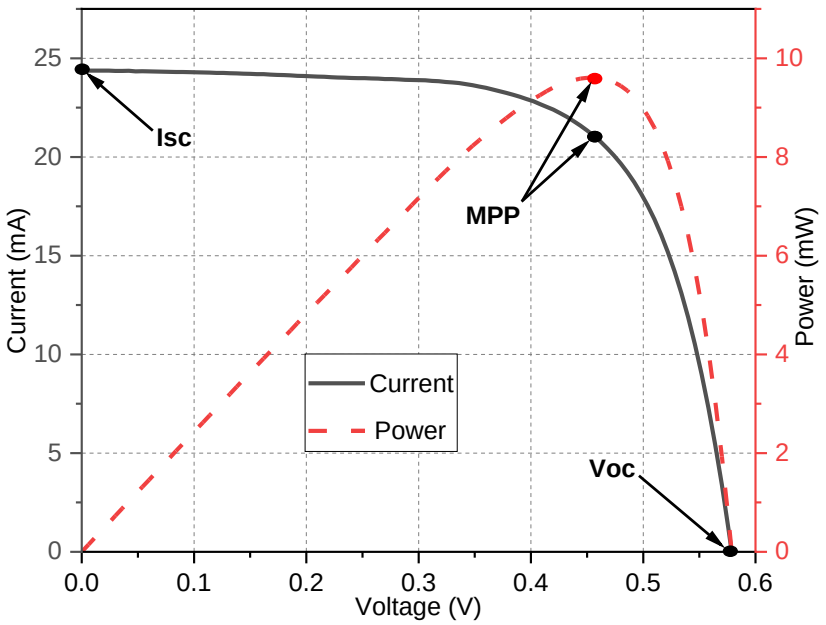

Figure 2.6. I-V and P-V characteristics of a typical solar cell at STC.

The I_{sc} is the maximum current that the cell can deliver when its terminals are short-circuited and hence the voltage equals to zero [1], [2]. It can be calculated from Equation (2.3) at the short circuit condition (setting $V = 0$) as shown in [34], [36]. The I_{sc} is usually

assumed to be equal to the photo-generated current (I_{ph}) [2], [37], which will be explained later in Section 2.7.5. If the I_{sc} value at STC is given, then the effects of irradiance and temperature variations on it are the same as those on the photo-generated current represented by [34], [41]:

$$I_{sc} = \left(I_{sc,ref} + K_{Isc}\left(T - T_{ref}\right)\right)\left(\frac{G}{G_{ref}}\right) \tag{2.7}$$

where $I_{sc,ref}$ is the short circuit current at STC, T and T_{ref} are the operational and STC temperatures, respectively. G and G_{ref} are the operational and STC irradiance intensities, respectively and K_{Isc} is the temperature coefficient of the short circuit current.

The V_{oc}, on the other hand, is obtained when the cell's terminal are open-circuited and the current equals to zero [1], [2]. While an expression for V_{oc} at any operational condition can be obtained by solving Equation (2.3) (setting $I = 0$) as shown in [34], [36], it is usually obtained from solving Equation (2.1) of the simplified model results in [1], [38]:

$$V_{oc} = V_{th}.n.ln\left(\frac{I_{sc}}{I_s} + 1\right) \tag{2.8}$$

The V_{oc} change with irradiation and temperature can be expressed by the following equation presented in [39], [45]:

$$V_{oc} = V_{oc,ref} + \left(V_{th}.n.ln\left(\frac{G}{G_{ref}}\right)\right) + K_{Voc}\left(T - T_{ref}\right) \tag{2.9}$$

where $V_{oc,ref}$ is the open circuit voltage at STC and K_{Voc} is the temperature coefficient of the open circuit voltage.

Under any operating condition, there is a unique operating point at which a PV device delivers its maximum possible power and it is referred to as Maximum Power Point (MPP). Practical PV generators operating point does not necessarily coincide with the MPP, but it is determined by the electrical characteristics of the load [34], [40]. The characteristics resistance at the MPP (also called the load matching resistance) represents the load resistance at the MPP (resistive load), which is used by MPP trackers to detect the MPP [34]. It can be calculated for a by simply using Ohm's law from:

$$R_{ch} = \frac{V_{mp}}{I_{mp}} \tag{2.10}$$

where V_{mp} and I_{mp} are the voltage and current at the MPP, respectively.

The fill factor (FF) of a solar cell is an estimation of its quality and it is given by [1], [2], [38]:

$$FF = \frac{V_{mp} I_{mp}}{V_{oc} I_{sc}} = \frac{P_{max}}{V_{oc} I_{sc}} \tag{2.11}$$

where P_{max} is the power at the MPP. As the FF becomes closer to unity, the quality of the solar cell becomes higher [38].

Another important aspect in determining the performance of real solar cells is the efficiency, which can be determined considering the solar cell active area (A_a) from [1], [2], [34]:

$$Efficiency = \frac{I_{sc}.V_{oc}.FF}{G.A_a} = \frac{P_{max}}{G.A_a} \tag{2.12}$$

The above-mentioned parameters, namely P_{max}, I_{sc}, V_{oc}, FF and efficiency, constitute the main parameters of a PV device that indicate its performance. In this thesis, besides R_{ch}, they will be called the performance parameters in order not to be confused with the equivalent circuit parameters that will be presented in the next section.

The characteristics of a solar cell vary with the irradiance and operational temperature as shown respectively in Figures 2.7 and 2.8, which were obtained experimentally from a 0.78 cm² active area mono-Si solar cell and shown here for the purpose of illustration. The effect of irradiance on a solar cell can be demonstrated by plotting the electrical characteristics under different irradiance levels and at a fixed cell temperature of 25 °C as depicted in Figures 2.7 (a) and (b). As illustrated in the figures, the irradiance level incident on a solar cell plays a vital role in determining its output characteristics. The I_{sc} of the solar cell is nearly linearly proportional to the level of irradiance incident on it. Moreover, the increase of irradiance level causes a logarithmic rise in the V_{oc}. Thus, P_{max} of a PV device increases as the incident irradiance level increases [34].

The cell's temperature, on the other hand, has a different effect as shown in Figures 2.8 (a) and (b). When it increases, it causes a slight increase in the I_{sc} and a strong decline in the V_{oc}. Hence, P_{max} and efficiency deteriorate with the increase in temperature because the decay in V_{oc} is much more significant than the small increase in the I_{sc} [1], [2], [38].

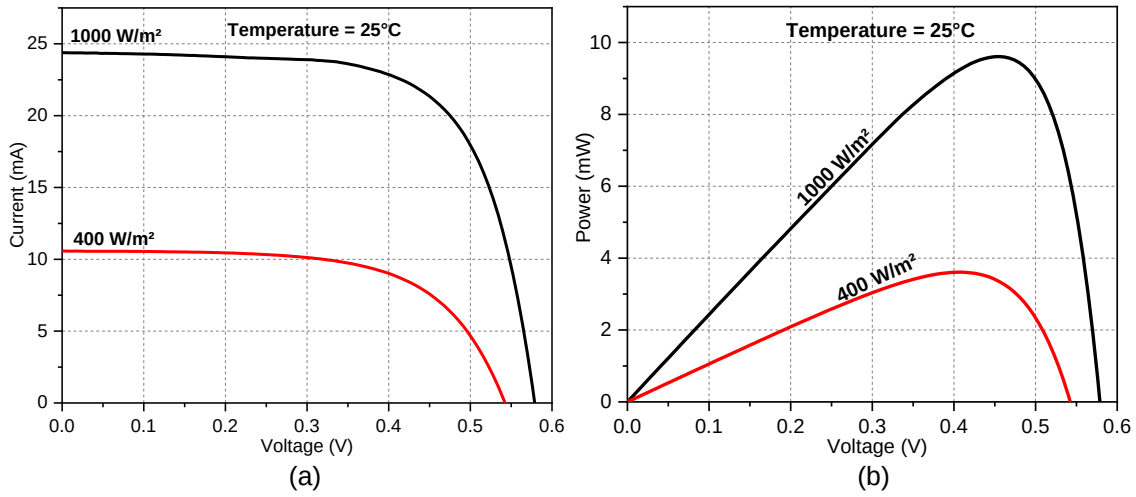

Figure 2.7. The effect of irradiance variation on: (a) the I-V and (b) the P-V characteristics of a solar cell.

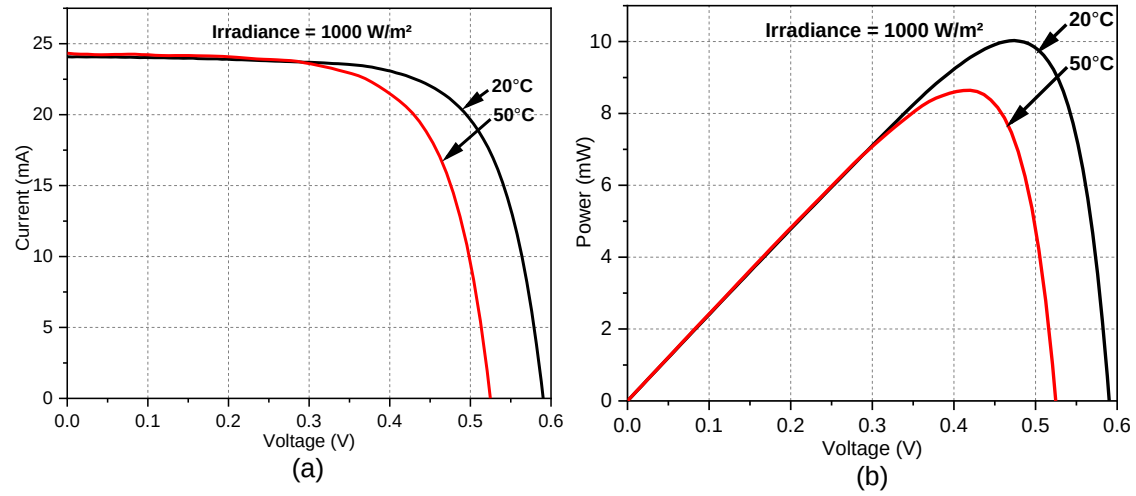

Figure 2.8. The effect of temperature variation on: (a) the I-V and (b) the P-V characteristics of a solar cell.

2.7. Single Diode Model Five Parameters

As mentioned previously, the single diode five-parameter model of Equation (2.3), which is commonly used by researchers, has five equivalent circuit parameters that need to be determined to solve its equation. These parameters are the series resistance (R_s), the shunt resistance (R_{sh}), the ideality factor (n), the reverse saturation current (I_s) and the photo-generated current (I_{ph}). However, this information is not usually provided in the manufacturer's data sheet of PV modules. The only data that can be obtained from a data sheet includes the I_{sc}, the V_{oc}, the current at the MPP, the voltage at the MPP, the current and voltage temperature coefficients (K_{Isc} and K_{Voc}). In addition, this information is

always provided only at STC [37]. The five parameters of the single diode model are subsequently discussed in the next sub-sections.

2.7.1. Series Resistance

The series resistance (R_s) is an important parameter that indicates the operational health of a PV module [46] as it affects the shape of the I-V curve near the MPP [40]. This resistance represents the losses in the interface between the semi-conductor and cell metal contacts in addition to the resistance of the contacts themselves [1], [37]. For a typical mono-Si solar cell, the effect of increasing R_s on its I-V curve is depicted in Figure 2.9. These I-V curves were obtained by solving Equation (2.3) for a set of five parameters with changing the value of R_s.

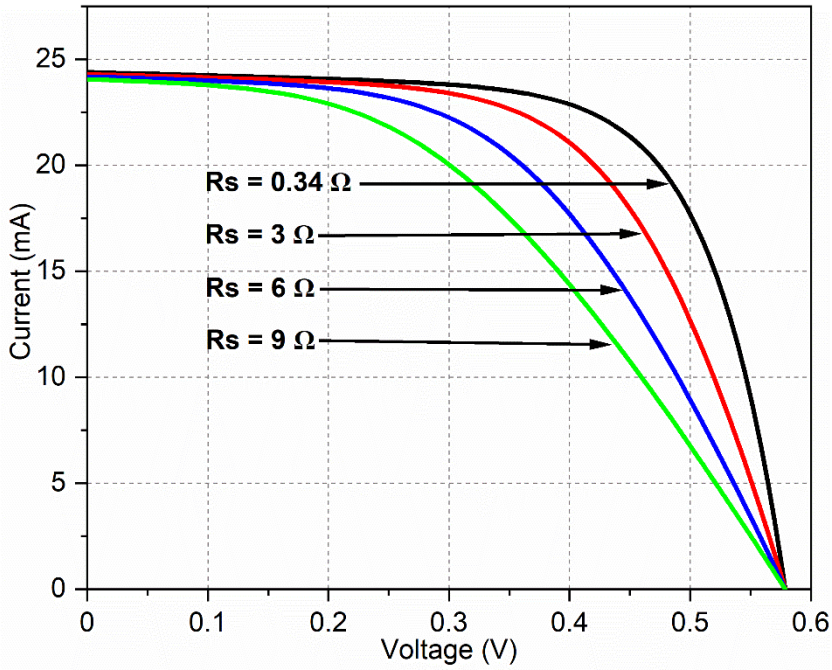

Figure 2.9. The effect of increasing the series resistance on the I-V characteristics of a solar cell. (The rest of the parameters used to plot the I-V characteristics are: shunt resistance = 687 Ω, ideality factor = 2.06, reverse saturation current = 0.42 μA and photo-generated current = 24.4 mA).

It is clear that R_s has a significant impact on the maximum power and the fill factor. In addition, its effect is more pronounced in the region between V_{oc} and MPP (also called the voltage source region [37]). The change in R_s with irradiance and temperature is given by the following expression [47]:

$$R_s = R_{s,ref}\left(\frac{T}{T_{ref}}\right)\left(1 - \beta ln\left(\frac{G}{G_{ref}}\right)\right) \quad (2.13)$$

where β is approximately equal to 0.217 and $R_{s,ref}$ is the series resistance value at STC.

2.7.2. Shunt Resistance

The shunt resistance (R_{sh}) represents the leakage originates from any short circuit paths exist in the p-n junction, especially near the solar cell edges [1], [38]. The R_{sh} value is usually much larger than R_s [2] and hence some authors neglect it from the five-parameter model, such as in [41]. Figure 2.10 illustrates the effect of reducing R_{sh} on the I-V curve of a mono-Si solar cell determined form solving Equation (2.3) for different R_{sh} values.

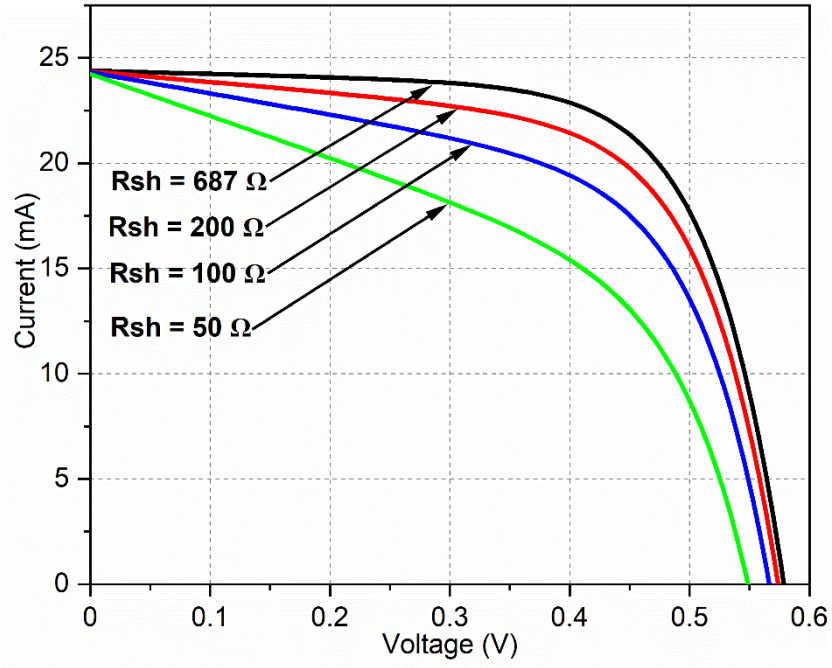

Figure 2.10. The effect of reducing the shunt resistance on the I-V characteristics of a solar cell. (The rest of the parameters used to plot the I-V characteristics are: series resistance = 0.34 Ω, ideality factor = 2.06, reverse saturation current = 0.42 µA and photo-generated current = 24.4 mA).

As shown in Figure 2.10, a clear distortion and reduction in the maximum power occur due to the decrease in R_{sh}. The most affected part of the I-V curve is between I_{sc} and MPP (also called the current source region [37]). The R_{sh} value is usually assumed constant with temperature, whereas its change with irradiation is given by [40]:

$$R_{sh} = R_{sh,ref}\frac{G_{ref}}{G} \quad (2.14)$$

where $R_{sh,ref}$ is the shunt resistance value at STC.

2.7.3. Diode Ideality Factor

The ideality factor (n) is added to the model in order to better represent real solar cells and its value is typically between 1 and 2 for crystalline-Si solar cells [1]. This parameter is empirical and it represents how close a solar cell's diode to a real diode. In addition, the effect of changing this parameter appears mainly in the curvature of the I-V curve [37]. In the literature, it is usually assumed independent of the change in irradiance and temperature (e.g. [35], [47]).

2.7.4. Reverse Saturation Current

The reverse saturation current of the diode (I_s) affects the shape of a solar cell's I-V curve near the MPP [36]. This parameter increases when the cell temperature rises because of the increase in the intrinsic carrier concentration. This causes a decline in the V_{oc} when the temperature rises [1]. A well-known equation governs the change of I_s with temperature is [34], [40], [48]:

$$I_s = I_{s,ref}\left\{\left(\frac{T}{T_{ref}}\right)^3 exp\left(\frac{E_g}{k}\left(\frac{1}{T_{ref}} - \frac{1}{T}\right)\right)\right\} \tag{2.15}$$

where $I_{s,ref}$ is the saturation current at STC, E_g is the bandgap of the material and it is equal to 1.12 eV for silicon. The bandgap has a weak dependence on temperature illustrated by the following equation for silicon solar cells [34], [40]:

$$E_g = E_{g,ref}\left(1 - 0.0002677(T - T_{ref})\right) \tag{2.16}$$

where $E_{g,ref}$ is the material bandgap at STC.

2.7.5. Photo-generated Current

The photo-generated current (I_{ph}) is generated from a solar cell when exposed to light. It depends on how many photons a solar cell absorbs from the incident light and contribute to the generation of electron-hole pairs and hence it is almost linearly proportional to the irradiance [1]. In addition, it is nearly equal to I_{sc} [2], [37] as previously stated. The effects of irradiance and temperature changes on I_{ph} are represented by [34], [41]:

$$I_{ph} = \left(I_{ph,ref} + K_{Isc}\left(T - T_{ref}\right)\right)\left(\frac{G}{G_{ref}}\right) \quad (2.17)$$

where $I_{ph,ref}$ is the photo-generated current at STC.

2.8. Parameters Extraction Methods

The problem of determining the parameters of the equivalent circuit of PV generators has attracted significant attention among researchers since the 1960s [49], in which the early attempts were published [50]. Over the past decades, many approaches have been proposed with different levels of simplicity, accuracy and applicability. These approaches can be mainly divided into four main categories: analytical methods, iterative methods, iterative-numerical methods and evolutionary computing methods [51]. In this context, analytical will be referred to the methods that only rely on explicit equations that are solved directly. Iterative methods are the ones that need an iterative process, while iterative-numerical methods are iterative techniques that depend on implicit equations, which need a numerical solver, such as the Newton Raphson method. Generally, some of the parameters extraction methods require only specific information usually provided in the data sheet of the PV generator, such as the I_{sc}, V_{oc} and MPP, as in [36], [37]. Others, however, require measurements of the complete I-V curve or part of it, as shown in some methods evaluated in [49].

The methods that require measurements of the whole I-V curve or part of it usually depend on calculating the slopes at I_{sc} and V_{oc} points [49]. In the remainder of this section, a brief outline of some approaches for selecting the proper location of points used to calculate the slopes is presented. In addition, as the single diode five-parameter model is the most commonly used model, a literature survey of some published methods of extracting the parameters of this model is presented. Although most the reviewed parameters extraction articles in this section present parameters extraction techniques in addition to methods to translate them to any operational irradiance and temperature, the main focus will be only on the techniques themselves. This is because parameters extraction is one of the main objectives of this research.

2.8.1. Calculating the Slopes of I-V Curves' Tangent Lines

The slopes of tangent lines on I-V curves at I_{sc} and V_{oc} points are used to get initial values of the shunt (R_{sh0}) and series (R_{s0}) resistances, respectively. An approximate value of R_{sh0} is obtained from the slope of the tangent line at I_{sc}, whereas an approximate R_{s0} is obtained from the slope of the tangent line at V_{oc} [1], [49]:

$$R_{sh0} = -\frac{\Delta V}{\Delta I}\ (I = I_{sc}) \tag{2.18}$$

$$R_{s0} = -\frac{\Delta V}{\Delta I}\ (V = V_{oc}) \tag{2.19}$$

Figure 2.11 illustrates how R_{sh0} and R_{s0} are obtained from an experimental I-V curve of a mono-Si solar cell obtained during experimental investigations in this research, where the points used for this purpose are labelled point-1, point-2, point-3 and point-4 [52]. Points 1 and 4 respectively represent the I_{sc} and V_{oc} points. Selecting proper locations along the linear parts of the I-V curve for points 2 and 3 can greatly affect the solution of a PV device parameters using extraction methods that depend on this data. In addition, this effect is more pronounced when the I-V curve has measurement noise or distortions [49].

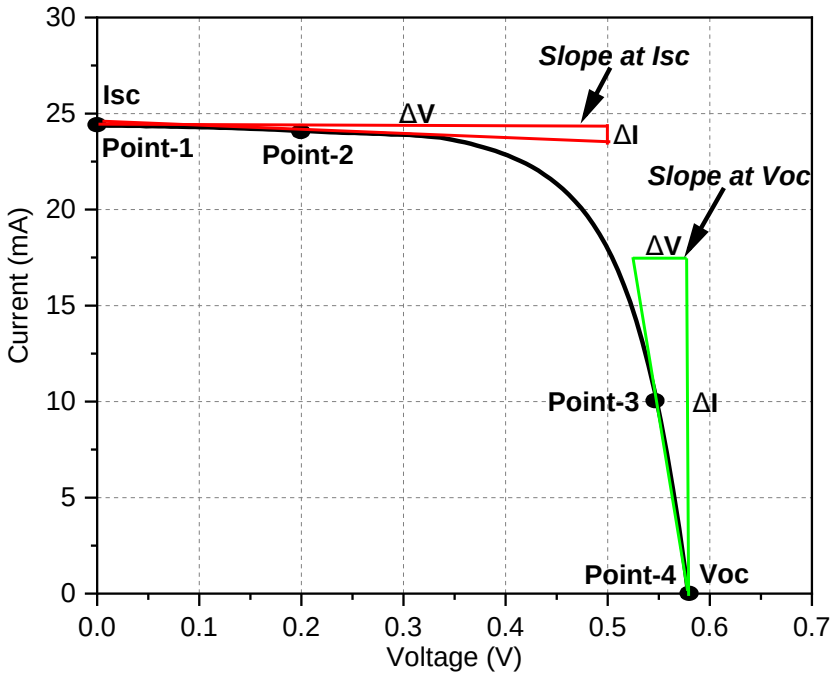

Figure 2.11. Determination of the slopes of tangent lines at short circuit current and open circuit voltage points.

Authors in [53], [54] proposed analytical parameters extraction methods that require experimental data of the I-V curve. However, the suitable locations of points 2 and 3 were not specified. Hence, parameters values obtained by these methods may vary depending on the selection of these points due to measurement noise in experimental I-V curves [49]. Thus, the results may not represent the correct values when unsuitable points are selected. However, studies in [47], [52], [55]–[57] claimed that the slopes can be obtained empirically from data sheet information when I-V curve data is not available.

Bai *et al.* [47] proposed using the four model parameters (neglecting R_{sh}) to obtain the I-V curve at STC as an initial step. Then, a piecewise curve fitting technique was used to obtain the slopes at I_{sc} and V_{oc} based on the nearly linear shape of the I-V curve near these two points. Two empirical equations were then derived to calculate R_{sh0} and R_{s0} using the four parameters and the data sheet information. Finally, the obtained values of R_{sh0} and R_{sh0} were used in an analytical approach to calculate the five parameters of the five-parameter model.

Benghanem and Alamri [52] suggested that for crystalline-Si PV modules, the best selection of point-2 to calculate R_{sh0} is located at a current equals to 95% of I_{sc}. Also, they proposed that the best location of point-3 to determine R_{s0} is a current equal to 50% of I_{sc}. The best point-3 for R_{s0} was obtained by iteratively varying point-3 current and then calculate the voltage and R_{s0} by solving Equations (2.5) and (2.19), respectively. This process is continued for the current range from 0 to I_{sc} until the calculated resistance matches the measured one obtained by an I-V curve tracer. The best point-2 for R_{sh0} was obtained in a similar fashion but using Equation (2.18) to calculate it. However, when varying the current of point-3, its voltage was calculated by the four-parameter model from Equation (2.5) (neglecting R_{sh}). Hence, an inadequate value of R_{s0} may be obtained because the four-parameter model is known to be less accurate than the five-parameter model [39]. This also applies to R_{sh0} calculation.

Orioli and Gangi [55] introduced two empirical expressions to calculate R_{sh0} and R_{s0} of crystalline-Si PV modules using only data sheet information. They developed these expressions by calculating R_{sh0} and R_{s0} from I-V curves of many PV modules using the following criterion. To calculate R_{sh0}, point-2 that has a voltage of 20% of V_{oc} was used. Likewise, to calculate R_{s0}, point-3 that has a current of 20% of I_{sc} was used. The yielded expressions of R_{sh0} and R_{s0} are respectively given by [55]:

$$R_{sh0} = 34.49692 \frac{V_{oc}}{I_{sc}} \tag{2.20}$$

$$R_{s0} = 0.11175 \frac{V_{oc}}{I_{sc}} \tag{2.21}$$

Similar approach to the work of [55] was proposed by Mares *et al*. [56], who also introduced two empirical equations to calculate R_{sh0} and R_{s0} from data sheet information and then used them to numerically calculate the five parameters. The procedure used to develop these equations is based on using many points on the I-V curve to determine R_{sh0} and R_{s0} and then selecting the best pair that provides the best fit with manufacturer issued I-V curves when the five parameters are calculated. Nevertheless, it was not indicated in [56] whether all possible pairs of points 2 and 3 to calculate R_{sh0} and R_{s0} were utilised or which range of points on the I-V curve were used. In addition, the procedure used to index the pairs in the iteration process was not shown (indexing points' pairs for R_{sh0} and R_{s0} calculation will be covered in detail in Chapter 4).

A very similar approach was presented by Senturk and Eke [57], who also introduced two empirical equations to obtain R_{sh0} and R_{s0} from data sheet information and then used them explicitly to extract the five parameters. R_{sh0} was estimated directly from the slope between I_{sc} and MPP points. The procedure followed to obtain the empirical equation of R_{s0} was by means of I-V curve digitising. First, a digitising software was used to obtain the actual R_{s0} from the slope of crystalline-Si PV modules' I-V curves published in their data sheets using Equation (2.19). Second, another approximated value of R_{s0} was estimated from the slope between V_{oc} and MPP points mentioned in the data sheet (without using the I-V curve). Subsequently, those two values were correlated, and it was found that the latter is higher than the former by about two orders of magnitude. Finally, R_{s0} equation was derived by calculating the slope between V_{oc} and MPP points and then dividing it by 2.

However, all of the above methods, that suggest specific points' locations to determine the slopes [52], [55] or use empirical approximations [47], [55]–[57], might not be applicable to PV technologies with different fill factor or to I-V curves that contain measurement noise. In other words, selecting specific points for a particular I-V curve might not provide an accurate solution for another curve that has a different shape as the solution is greatly affected by these initial values [56]. Furthermore, these techniques can be useful only when experimental I-V curve data is not available. Even if experimental

data is handy, it is still a challenging task to select the locations of these points that provide accurate parameters [49]. This task will be dealt with in the work presented in Chapter 4.

2.8.2. Analytical Methods

The analytical parameters extraction methods in general rely on a number of simplifications and empirical assumptions in deriving explicit equations from the main model Equation (2.3). These explicit equations do not require iterations or a numerical solver for their solution. Compared to other techniques, analytical methods do not have convergence issues thanks to their simplicity. Yet, they suffer from low accuracy due to their direct solution and absence of any optimisation [51].

Phang *et al*. [53] proposed an analytical method that was tested and verified experimentally in [39], [45]. The five parameters of an illuminated I-V curve are extracted at a particular irradiance and temperature from analytical expressions based on calculating R_{sh0} and R_{s0} using the slopes at I_{sc} and V_{oc} points, respectively. These analytical expressions were derived based on some simplifications of Equation (2.3) when this equation is extrapolated into the three main points on the I-V curve, namely, I_{sc}, V_{oc} and MPP. The equations of the analytical method proposed in [53] will be presented in Chapter 4. Similar analytical expressions that depend on R_{sh0} and R_{s0} were proposed in [47], [54], [57]. Once the slopes are estimated, the five parameters are analytically extracted, hindering the need for an iterative or numerical solvers. Some authors introduced analytical techniques that require only R_{sh0} [58], [59], although the method of [59] needs also other three points from I-V curve data to explicitly determine the five parameters.

There are also analytical methods that do not require the slopes. Saleem and Karmalkar in [60] proposed an analytical method that requires only two points on the I-V curve in addition to I_{sc} and V_{oc} points, which are provided in the data sheet. In this work, the five-parameter model Equation (2.3) was transformed to a power law model and the five parameters are extracted using two auxiliary parameters found from the above four points.

Another method that requires only data sheet information and does not need the slopes was introduced by Batzelis and Papathanassiou [61]. The temperature coefficients of the short circuit current and open circuit voltage, which are commonly given in the data sheet,

were used to introduce a new coefficient evaluated at STC. This coefficient is then used to solve for the five parameters analytically.

Analytical parameters extraction by using the explicit form of the five-parameter Equation (2.3) incorporating the Lambert W-function was first proposed by Jain and Kapoor [62]. The current can be expressed in terms of voltage in an explicit form and thus hindering the need for numerical solvers. In addition, this method features determining the parameters using the exact solution as shown by [63] without the need for simplifications of Equation (2.3) used in other methods, such as the methods in [47], [53], [54]. Some other authors, however, made further simplifications to the approach of using the Lambert W-function by expressing only R_s [64] and both R_s, R_{sh} [65] using this function. The rest of the parameters are explicitly calculated using simplifications of Equation (2.3) in a similar fashion to the works of [47], [53], [54].

Ortiz-Conde *et al.* [63] transformed the Lambert W-function analytical form of Equation (2.3) to a co-content function with five coefficients. These coefficients are then obtained from an experimental I-V curve by bi-dimensional fitting and then used explicitly to calculate the five parameters of the solar cell. However, this method is not a straightforward analytical method because of the need to the bi-dimensional fitting to experimental I-V curve to obtain the coefficients of the co-content function.

Besides using solely the analytical methods, in some works, the analytical solution of the five parameters was utilised as initial guesses for other advanced algorithms to insure convergence [66]–[69]. The method presented in [66] uses the Lambert W-function to explicitly estimate initial values of parameters and then enhances the solution using a polynomial curve fitting, which fits the theoretical I-V curve with the experimental one. In [67], approximate values of the parameters are extracted analytically using data sheet information after a set of assumptions and approximations. Then, they are used as initial guesses for the Newton Raphson method. In addition, the analytical solutions of parameters were used as initial values for the numerical Levenberg-Marquardt algorithm in [68] and for least-square curve fitting in Microsoft Excel in [69]. In [70], a quasi-explicit technique is presented in which the parameters are explicitly extracted using four arbitrary points on the I-V curve, in addition to numerically solving one fifth-degree polynomial equation.

2.8.3. Iterative and Iterative-Numerical Methods

These methods rely, in general, on solving a set of non-linear equations using an iterative process with a numerical solver as in [71] or using an iterative process only as in [72], [73]. The equations are usually derived by extrapolating Equation (2.3) to the three main points on the I-V curve. In general, these techniques are more accurate than the analytical techniques, but at the cost of higher complexity and computational burden [61]. Further, convergence errors will be present if initial parameters' values for the solution are not properly selected [56], [68], [72].

In order to calculate the five parameters from the data sheet information, De Soto *et al.* [40] used a numerical solver called Engineering Equation Solver to solve a system of non-linear equations obtained from applying the conditions of I_{sc}, V_{oc} and MPP to Equation (2.4). Similarly, the newton Raphson numerical method was utilised in [71], [74] for solving a set of non-linear equations to determine the five parameters from data sheet.

De Blas *et al.* [72] proposed an iterative procedure to calculate the five parameters starting from estimating the slopes of the I-V curve. This technique is based on extrapolating Equation (2.3) to the three main points on the I-V curve. After some simplifications, the following five equations are derived to calculate the parameters [72]:

$$R_{sh} = R_{sho} - R_s \tag{2.22}$$

$$R_s = \frac{\left(1-\frac{I_{sc}R_{s0}}{V_{th}n}\right)R_{sh0}+\left(\frac{V_{oc}}{V_{th}n}-1\right)R_{s0}}{\left(\frac{V_{oc}-I_{sc}R_{sh0}}{V_{th}n}\right)} \tag{2.23}$$

$$n = \frac{\left(V_{mp}-V_{oc}+I_{mp}R_s\right)}{V_{th}Ln\left(\frac{I_{sc}-\frac{V_{mp}}{R_{sh}}-\left(1+\frac{R_s}{R_{sh}}\right)I_{mp}}{\left(1+\frac{R_s}{R_{sh}}\right)I_{sc}-\frac{V_{oc}}{R_{sh}}}\right)} \tag{2.24}$$

$$I_s = \frac{\left(1+\frac{R_s}{R_{sh}}\right)I_{sc}-\frac{V_{oc}}{R_{sh}}}{exp\left(\frac{V_{oc}}{V_{th}n}\right)} \tag{2.25}$$

$$I_{ph} = I_s\left(exp\left(\frac{V_{oc}}{V_{th}n}\right)-1\right)+\frac{V_{oc}}{R_{sh}} \tag{2.26}$$

Accuracy of this method will be evaluated in Chapter 4. First, R_{sh0} and R_{s0} are determined using Equations (2.18) and (2.19), respectively. Second, an initial value of R_s is assumed. Then, R_{sh} and n are calculated respectively from Equations (2.22) and (2.24).

Subsequently, an iterative process is executed to calculate R_s from Equation (2.23) until it converges with a specified tolerance. Then, R_{sh} is recalculated using Equation (2.22). Finally, I_s and I_{ph} are determined from Equations (2.25) and (2.26), respectively [72], [75]. De Blas *et al.* method [72] is similar to Phang *et al.* method [53] as both rely on determination of R_{sh0} and R_{s0}. Nevertheless, in [72], the technique was proposed to calculate the parameters based on the data sheet and hence fixed values of R_{sh0} and R_{s0} were assumed under any operating conditions. A similar iterative technique was introduced by Orioli and Gangi [55], although with slightly different equations. The main difference is that these authors [55] assumed that I_{ph} is equal to I_{sc} in addition to proposing Equations (2.20) and (2.21) to estimate R_{sh0} and R_{s0} using data sheet information.

Villalva *et al*. [37] proposed an iterative-numerical method to calculate the five parameters of PV modules based on equating the maximum power obtained from experimental data (or from the data sheet) with the calculated maximum power and solving for R_{sh} as per the following equation [37]:

$$R_{sh} = \frac{V_{mp}\left(I_{mp}R_s+V_{mp}\right)}{\left(I_{ph}V_{mp}-I_sV_{mp}exp\left(\frac{I_{mp}R_s+V_{mp}}{N_sV_{th}n}\right)+I_sV_{mp}-P_{max,e}\right)} \tag{2.27}$$

where: $P_{max,e}$ is the experimental maximum power. The authors suggested that an arbitrary value of the ideality factor (n) can be assumed. They also used the following equation to determine the reverse saturation current [37]:

$$I_s = \frac{I_{sc}}{exp(V_{oc}/N_sV_{th}n)-1} \tag{2.28}$$

First, I_s is calculated from Equation (2.28), an initial value of zero is assumed for R_s and I_{ph} is assumed to be equal to I_{sc}. Second, R_{sh} is calculated from Equation (2.27). Then, Equation (2.4) is solved by Newton Raphson method to produce the theoretical I-V curve and hence the theoretical maximum power ($P_{max,c}$). This process is continued iteratively by incrementing R_s until $P_{max,c}$ converges to $P_{max,e}$ with a specified tolerance. To enhance the model accuracy, the authors added some equations to the model:

- Initial minimum value is assigned for R_{sh}, which is the minimum value that this parameter could take obtained from [37]:

$$R_{sh,min} = \frac{V_{mp}}{I_{sc}-I_{mp}} - \frac{V_{oc}-V_{mp}}{I_{mp}} \quad (2.29)$$

- I_{ph} is initially assumed as it is equal to I_{sc}. However, for enhancing the model accuracy, after each iteration, it is re-calculated considering the effect of R_s and R_{sh} as follows [37]:

$$I_{ph} = I_{sc}\left(\frac{R_s+R_{sh}}{R_{sh}}\right) \quad (2.30)$$

- For more enhancement of the model, the program code of this model, which is available online from the webpage provided by the authors [76], added an equation to update I_s after each iteration considering the new values of I_{ph} and R_{sh}:

$$I_s = \frac{I_{ph}-(V_{oc}/R_{sh})}{exp(V_{oc}/N_s V_{th} n)-1} \quad (2.31)$$

This method utilises only information available in data sheets and based on fitting the curve only at the MPP point by assuming that only one pair of R_{sh} and R_s will fit the theoretical power with the experimental power (or the value provided in the data sheet) at this point. Evaluation of the accuracy of this method will be presented in Chapter 4.

Lo Brano *et al*. [36] developed an iterative technique based on the three main points on the I-V curve provided in the data sheet under STC. In addition, a new lumped equation was proposed based on altering the five-parameter Equation (2.3) to account for any irradiance and temperature conditions when calculating the parameters. Starting with initial guesses of R_s and n, the five parameters are obtained in a trial and error manner using similar equations to the ones proposed by De Blas *et al.* [72]. Furthermore, it was compared to the models of [37], [45], [72] elsewhere [75] and it provided more accurate results. This is because the parameters are extracted by solving a set of non-linear equations without any simplifications [36], [75]. Mares *et al*. [56] used the same procedure proposed in [36], but further simplified the iterations towards the solution and also proposed how to obtain the values of R_{sh0} and R_{s0} from data sheet information.

Authors in [73] proposed an iterative procedure to calculate R_{sh}, R_s and n from data sheet information. Instead of only changing R_s with each iteration as in [72], they changed R_{sh},

R_s and n until the difference in R_s between two subsequent iterations is less than a specified tolerance. After that, I_{ph} and I_s are explicitly calculated using R_{sh}, R_s and n.

Authors in [77] introduced an iterative algorithm to extract the five parameters from data sheet information. This method depends on the fact that at the MPP, a pair of R_{sh} and R_s will meet the condition at which the derivative of the power with respect to the voltage is equal to zero. In this work, n was assigned a fixed value and I_s is calculated by Equation (2.28). The other three parameters are extracted by an iterative procedure without solving any implicit equations. This technique is quite similar to the method of Villalva *et al*. [37] as both rely on the MPP for calculating the parameters.

There are some other methods that require measurements of the I-V curve or some points from it. In [78], Ishibashi *et al.* proposed an iterative process that requires determination of the slope at discrete experimental data points on the I-V curve. The work in [79] performed orthogonal distance regression in Origin Lab software on Equation (2.3) with experimental I-V curves. The equation is fitted in an iterative way with the I-V curve until the best fit is achieved. Both techniques in [78], [79] were validated by extracting the parameters of different types of solar cells.

Similar work is presented in [80], where the authors applied the least square fitting technique to experimental data of organic solar cells to calculate R_s and n. The photo-generated current I_{ph} was assumed to be equal to I_{sc}. The shunt resistance R_{sh} was obtained by linear fitting at either forward or reverse bias conditions. Finally, I_s was calculated graphically form the calculated I-V curve that takes into account the calculated value of R_s.

Authors in [81], introduced an approach to extract the five parameters from measurement of R_{sh} of a PV module and information provided in the data sheet. Once R_{sh} is measured by applying a negative voltage to a PV module under a dark condition, its value is used alongside with the data sheet information to solve two non-linear equations numerically in order to get the other parameters.

2.8.4. Evolutionary Computing Methods

Recently, artificial intelligence has played a key role in the accurate determination of PV devices parameters. In evolutionary computing techniques, the iterative process is

combined with an optimisation random search to extract the parameters [51]. Different methods are available in the literature with different degrees of complexity and accuracy, such as particle swarm optimisation (PSO) [82], generic algorithm (GA) [83], differential evolution (DE) [84], simulated annealing (SA) [85], pattern search (PS) [86], artificial bee colony (ABC) [87], multi-verse optimiser (MVO) [88], and teaching-learning-based optimisation (TLBO) [89], among others. Some authors also proposed hybrid techniques, such as in [90], in which the ABC was combined with the TLBO optimisation technique. Besides hybridising two evolutionary computing techniques, some researcher also investigated hybridising them with analytical methods, such as the work in [91], which combined an analytical approach to calculate I_{ph}, R_{sh} and I_s with the DE to determine R_s and n.

Generally, although very accurate solution can be achieved using the evolutionary computing methods, this is associated with an intensive computation, a high level of complexity and convergence issues [51], [61] similar to the case in iterative and iterative-numerical methods. Therefore, in most applications, a simple but accurate enough technique is demanded. This will be dealt with in Chapter 4 by introducing a simple iterative process to optimise the accuracy of calculating the slopes of I-V curves.

2.9. Partial Shading in PV Systems

Partial shading is an unavoidable issue that severely degrades the performance of PV devices. As briefly explained in Section 1.2, it is caused by objects near the PV system or by clouds. Figure 2.12 depicts a typical example studied in [92], in which a light pole casts shadow on a nearby PV system. In the next sections, the impact of partial shading on PV devices is briefly discussed. After that, a literature survey of the representative modelling attempts of PV systems response under partial shading is given.

Figure 2.12. Partially shaded PV system by a light pole [92].

2.9.1. Consequents of Partial Shading

A PV module is the commercially available unit in PV systems. It typically consists of series-connected solar cells, which could be 72, 60, 48 or 36 cells [1]. The cells are divided into a number of groups. Each group is called a cell-string or sub-module [5] and usually equipped with a bypass diode in order to bypass it in the case of partial shading to protect cells from over-heating and hot spots [1], [2], [5], [93]. Figure 2.13 shows the cells' configuration with bypass diodes in a typical mono-Si 10 W PV module that was used in characterisation experiments within the scope of this research. The module consists of two cell-strings, each one containing 18 cells connected in series separated by bypass diodes. In order to illustrate the power loss caused by shading in PV modules, Figures 2.14 (a) and (b) presents the output I-V and P-V curves, respectively, of the module without shading and when only one cell is half shaded by an opaque tape. These measurements were taken under an irradiance of 1000 W/m^2 and at a module temperature of 25 °C and they are shown in this context for illustration purpose.

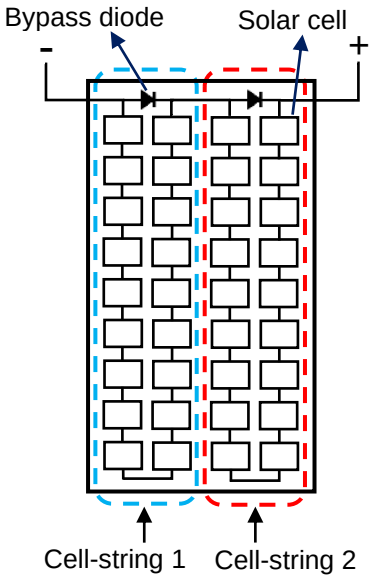

Figure 2.13. The schematic diagram of cells and bypass diode configuration in a mono-Si 10 W PV module.

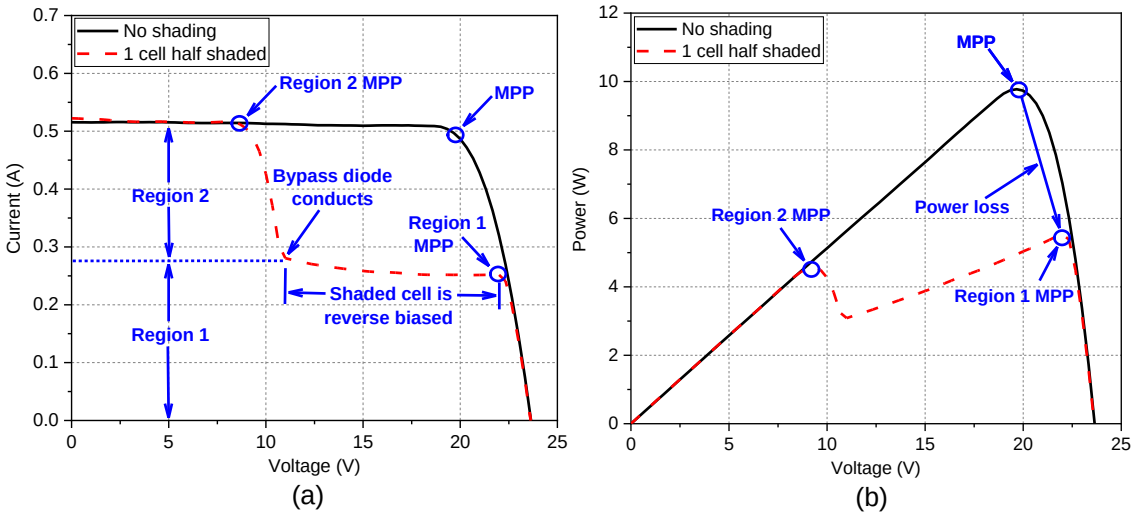

Figure 2.14. The output characteristics of a mono-Si 10 W PV module under no shading and when one solar cell is half shaded: (a) the I-V curve and (b) the P-V curve.

As illustrated in Figures 2.14 (a) and (b), initially, before half shading of a single cell, the module was delivering a maximum power of 9.775 W. However, when one cell is half shaded, the I-V and P-V curves are divided into two regions [94] annotated in Figure 2.14 (a) as region 1 and region 2. In addition, the I-V and P-V curves show multiple steps (knees) and peaks, respectively, because of bypass diode conduction, that is two MPPs. One of them is the real MPP of the module and it is usually called the global MPP (GMPP), whereas the other one is called a local MPP (LMPP) [10]. In this shading case, the peak point at region 1 represents the GMPP with a power of 5.539 W. Thus, a significant drop in maximum power of about 43.3% occurs while shading a small area of the module representing only about 1.4% of the total area of the 36 cells. However, if the shading increases to a certain extend, the GMPP of the shaded module in Figures 2.14 (a) and (b) will be shifted from region 1 MPP to region 2 MPP and it will remain constant regardless of the shading extend on the cell-string [94]. Maximum power point tracking (MPPT) in partially shaded PV systems is an intricate task due to the appearance of multiple peaks, hindering the conventional MPPT techniques from finding the GMPP [10], [95]. It is also to be noted that the power loss, in fact, becomes even worst if the module does not have bypass diodes [1].

In region 1, the shaded cell limits the current of the whole module. However, when the current of the unshaded cells exceeds the maximum current of the shaded cell (shaded cell I_{sc}), the shaded cell begins to be reverse biased by the voltage of the unshaded cells. When this reverse voltage exceeds the bypass diode threshold voltage (about 0.7 V), the

diode conducts and bridges the whole cell-string that contains the shaded cell as illustrated in Figure 2.14 (a). The module is thus now operating in region 2 and only one cell-string delivers power [1], [94]. Moreover, when the bypass diode conducts, there will also another small amount of power loss dissipated in the bypass diode because of the current flows through it [96].

If the module is not equipped with bypass diodes, the shaded cell will continue to be reverse biased by the unshaded cells at high negative voltages and thus consumes their produced power [2]. This will cause the shaded cell to heat-up significantly and result in the so-called hot spot, which could have a destructive impact on the whole PV module [1], [8].

2.9.2. Modelling of PV Systems Under Partial Shading

In light of the consequents of partial shading discussed in the previous section, it is indeed important to study and investigate the behaviour of PV systems affected by this phenomenon. A variety of models have been proposed in the literature with different equivalent circuit models and different system sizes [5]. Most researchers adopted the five-parameter model [6], [12], [97]–[121], whereas others used the four-parameter model, neglecting R_{sh} [122]. On the other hand, some works sought more accuracy and employed the double-diode model [9], [42], [93], [94], [123]–[127].

In order to gain more accuracy in modelling the reverse bias characteristics of shaded solar cells, an avalanche breakdown term is included in the five-parameter model [12], [97], [100], [105], [108], [109], [112], [113], [116], [121] and the double-diode model [93], [94], [123]. The inclusion of avalanche breakdown was initially proposed in 1988 by Bishop [12]. Since then, it has become a common practice to add this term, which is commonly called the Bishop's term. When a PV module is not equipped with bypass diodes, the reverse bias behaviour of a shaded solar cell appears in a wide voltage range as shown by Quaschning and Hanitsch [123] covering nearly all the first quadrant (from MPP to I_{sc}). However, when bypass diodes are provided, the reverse bias behaviour of the shaded solar cell dominates in region 1, as illustrated in Figure 2.14 (a), in the area between region 1 MPP and the point at which the bypass diode conducts as shown by [98], [128]. The equivalent circuit proposed by Bishop [12] for a solar cell using the avalanche breakdown term is shown in Figure 2.15.

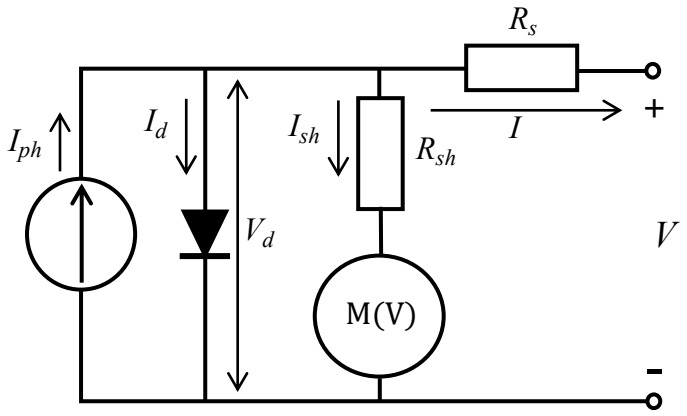

Figure 2.15. The equivalent circuit of the five-parameter model including the avalanche breakdown term connected in series with the shunt resistance and denoted M(V). (Adapted from [12]).

The five-parameter model of a solar cell including the avalanche breakdown term is expressed by [12]:

$$I = I_{ph} - I_s\left(exp\left(\frac{IR_s+V}{V_{th}.n}\right)-1\right) - \frac{IR_s+V}{R_{sh}}\left(1+a\left(1-\frac{IR_s+V}{V_b}\right)^{-m_a}\right) \qquad (2.32)$$

where V_b is the breakdown voltage, m_a and a respectively represent the avalanche breakdown exponent and the avalanche breakdown current fraction. The double-diode model version of this equation is [93]:

$$I = I_{ph} - I_{s1}\left(exp\left(\frac{IR_s+V}{V_{th}n_1}\right)-1\right) - I_{s2}\left(exp\left(\frac{IR_s+V}{V_{th}n_2}\right)-1\right) - \frac{IR_s+V}{R_{sh}}\left(1+a\left(1-\frac{IR_s+V}{V_b}\right)^{-m_a}\right) \qquad (2.33)$$

Slight alterations to Bishop's model are also available in the literature. Quaschning and Hanitsch [123] presented a benchmark model by including the avalanche breakdown term shown in Figure 2.15 in parallel with R_{sh} of the double diode model and not in series with R_{sh} of the the five-parameter model as proposed by Bishop [12]. In addition, another modification was presented by Jung *et al.* [105], who modelled a PV module by adding another term in series with the diode and another branch in parallel with R_{sh} of the five-parameter model. A similar approach was introduced in [124] adding Thevenin voltage sources, resistances and diodes to the double-diode equivalent circuit to represent the reverse bias mode. However, all these approaches and publications that follow them use a similar approach to describe the avalanche breakdown to the one introduced by Bishop [12]. Nevertheless, Bishop's avalanche breakdown term requires the knowledge of

additional parameters as shown by Equation (2.32), which are the two constants (a and m_a) and the breakdown voltage. A lumped equation that does not depend on the equivalent circuit and allows characterisation of solar cells under only reverse bias was proposed in [129] and applied to modelling of PV modules under partial shading in [98]. Similar to Bishop's approach, this equation also requires additional parameters, one of which is the breakdown voltage.

Regarding the modelling scale of PV systems, in [6], [9], [42], [101], [106], [122], [126], [127], the PV module was considered as the basic block and then it was extended to model larger systems. Some authors also started from the cell-string level [114], [119]. Majority of the published researches, on the other hand, started from a single cell model [12], [93], [94], [97]–[100], [102]–[105], [107]–[113], [115]–[117], [120], [121], [123]–[125] or even a cell fraction level [118] seeking more sophisticated and accurate modelling. All of these models used the cell-level irradiance as input in the model. Nevertheless, except a few publications [110], [118], [120], [121], all the cell-level reported works did not take into account the variations of the cell's equivalent circuit parameters because of shading. In other words, they assumed that R_s, R_{sh}, n and I_s are irrelevant to the change of irradiance caused by shading and that only I_{ph} changes with shading. The linear change of I_{ph} with irradiance variation is well-known as shown previously by Equation (2.17).

Furthermore, the effects of partial shading and reducing light on the total cell area (with the equivalent intensity of shading) on solar cells parameters have been previously assumed identical in the models. Considering the shaded area and the shadow intensity, this was realised in a way so that a partially shaded solar cell would receive a reduced averaged light intensity on its total surface [107], [109], [110], [115]–[118], [120], [121], [125]. This light was then used as an input to the model. However, an experimental comparison between shading and irradiance reduction in terms of their influence on solar cells' characteristics and parameters have not been previously published in order to validate this assumption.

As stated above, only the works of [110], [118], [120], [121] considered some parameters' variations with shading in the model. Wang *et al.* [110] modelled the influence of shading caused by the frame of a PV/thermal system using the five-parameter model. The authors took into account the variations in single cell R_s and R_{sh} with shading in addition to I_{ph}. The variations in R_s, R_{sh} and I_{ph} were obtained through Equations (2.13), (2.14) and

(2.17), respectively, with assuming a constant temperature at STC. The input irradiance (G) to these equations was determined as the average of both shaded and unshaded areas irradiance levels. However, the authors did not specify which parameter change with shading (R_s or R_{sh}) would enhance the model accuracy because of the lack of comparison with experimental data. Furthermore, the possibility of model accuracy enhancement by evaluating the change in n and I_s with shading was not assessed.

Bharadwaj and John [118] presented a model to predict the performance of partially shaded PV modules starting from a fraction of a solar cell. In this model, solar cells are divided into fractions, called sub-cells, connected in parallel. Including I_{ph}, the parameters considered variable with shading are R_s, R_{sh}, and I_s. The variations of these parameters with shading for each shaded cell were calculated using the number of unshaded sub-cells, and not by using the average irradiance of the shaded and unshaded areas of the cell as in [110]. The sub-cell fraction approach is given in the following equations for an opaque shading [118]:

$$R_s = \frac{R_{s,nsh}}{k_f} \tag{2.34}$$

$$R_{sh} = \frac{R_{sh,nsh}}{k_f} \tag{2.35}$$

$$I_s = k_f . I_{s,nsh} \tag{2.36}$$

$$I_{ph} = k_f . I_{ph,nsh} \tag{2.37}$$

where the parameters with the sub-script nsh represent their values without shading, the parameters without this sub-script represent the values under partial shading and k_f represents the fraction of the unshaded sub-cells inside the solar cell ($k_f < 1$). Except Equation (2.37) for I_{ph}, which follows the well-known linear dependency of this parameter on irradiance, the above equations of R_s, R_{sh}, and I_s were not obtained in [118] from experimental investigations. Moreover, similar to the work of Wang *et al.* [110], there is no investigation on which one of the three parameters (R_s, R_{sh}, and I_s) variation with shading would enhance the accuracy of the model.

A similar approach was very recently proposed by Shen *et al.* [120], who accounted for the variation of only R_{sh} with shading when modelling PV modules under different

shading conditions. The R_{sh} of a partially shaded solar cell was empirically obtained based on dividing the cell into shaded and unshaded parts. In addition, its value at reverse bias was empirically found 6 times higher than the equivalent R_{sh} of the partially shaded solar cell. Although an improvement in modelling accuracy was achieved when taking into account the R_{sh} value in reverse bias, there was no investigation on the influence of taking into account the variations of the other parameters on the model accuracy.

A very recent published study by Chepp *et al.* [121] considered the variations of R_s and R_{sh} with shading in modelling PV modules in addition to including Bishop's term. The variation of R_{sh} with the irradiance change due to shading was implemented using Equation (2.14) proposed by De Soto *et al.* [40]. Whereas the variation of R_s was implemented following an increased value with reducing the irradiance proposed by a power low in [130]. However, the authors did not provide an individual assessment of modelling accuracy improvement imposed by those two parameters. Furthermore, they did not investigate whether considering the variations in n and I_s with shading would lead to accuracy improvement.

The lack of concise and complete experimental study on the variations of single solar cells' parameters with shading or reducing the irradiance may in fact explain why they are treated constant in most of the modelling published works. Note that partial shading effect on solar cells was compared with that of reducing light in the present work and will be presented in Chapter 5. Hence, the works that investigated the effect of changing the irradiance on parameters instead of partial shading were also included in this literature review.

Zhu *et al.* [117] experimentally studied the variations of R_s and I_{ph} of a single solar cell with shading. Yet, the variation of R_s was neglected and not taken into account when extending the model to larger PV systems. In addition, the variations of the other parameters with shading were not investigated. Sabry and Ghitas [131] carried-out edge shading experiments of a solar cell and investigated its effect on the cell's parameters. However, only variations of R_s and R_{sh} with shading were studied. The rest of the equivalent circuit parameters' variations were not investigated. Furthermore, only a small portion shading at the cell's edges was applied, which does not show the variations of parameters over a wide range of shading proportions from the total cell area. Hence, no equations that govern the variations of parameters with shading can be deduced.

Khan *et al.* [132] studied the influence of irradiance reduction on the parameters of a mono-Si solar cell. Four parameters form the equivalent circuit were investigated, which are R_s, R_{sh}, I_s and n. Again, no relationships between parameters and irradiance change were derived and hence the resulted variations of parameters were not previously used for modelling of PV devices under different irradiance levels or partial shading. Ghitas and Sabry [133] compared the effects of edge shading and central shading on a solar cell. However, the equivalent circuit parameters were not investigated and only the performance parameters were studied, namely, I_{sc}, V_{oc}, FF and efficiency. Similarly, studies in [134]–[136] covered only the effect of shading on some performance parameters.

Some authors studied the variations of equivalent circuit parameters of PV modules, but not single solar cells. The R_s and R_{sh} variations with shading were investigated in [137]. The R_{sh} variation with reducing the irradiance was studied in [40], [138]. Whereas the variations of all the equivalent circuit parameters with reducing the irradiance were recently investigated in [130], in which no defined trend for the variations of n and I_s was obtained.

It is to be emphasised that models harness the avalanche breakdown effect may accurately model the characteristics of PV modules with shaded solar cells, particularly at the region of the characteristics at which the shaded cells are reverse biased (see Figure 2.14 (a)), as shown by several publications [12], [97], [100], [105], [116], [121], [123]. This is mainly due to the inclusion of the avalanche breakdown term. Hence, one may not need to account for the variations of single cells' parameters with shading in the model in order to obtain accurate modelling. Nevertheless, as mentioned previously, adding the avalanche breakdown term to the model requires the knowledge of additional parameters, such as the breakdown voltage. This voltage can take different values in a wide range within solar cells, although they belong to the same module [129] or even to the same manufacturing batch [139]. In addition, the value of this voltage is not commonly supplied in PV modules' data sheets. Although a method to calculate it was proposed in [129], it requires the measurement of the dark reverse bias characteristics of each single solar cell.

Therefore, it is beneficial to investigate the possibility of having a model that does not require the breakdown voltage and the avalanche breakdown term, but still capable of adequately simulating the behaviour of PV modules with shaded solar cells. It is also

favourable to assess which one of the parameters better improves modelling accuracy when its variation with shading is taken into account. These topics were explored in this research and they are presented in Chapter 5.

2.10. Broken Contact Fingers and Cracks in Solar Cells

Solar cell front contact fingers may break because of cell cracks that occur during manufacturing stages. Thermal and mechanical cycles that the cells face during lifetime may also cause existing cracks to propagate into the cell's material and disconnect parts of the cell area [14], [19], [140]. This prevents the current from flowing to the main busbar of the cell and hence deteriorates its performance [13], [19]. An example of broken contact fingers caused by poor soldering of the busbar ribbon wire is depicted in Figure 2.16. This figure shows an EL image of a solar cell with a dark region between busbars (shown by the white box in the figure), which was attributed to broken contact fingers by Chaturvedi *et al.* [14].

Manufacturers of PV modules tend to reduce the silicon wafer thickness in order to reduce the manufacturing cost and consumption of silicon, which has made solar cells more prone to cracking and cell breakage [141], [142]. This has triggered significant attention among researchers to investigate cracks origin, their effect on PV systems performance and detection techniques.

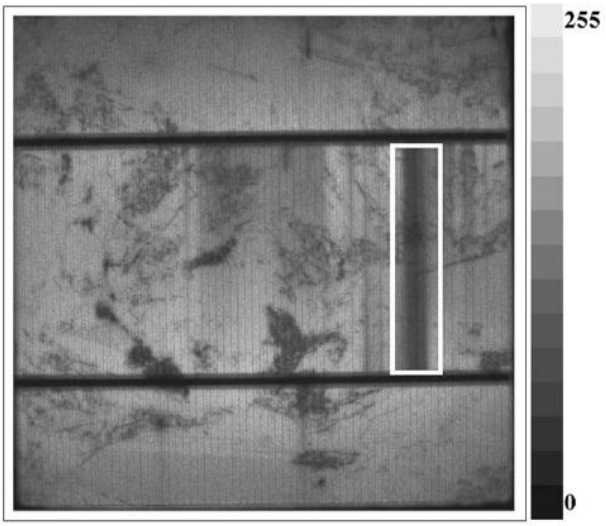

Figure 2.16. EL image of a solar cell shows a dark region caused by broken contact fingers due to poor soldering [14].

2.10.1. Types of Solar Cell Cracks

Cracks of crystalline-Si solar cells can be classified into six types based on their orientation. Namely, parallel to busbar, perpendicular to busbar, diagonal (could be +45° or -45°), multiple directions and dendritic [13], [143] as depicted in the EL images in Figure 2.17.

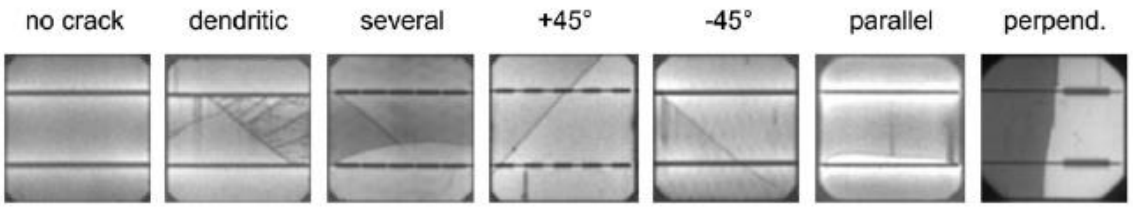

Figure 2.17. EL images showing different types of PV cracks depending on their orientation in silicon solar cells [13].

In terms of their width, cracks can be micro or macro-cracks. A crack is usually called a micro-crack if it has a width of less than 30 µm [144]. Moreover, in terms of their depth, according to [145], cracks that affect the surface of the silicon wafer are called facial cracks, whereas those occur deeper in the wafer or start at the surface and propagate inside the wafer are called sub-facial cracks. The latter is also divided into two types depending on its depth, which are shallow-layer and deep-layer cracks [145].

Broken front contact fingers lead to disconnected cell areas and are caused by cracks with an orientation that cuts the contact fingers, which could be any one of the types shown in Figure 2.17, except the perpendicular to busbar [13]. Among those types of cracks, the parallel to busbar type has the highest occurrence within PV modules according to a study performed by Kajari-Schröder *et al.* [13]. They carried-out mechanical load tests on 27 crystalline-Si PV modules simulating actual stress seen by the modules in the field and found that 50% of the resulted cracks are parallel to busbar. Besides, data collected from PV installations in the field in [146] revealed that parallel to busbar cracks represented 21% of the total observed cracks. Furthermore, in another study by the same authors [140], they applied artificial aging tests to 12 modules already affected by cracks from the mechanical load tests. They observed that 7% of the cracks worsened and caused disconnected cell areas. Thus, parallel to busbar cracks are of high criticality as they have the highest occurrence and highest possibility to break the contact fingers and cause disconnected cell areas [13], [140].

2.10.2. The Effect of Solar Cell Broken Contact Fingers on the Output Power of PV Modules

As cracks and the resulted broken contact fingers may occur or worsen in any stage of the module's lifetime, it is quite difficult to quantify their effect on the module's performance [19]. However, in order to perform controlled experiments for modules' aging, mechanical load and accelerated aging tests are commonly used by researchers to simulate the stress on modules caused by environmental conditions, such as wind, snow and temperature cycling. These tests are usually applied in such a way so that they match the IEC 61215 standards [18].

Many works in the literature showed that cracks that disconnect parts of a cell's area are the worst type of cracks in terms of power loss [19], [147]–[149]. Grunow *et al.* [147] compared the influences of different types of cracks on the I_{sc}, V_{oc} and FF of individual poly-Si solar cells. The cracks investigated were parallel to busbar, perpendicular to busbar and diagonal. These cracks were intentionally introduced to solar cells using a metal pen in addition to a random crack with unknown orientation created by bending. The results show that the parallel to busbar cracks, that cause broken contact fingers, have the greatest impact on the investigated parameters, especially the I_{sc}.

Köntges *el. al.* [19] assessed and quantified the power loss in poly-Si PV modules because of micro cracks. Output power and EL imaging of PV modules were measured before and after mechanical load tests and also before and after accelerated aging tests. Several cracks of different types were noticed after the mechanical load test and some of them worsened after the aging test. The power loss investigations in [19] show that cracks that do not disconnect parts of the cell area cause negligible power loss to the module. On the other hand, a simulation study was also performed to determine the module's power loss due to disconnected cell area. The results depicted in Figure 2.18 show the power loss and the MPP current of a 60-series-connected-cells module when the disconnected area of one cell was increased from 0 to 100% at different cell breakdown voltages. These results show that there is no appreciable power loss when the disconnected cell area is less than 8% of the total cell area regardless of the value of the breakdown voltage of the solar cell.

By contrast, with a breakdown voltage of 15 V or above, the power loss increases nearly linearly from zero to the power of one cell-string when the disconnected cell area increases from 12 to 50%. There is also a considerable amount of power loss for breakdown voltages of less than 15 V. For instance, about 20% of the module's power is lost when the disconnected cell area is 50% and with a breakdown voltage of 10 V. In addition, there is also a decline in the MPP current of the module at different cell breakdown voltages.

Due to the commonly used series connection of cells in a cell-string, when there are many cracked cells in a cell-string, the cell with the largest disconnected area governs the amount of power loss, same as partial shading. Thus, when the module with a cracked cell is connected in series with other modules, the cracked cell may lower the power output of the whole string significantly [19].

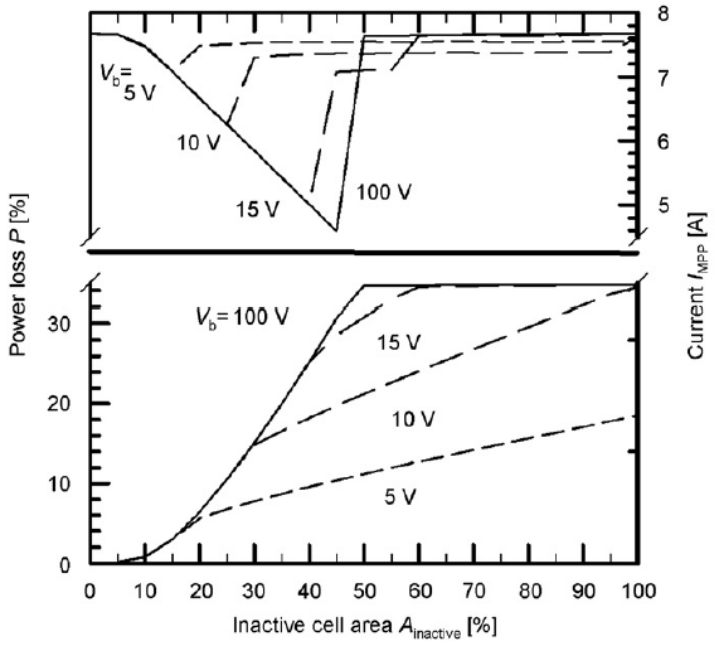

Figure 2.18. The power loss (bottom) and the MPP current (top) of a module with 60 series-connected cells as a function of the percentage of the disconnected area of one cell from the total cell area at different cell breakdown voltages [19].

Chaturvedi *et al.* [14] performed mechanical load and thermal cycling tests on a PV module. Electrical parameters and EL images were taken before and after the tests. The EL images showed dark rectangular regions after the tests, which were attributed to broken contact fingers. The maximum power of the module reduced from 236 W to 228 W because of the mechanical load test. Moreover, it reduced from 241 W to 226 W

because of the thermal cycling test. Those power losses occurred due to cracks and broken contact fingers.

Dolara *et al.* [150] also measured the maximum power at STC of PV modules that significantly affected by cell breakage and compared it with data sheet value. The results revealed a reduction of 26 to 27% due to cracks and broken contact fingers. In addition, from EL and thermal images, the authors found that there is a correlation between broken contact fingers and hot spots. Similarly, Dhimish *et al.* [151] studied the power loss of 10 PV modules in the field using long-term maximum power measurements. The measured maximum power over one day was compared with the theoretical one and the results showed that there were two modules with significant power loss because of cracks and broken cells. The broken cells were also detected by EL imaging. These modules gave a power output percentage of 85.43 and 80.73% from the theoretical power. These findings indicate that cracks that cause cell parts disconnection and cell breakage have a significant impact on PV modules' performance.

Dhimish [148] investigated the impact of cracks of 4000 samples of poly-Si solar cells. The power loss was assessed by comparing the measured power with the theoretical one. It was found that cracks that affect the contact fingers caused a power loss ranging from 1.7 to 13.5% due to the decrease in finger width. Moreover, the thermal imaging results indicate that there is a correlation between damaged contact fingers and hot spots. In another recent publication, Dhimish *et al.* [149] examined a number of solar cells affected by cracks that are uniformly and non-uniformly distributed over the cell area. The authors found that contact fingers are severely affected in all cracked cells. Further, they linked the large amount of power loss and hot spots in the non-uniformly cracked cells to broken contact fingers and busbars.

2.10.3. Detection Techniques of Solar Cell Broken Contact Fingers

Considering the consequents of broken contact fingers mentioned in the previous section, it is imperative to detect them in an early stage. PV modules may be inspected for cracks before they leave the factory [152] to alleviate the issue of cracks propagation and creation of broken contact fingers during modules' aging [19], [140]. However, during operation in the field, bypass diodes may conduct to bridge the cell-strings that contain broken cells and hence the power loss may be significant [19]. Furthermore, researchers

noticed a clear correlation between broken contact fingers and hot spots [148]–[150]. These consequents imply that severely affected PV modules in the field may need to be replaced for an efficient and safe operation [153]. Therefore, regular inspection of PV modules for cracks and broken cells is of great importance.

There are various cracks detection techniques reported in the literature, which differ in terms of their applicability, reliability, complexity and cost. They include EL imaging [13], [14], [143], [150]–[162], thermal imaging [150], [153], photoluminescence imaging (PL) [163], [164], ultraviolet (UV) fluorescence imaging [17], [153], lock-in thermography [165], [166], optical transmission [167], resonance ultrasonic vibration [168], scanning electron microscopy [14], [149], interferometry of electronic speckle pattern [169], lamb-wave air coupled ultrasonic testing [170] and mechanical impact testing [171]. However, for the sake of brevity and consistency with the findings of this research, only EL and thermal imaging will be briefly reviewed in the following text. This is also because they are widely used in fault diagnostics of PV installations in the literature due to their simple and fast implementation as shown by several publications, e.g. [143], [153]. Furthermore, EL imaging is already used in the production lines of solar cells for detection of cracks [152].

El imaging is a powerful tool for inspecting solar cells and modules for defects and cracks and it was first proposed in 2005 by Fuyuki *et al.* [154]. Solar cells are capable of emitting infrared light when forward biased because of radiative recombination of charge carriers [153], [155]. Cooled silicon charge-coupled device (CCD) camera is usually used under dark environment to capture the EL radiation that has a peak of around 1150 nm spectrum [155]. Dark areas in the EL images indicate defects because of low radiation emission [150]. A schematic diagram shows the experimental set-up of an El imaging system of a poly-Si solar cell introduced by Fuyuki *et al.* [154] is presented in Figure 2.19.

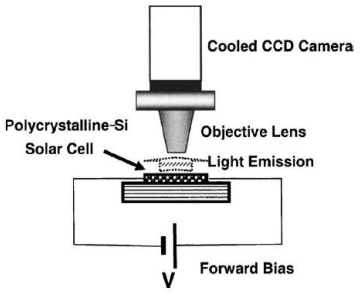

Figure 2.19. The experimental set-up of an El imaging system proposed by [154].

Although EL imaging is performed in the dark [155], some researchers [156], [161] proved the ability to take EL images under day light with applying some light filtering techniques. In addition, in order to perform EL imaging in a cost-effective manner, some authors used a consumer grade low-cost digital single-lens reflex (DSLR) camera. The infrared (IR) blocking filter is removed in this case to allow image capturing in the near infrared range [143], [153], [157], albeit the captured image in this case is of less quality than that taken by a special camera [1].

In order to enhance the performance of EL imaging, machine vision techniques [159], [160], [162] and evolutionary computing [152], [158], [162] techniques have recently been emerged in this field. In these approaches, EL images undergo further processing and refinement stages in order for cracks and broken contact fingers to be reliably detected.

Thermal imaging (also called thermography) can also be used to detect broken solar cells in PV modules, although with a much less informative images than EL imaging as shown by [150]. The sensor in a thermal imaging device receives the emitted radiation by the PV device under test in the infrared range of the spectrum. The imaging device then converts this radiation into a thermal image [1], [153]. In order for the defected cells to be clearly detected as hot spots in the images, the imaging needs to be captured at the short circuit condition [1]. Nevertheless, it was shown by [153] that thermal imaging was not capable of detecting damaged cells in a PV installation occurred due to a hailstorm. Thus, thermal imaging is not as reliable as EL imaging in detecting broken contact fingers as shown by the results presented in [150], [153]. This also will be shown during experimental investigations within the scope of this project presented in Chapter 6.

As previously mentioned, EL imaging is widely used due to its simplicity. Add to this is the cheap implementation when using a low-cost DSLR camera [143], [153], [157]. Its main drawback, however, is that it cannot directly detect faults under day light because EL radiation is weaker than sunlight by several orders of magnitude [156], [161]. Day light EL imaging needs special hardware, filtering techniques and background images as shown by [161], which makes it an intricate task. Similarly, PL imaging under day light also requires a special camera and filtering techniques [164]. Furthermore, detecting cracks and broken contact fingers from EL images of poly-Si PV modules can be challenging and needs an experienced user. This is due to the structural nature that poly-

Si solar cells have, which obscures the cracks and broken contact fingers in the image [13].

An alternative way for modules inspection is to take I-V curve measurements of PV systems in the field to investigate the quality of PV modules [1]. In particular, measuring I-V curves of a PV module when applying shading to individual solar cells can provide valuable information about the health of solar cells [139], [172], [173]. This procedure is also a part of the IEC 61215 standards [18] in hot spot endurance testing. The subsequent section briefly discusses this technique.

2.10.4. Using I-V Curves of Partially Shaded PV Modules for Defect Detection

When shading a solar cell in a PV module equipped with bypass diodes, the characteristics of the shaded solar cell govern region 1 (see Figure 2.14 (a)) of the I-V curve measured at the module's terminals as shown by [1], [139], [174]. Hence, health state of individual cells can be conveniently obtained. This feature was used for detection of hot spots of individual cells in PV modules in [11], [175]. The detection is based on the fact that the worst cell in a module is dictated by the steepest I-V curve (with higher slope) in region 1 [139] as witnessed by Figure 2.20. This is mainly due to a reduced shunt resistance of this cell [172].

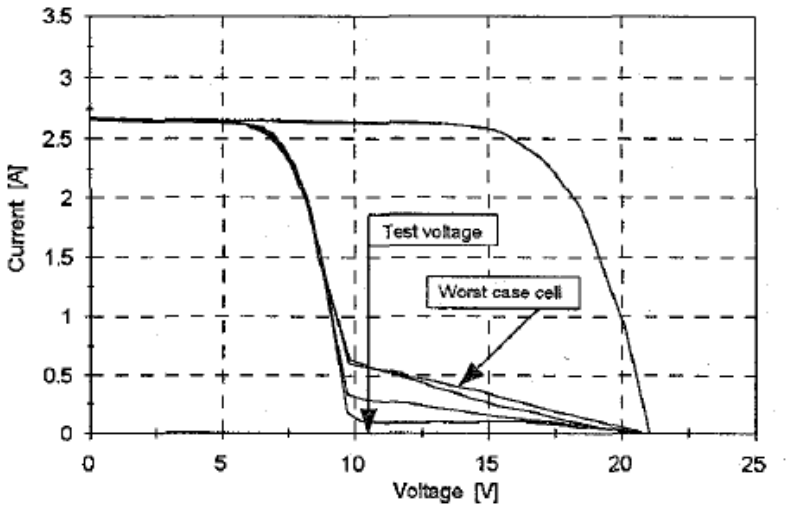

Figure 2.20. Hot spots detection from I-V curves of a PV module when shading some solar cells individually [139]. (The indicated test voltage point in the figure is used for detecting the highest current at this point, which belongs to the worst cell [139]).

In addition to utilising individual cell shading for hot spot detection, some researchers used this feature to extract some parameters of individual solar cells. These parameters are important for assessing the health state of solar cells [172], [173], [176]. Kim *et al.* [173] proposed a technique to determine the series resistance of solar cells encapsulated in PV modules by individually applying partial shading to them. They used specific points in region 1 to calculate it, thereby allowing cells with low series resistance to be identified. A similar approach was introduced by Alessandro *et al.* [172], but for determining the shunt resistance of individual cells in PV modules' strings. Another similar work was published in [176], in which the authors extracted the short circuit current and shunt resistance of individual encapsulated solar cells. The results in [176] indicated that stressed solar cells because of artificial aging tests were identified by their low shunt resistance.

However, for detection of broken cell contact fingers, only a few publications used measurements of PV modules' parameters [177], [178] and I-V curves [179], but without shading of individual cells. Wang *et al.* [177] proposed an online fault diagnostic device that is capable of detecting cracks in PV modules. The device was programmed to estimate the dynamic parameters of the module while it is in operation. The drift in parameters, namely the capacitance and series resistance, from their initial values was then monitored to detect the cracks. The system was successfully tested to detect cracks of two a-Si modules. However, this system requires a powerful computing in addition to complicated circuitry. Moreover, the system components are powered by the module itself, causing a loss in the produced power. Similarly, Al-Soeidat *et al.* [178] proposed to use the dynamic parameters, represented in the cell capacitance, as an indicator for a PV module's cracking. Yet, individual cells that suffer from cracks or broken contact fingers cannot be identified within the module.

More recently, Ma *et al.* [179] proposed a technique for fault diagnosis of PV modules including cracks that breaks the contact fingers. The technique is based on analysis of region 1 MPP knee (see Figure 2.14 (a)) of I-V curves under mismatch conditions caused by broken contact fingers. Nevertheless, individual solar cells that have broken contact fingers cannot be identified. In addition, only severe cracks can be detected, which are the ones that make the module's I-V curve to exhibit a step under no shading condition. Moreover, if other more serious faults exist in the same cell-string that contains the

cracks, such as partial shading or hot spots, cracks cannot be detected because the shape of the step on the I-V curve will be governed by the most serious fault as shown in [179]. Those issues may be alleviated if partial shading of individual cells within the module is used for the detection.

Generally speaking, using the interesting feature of shading individual cells in PV modules for detection of broken contact fingers has not been hitherto investigated. This topic will be explored in Chapter 6 of this thesis.

2.11. Summary

This chapter has presented a background and a literature survey about different aspects of solar cells and PV modules. A comprehensive literature survey revealed that despite the fast-growing developments and innovations in this field, there are still topics that need further research and investigations. Based on the previously published works discussed in this chapter, the directions of the research carried-out within the scope of this project and presented in this thesis were identified.

After presenting a general background about PV history, solar cells operation, types, characteristics and modelling, this chapter firstly focused on solar cells equivalent circuit parameters extraction in Section 2.8. It has been shown that the iterative, iterative-numerical and evolutionary computing parameters extraction methods are accurate, but they suffer from convergence issues, high computational cost and complexity. By contrast, the analytical methods offer very simple calculations, but associated with a lower accuracy. Thus, it is highly demanded to have a technique that is simple and accurate at the same time for obtaining the parameters of illuminated solar cells' I-V characteristics. This research problem will be picked-up in Chapter 4 of this thesis, in which the accuracy of a simple analytical technique will be improved. This will be accomplished by optimising the selection of points on the I-V curve used to calculate the slopes at I_{sc} and V_{oc}.

A literature survey was also carried-out about modelling of solar cells and modules under partial shading in Section 2.9. In PV models that start from the cell level, it has been found that most of the published models do not take into account the variations of single cell parameters with shading. In addition, to the best of the author's knowledge, there is no publication that compares possible improvements in model accuracy gained by

considering the variation of each parameter in turn with shading. Thus, it is not clear which parameter variation with shading would improve modelling accuracy. This might be attributed to the lack of a comprehensive experimental study that investigates the variations in solar cells' parameters with shading. Moreover, it can be deduced from the literature survey that accurate modelling of the reverse bias characteristics of PV modules needs the inclusion of the avalanche breakdown term, which adds more complexity and increases the number of unknown parameters. Further, it has been found that although partial shading and irradiance reduction over the whole cell area have been previously treated identically in terms of their influence on solar cells parameters, there is no experimental evidence for this fact.

These issues will be investigated in Chapter 5 by providing a systematic experimental study of partial shading phenomenon and its modelling. Starting from investigating the change of each parameter of a single cell with shading, modelling accuracy of PV modules will be adequately optimised by considering each parameter variation in turn in the model. Thereby allowing to investigate which parameter variation would enhance modelling accuracy of PV modules and thus hindering the need for the avalanche breakdown term. In addition, partial shading and irradiance reduction will also be experimentally compared in terms of their influences on solar cells' parameters and output characteristics.

In another context, a literature survey in Section 2.10 about broken contact fingers of solar cells revealed that they are difficult to prevent and hence it is important to detect them during different stages of the PV module's lifetime. However, except the EL imaging, most of the available techniques are based on either complex or non-reliable imaging systems. Further, even though shading of individual cells in PV modules was successfully used by different researchers to detect hot spots and calculate series and shunt resistances, it has not previously investigated for the detection of broken contact fingers. This will be explored in Chapter 6 by investigating the behaviour of PV modules when partially shading individual cells that have broken contact fingers.

Chapter 3: Experimental Methods

3.1. Introduction

Characterisation of PV devices in this research requires a controlled environment in terms of irradiance and temperature. This chapter presents all equipment preparations, calibrations and test arrangements performed within the scope of this research. The solar simulator testing procedure is demonstrated in terms of spectral match, spatial non-uniformity and temporal stability in order to ensure that it meets the standards. Then, the solar cell samples preparations and contacts soldering are described alongside building the cells' test rig. After that, PV module samples preparations and soldering are presented.

Subsequently, temperature control and I-V curve tracing procedures are explained followed by constructing the complete experimental set-up and evaluating its repeatability error analysis. Shading object fabrication by 3D printing is then illustrated followed by thermal and EL imaging systems set-ups.

3.2. Solar Simulator Tests

The solar simulator system used in this research had been previously constructed at the Solar and Environmental Research Laboratory, Cardiff University. The simulator shown in Figures 3.1 (a) to (e) consists of a light source housed inside a walk-in environmental chamber from Thermotron [180] model WP-563-THCM1-5-5-AC. The 6000 W ARRISUN 60 light source form ARRI [181] is fixed using aluminium rails at the top of the chamber facing downward without its protective glass and equipped with a separate filter as depicted in Figures 3.1 (b) and (c). The chamber has a shutter that was equipped with a remotely operated 12 V DC linear actuator to block the light if needed as Figure 3.1 (b) shows.

The light source is fitted with a Philips medium source rare-earth hot-restrike lamp model MSR 6000 HR UNP [182] that has a power rating of 6000 W and lifetime to 50% failure of 300 hours. The light source is controlled by an electronic ballast model 6000 EB from ARRI [183] shown in Figure 3.1 (d). The electronic ballast is used to switch the light ON and OFF in addition to adjusting the light intensity using a dedicated knob. The

environmental chamber is fitted with a height-adjustable test table with a horizontal plane surface that is used for placing the samples under the light source as witnessed by Figure 3.1 (e). The centre point of the test table was approximately aligned with that of the light source. In addition, the test table is not perfectly rectangular as it has curved edges. However, a rectangular test area of 160 cm x 100 cm was taken from the table in order to allow for dividing it into equal squares for the spatial non-uniformity test that will be discussed in detail in Section 3.2.2.

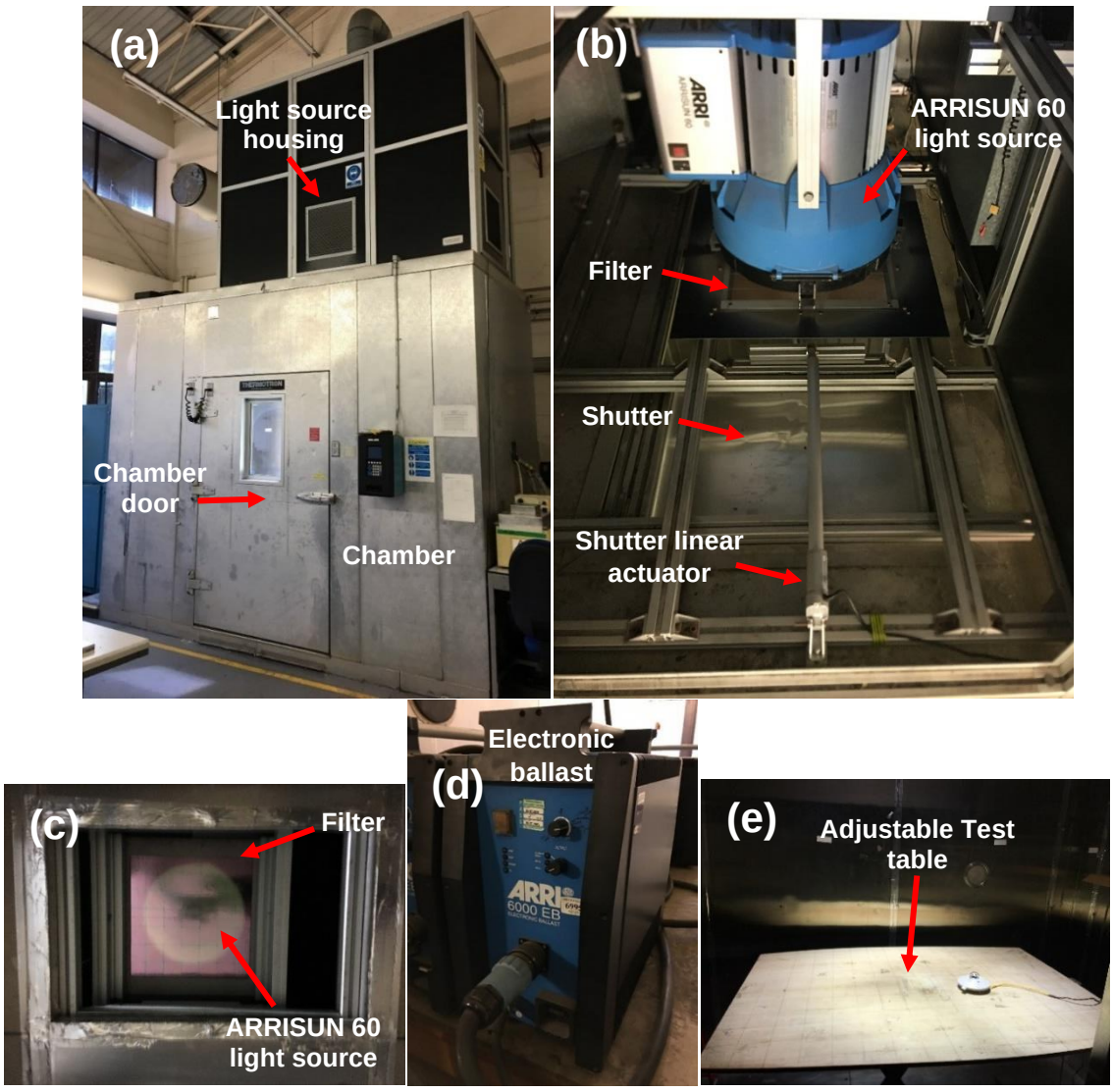

Figure 3.1. The solar simulator system: (a) environmental chamber from outside, (b) ARRISUN 60 light source fitted at the top of the chamber, (c) ARRISUN 60 light source viewed from inside the chamber, (d) electronic Ballast and (e) adjustable test table.

When using solar simulators for PV devices testing, they need to meet the E927-10 standards issued by the American Society for Testing and Materials (ASTM) [184]. According to these standards, a solar simulator that is used for testing PV devices could

be of either Class A, B or C in each one of the performance measures, which are spectral match, spatial non-uniformity and temporal instability, as shown by Table 3.1. These qualification tests were performed on the solar simulator used in this study in a collaborative[1] work with a fellow PhD student, Mr. Ali Bahr.

Table 3.1. Classification of large area solar simulators according to their performance. (Adapted from E927-10 standards [184]).

Performance measure	Solar simulator class		
	A	B	C
Spectral match	0.75 to 1.25	0.6 to 1.4	0.4 to 2
Spatial non-uniformity (%)	3	5	10
Temporal instability (%)	2	5	10

3.2.1. Spectral Match

The spectrum of ARRISUN 60 light source was measured and compared with the Sun spectrum and with E927-10 standards limits in order to define its class in terms of spectral match. Figures 3.2 and 3.3 respectively illustrate the schematic diagram of the spectrum measurement set-up and its photograph. The spectrometer used in this work is from StellarNet [185] and it consists of two devices that measure the electromagnetic spectrum instantly covering a wavelength range of about 200 to 1700 nm. The Blue-Wave spectrometer is used for measuring the UV and visible light spectrum within the range of 200 to 1100 nm. Whereas the Dward-Star spectrometer covers a range of 900 to 1700 nm.

[1] The measurement raw data of spectrum, large area non-uniformity and temporal instability, presented respectively in Sections 3.2.1, 3.2.2.1 and 3.2.3, were obtained in a collaborative work with a fellow PhD student colleague, Mr. Ali Bahr. Although only the original raw data of those tests were obtained in the collaborative work and shared with the fellow colleague, all calculations, data analysis, presentations, figures' production, explanations, and interpretations of the results in those sections of this thesis were carried-out solely by the author.

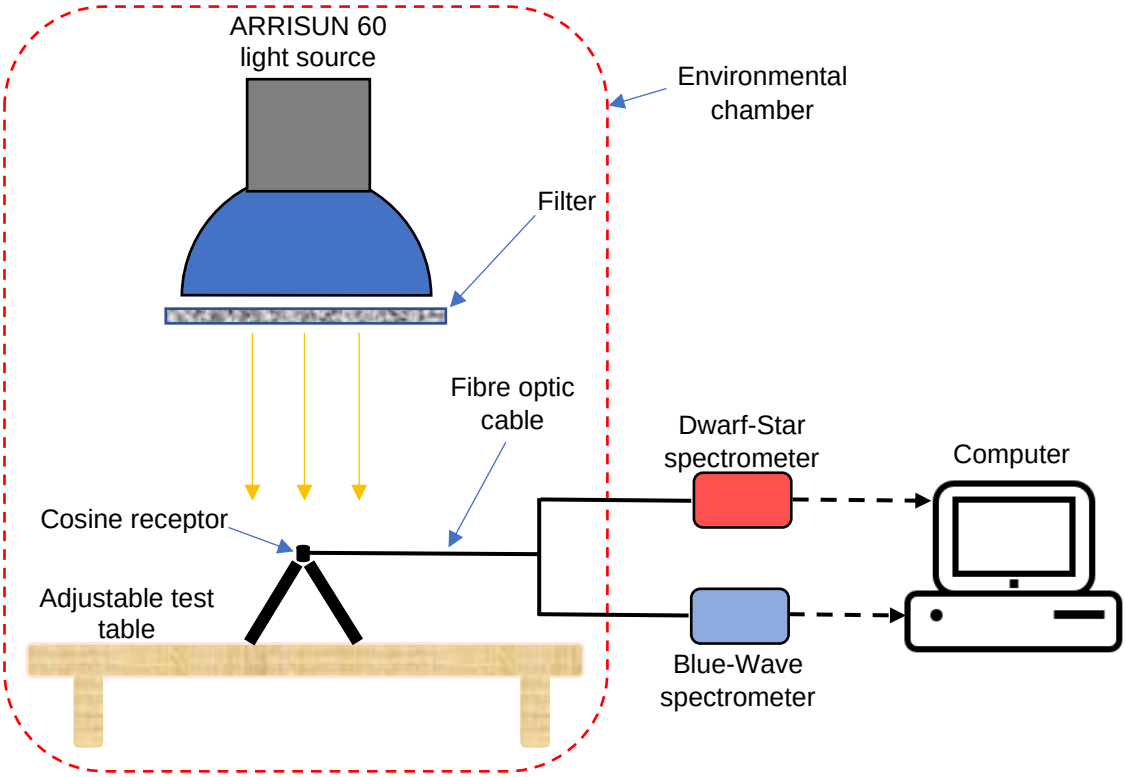

Figure 3.2. Schematic diagram of light source spectral measurement.

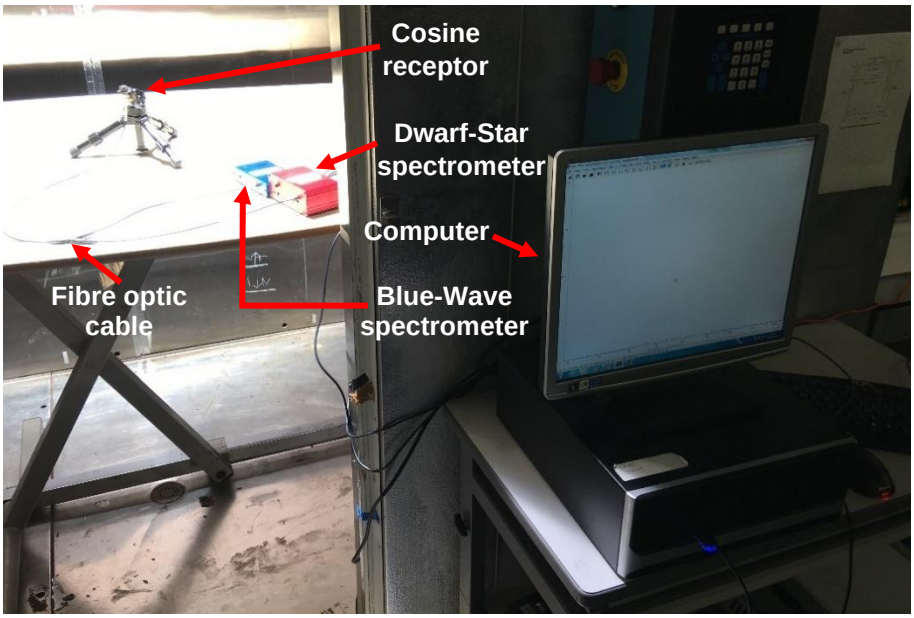

Figure 3.3. Set-up for light source spectral measurement.

Both devices were attached to a cosine receptor via a fibre optic cable. The cosine receptor was placed under the simulator at the centre of the test table and both devices were interfaced with a computer using an appropriate software as depicted in Figures 3.2 and 3.3. The spectrum of the ARRISUN 60 light source was measured using the mentioned

set-up at a range of 194 to 1749.5 nm. Yet, according to E927-10 standards, only 400 to 1100 nm range is used for spectral match measurements of solar simulators and hence this range was utilised in this work. The procedure of calculating the spectral match of the light source was implemented following illustrations given in the E927-10 standards.

First, the normalised spectral irradiance of the ARRISUN 60 light source was obtained for each wavelength interval shown in the first column of Table 3.2. This was obtained by summing up the spectral irradiance for each interval at a resolution of 1 nm and normalise it by the total irradiance of all intervals (400 to 1100 nm). The percentage of the ARRISUN 60 spectral irradiance of each interval normalised by the total irradiance is presented in the first sub-column of the second column in Table 3.2. Second, the ideal spectral match requirement according to E927-10 standards for each wavelength interval is listed in the second sub-column of the second column in Table 3.2. Third, upper and lower limits of Classes A and B were obtained by multiplying the ideal spectral match (second sub-column of the second column in Table 3.2) by the upper and lower limit values of each class shown in Table 3.1. The resulted upper and lower limits of classes A and B are listed in the third and fourth columns in Table 3.2, respectively. Figure 3.4 presents the spectral match response of the ARRISUN 60 light source compared with the ideal match requirement and with upper and lower limits of Classes A and B for each wavelength interval. The results revealed that ARRISUN 60 slightly exceeds the limits of Class A in the intervals 400 to 500 nm and 700 to 800 nm, but still within the limits of Class B. Therefore, the light source was defined as Class B in terms of its spectral match.

Table 3.2. Spectral match response, which is the total irradiance for each wavelength interval normalised by the total irradiance of all intervals, of ARRISUN-60 light source compared with the ideal match requirements and Classes A & B limits according to E927-10 standards [184].

Wavelength interval (nm)	Irradiance normalised by total irradiance (%)		Spectral match of Class A (E927-10 standards) (%)		Spectral match of Class B (E927-10 standards) (%)	
	ARRISUN 60	E927-10 standards ideal match requirements	Upper limit	Lower limit	Upper limit	Lower limit
400-500	24.4	18.4	23.00	13.80	25.76	11.04
500-600	21.3	19.9	24.88	14.93	27.86	11.94
600-700	17.3	18.4	23.00	13.80	25.76	11.04
700-800	10.6	14.9	18.63	11.18	20.86	8.94
800-900	11.7	12.5	15.63	9.38	17.5	7.5
900-1100	14.7	15.9	19.88	11.93	22.26	9.54

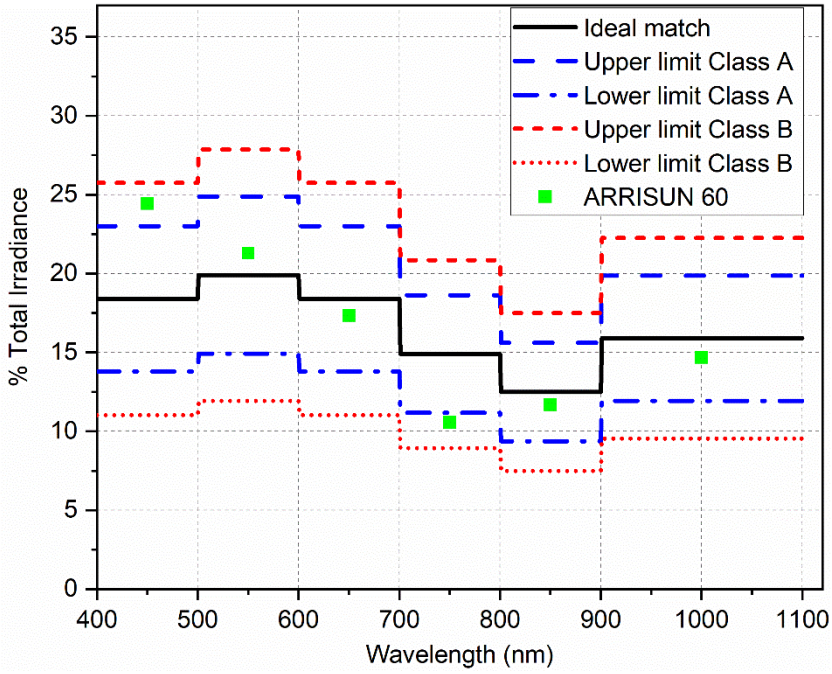

Figure 3.4. Spectral match response of ARRISUN-60 light source compared with the ideal match requirements and limits of Classes A & B according to E927-10 standards [184].

In order to perform further analysis, the deviation of the ARRISUN 60 total spectral irradiance (at a resolution of 1 nm) from the Sun AM 1.5 global (AM 1.5G) spectrum in each wavelength interval was calculated [1] and presented in Table 3.3. The data of the Sun AM 1.5 spectrum was obtained from the G-173-03 table developed by ASTM and available from the NREL website [186]. The most significant deviation of 44.7% was recorded between 400 and 500 nm. On the other hand, other intervals showed much smaller deviations ranging from 1.5 to 22.1%. Moreover, the deviation of the total spectral irradiance from 400 to 1100 nm of the light source from that of the Sun AM 1.5G is 9.9% indicating that the light source simulates sun light quite decently.

Another proof of the well simulation of Sun light is shown by the comparison between the ARRISUN 60 spectrum, measured at a range of 194 to 1749.5 nm, and the Sun AM 1.5G spectrum plotted in Figure 3.5. The results indicate a good agreement as both plots have similar trends.

Table 3.3. Total irradiance for each wavelength interval of ARRISUN-60 light source compared with the Sun AM 1.5G spectrum data of ASTM [186].

Wavelength Interval (nm)	Irradiance (W/m²)		Absolute Percentage Error (%)
	ARRISUN 60	Sun Spectrum AM 1.5G	
400-500	203.92	140.91	44.7
500-600	177.68	150.98	17.7
600-700	144.65	139.14	4.0
700-800	88.14	113.08	22.1
800-900	97.45	94.37	3.3
900-1100	122.53	120.78	1.5
Total Irradiance	834.37	759.26	9.9

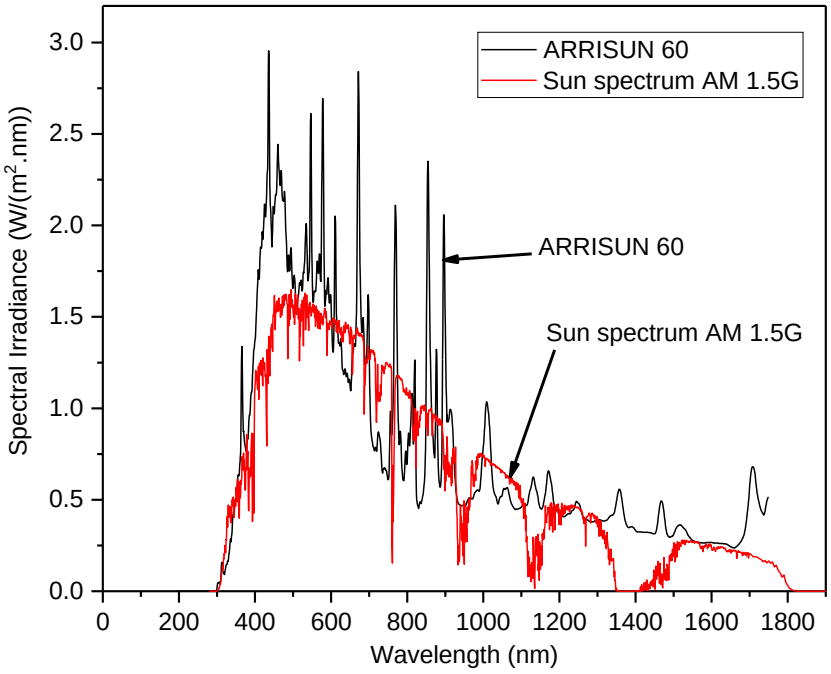

Figure 3.5. Spectrum of ARRISUN 60 light source compared with the Sun AM 1.5G spectrum data of ASTM [186].

3.2.2. Irradiance Spatial Non-uniformity

The spatial non-uniformity is the second qualification test of the E927-10 standards and it provides a measure of how uniform the light is over the test area. Since the PV devices used in this research have different sizes as will be explained later, this test was divided into two parts: large and small area non-uniformity tests.

3.2.2.1. Large Area Non-uniformity Test

This test was performed on the complete test area of 160 cm x 100 cm. First, the test area was divided into 10 cm x 10 cm squares. Subsequently, the light source irradiance was adjusted to 1000 W/m² at the centre and then it was measured in each square using a pyranometer. The pyranometer is a very accurate device used to measure the global irradiance with a spectrum of 300 to 2800 nm and it provides a voltage output signal [1]. The used pyranometer in this work was the CM 21 model from Kipp & Zonen [187], which has a sensitivity of 12.32 μV/W.m^{-2} and a resolution of ±0.5 W/m². In addition, it can measure an irradiance within the range of 0 to 4000 W/m² with a maximum error of 2% for total hourly and daily irradiances. When performing irradiance measurements in this work, the output voltage of the pyranometer was measured by a multimeter. The irradiance was then simply calculated through dividing the output voltage by the sensitivity.

A photograph of the large area non-uniformity test experimental set-up is given in Figure 3.6 and the irradiance spatial distribution is given as a heat-map plot in Figure 3.7. As shown, the light is significantly non-uniform with the highest intensities located at the centre. Hence, the largest PV device used in this research was selected to be a 10 W PV module with dimensions of 34 cm x 24 cm. The test area of interest from the total test area was thus selected to be 40 cm x 40 cm for this PV module's testing as indicated by the black box in Figures 3.6 and 3.7.

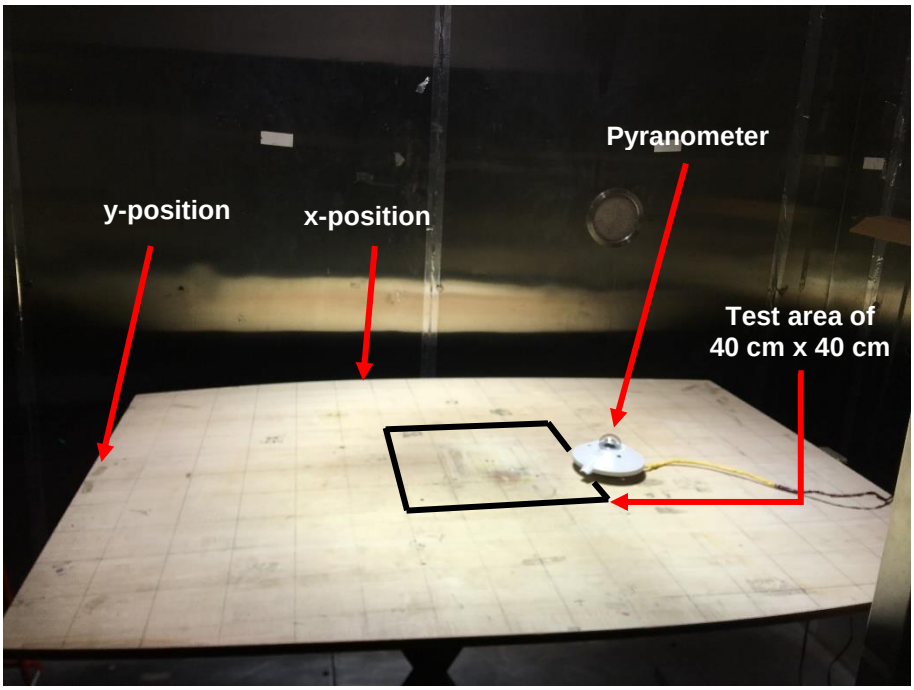

Figure 3.6. Spatial non-uniformity test using a pyranometer for a test area of 160 cm x 100 cm (total test area) divided into 10 cm x 10 cm squares. The area inside the black box is 40 cm x 40 cm and was used for characterisation of a 10 W PV module.

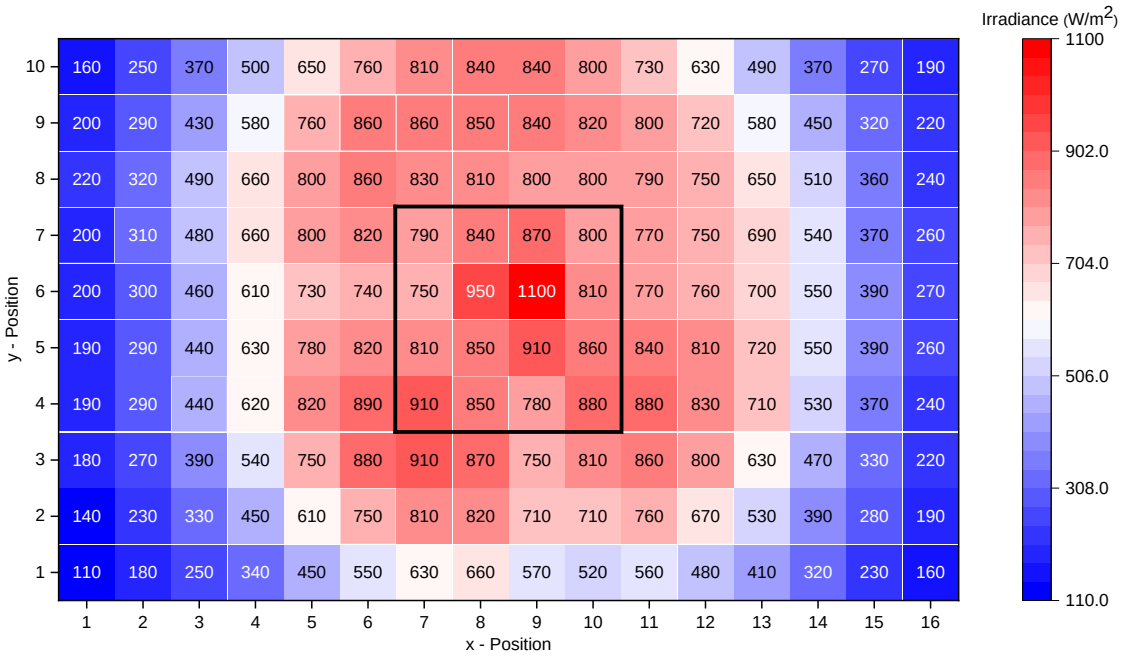

Figure 3.7. Irradiance spatial distribution over a test area of 160 cm x 100 cm (total test area) divided into 10 cm x 10 cm squares. The area inside the black box is 40 cm x 40 cm and was used for characterisation of a 10 W PV module.

The spatial non-uniformity was calculated according to E927-10 standards for both test areas, which are the total area of 160 cm x 100 cm and the selected smaller area for the PV module's characterisation of 40 cm x 40 cm. Given the maximum irradiance (G_{max})

and the minimum irradiance (G_{min}) within a test area, the spatial non-uniformity (S_N) can be calculated from [184]:

$$S_N = 100\% * \left(\frac{G_{max}-G_{min}}{G_{max}+G_{min}}\right) \quad (3.1)$$

From Figure 3.7, using the maximum and minimum irradiances of the 160 cm x 100 cm area and solving Equation (3.1) yield a spatial non-uniformity of about 82%. This shows that the light is significantly non-uniform with this large test area and hence the light source does not meet the E927-10 standards of spatial non-uniformity in Table 3.1. Hence, this area was not used in this research.

Using the maximum and minimum irradiances of the 40 cm x 40 cm area shown in Figure 3.7 by the black box provide a spatial non-uniformity of about 19% from Equation (3.1). It is apparent from those results that the light source also failed to meet the E927-10 standards of spatial non-uniformity in Table 3.1 when using this area of the test table. Hence, the largest PV module size characterised in this research was selected to be 34 cm x 24 cm (including frame as will be explained in Section 3.4). However, when different cells are partially shaded within this PV module, the I-V curve exhibits a shift along the vertical axis due to the non-uniformity. The shape of the I-V curve (slope of the reverse bias region) did not significantly change (see Figure 6.2). Hence, this non-uniformity has no significant effect on the reliability of the results in this research as the main focus when using this module is on the reverse bias region (Section 5.5.2). The other PV devices used in this research have smaller sizes than this module and thus a small area non-uniformity test was needed.

3.2.2.2. Small Area Non-uniformity Test

The small area test was performed in order identify the simulator's class in terms of spatial non-uniformity when using it for characterising small PV devices. A reference cell from SEAWARD (solar survey 200R) [188] was used in this test because it is much smaller in size that the pyranometer and can perform measurements in small areas. The solar survey 200R, shown in Figure 3.8, is a battery powered handheld device that provides quick irradiance measurements. Furthermore, it has a resolution of 1 W/m² and capable of measuring an irradiance range of 100 to 1250 W/m². It can also measure the temperature and inclination in addition to the built-in compass function. However, it was utilised only for irradiance measurements in this work. The main advantage of reference cells is the

fact that they usually use a crystalline-Si solar cell to measure the irradiance, which behaves as the crystalline-Si PV devices under test [1]. It is to be noted that when using the solar survey 200R with the light source used in this work, the measurement was not stable and it fluctuated between two readings. Hence, the average value of the two readings was taken for each measurement.

A test area of 14 cm x 14 cm was selected at the centre of the test table as indicated by the yellow dashed line box in Figure 3.8 in order to characterise one small in-house assembled PV module that has dimensions of approximately 9 cm x 12.5 cm (area covering the solar cells only as will be explained in Section 3.4.2). The test area of 14 cm x 14 cm was divided into 2 cm x 0.7 cm rectangles, which are approximately the dimensions of the used reference cell. Subsequently, the irradiance was measured in each rectangle by attaching a foam adhesive tape, that has the same size of the reference cell, to the back of the 200R. The 200R was then carefully placed so that the tape covers the desired rectangle. Irradiance measurements were finally taken at each rectangle and the values were recorded while it was measured as 1000 W/m² at the centre. The experimental set-up of the small area non-uniformity test and the irradiance spatial distribution are depicted in Figures 3.8 and 3.9, respectively. Figure 3.9 shows that the light has much more better uniformity than that of the large area non-uniformity test shown previously in Figure 3.7. The black boxes in Figures 3.8 and 3.9 indicate a smaller test area of 6 cm x 5.6 cm selected to be used for characterising all solar cells in this research.

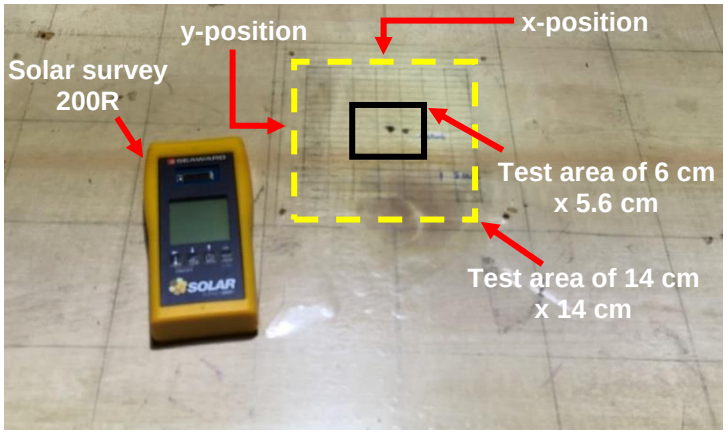

Figure 3.8. Spatial non-uniformity test using solar survey 200R reference cell for a test area of 14 cm x 14 cm divided into 2 cm x 0.7 cm rectangles (reference cell area). (This 14 cm x 14 cm area was used for characterisation of a small in-house assembled PV module. The area inside the black box is 6 cm x 5.6 cm and was used for characterisation of all single solar cells).

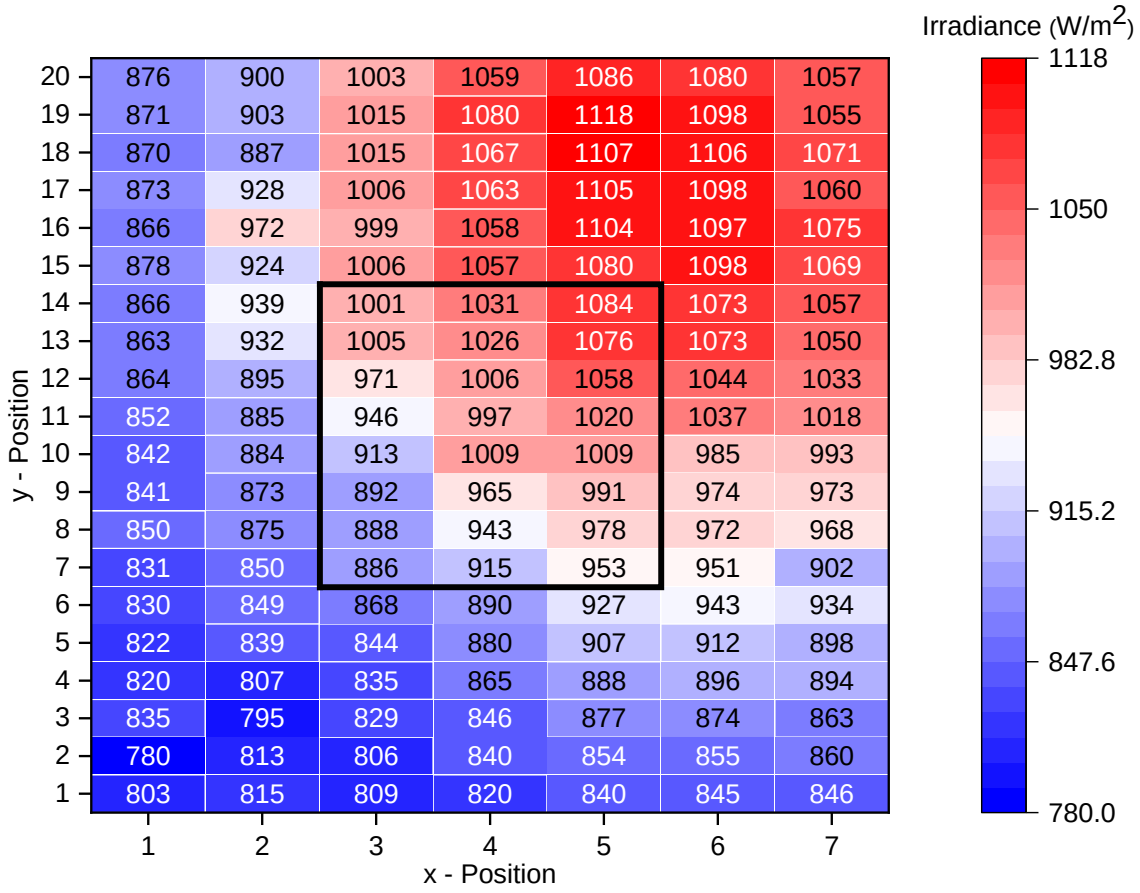

Figure 3.9. Irradiance spatial distribution over a test area of 14 cm x 14 cm divided into 2 cm x 0.7 cm rectangles (reference cell area). (This 14 cm x 14 cm area was used for characterisation of a small in-house assembled PV module. The area inside the black box is 6 cm x 5.6 cm and was used for characterisation of all single solar cells).

The 14 cm x 14 cm test area has a spatial non-uniformity of about 18% from Equation (3.1). This indicates that the light source does not meet the E927-10 spatial non-uniformity standards of Table 3.1 when used with the 14 cm x 14 cm area. However, this area was used only for characterising the 9 cm x 12.5 cm in-house assembled PV module under individual cell shading for investigating the influence of broken contact fingers. The area of interest in this investigation is the shape of region 1 MPP (see Figure 2.14 (a)), which is not affected by the non-uniformity as will be discussed in Section 6.4.4.

The smaller test area of 6 cm x 5.6 cm has a spatial non-uniformity of about 10%, which matches the 10% limit of Class C according to Table 3.1. Hence, the light source was classified as Class C when used with this area. Therefore, for all single solar cells' characterisation in this research, the light source was considered of Class C in terms of its spatial non-uniformity.

3.2.3. Irradiance Temporal Instability

The third and last qualification test of the light source is the temporal instability, which evaluates its performance in terms of the light stability over a period of time. The E927-10 standards recommended carrying-out temporal instability tests for steady state simulators by taking at least 20 irradiance measurements over a period of 1 second. However, due to the lack of a data acquisition system that is capable of recording measurements at this frequency, the irradiance was measured in this work manually once every 5 minutes over a period of 4 hours (240 minutes). The pyranometer was used for this purpose and it was placed at the centre of the test table with the light source irradiance adjusted to 1000 W/m². In Figure 3.10, the change of irradiance over the 4 hours period is reported. The plot in Figure 3.10 indicates that the light source has a reasonably good stability.

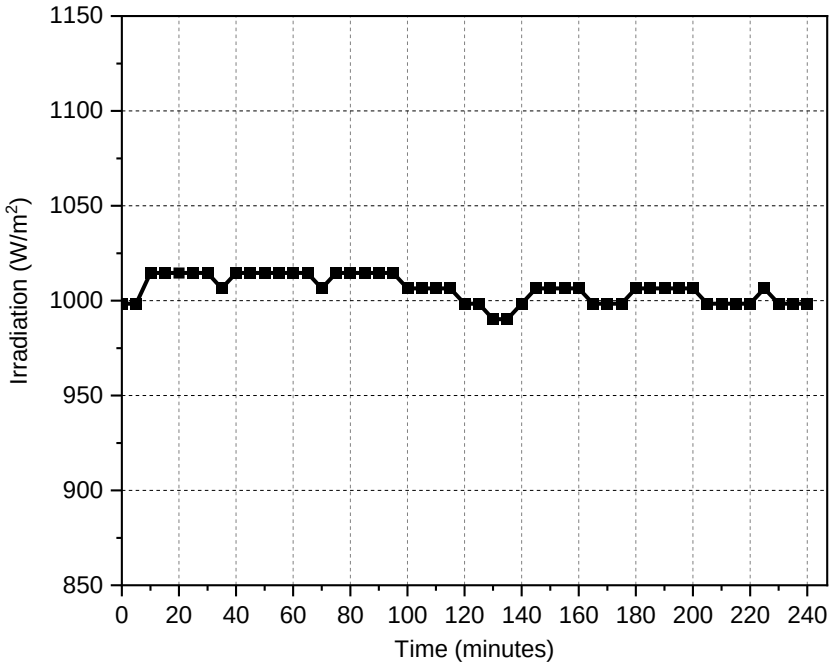

Figure 3.10. Irradiance temporal instability of the light source over a period of 4 hours.

According to E927-10 standards, the temporal instability can be calculated using Equation (3.1) of the spatial non-uniformity considering the maximum and minimum irradiances measured, which are respectively 1014.6 and 990.3 W/m² in this case. The results yielded a temporal instability of 1.2% revealing that the light source is of Class A in terms of its temporal instability according to Table 3.1.

3.2.4. Overall Performance Classification of the Solar Simulator

The previous three Sections 3.2.1, 3.2.2 and 3.2.3 presented the experimental evaluation of the light source class according to E927-10 standards in terms of spectral match, spatial non-uniformity and temporal instability, respectively. Only spatial non-uniformity test showed that the light source does not meet the standards when used with large test areas, which are only required for characterising two PV modules in this research. However, it does meet the standards of Class C when applied to a small area of 6 cm x 5.6 cm. Thus, all single solar cells used in this research were selected to be much smaller than 6 cm x 5.6 cm. Further, the PV modules used were selected with small sizes to minimise the impact of non-uniformity. Despite this non-uniformity, the light source was successfully used to characterise those PV modules for the purpose of this research as previously discussed in Sections 3.2.2.1 and 3.2.2.2.

The overall performance classification of the solar simulator was therefore established for testing single solar cells in this research and it is given in Table 3.4 indicating that the simulator is of Class BCA.

Table 3.4. Performance classification of the ARRISUN 60 light source for single solar cell testing.

Performance measure	Class
Spectral match	B
Irradiance spatial non-uniformity	C
Irradiance temporal instability	A

3.3. Solar Cells and Testing Rig Preparations

This section presents various stages of solar cells' samples preparations. The printed circuit board (PCB) design and fabrication is first explained followed by the cell contacts soldering process and finally the test rig arrangements. Three different mono-Si solar cell sizes were used in different experimental studies in this research with active areas (excluding soldered busbar ribbon wire) of 0.78 cm² (1 cm x 0.78 cm), 0.8 cm² (1 cm x 0.8 cm) and 6.25 cm² (2.5 cm x 2.5 cm). The total areas of these three sizes (including busbar) are respectively 1 cm² (1 cm x 1 cm), 1 cm² (1 cm x 1 cm) and 6.7 cm² (2.5 cm x 2.68 cm). In the remainder of this thesis, only the active area of single solar cells will be recalled unless otherwise stated.

All solar cells were supplied by Solar Capture Technologies [189] as a cut wafer without soldered contacts and have a single busbar. Apart from the 0.78 cm² cell, all other cells were supplied from the same batch. All cells do not have a specific data sheet as they were custom-made by Solar Capture Technologies. In this section, the process of solar cell sample preparation is explained for the 0.78 cm² cell. All other cells and their test rig were prepared in the same manner. The photograph of each used solar cell will be shown in the respective section of this thesis.

3.3.1. Solar Cells PCB Design and Fabrication

As mono-Si solar cells are very fragile, it is imperative to provide a mechanical support for the solar cell to protect it from breakage during handling for experimental studies. The idea of using a supporting board for solar cells was taken from Al-Shidhani *et al.* [190], who used a direct copper bonded (DCB) board. However, in this work, the PCB was selected as a supporting board due to its availability, low-cost and easy fabrication.

A computer aided design (CAD) drawing of the designed PCB for the 0.78 cm² solar cell is depicted in Figure 3.11 (a) drawn in SolidWorks software, while a photograph is given in Figure 3.11 (b). The PCB has dimensions of 6 cm x 6 cm, which are slightly larger than the small test area discussed in Section 3.2.2.2. Further, it has a small thickness of 0.5 mm in order to improve thermal conductivity for water cooling as will be explained later in Section 3.5.2. The copper part of the PCB was designed to be attached to the back of the solar cell and hence it was designed with slightly larger dimensions of 10.5 mm x 10.5 mm than the total cell dimensions (10 mm x 10 mm). The upper copper appendage shown in Figures 3.11 (a) and (b) was designed in order to attach the thermocouple for temperature measurements. Whereas the lower two copper appendages were dedicated to solder the positive and negative terminals. The positive terminal appendage was extended from the copper part, but the negative terminal one was separated by 1 mm in order to avoid short circuiting the terminals. The PCB was fabricated in the Electrical Workshop, Cardiff University using a Circuit Board Plotter Machine model ProtoMat S100 from LPKF Laser & Electronics [191].

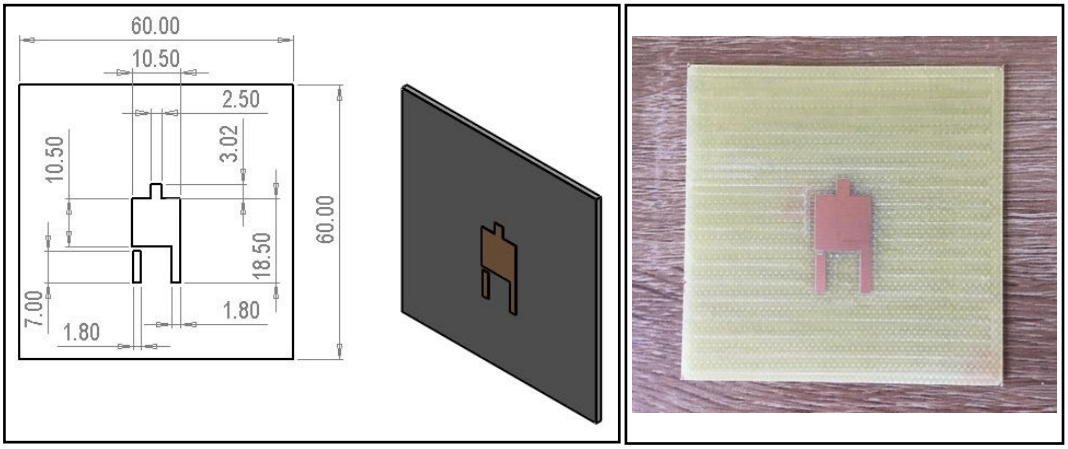

Figure 3.11. The PCB design for solar cell housing: (a) CAD drawing and (b) PCB photograph. (Dimensions in the CAD drawing are in mm).

3.3.2. Solar Cells Preparation and Soldering

A photograph of the 0.78 cm² solar cell supplied as a wafer without contacts is given in Figure 3.12 (b). The solar cell sample preparation process was divided into two stages: soldering the solar cell to the PCB and soldering the cell contacts. In the first stage, the PCB copper part was carefully cleaned using Isopropyl Alcohol. Then, a hotplate was heated to a temperature just above the melting point of the soldering wire lead, which is from 183 °C to 188 °C [192]. This was done in order to avoid high temperatures that may damage the cell or burn the PCB. The hotplate temperature was monitored using a K-type thermocouple placed inside a hole of a copper sheet as shown in Figure 3.12 (b). A thermal paste from RS components [193] that has a thermal conductivity of 2.9 W/(m.K) was used when placing the thermocouple inside the hole (this thermal paste was also used in all other experiments). Subsequently, the PCB was placed on the hotplate and a small amount of soldering wire lead was added to its copper part. Once the wire lead was melted, the solar cell was carefully placed on the copper part of the PCB and then removed quickly and left to cool down. This process provided a good bond between the PCB and the solar cell.

The second stage in solar cell preparation involved soldering the contacts. As the positive contact was already created by soldering the back sheet of the solar cell to the PCB, the positive terminal was realised by soldering a wire to the appendage extended from the copper part of the PCB as Figure 3.12 (c) shows. The negative terminal was established by soldering a 0.16 mm thick wire ribbon to the front busbar and then soldering it to an

external wire via the appendage that is separated from the copper part as depicted in Figure 3.12 (c). Soldering flux was applied using a flux pen to the wire ribbon before soldering in order to have a good bond with the solar cell's busbar. Note that the thermocouple attached to the PCB in Figure 3.12 (c) is for temperature measurements of the solar cell as will be explained later in Section 3.5.1.

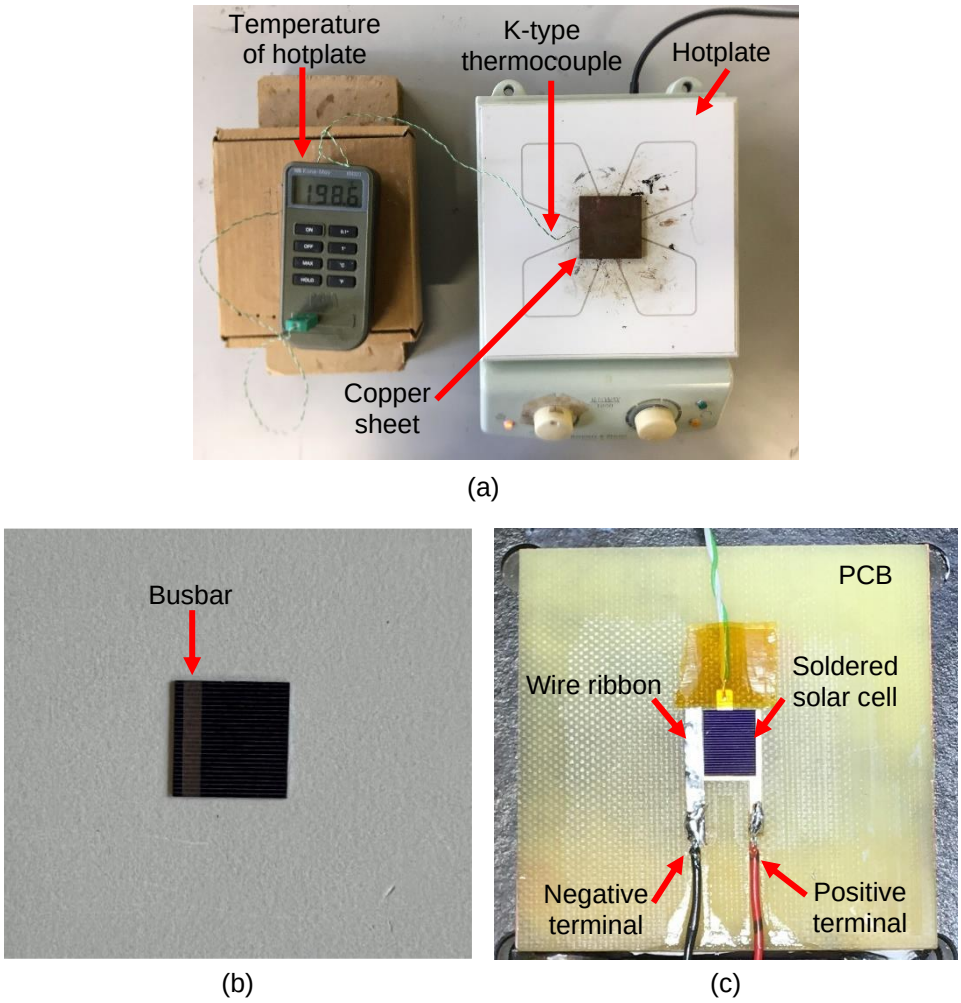

Figure 3.12. Soldering process of the solar cell: (a) the heated hotplate used for solar cell and PCB soldering and its temperature measurement using a K-type thermocouple, (b) the solar cell with a total area of 1 cm^2 (1 cm x 1 cm) without contacts and (c) the solar cell after soldering the PCB and terminals resulting in an active area of 0.78 cm^2 (1 cm x 0.78 cm).

It is worth noting that for this particular solar cell, there was a small part of the excess wafer between the busbar and the left edge as shown in Figure 3.12 (b). Hence, a wide ribbon wire with a width of 3 mm was used in order to completely cover this area and avoid penetration of light through it. The purpose of doing that was to have an active cell area in only one side of the busbar in order to conveniently perform partial shading

experiments on it. All other cells used in this research did not have this issue and hence a standard wire ribbon that has a width of 1.8 mm and a thickness of 0.16 mm was used.

3.3.3. Solar Cells Test Rig under the Simulator

Once the solar cell sample had been soldered and prepared, the test rig used to properly place the cell under the simulator was built. A black plastic plate of 20 cm x 20 cm was fabricated and grooved by the Mechanical Workshop, Cardiff University in order to hold the solar cell assembly in place. Three grooves were introduced into the plate as shown in Figure 3.13 (a). The first one was for holding the heat exchanger and the other two were for holding the insulated water tubes as Figure 3.13 (b) shows. First, the plate was connected at the middle of the test table by four screws. Second, the heat exchanger and water tubes were placed inside the grooves with the help of an adhesive tape. Third, the solar cell assembly was attached to the heat exchanger using the thermal paste. Using the heat exchanger and water tubes for cooling will be discussed in Section 3.5.2. Figure 3.13 (d) shows the complete cell assembly with its cooling system placed inside the chamber.

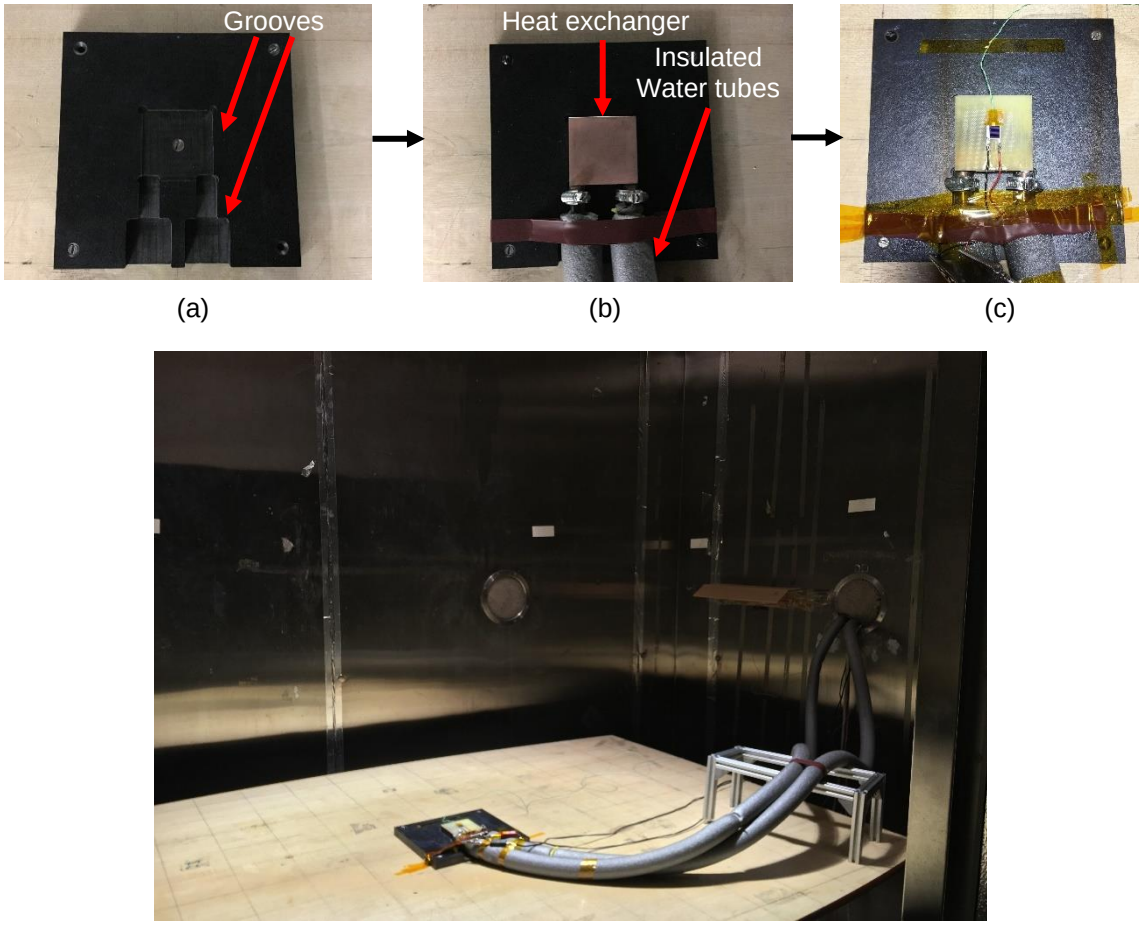

Figure 3.13. Steps of preparing the solar cells' test rig: (a) plastic supporting plate with grooves for heat exchanger and tubes, (b) heat exchanger and tubes are placed on the supporting plate, (c) the solar cell assembly is placed on the heat exchanger and (d) the complete test platform with the solar cell under the solar simulator.

3.4. PV Modules Preparations

This section presents the preparations of PV modules used in this research and their soldering work. Three PV modules were used in the experimental investigations of this research. A mono-Si 10 W PV module with total dimensions (including frame) of 34 cm x 24 cm from Betop-camp [194], an in-house assembled mono-Si PV module with total dimensions of 15 cm x 15 cm and a small SANYO a-Si PV module model AM-8701 purchased from Rs Components [195] with total dimensions of 5.51 cm x 5.77 cm. The latter did not need any soldering work and hence only the preparations of the 10 W module and the in-house assembled module will be presented.

3.4.1. Mono-Si 10 W PV Module Preparation

This mono-Si 10 W module has 36 solar cells connected in series without bypass diodes, as shown in Figure 3.14 (a). However, it was required to add two bypass diodes, one for each cell-string per 18 cells, in order to investigate partial shading. The back sheet and adhesive encapsulant were removed and one bypass diode was soldered in parallel across each cell-string. It was also required to cut part of the frame in order to easily access the locations of the soldering joints and also for cooling purpose as will be explained in Section 3.5.2. In addition, the blocking diode, which is available in the module junction box for protection against battery discharge at night, was removed because the module was characterised without a battery system in this work. Figures 3.14 (b) and (c) illustrate the back side of the PV module before and after insertion of the bypass diodes, respectively. The bypass diodes used were the 1N5819 Schottky rectifiers from STMicroelectronics [196] purchased from RS Components [197]. A schematic diagram shows the internal configuration of cells and bypass diodes of this module was previously given in Figure 2.13 to illustrate the consequents of partial shading in Section 2.9.1.

(a) (b) (c)

Figure 3.14. The mono-Si 10 W PV module and its bypass diodes soldering: (a) front of PV module, (b) back of PV module before removing frame and bypass diodes soldering and (c) back of PV module after removing frame and bypass diodes soldering.

3.4.2. In-house Made Mono-Si PV Module Preparation

An in-house made PV module consists of 12 mono-Si solar cells was prepared within the scope of this research. The solar cells were of central busbar as shown in Figure 3.15 with an active area of 6.25 cm² (2.5 cm x 2.5 cm). The module has two cell-strings, each one

has 6 cells and one anti-parallel bypass diode. The solar cells were first soldered into strings of 3 series connected cells using the 1.8 mm wide wire ribbon connecting the front busbar of each cell to the back contact of the next one. Then, the strings of 3 cells were soldered in series using a main bus wire ribbon that has a width of 5 mm and a thickness of 0.16 mm. Soldering flux was applied to all wire ribbons throughout the soldering process. Subsequently, the bypass diodes were soldered in anti-parallel across each cell-string. The positive and negative wires were then soldered. Finally, the soldered cell-strings were placed on a 1.5 mm thick self-adhesive thermal interface sheet purchased from RS components [198] with a thermal conductivity of 1.95 W/(m.K) for cooling purpose and mechanical support. The complete PV module has total dimensions of 15 cm x 15 cm (area of the thermal sheet) and it is depicted in Figure 3.15. The area including only the cell-strings is approximately 9 cm x 12.5 cm.

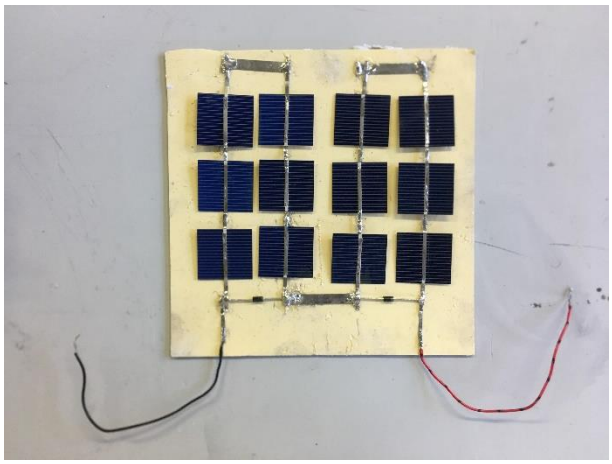

Figure 3.15. The in-house assembled PV module consists of 12 solar cells connected in series with two bypass diodes.

3.5. Temperature Control

The change in a solar cell temperature has a noticeable effect on its output characteristics as shown previously in Figures 2.8 (a) and (b). Since this work used a light source that has a lamp with a high power rating inside a closed chamber, the rise in temperature of the PV device under test is inevitable. Moreover, in order to carry-out a comparative study between different experiments, it is important that they are performed under the same temperature. Therefore, temperature measurements and cooling are required in this research and are presented in the following two sub-sections.

3.5.1. Temperature Measurements by Thermocouples

A K-type thermocouple from RS Components [199] that has a length of 5 m and capable of measuring a temperature range of -75 to 260 °C was used in this work for measuring the solar cells and modules temperatures. The accuracy depends on the temperature range as per the Thermocouple Selection Guide from RS Components. For a range of -40 to 1000 °C, which covers all temperatures used in this work (20 to 50 °C), the accuracy is ±0.004 multiplied by the actual temperature or ±1.5 °C, whichever is greater. However, for the range used in this work, ±1.5 °C is always greater.

The thermocouple was attached to a data logger model TC-08 from Pico Technology [200] purchased from RS Components [201] as shown in Figure 3.16 (a). The TC-08 data logger can be interfaced with a computer using the USB port via a dedicated software for temperature monitoring and recording. In addition, it can be connected to a maximum of eight thermocouples and can take up to 10 measurements per second. Further, it supports a measurement range of -250 to +1370 °C at a resolution of 0.025 °C when using K-type thermocouples. The accuracy is the summation of ±0.5 °C and ±0.2% of measurement. For the lower and upper limits of the temperature range used in this work (20 and 50 °C), this yields an accuracy of ±0.54 °C and ±0.6 °C, respectively. Adding these values to the accuracy of the thermocouple provides an uncertainty of ±2.04 °C and ±2.1 °C in the lower and upper temperature range limits, respectively. Therefore, the uncertainty in all temperatures measured in this work is between those two values. However, in Section 3.7, the repeatability error of measuring several I-V curves at a fixed temperature will be assessed and the error in temperature measurements accuracy will be accounted for.

The solar cell temperature was measured by attaching the thermocouple to the copper appendage using an adhesive tape that has a high temperature resistance manufactured by Tesa [202] and supplied by RS Components [203] as Figure 3.16 (b) shows. The purpose of using a high temperature resistive tape was to protect the thermocouple from being affected by the environment temperature, thereby measuring only the temperature of the copper appendage. Since the solar cell is soldered to the copper part of the PCB and copper is known to have a high thermal conductivity, it is expected that the difference

between the solar cell back contact temperature and the copper appendage temperature is negligible.

The PV modules' temperature, on the other hand, was measured by attaching the thermocouple to the back sheet using the adhesive tape. Figure 3.16 (c) for instance shows the thermocouple attached to the back sheet of the 10 W PV module. The same technique was also used with other PV modules used in this research.

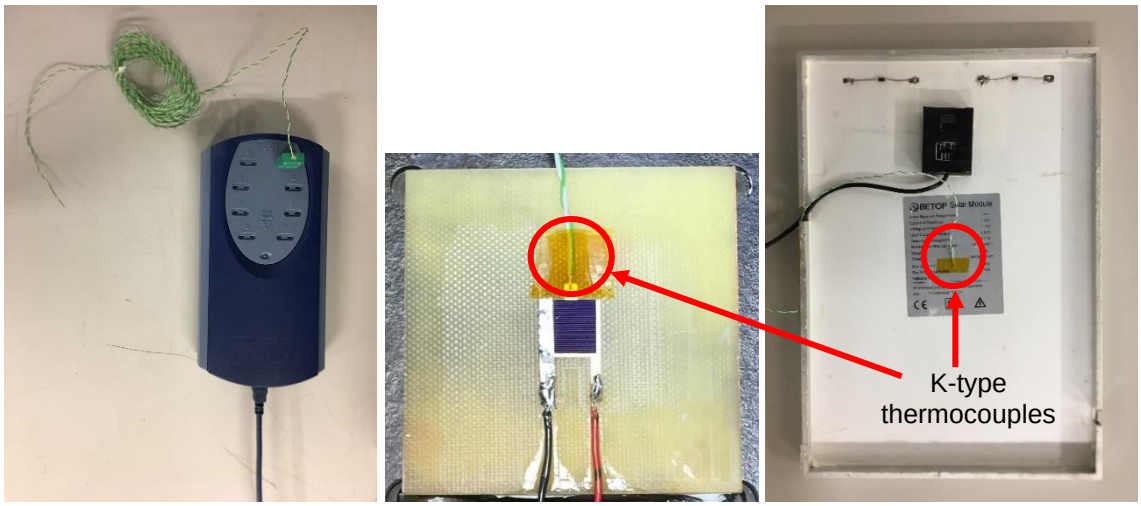

(a) (b) (c)

Figure 3.16. Temperature measurement of solar cells and modules: (a) a K-type thermocouple is attached to Pico TC-08 data logger, (b) the thermocouple is attached to the PCB copper appendage to measure the solar cell temperature and (c) the thermocouple is attached to the back of the 10 W PV module.

3.5.2. Water Circulation Cooling

The solar cells and modules cooling was achieved using water circulation by means of a heat exchanger and a water circulator. The heat exchanger used in this work for solar cells cooling was designed and fabricated by the Mechanical Workshop, Cardiff University as depicted in Figures 3.17 (a) and (b). It was made from copper with dimensions of 6 cm x 6 cm, which match the PCB dimensions as shown by the CAD drawing in Figure 3.17 (a). A photograph is given in Figure 3.17 (b) showing the heat exchanger before welding the copper cover plate. The 1.2 cm thick heat exchanger has two identical copper tubes for water inlet and outlet at each side designed to be connected with flexible water tubes that have an inner diameter of 0.8 cm. Connecting the heat exchanger with the PCB, water tubes and the experimental test rig was previously shown by Figures 3.13 (a) to (d). In

addition to cooling all solar cells used in this research, this set-up was also used to cool the SANYO a-Si PV module because it is smaller in size than this copper heat exchanger.

The water tubes were then attached to a water circulator model GP-300 from NESLAB Instruments [204] that has a water bath capacity of 20 litres. While the test rig with the heat exchanger were placed inside the chamber, the water circulator was placed outside of it. The water tubes were extended between the heat exchanger and the water bath through a hole in the chamber side wall. Since the tubes extended from the heat exchanger inside the chamber are exposed to the simulator's light when it is switched ON, the water inside the tubes will be heated rapidly and hence may not allow an efficient cooling. In order to alleviate this issue, the water tubes inside the chamber were covered by a polyethylene pipe foam insulator from RS Components [205] (see Figure 3.13 (d)).

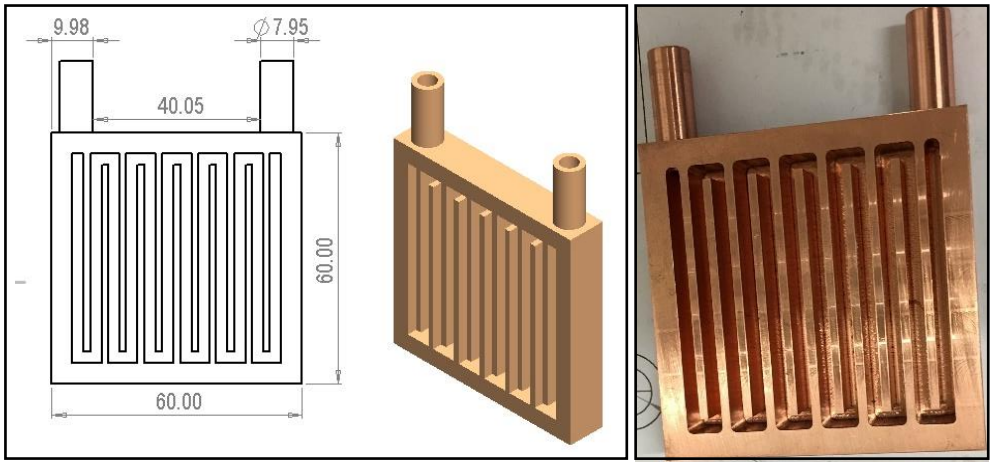

Figure 3.17. Inner view of the heat exchanger used for solar cells cooling designed by the Mechanical Workshop at Cardiff University: (a) CAD drawing and (b) photograph. (Dimensions in the CAD drawing are in mm).

The mono-Si PV modules cooling process harness the same technique, albeit with a larger aluminium heat exchanger with dimensions of 22 cm x 22 cm shown in Figure 3.18 (a). The back side of this heat exchanger was covered using a Perspex sheet by the Mechanical Workshop as shown in Figure 3.18 (b) creating a total thickness of 1.5 cm. The 10 W PV module, shown in Figure 3.14, was attached to the heat exchanger front aluminium plate using the thermal paste as illustrated in Figure 3.18 (c) and then the whole assembly was placed at the centre of the test table under the simulator. It is to be noted that the module's frame was cut to allow for the heat exchanger housing and also grooves were made in the frame as shown in Figure 3.18 (c) in order to insert the inlet and outlet tubes.

A similar procedure was followed for cooling the in-house assembled PV module shown previously in Figure 3.15 by placing the thermal interface sheet on the heat exchanger using the thermal paste as Figure 3.18 (d) shows. Note that for cooling both mono-Si modules, the heat exchanger was placed directly on the test table without a plastic plate used in the case of single solar cells set-up (see Figures 3.13 (a) to (d)). This is because the heat exchanger behaves like a test rig for the PV modules that holds them in place.

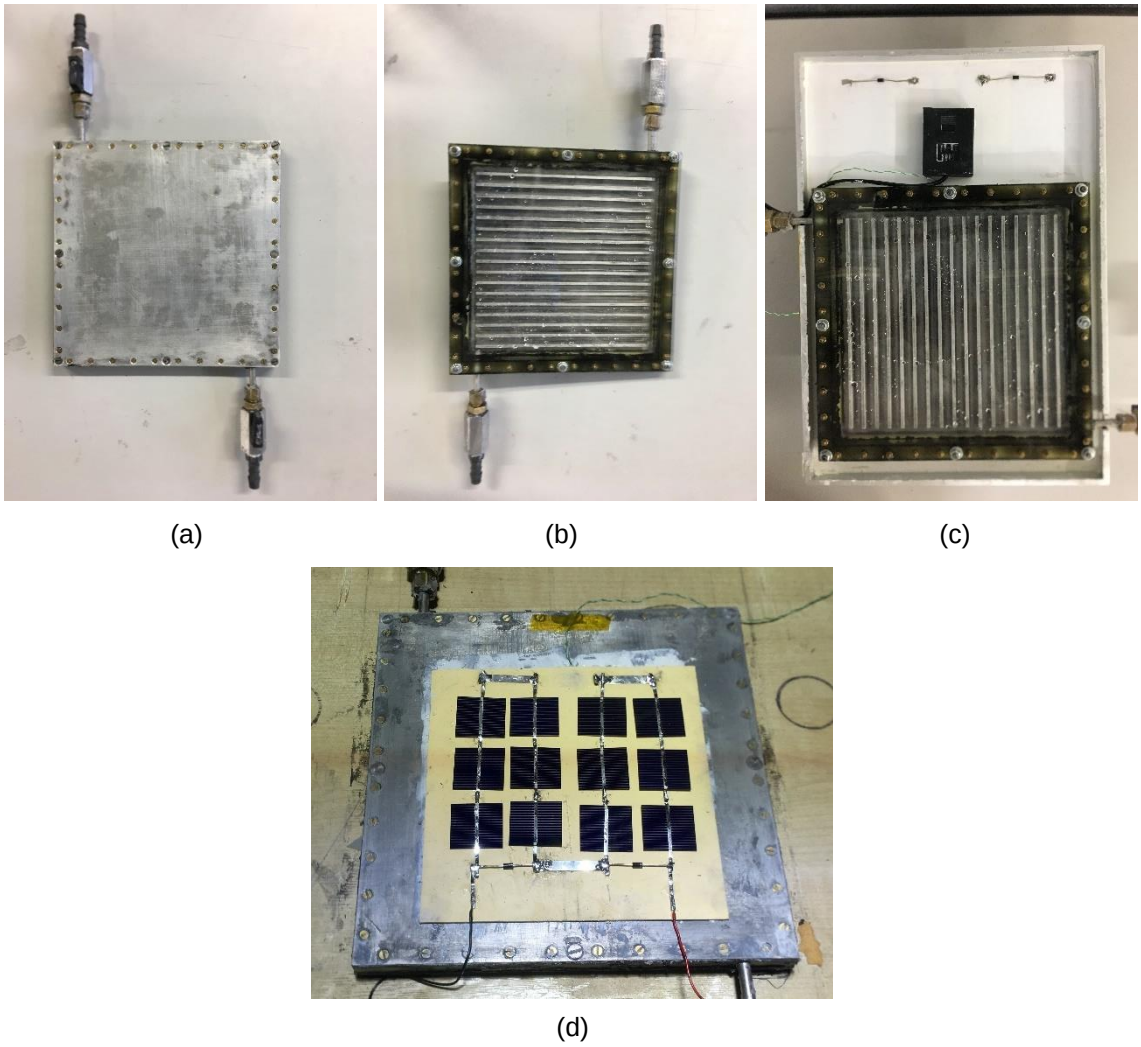

(a) (b) (c)

(d)

Figure 3.18. The heat exchanger used for PV modules cooling; (a) front aluminium plate, (b) back Perspex sheet, (c) the heat exchanger is attached to the back of the 10 W PV module and (d) the heat exchanger is attached to the back of the in-house assembled PV module.

It is crucial in this research that PV devices have an efficient cooling system in order to perform I-V curves tracing at a stabilised temperature. The solar cell cooling system was thus tested under the light source before starting I-V curve tracing in this research. The solar cell test rig was placed inside the chamber and the water circulator GP-300 was placed outside of it as explained previously. A schematic diagram of this experimental

set-up is given in Figure 3.19. K-type thermocouples were used to monitor the solar cell, the water bath and ambient temperatures via the Pico TC-08 data logger and a computer. The solar cell's thermocouple was attached to it as shown previously in Figure 3.16 (b). The water bath's thermocouple was immersed in the water, whereas the ambient temperature's thermocouple was attached to the chamber side wall using an adhesive tape. Since the thermocouples used to measure the solar cell and ambient temperatures were measuring those temperatures inside the chamber, they were inserted through the hole in the chamber's wall in order to be connected to the TC-08 data logger located outside the chamber. It is also to be noted that the thermocouples used to measure the water bath and ambient temperatures were of the same make as that of the one used to measure the PV devices' temperatures, but with smaller lengths of 1 m and 2 m, respectively.

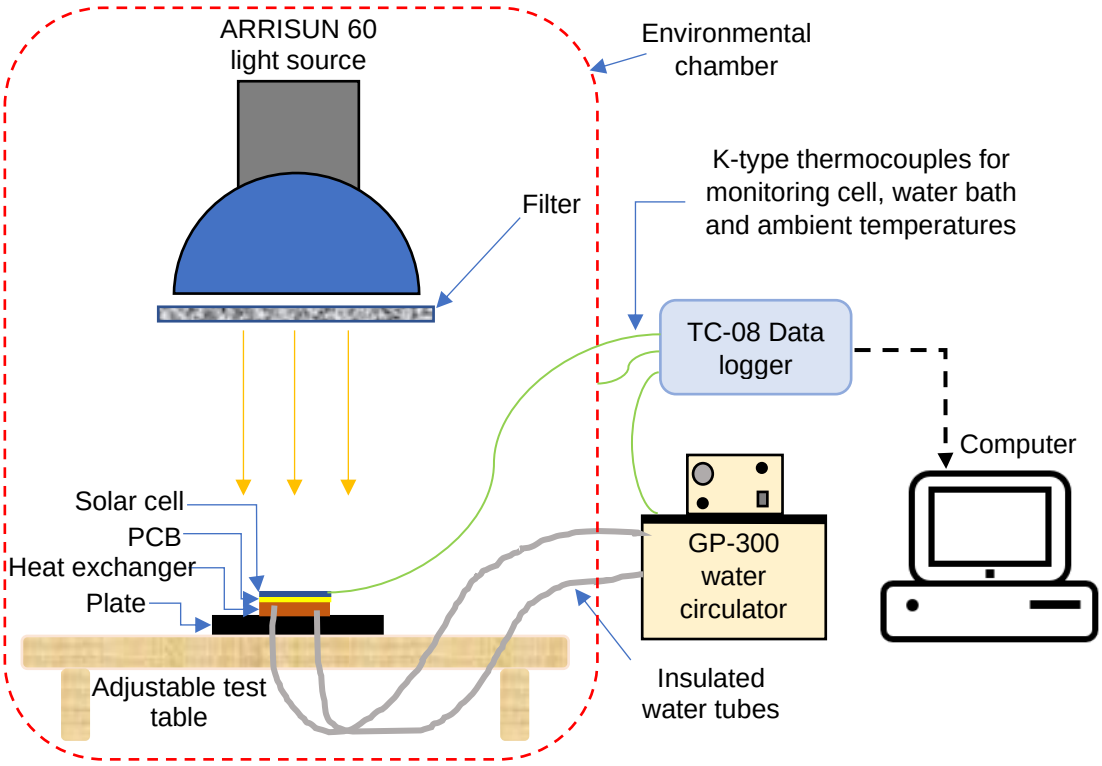

Figure 3.19. Schematic diagram of temperature control set-up.

The light source was switched ON at in irradiance of 1000 W/m² for a period of 3 hours and the chamber door was permanently closed during this time. The three temperatures were recorded using the data logger and plotted against time in seconds in Figure 3.20. As shown, there was a sharp increase in the ambient temperature starting from about 14 °C and reaching nearly 52 °C after the 3 hours. On the other hand, the solar cell and water bath temperatures had a similar trend with a much slower increase throughout the period.

The initial solar cell temperature was about 15 °C and rose to about 26 °C at the end of the test, indicating a fairly stable temperature considering this long period of time.

The cell temperature stayed at STC (25 °C) for a period of about 6 minutes and stayed within 25 ± 0.5 °C for a period of approximately 26 minutes. This time was sufficient for taking I-V curve measurements. Similarly, if it is desired to take I-V curve measurements at other cell temperatures, the cell temperature is monitored while it is slowly increasing and the measurement is taken once it reaches the desired value.

In this particular test, the STC cell temperature was reached at about 8500 second (2 hours and 22 minutes). This can be attributed to the low initial temperature of the water bath (about 13 °C), which caused the slow cell temperature rise when exposed to the light. However, it was noticed in some experiments performed in this research that when the water bath initial temperature was higher, at 20 °C for instance, the STC cell temperature was reached in a much shorter time.

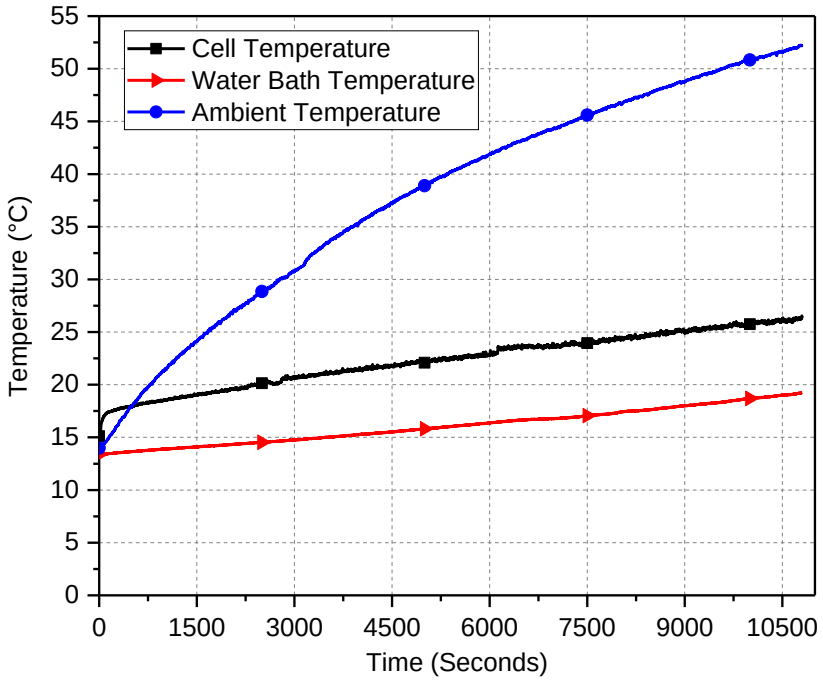

Figure 3.20. Change of the solar cell, water bath and ambient temperatures over a period of 3 hours. Measurements were recorded every one second.

3.6. I-V Curve Tracing

I-V curve measurement is the main characterisation technique in this research used to study the behaviour of solar cells and modules. The used I-V curve tracing system is

shown in Figure 3.21 and was previously established at the Solar and Environmental Research Laboratory, Cardiff University. Keithley 2601 source meter [206] was used to perform I-V curve tracing. The positive and negative terminals of the PV device under test is connected to the Keithley source meter. The source meter itself is interfaced with a computer that harness Test Script Builder (TSB) software via General Purpose Interface Bus (GPIB) control device from National Instruments [207].

According to its data sheet [206], the Keithley 2601 source meter can be used for measuring I-V characteristics of a wide range of electronic components. It has a built-in electronic load and analogue to digital converters for current and voltage, hence it provides current and voltage characterisations in the source and sink modes of operation (when the instrument is used either as a source or as a load). In this work, this instrument was used for I-V curve measurements of PV devices only in the first quadrant, except a few points in the fourth quadrant measured in order to obtain the open circuit point as will be explained later in this section. The current measurement accuracy of the source meter was specified by the manufacturer under specific test conditions, and it is valid for only one year. However, as the used source meter had been in the Laboratory for a few years before using it in this research, these specifications are considered out of data. Hence, the error caused by the source meter on I-V curve measurements will be accounted for in this work when assessing the repeatability of the whole experimental set-up in Section 3.7.

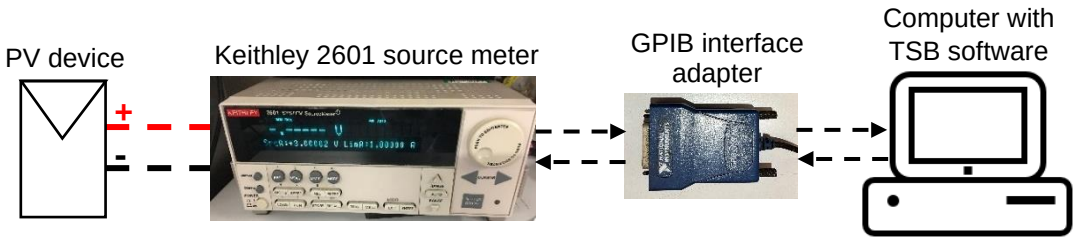

Figure 3.21. I-V curve tracing system configuration.

The TSB software is used to create and debug the source code for I-V curve tracing in addition to sending commands and receiving measurements through the GPIB. Particularly, this software was useful in this work for adjusting the required voltage range according to the size of the PV device under test. Moreover, the measurement resolution can also be set within the software allowing to adjust the number of data points on I-V curves. The more the number of data points is, the longer the I-V curve sweep time will be. Large number of data points make I-V curves more informative and hence is useful

for calculating the equivalent circuit parameters. Nevertheless, large number of data points may make the measurement prone to random errors and temperature variations effect because of long I-V curve sweep time. Therefore, a compromise between large number of data points and short sweep time was selected in this work by not exceeding 106 points in all experiments resulting in a sweep time of less than 3 seconds. Throughout this research, the number of data points of all I-V curves that are compared with each other are consistent.

The current for each voltage point within the specified voltage range was measured by the source meter and received in the TSB software. This I-V data was then exported to a Microsoft Excel file for further adjustment, which constituted calculating the open circuit voltage point and deleting any extra points in the fourth quadrant. Figure 3.22 (a) shows a measured I-V curve of the solar cell that has an active area of 0.78 cm² depicted here as an example to illustrate this procedure. As shown, the open circuit voltage (V_{oc}) point (I = 0) cannot be obtained experimentally and hence the current was measured with some data points in the fourth quadrant. The V_{oc} can be calculated from the two points located in the red circle in Figure 3.22 (a) using linear interpolation due to the fact that these points form nearly a straight line and they are close to each other. Assume that the upper and lower points' coordinates are (x_1, y_1) and (x_2, y_2), respectively. The V_{oc} coordinates are (x_0, y_0). Then we can write:

$$\frac{(y_0-y_1)}{(x_0-x_1)} = \frac{(y_2-y_1)}{(x_2-x_1)} \tag{3.2}$$

The V_{oc} coordinate (x_0) can then be calculated from:

$$x_0 = V_{oc} = \frac{(y_0-y_1)(x_2-x_1)}{(y_2-y_1)} + x_1 \tag{3.3}$$

For this particular I-V curve, using the coordinates of (x_1, y_1), (x_2, y_2) and given a current of zero at open circuit $(y_0 = 0)$, the calculated V_{oc} using Equation (3.3) is 0.576 V. Once V_{oc} is obtained, the extra fourth quadrant points are deleted from the data including the lower point (x_2, y_2) in the red circle in Figure 3.22 (a), resulting in an I-V curve in the first quadrant as depicted in Figure 3.22 (b). Once the I-V curve is obtained, the P-V curve can be simply determined by calculating the power for each point $(I.V)$ and then plotting it versus the voltage.

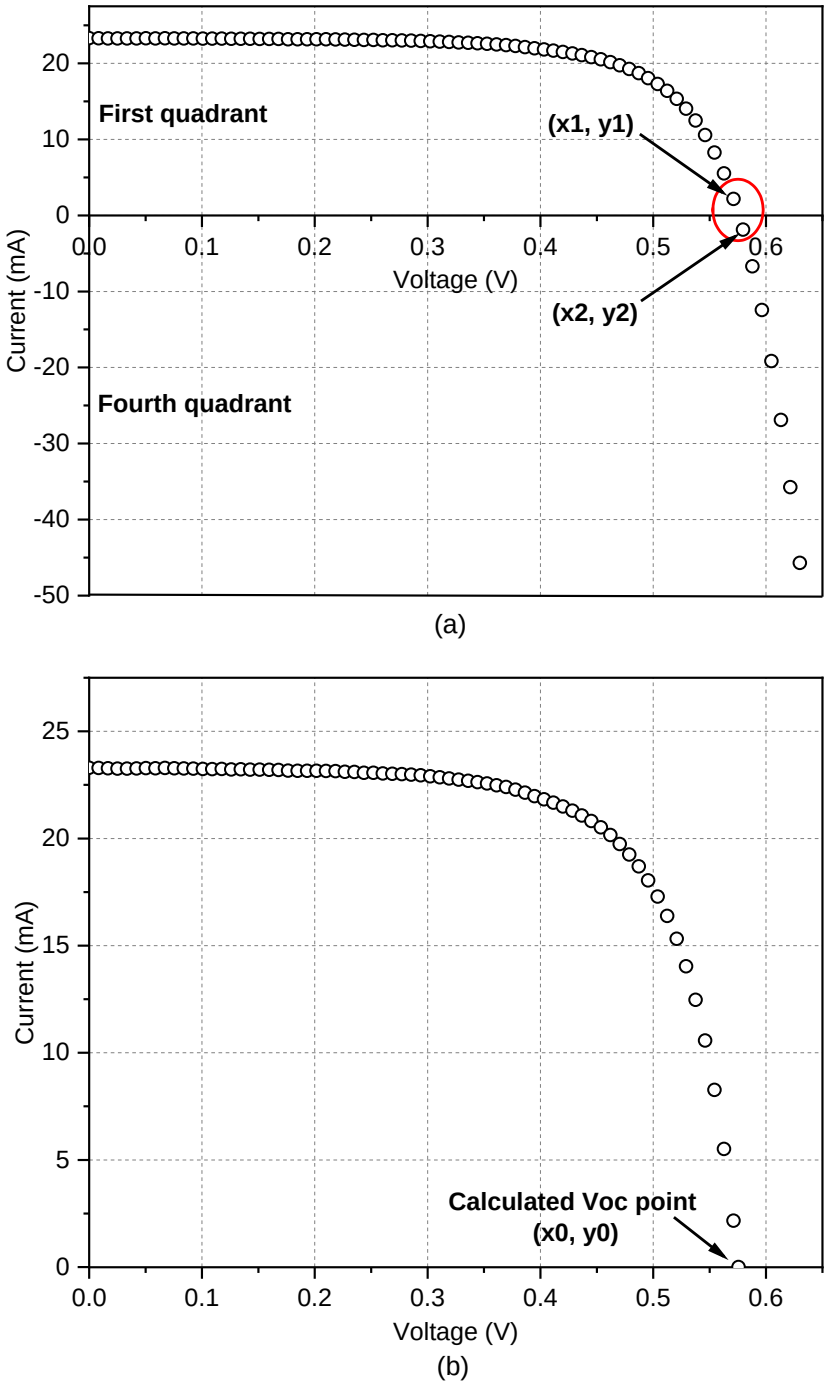

Figure 3.22. Experimental I-V curves of the 0.78 cm² active area solar cell depicted to illustrate the open circuit voltage point calculation process: (a) the complete measured I-V curve and (b) the I-V curve in the first quadrant with the open circuit point added and the fourth quadrant points deleted.

It is important to point out that in some I-V curves, the upper point (x_1, y_1) in Figure 3.22 (a) is very close to the x-axis with a very low current value. When calculating the V_{oc}, the upper point (x_1, y_1) and the V_{oc} point will be very close and nearly overlapped with each other. In order to avoid this issue of overlapped two points, a criterion was developed

depending on how close the point (x_1, y_1) to V_{oc}. If the current of this point is ≥1% of the I_{sc}, this means that this point is not very close to V_{oc} and hence it is retained as it is the case in the example given in Figures 3.22 (a) and (b). On the other hand, if the current of this point is < 1% of the I_{sc}, then this point is very close to V_{oc} and thus it is deleted from the data. This procedure was applied to all solar cells and modules that was required to calculate their equivalent circuit parameters in this research. However, this procedure was not applied to I-V curves that were not used for calculating the parameters and were only presented for experimental comparison.

3.7. Complete Experimental Set-up and Repeatability Error Analysis

The solar cells and modules characterisation set-up was assembled as discussed in the previous sections. After placing the solar cell or module assembly at the centre of the test table, the water cooling and I-V curve sweep systems were configured establishing the complete characterisation set-up. A schematic diagram of the solar cell under the characterisation set-up is given in Figure 3.23 and a photograph of the facility is given in Figure 3.24 where all main parts are annotated.

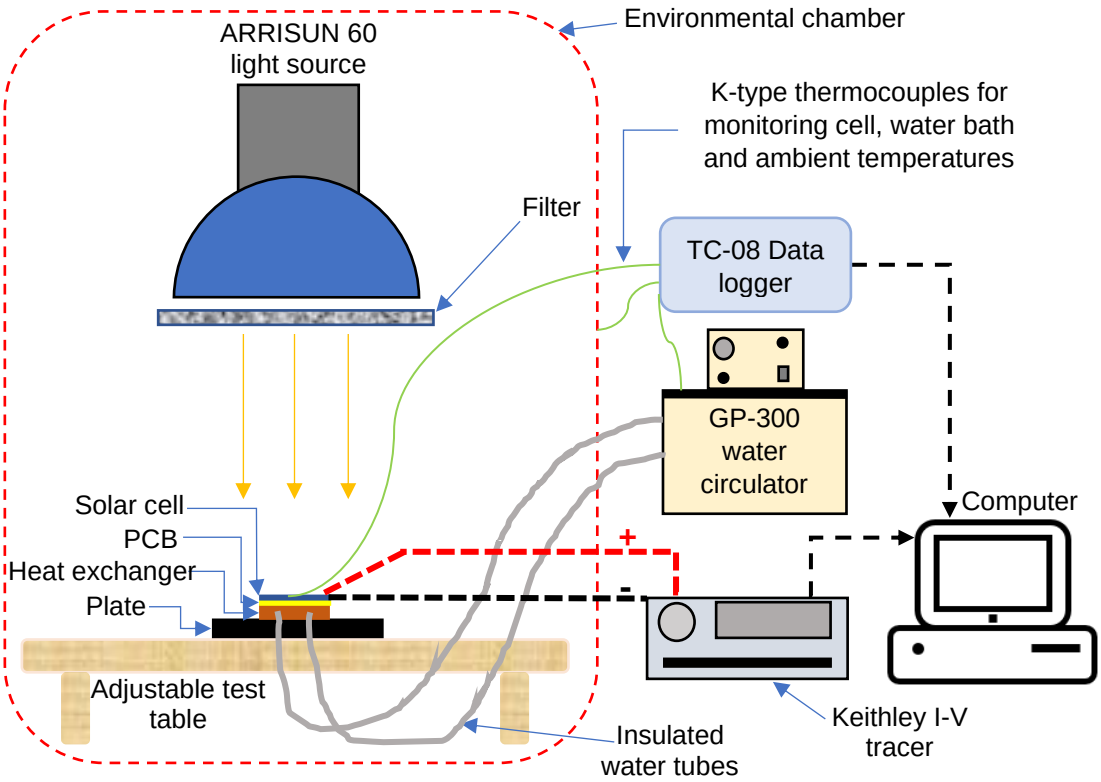

Figure 3.23. Schematic diagram of the facility for solar cells and modules characterisation.

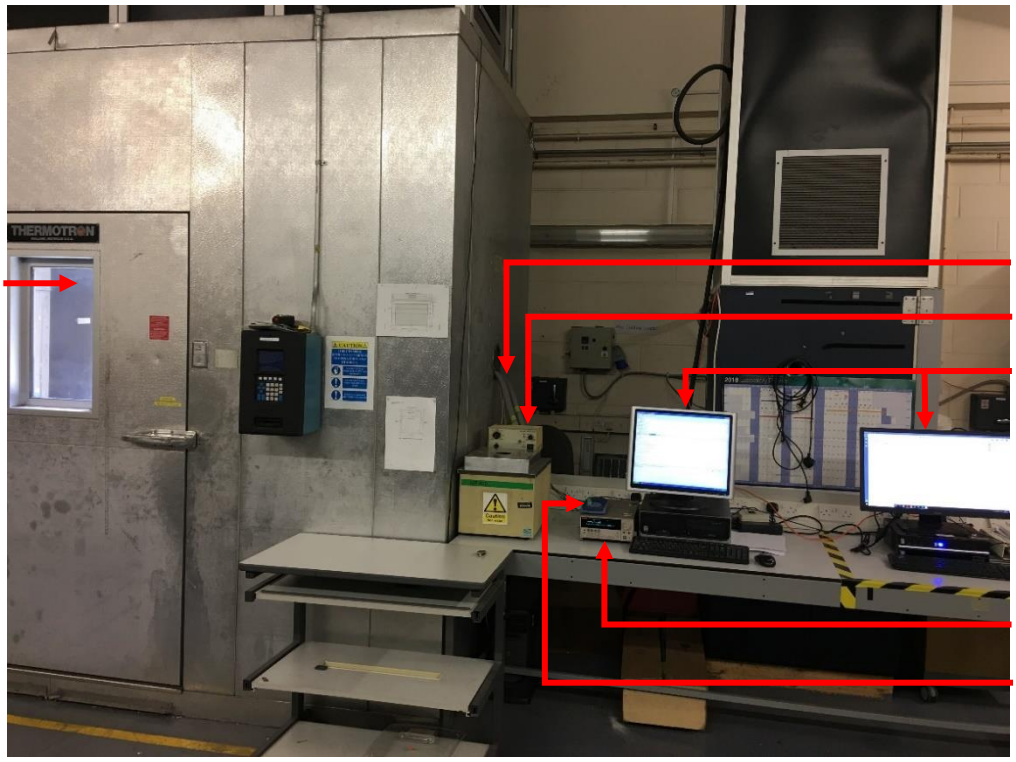

(1) Environmental chamber with ARRISUN 60 light source
(2) Insulated water tubes
(3) GP-300 water circulator
(4) Computers for I-V tracing and temperature monitoring
(5) Keithley 2601 I-V tracer
(6) TC-08 temperature data logger

Figure 3.24. Photograph of the facility for solar cells and modules characterisation.

The next step was to test the system and determine its repeatability error by measuring I-V curves of a solar cell several times under the same condition. The I-V curve of the solar cell that has an active area of 0.78 cm² was measured 12 times at STC over three days, with four measurements obtained per day, during which the light source and all test equipment were switched OFF after each four measurements. The 12 I-V curves are plotted in Figure 3.25 indicating a reasonably good consistency, especially near V_{oc} point. The performance parameters of each I-V curve were extracted from experimental data. In addition, the mean value and relative standard deviation (RSD) of the population were calculated using Microsoft Excel and presented in Table 3.5. The RSD was calculated from the following equation:

$$RSD = 100\% * \left(\frac{SD}{\bar{x}}\right) \tag{3.4}$$

where $\bar{x}$ is the mean and SD is the standard deviation of the samples' population, which is calculated from:

$$SD = \sqrt{\frac{\sum_{i=1}^{N}(\bar{x} - x_i)^2}{N}} \tag{3.5}$$

where x_i represents the i_{th} point of the samples' population and N is the number of samples.

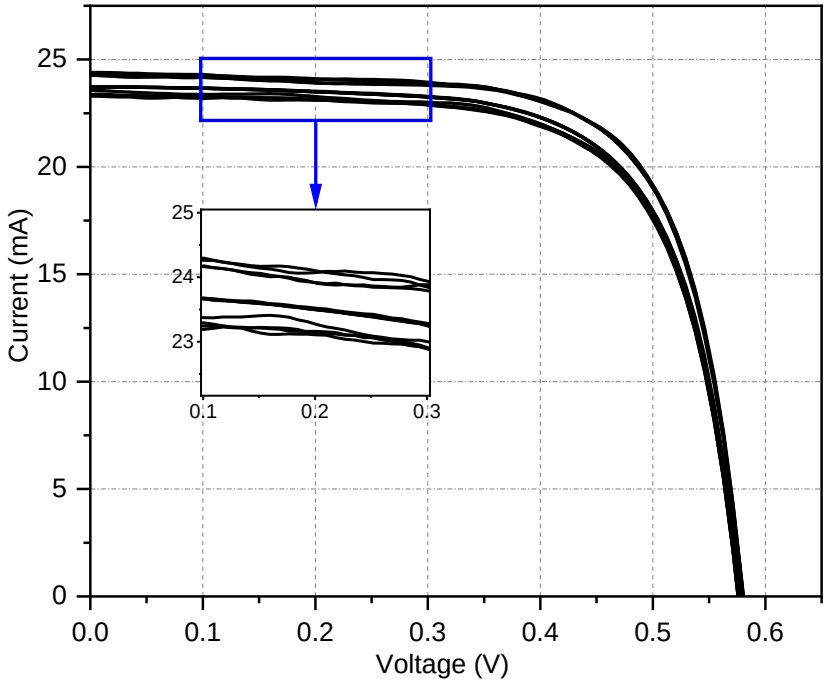

Figure 3.25. 12 I-V curve measurements taken at STC over three days, with four measurements obtained per day.

Table 3.5. Performance parameters of the mono-Si solar cell extracted under STC. (Each parameter value was calculated by averaging 12 values from 12 I-V curve measurements taken over three days, with four measurements obtained per day. The relative standard deviation of each parameter is also shown).

Parameter at STC	Mean value	Relative standard deviation (%)
P_{max} (mW)	9.6	±3
I_{sc} (mA)	23.8	±1.6
V_{oc} (V)	0.578	±0.3
FF	0.694	±1
Efficiency (%)	12.3	±2.7

The RSD was also calculated using Equation (3.4) for each point of the measured current on the 12 I-V curves in Figure 3.25 and then it was averaged resulting in a value of about 5%. The V_{oc} points of the first four I-V curves were not included in the RSD calculations because those four curves have 71 data points, whereas the other curves have 70.

Furthermore, the data in Table 3.5 indicates fairly small RSDs of the main parameters. The slightly higher RSDs of P_{max}, efficiency and I_{sc} may be attributed to the slight attenuation in light source intensity because of switching it OFF and then ON again. However, the FF and V_{oc} showed lower RSDs of ±1 and ±0.3%, respectively. The consistency of V_{oc} among the 12 I-V curves indicates that the temperature cooling system is effective in maintaining a stable cell temperature of 25 °C because this parameter is sensitive to the change in the cell temperature [1]. All the above results imply that the experimental set-up has a reasonably good repeatability.

The measurement error, which is presented above as RSD of the performance parameters and I-V curves, is an accumulation of any random errors caused by the light source attenuation, I-V curve tracing and accuracy of temperature measurements. Therefore, throughout this thesis, the RSD calculated from Equations (3.4) and (3.5) will be used as a measure of repeatability and measurement error in performance parameters, equivalent circuit parameters and I-V curves.

3.8. Shading Objects Fabrication

It is required in the shading experiments performed in this research to use opaque objects to block parts of the solar cells and prevent light from reaching them. Since most of the used solar cells are quite small in size and do not have a front glass sheet, it was decided to fabricate the shading objects using 3D printing technology. This is with the exception of the 10 W PV module shown in Figure 3.14, which has larger solar cells (active area of 15 cm² (3 cm x 5 cm)) encapsulated into a front glass sheet, hence a double-sided foam adhesive tape was used. The adhesive tape worked well with this module for prevention of light penetration through the shaded cell edges because of its firm adherence to the glass. Nevertheless, it cannot be used with other cells and modules that do not have a front glass sheet because the tape might damage the cells when it is peeled off. The 3D printing process is presented below for the 0.78 cm² active area cell. It is the same for all other PV devices used in this research, expect the 10 W module as stated above.

The 3D objects were made of black Polylactic acid (PLA) filament using Ultimaker 2 Extended Plus 3D printer [208] located at the Electrical Workshop, Cardiff University and shown in Figure 3.26. First, the objects were designed in SolidWorks software with sizes depending on the cell area. For instance, a shaded area of 25% from the total cell

area requires an object that has a width covers 25% of the cell. Three objects were fabricated for three shaded area percentages of 25, 50 and 75%. The thickness of all objects was selected to be 2 mm.

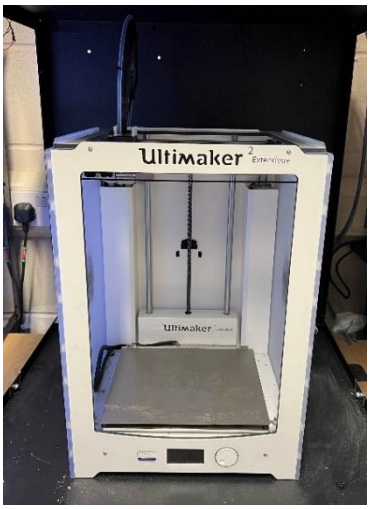

Figure 3.26. Ultimaker 2 Extended Plus 3D printer used to fabricate the shading objects.

Second, once the CAD drawing file was ready in SolidWorks, it was converted to a stereolithography (STL) file type and then opened by Ultimaker Cura software. In this software, the printing features can be adjusted if needed, such as the layer height and object filling percentage. Third, the file was exported to the 3D printer in order to perform the printing process. In Figure 3.27 (a) to (c), CAD drawing in SolidWorks and photographs of the shading objects for the 0.78 cm² cell are depicted. The left-hand side of each figure shows the CAD drawing, while the photographs are given in the right-hand side. As shown in the CAD drawings, the length of all objects was increased by 0.5 mm beyond the length of the cell (10 mm) in order to minimise light penetration through the upper and lower shaded edges of the cell.

It is also to be mentioned here that the used 3D printer is very accurate in fabricating objects with the required dimensions. Its accuracies along the x, y and z directions are 12.5, 12.5 and 5 µm, respectively [208]. This high precision in addition to carefully placing the objects on the cell helped in blocking the area that intended to be shaded. Moreover, in all solar cells and modules used in this research, the well-known linear decrease of the I_{sc} with shading was also used to verify that the shaded percentage is correct.

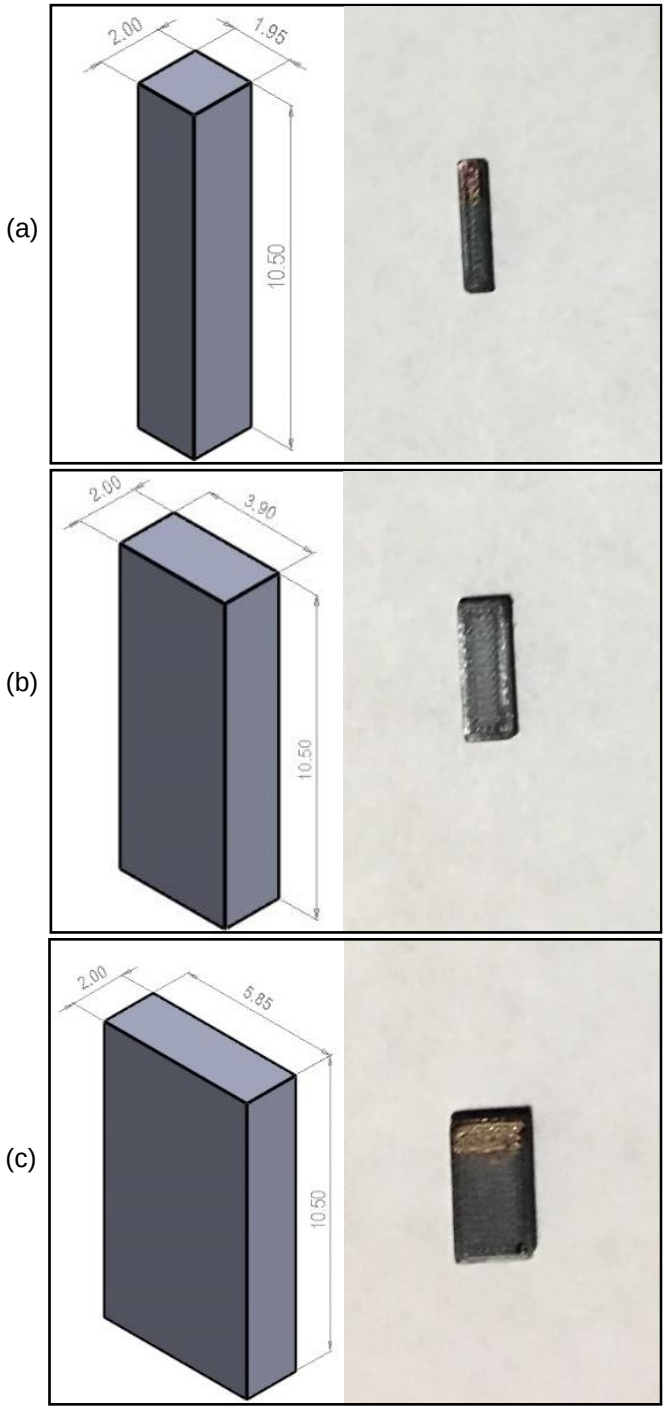

Figure 3.27. The 3D printed shading objects of the 0.78 cm² active area cell: ((left) CAD drawings and (right) photographs): (a) 25% shading object, (b) 50% shading object and (c) 75% shading object. (Dimensions in the CAD drawings are in mm).

3.9. Thermal Imaging Set-up

Thermal imaging was used in this work in an attempt to detect hot spots of cells that have broken contact fingers in PV modules. FLIR C2 thermal camera [209] shown in Figure 3.28 was used for capturing thermal images of the 10 W module shown in Figure 3.14.

The main specifications of the thermal camera according to its data sheet are given in Table 3.6. Thermal images present temperatures of objects as a heat map. The temperature at any position in the image can be determined when exporting the image from the camera to its FLIR software. Furthermore, the camera offers three main settings that can be adjusted by the user, which are the emissivity, the reflected temperature and the distance from the target object.

According to a thermal imaging guidebook from FLIR [210], the emissivity, which is a measure of the object's capability of emitting IR radiation, is a very important parameter that needs to be set properly in the camera setting to achieve accurate thermal measurements. Moreover, glass emissivity mainly influences the thermal imaging of PV modules due to its specular reflections. As mentioned in this guidebook, thermal images of PV modules need to be taken while the camera is being held at an angle of 5 - 60º, with 0º means that the camera is perpendicular to the PV module. In addition, it is shown in the guidebook that emissivity of glass changes with the angle of imaging. At an angle of approximately 45º, which is the one used in this work, the emissivity of glass is about 0.8. Hence, the emissivity in the camera settings was set to 0.8 in this work.

The reflected temperature, on the other hand, is only important when imaging objects with a low emissivity [210]. This temperature was therefore left at its default value of 20 °C. Similarly, the distance from the target object was also left at its default value of 1 m, which was roughly the actual distance between the camera and the module when capturing the thermal images in this work.

Figure 3.28. FLIR C2 thermal camera used in capturing thermal images [209].

The module thermal images were captured under 1000 W/m² illumination and short circuit condition. The latter is the condition under which thermal imaging should be taken [1]. The module was imaged without the cooling system in order to allow increasing of solar cells' temperatures by the light source, thereby increasing the thermal gradient and facilitating the appearance of hot spots. A thermal image of the module will be presented later in Chapter 6, Section 6.4.2.

Table 3.6. Main specifications of the FLIR C2 thermal camera [209].

Specification	Value
Measured temperature range	-10℃ to +150℃
Thermal sensitivity	< 0.1℃
Accuracy at 25℃	±2℃ or 2% (whichever is greater)
IR sensor	80 × 60 pixels
Image frequency	9 Hz
Field of view	41° × 31°

3.10. Electroluminescent Imaging Set-up

EL imaging was employed in this work for detection of cell broken contact fingers in PV modules. An EL experimental set-up was built as shown in Figure 3.29. The PV device under test was placed inside the environmental chamber and the shutter was closed using the linear actuator (see Figure 3.1 (b)), hence creating a dark environment. In addition, the glass window of the chamber door (see Figure 3.1 (a)) was closed using a black neoprene sheet in order to prevent any light penetration when the door is closed. The PV device was then forward biased by a current nearly equal to its I_{sc} under STC. This bias level provides good quality EL images as shown by [14], [160]. Subsequently, EL images were captured using a Nikon D40 camera [211], which is a consumer grade DSLR camera, with the IR filter removed following the work of [157]. The D40 camera has a CCD sensor with an image resolution of 3008 x 2000 pixels (6 megapixels) and was equipped with a lens that has a focal length of 18 – 55 mm. Furthermore, the camera was connected on a tripod in order to allow a stable image capturing.

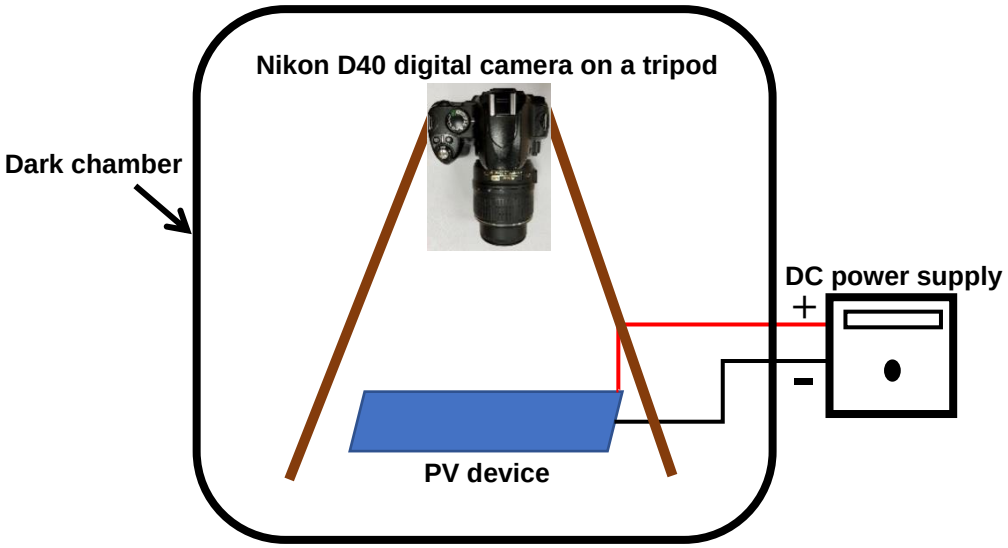

Figure 3.29. Schematic of the EL imaging experimental set-up. The PV device under test could be a solar cell or a PV module.

In order to adequately capture EL images of PV devices, some camera settings need to be adjusted beforehand. Since EL imaging was employed in this work for taking images of solar cells and modules, the camera settings for solar cells were different from those for PV modules due to the difference in size. The solar cell imaged by EL is the 2.5 cm x 2.5 cm cell, whereas the imaged modules are the 10 W module shown in Figure 3.14 and the in-house assembled module shown in Figure 3.15. Same EL set-up and camera settings were used for both PV modules, so only the EL of the 10 W module is presented in this section. Photographs of the EL imaging experimental set-up of the solar cell and the 10 W module are given in Figures 3.30 (a) and (b), respectively.

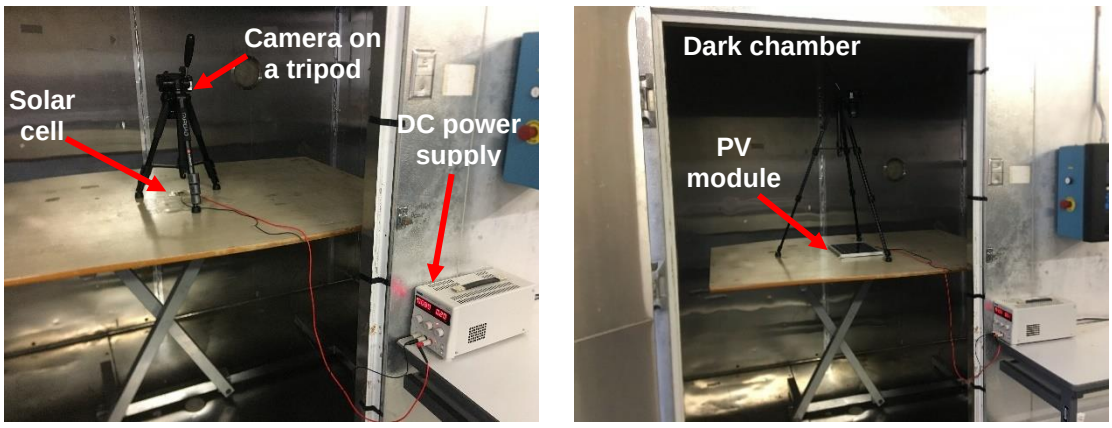

(a) (b)

Figure 3.30. EL imaging experimental set-up used to capture the EL images: (a) of the 2.5 cm x 2.5 cm solar cell and (b) of the 10 W PV module.

Before the camera settings adjustment started, the mode dial had been adjusted to manual to allow for manual adjustment of settings. Moreover, the camera focus had been set to automatic mode initially and then once the lens focused on the PV device, it was set to manual mode and left in this position throughout all EL experiments. This was done in order for the focus to be fixed on the PV device and to prevent the camera from changing it automatically.

There were five camera settings that were adjusted in this work as depicted in Table 3.7. First, the camera sensitivity (also called ISO) was set to a typical value of 800, which is the middle value of the camera maximum ISO of 1600. Second, the distance from the lens to the PV device and the focal length were simultaneously adjusted by trial and error through taking different ordinary digital images. The distances were set respectively to 29 cm and 76 cm for the solar cell and the module. Whereas the focal length was adjusted to 55 mm and 45 mm for both devices, respectively. Subsequently, the aperture was adjusted to its widest opening according to the focal length. Apertures of F/5.6 and F/5.3 were set according to the focal lengths of 55 mm and 45 mm for the solar cell and the module, respectively.

Finally, the shutter speed was found to be the most important parameter affecting the quality of the EL images. The solar cell and module EL images were captured under different shutter speeds from 5 seconds to 30 seconds in a 5 second step as shown in Figures 3.31 and 3.32. It was observed that the higher the shutter speed is, the brighter and more informative the EL image will be. Therefore, a shutter speed of 30 seconds was selected for both PV devices.

Table 3.7. Nikon D40 camera settings for capturing EL images of the 2.5 cm x 2.5 cm solar cell and the 10 W PV module.

Camera setting	PV device under test	
	Solar Cell	10 W Module
ISO	800	800
Distance from lens to PV device (cm)	29	76
Focal length (mm)	55	45
Aperture	F/5.6	F/5.3
Shutter speed (seconds)	30	30

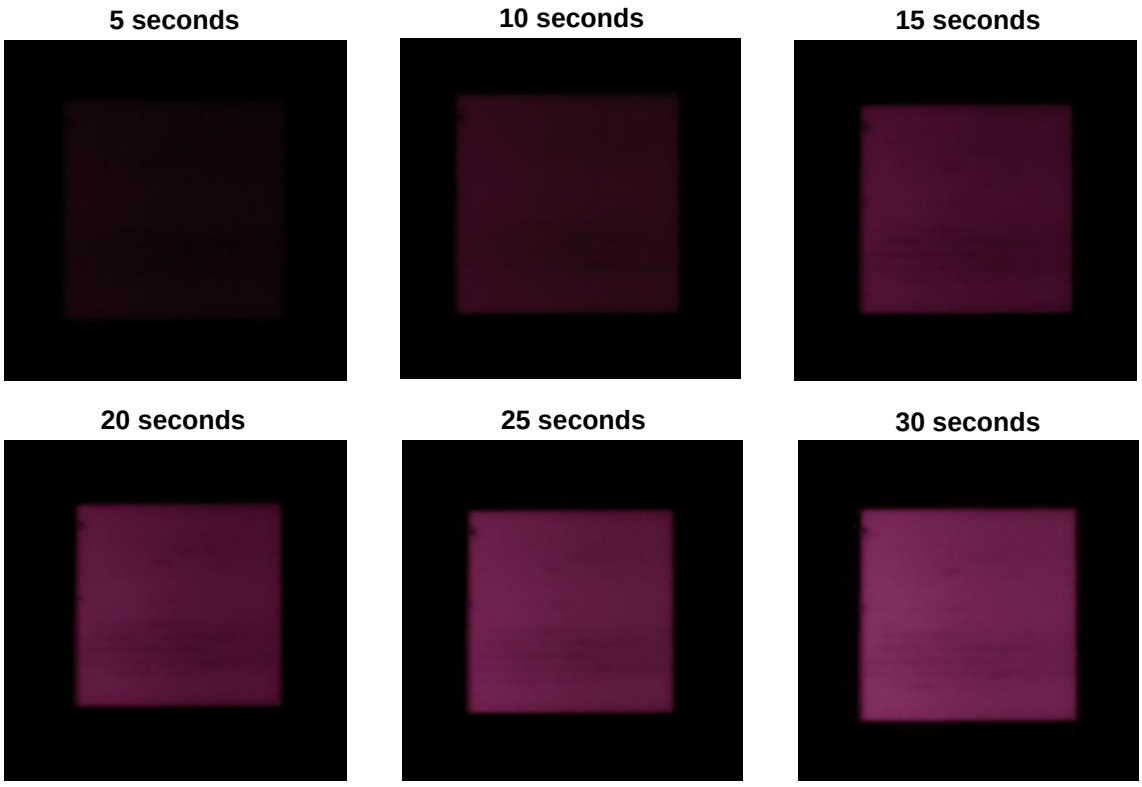

Figure 3.31. Camera shutter speed selection for EL imaging of the 2.5 cm x 2.5 cm solar cell.

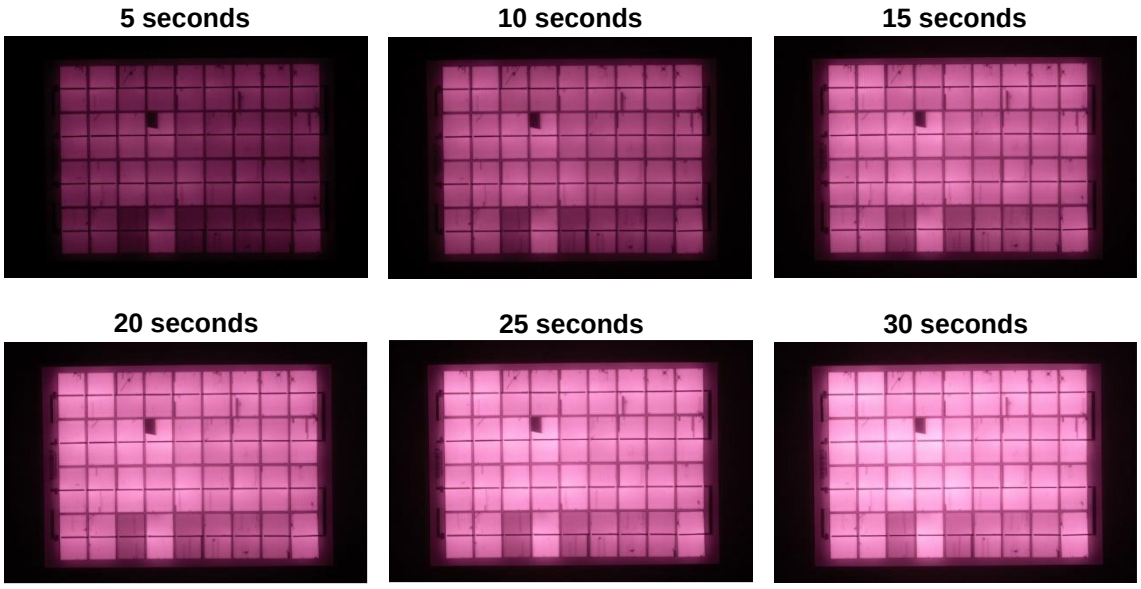

Figure 3.32. Camera shutter speed selection for EL imaging of the 10 W PV module.

It is to be noted that as EL imaging must be performed under a dark environment, the chamber door must be closed while the image is being captured. Thus, the self-timer feature of the camera was used for this purpose. The self-timer makes the camera waits

for 10 seconds after pressing the capture button. This time is sufficient to leave the chamber and close the door before the image capturing process begins.

3.11. Summary

The experimental methods of this research have been reported in detail in this chapter. The light source calibration tests were performed according to the E927-10 standards in terms of spectral match, spatial non-uniformity and temporal stability. The results revealed that it is of Class BCA for testing single solar cells used in this research. Nevertheless, it does not meet the standards only in terms of spatial non-uniformity when testing PV modules. However, as will be shown in Chapters 5 and 6, small PV modules can still be characterised adequately enough to satisfy the purpose of this research.

After that, the soldering and test rig preparations have been presented for the 0.78 cm^2 solar cell. The same process was applied to all other solar cells used in this research. The use of a PCB as a support for the fragile solar cells was found to be a very useful technique for cells handling during experiments and for cooling purpose. Then, the preparation and soldering process of the used PV modules have been explained.

Subsequently, the design and testing of the temperature control system has been reported. Thermocouple configuration for measuring the temperature of solar cells and modules has been first discussed followed by explaining the construction of the water cooling system. Testing the temperature cooling system showed that the cell temperature could remain reasonably stable for a sufficient period of time to take the I-V measurements. The last step in building the complete experimental set-up was the I-V curve tracing system. This system was tested and the issue of obtaining the open circuit voltage point from experimental data was alleviated thanks to the linear interpolation method.

When the complete characterisation experimental set-up was established, its repeatability error was assessed by repeating I-V curve measurements of a solar cell 12 times at STC over three days, with four curves measured in each day. The results of calculating the RSDs of performance parameters and I-V curves indicated that the set-up performed quite decently. The RSD was used as an indicator of the measurement error of the experimental set-up throughout this research.

Subsequently, fabrication of solar cells' shading objects using 3D printing technology was carried-out and reported. It was found that for small solar cells that are not encapsulated, 3D printed shading objects can be used to apply shading without damaging the cells in contrast to the foam adhesive tape. On the other hand, the foam adhesive tape was found to be performing better for shading of the 10 W PV module, which has encapsulated solar cells within the module's glass, by adhering well to the glass and hence preventing light penetration.

Finally, thermal and EL imaging experimental set-ups were built, tested and presented in this chapter. Camera settings adjustment experiments indicated that the shutter speed is the most crucial setting for EL imaging that needs to be carefully selected. Thermal and EL imaging were used in this work for detection of cells that have broken contact fingers in order to validate the correlation between I-V curves and broken contact fingers as will be presented in Chapter 6.

Chapter 4: Parameters Extraction of Solar Cells

4.1. Introduction

In this chapter, a technique for improving the accuracy of equivalent circuit parameters extraction methods of PV devices from experimental I-V curves is introduced. As discussed previously in Section 2.8.2, the analytical parameter extraction methods are simple compared with the other methods, yet at the cost of lower accuracy [51]. Nevertheless, in this research, a simple but accurate approach to extract the parameters form experimental I-V curves was desired in order to study their behaviour under different operational conditions. Therefore, this issue has been tackled by improving the accuracy of an analytical method available in the literature, while maintaining its simplicity. This was achieved by developing a simple new strategy for selecting the points used to calculate the slopes of tangent lines at I_{sc} and V_{oc} (points 2 and 3 in Figure 2.11). Moreover, the development of this technique has alleviated the issue represented in the perplexity of selecting the proper locations of those points on I-V curves.

The high accuracy of the technique was validated by comparing the calculated I-V curves from the extracted parameters with the experimental data of two types of PV devices, which are a mono-Si solar cell and an a-Si PV module. The results were also compared with an iterative and an iterative-numerical methods from the literature and showed superior accuracy for the developed technique. Further, the computational time was evaluated and compared with the other methods in addition to assessing the technique's repeatability and capability of detecting the change in parameters caused by re-positioning the solar cell or re-soldering its contacts. The developed technique was used in all experimental investigations of this research which require equivalent circuit parameters extraction.

4.2. New Strategy for Accurate Extraction of Solar Cells Parameters from Experimental I-V Curve Data

The slopes of tangent lines at short circuit point (R_{sh0}) and at open circuit point (R_{s0}) were previously shown to be calculated from Equations (2.18) and (2.19), respectively.

In Figure 2.11, the four points used to calculate the slopes for a mono-Si solar cell were denoted point-1, point-2, point-3 and point-4. The voltages and currents of each point are now denoted (V_1, I_1), (V_2, I_2), (V_3, I_3) and (V_4, I_4), respectively, as shown in Figure 4.1. Therefore, Equations (2.18) and (2.19) can now be re-written as the following two equations, respectively [52]:

$$R_{sh0} = \frac{V_2 - V_1}{I_1 - I_2} = \frac{V_2}{I_{sc} - I_2} \tag{4.1}$$

$$R_{s0} = \frac{V_4 - V_3}{I_3 - I_4} = \frac{V_{oc} - V_3}{I_3} \tag{4.2}$$

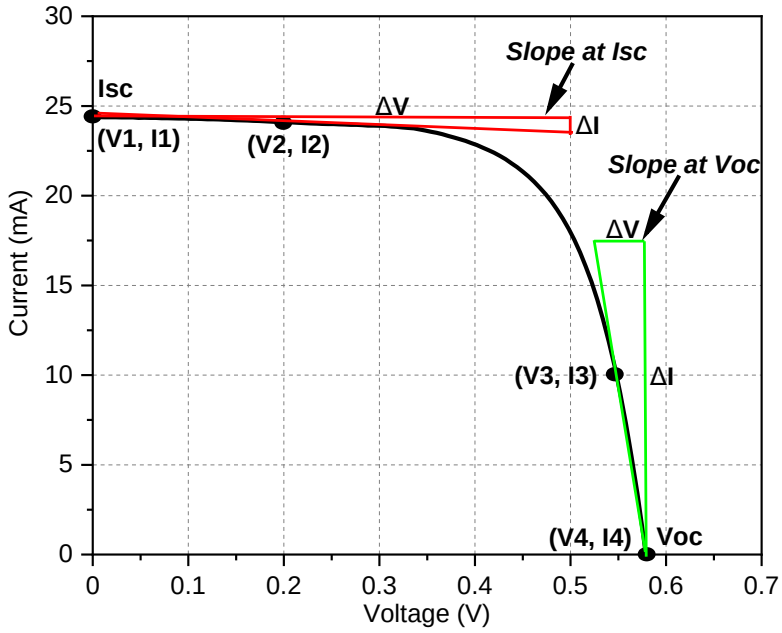

Figure 4.1. I-V curve of a solar cell shows the voltages and currents of the four points used to calculate the slopes of tangent lines at short circuit current and open circuit voltage points.

Accurate determination of the parameters needs the proper selection of the locations of the pair of points 2 and 3. The developed technique uses all the points on a portion of the I-V curve to calculate the slopes and the five parameters and then selects the pair that provides the best fit with experimental data. This strategy can be used to improve the accuracy of all parameters extraction methods that are based on the slopes, such as the ones in [47], [53], [54], [57]. However, in this work, the analytical method proposed by Phang *et al*. [53] was used as it is very simple and performs well in calculating the parameters [49]. In this method, after some simplifications and assumptions, the derived equations for calculating the five parameters are [53]:

$$R_{sh} = R_{sh0} \tag{4.3}$$

$$n = \frac{(I_{mp}R_{s0}+V_{mp}-V_{oc})}{V_{th}\left[\left(\frac{I_{mp}}{I_{sc}-\frac{V_{oc}}{R_{sh}}}\right)-Ln\left(I_{sc}-\frac{V_{oc}}{R_{sh}}\right)+Ln\left(I_{sc}-\frac{V_{mp}}{R_{sh}}-I_{mp}\right)\right]} \quad (4.4)$$

$$I_s = exp\left(-\frac{V_{oc}}{V_{th}n}\right)\left(I_{sc} - \frac{V_{oc}}{R_{sh}}\right) \quad (4.5)$$

$$R_s = R_{s0} - exp\left(-\frac{V_{oc}}{V_{th}n}\right)\left(\frac{V_{th}n}{I_s}\right) \quad (4.6)$$

$$I_{ph} = \left(\frac{R_s}{R_{sh}}+1\right)I_{sc} + \left(exp\left(\frac{R_s I_{sc}}{V_{th}n}\right)-1\right)I_s \quad (4.7)$$

MATLAB software was used to implement the developed technique code. In Figure 4.2, the flow chart of the technique is shown, while the MATLAB code is given in Appendix A. The technique is based on taking every possibility to calculate R_{sh0} and R_{s0} from Equations (4.1) and (4.2) by harnessing a specific range of points for points 2 and 3, respectively, as illustrated in Figure 4.3. First, the experimental I-V curve data and the PV device temperature value are entered in the program. Second, an iterative program routine is invoked to determine R_{sh0} using a range of points for point-2 starting from the vicinity of I_{sc} and ending at the point that has a voltage equals to 50% of V_{oc} (or the point with the nearest voltage value to 50% of V_{oc}). When calculating R_{sh0} from every point in this range, R_{s0} is instantly calculated using a range of points for point-3 starting from the vicinity of V_{oc} and ending at the point that has a current equals to 50% of I_{sc} (or the point with the nearest current value to 50% of I_{sc}). The limits of the first and second ranges were selected respectively as 50% of V_{oc} and 50% of I_{sc} in order to only utilise the linear parts of the I-V curve in both ranges without utilising points on the MPP knee as depicted in Figure 4.3.

In Figure 4.3, a graphical illustration of indexing the pairs of points 2 and 3 in the program is given. The first indexed pair, for instance, contains the point with the first index in the vicinity of I_{sc} and the point with the first index in the vicinity of V_{oc}. The second indexed pair contains the point with the first index in the vicinity of I_{sc} and the point with the second index in the vicinity of V_{oc}. The program continues invoking this process until utilising all points between the vicinity of V_{oc} and 50% of I_{sc}. After that, it moves to the second index near I_{sc} and uses it with all points between the vicinity of V_{oc} and 50% of I_{sc} and so forth until using all points between the vicinity of I_{sc} and 50% of V_{oc}. Therefore, all possibilities of points within both ranges are iterated by taking every point in the first range with every point in the second range, apart from the points very near to V_{oc} because

they resulted in unrealistic negative R_s values in some I-V curves. For each pair, the five parameters are calculated using Equations (4.1) to (4.7) and then the theoretical I-V curve is obtained by solving Equation (2.3) for the current at each voltage value from the experimental curve. Equation (2.3) was solved in this work using the Newton Raphson method implemented following the program code published in [76].

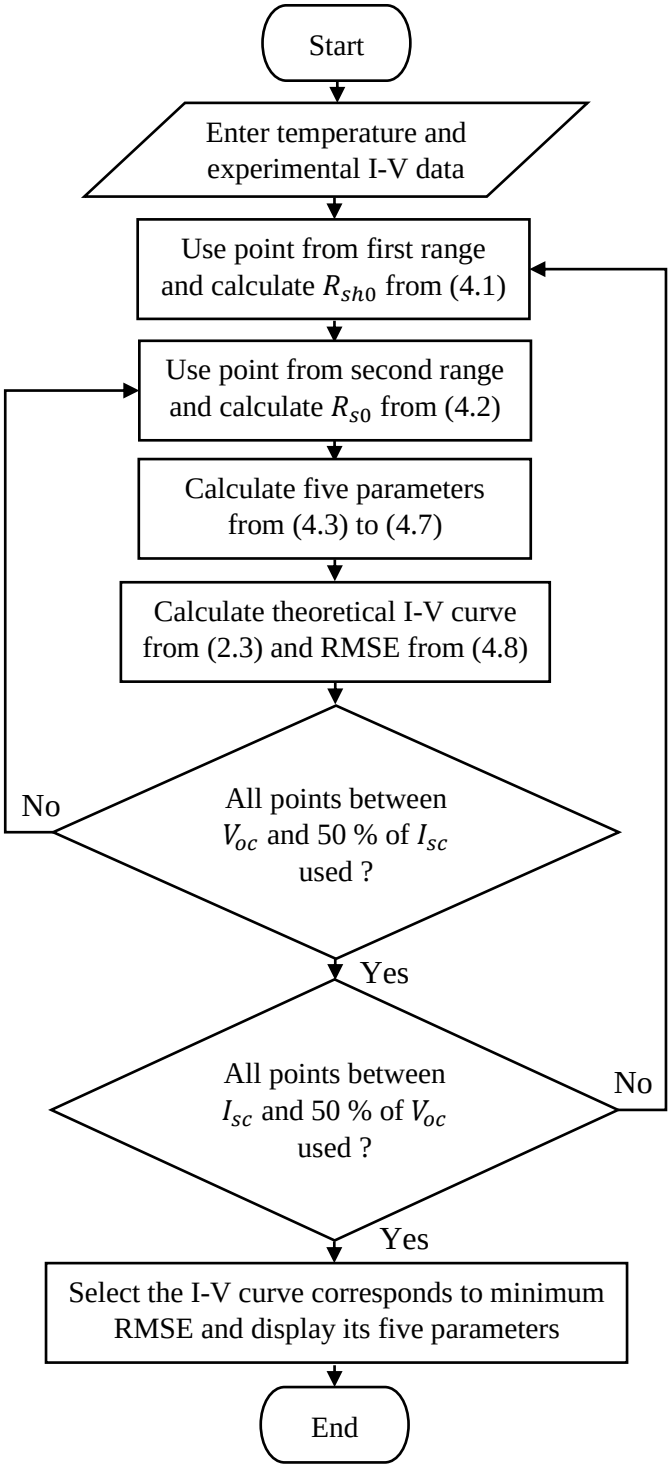

Figure 4.2. A flow chart shows the steps of the developed technique.

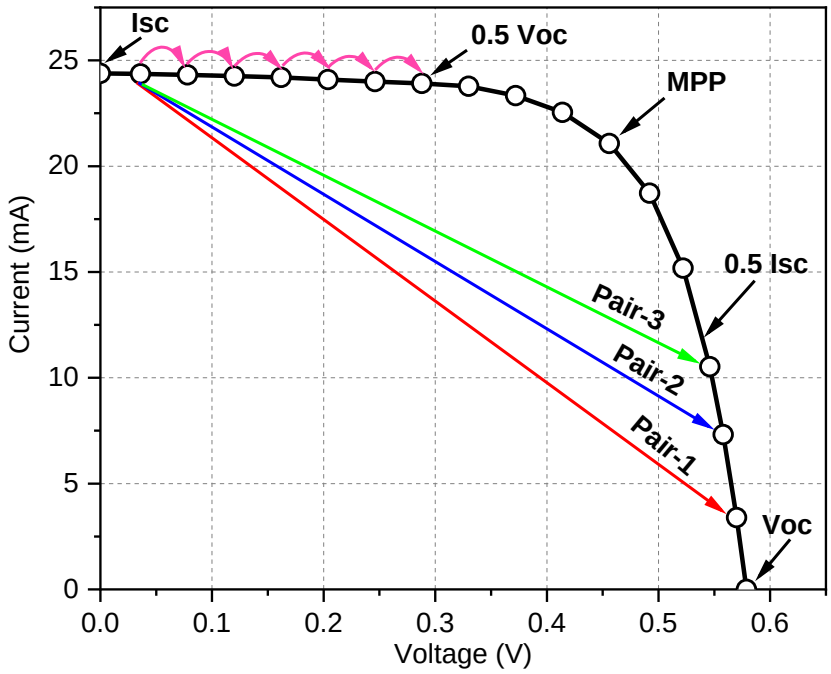

Figure 4.3. I-V curve illustration of points' indexing in the technique for calculations of the slopes of tangent lines.

All obtained theoretical I-V curves are compared with experimental data by calculating the Root Mean Square Error (RMSE) from [80]:

$$RMSE = \sqrt{\frac{\sum_{i=1}^{N} (I_{i,exp} - I_{i,cal})^2}{N}} \tag{4.8}$$

Where $I_{i,exp}$ and $I_{i,cal}$ are respectively the experimental and calculated current values of the i_{th} point. N represents the number of points on the I-V curve data. Finally, the I-V curve corresponds to the smallest RMSE value is considered to be the best theoretical fit and hence its parameters are selected as the PV device equivalent circuit parameters.

It is important to emphasise that the second range (between the vicinity of V_{oc} and 50% of I_{sc}) starting point was selected to be the second index near V_{oc} in all I-V curves solved in this chapter to avoid negative R_s values. Nevertheless, in the other chapters of this thesis, in which many I-V curves' parameters where compared, the starting point was selected to be the third index near V_{oc} because the second index resulted in negative or very small R_s values in some cases as well. However, consistency in this work was guaranteed so that in each comparison, the same starting index of this range was used for all compared I-V curves.

4.3. Results and Discussion

Different experiments were performed and presented in this section to validate the above technique. A mono-Si cell and an a-Si module were characterised using the experimental set-up detailed in Chapter 3. The technique accuracy was first assessed for both PV devices under different operational conditions and compared with other methods from the literature. The computational time and repeatability were then evaluated for the mono-Si solar cell.

The first set of measurements was taken for both PV devices at a fixed device temperature of 25 °C and two irradiance levels of 1000 and 400 W/m². The second set was taken at a fixed irradiance of 1000 W/m² and two temperatures of 20 and 50 °C. Then, the parameters of those experimental cases were first extracted using the developed technique and the calculated I-V curves were obtained. Further, the parameters and I-V curves were also calculated using an iterative method from the literature introduced by De Blas *et al.* [72] and an iterative-numerical method introduced by Villalva *et al.* [37]. The calculated I-V curves from all techniques were finally compared with experimental data. The methods of De Blas and Villalva were briefly discussed in Chapter 2, Section 2.8.3.

De Blas method needs the slopes and therefore it was combined with two approaches to calculate them from experimental data introduced by [52] and [55]. Both approaches suggest using specific locations on the I-V curve for points 2 and 3 as discussed in Section 2.8.1. Moreover, the method of De Blas was implemented in the present work using Equations (2.22) to (2.26**)** with the tolerance of R_s, which determines the accuracy of convergence, was set equals to its minimum value for each I-V curve. This was done in order to ensure high precision in determining the parameters. Furthermore, in each iteration, R_s was incremented with a very small value of 1×10^{-5} Ω for all I-V curves. For instance, when using De Blas method with the approach of [55] for the I-V curve of the mono-Si solar cell that corresponds to an irradiance of 1000 W/m² and a cell temperature of 25 °C, R_s tolerance was set to 4×10^{-4} Ω. This value was achieved by decrementing R_s tolerance by 1×10^{-4} Ω until the minimum value that provides accurate convergence is acquired. Hence, any value less than 4×10^{-4} Ω will cause De Blas method to have convergence errors with this particular I-V curve. The procedure of adjusting R_s tolerance and its incremental value was implemented for all other I-V curves included in this study.

De Blas method was implemented in a MATLAB program code following the illustrations provided in [72], [75].

Villalva method is based on matching the maximum power obtained from experimental data with the calculated maximum power in order to extract R_{sh} from an assumed value of R_s, and then extracting the other parameters as explained in Section 2.8.3. This can be achieved using Equations (2.27) to (2.31), with equating N_s to 1 as this method was applied to a single solar cell in this work. Again, when using this method in this study, the maximum power tolerance and the incremental value of R_s were adjusted to very small values for more precision [76]. For instance, when solving for the parameters of the mono-Si solar cell at an irradiance of 1000 W/m² and a cell temperature of 25 °C, they were set to 1×10^{-8} W and 1×10^{-5} Ω, respectively. This method was programmed in MATLAB following the sample program code provided by the authors in a web page [76].

4.3.1. Accuracy Evaluation

The accuracies of the developed technique and other methods were validated through comparing the calculated I-V curves against experimental data. Three measures of accuracy were calculated, namely, the RMSE the mean absolute percentage error (MAPE) and the absolute percentage error (APE). While the RMSE is calculated from Equation (4.8), the MAPE and APE are obtained respectively from the following two equations [80]:

$$MAPE = \frac{\sum_{i=1}^{N}\{(|I_{i,exp} - I_{i,cal}|)(100/I_{i,exp})\}}{N} \tag{4.9}$$

$$APE = \left(\left|I_{i,exp} - I_{i,cal}\right|\right)\frac{100}{I_{i,exp}} \tag{4.10}$$

The RMSE and MAPE provide a single error value for the whole I-V curve. By contrast, the APE determines the error at each point on the I-V curve and hence accuracy at different parts of the I-V can be visualised. In addition, it is worth noting here that the MAPE and APE contain the current in the denominator. An undefined value will thus be obtained when calculating them at the V_{oc} because of zero current. Therefore, only the V_{oc} point was not included in the MAPE and APE calculations.

4.3.1.1. Results of Mono-crystalline Silicon Solar Cell

The mono-Si solar cell that has an active area of 0.78 cm² was used here. The preparations of the solar cell sample and its test rig were presented in Section 3.3 and a photograph of the cell is given in Figure 3.12 (c). The performance parameters of this solar cell were obtained at STC using the experimental set-up and they were previously given in Table 3.5. The experimental and calculated I-V curves by all methods at two irradiance levels and a constant cell temperature of 25 °C are depicted in Figure 4.4. The calculated five parameters, the RMSE and the MAPE for those experimental cases are presented in Table 4.1.

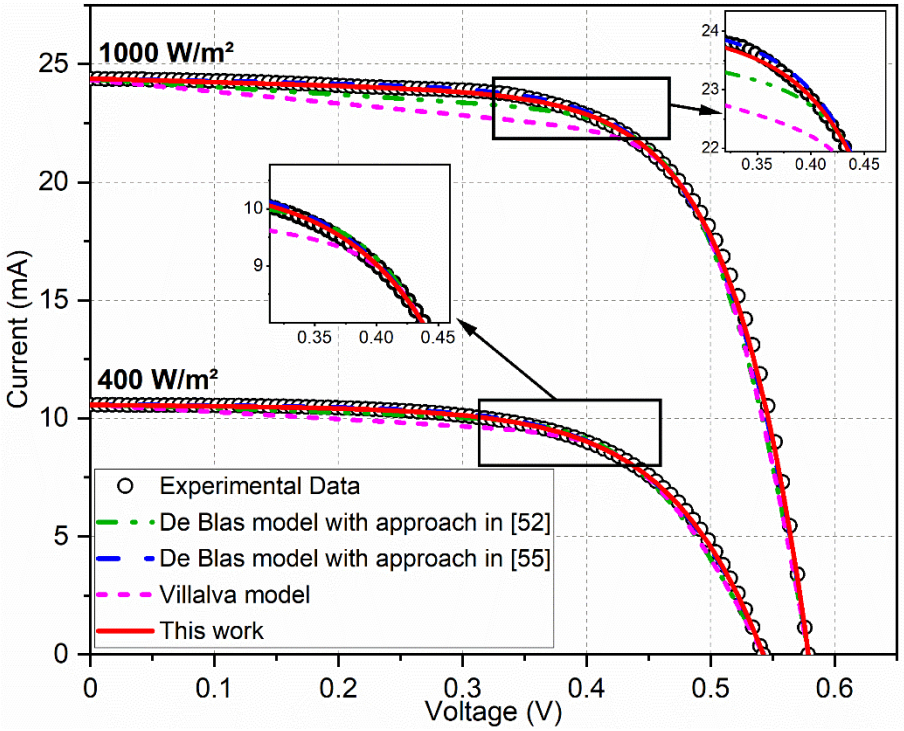

Figure 4.4. Experimental and calculated I-V curves at two irradiance levels and a constant cell temperature of 25 °C applied to the mono-Si solar cell.

Table 4.1. Parameters, RMSE and MAPE between experimental and calculated I-V curves at two irradiance levels and a constant cell temperature of 25 °C applied to the mono-Si solar cell.

Extraction Method	**Irradiance = 1000 W/m²**						
	R_s (Ω)	R_{sh} (kΩ)	n	I_s (μA)	I_{ph} (mA)	RMSE(A)	MAPE (%)
De Blas model with approach in [52]	1.829	0.309	1.271	4.572×10^{-4}	24.532	5.300×10^{-4}	2.897
De Blas model with approach in [55]	0.504	1.015	2.058	0.420	24.399	2.301×10^{-4}	1.093
Villalva model	2.133	0.198	1	3.575×10^{-6}	24.650	7.572×10^{-4}	3.976
This work	0.344	0.687	2.060	0.418	24.400	1.444×10^{-4}	0.694
	Irradiance = 400 W/m²						
De Blas model with approach in [52]	5.968	0.590	1.363	1.822×10^{-3}	10.682	2.267×10^{-4}	3.150
De Blas model with approach in [55]	1.391	3.353	2.540	2.558	10.577	7.501×10^{-5}	0.971
Villalva model	6.821	0.325	1	6.170×10^{-6}	10.797	3.569×10^{-4}	4.534
This work	0.922	2.163	2.584	2.913	10.580	4.545×10^{-5}	0.605

It can be seen from the above results that the developed technique in this work is more accurate than iterative and iterative-numerical methods included in this comparison at both irradiance levels. The I-V curve produced by the developed technique is the closest one to experimental data as shown in Figure 4.4. This superior accuracy can also be revealed from the minimum RMSE and MAPE among all methods in Table 4.1. It can also be observed that the method of De Blas combined with the approach of [55] is also reasonably accurate with a MAPE of about 1% in both experimental cases. By contrast, De Blas method using the approach of [52] and also Villalva method showed larger deviations from experimental data. The deviation of the former may be attributed to using a point away from V_{oc} (50% of I_{sc}) to calculate R_{s0}. This can be explained by the much less error provided by the approach of [55], which also used De Blas method but with a point located at only 20% of I_{sc}. The largest deviation of Villalva method from experimental data might be postulated to assuming an ideality factor of 1, because this method does not provide a way to calculate it. This parameter should take a value larger than 1 for a better representation of real solar cells [1]. Furthermore, this method uses only the MPP as a fitting parameter, rendering it not accurate at other regions of the I-V curve.

In terms of the calculated parameters given in Table 4.1, they have a large discrepancy due to the different approaches used, except for I_{ph}. Nevertheless, the developed technique and that of De Blas with the approach of [55] resulted in similar parameter

values compared with the higher discrepancy occurred due to the other techniques. This can be explained by the fact that in some I-V curves, the fixed point used to calculate R_{s0} by the approach of [55] (20% of V_{oc}) is also selected by the proposed technique as the best point in this range. This will be further interpreted later from Figure 4.6.

In the case of an irradiance of 1000 W/m² and a cell temperature of 25 °C, the APE was evaluated at each point on the I-V curve, except the V_{oc} point, and depicted in Figure 4.5. These results also validate the effectiveness of the developed technique in terms of accuracy. It shows a small APE compared to the other approaches, especially at points near V_{oc}. It can also be noted that the APE at MPP is very small for all techniques with the developed technique being the most accurate as depicted by the zoom-in view in Figure 4.5. Moreover, although De Blas method with the approach of [55] has also very small APE, the developed technique surpasses it significantly between the MPP and V_{oc} point.

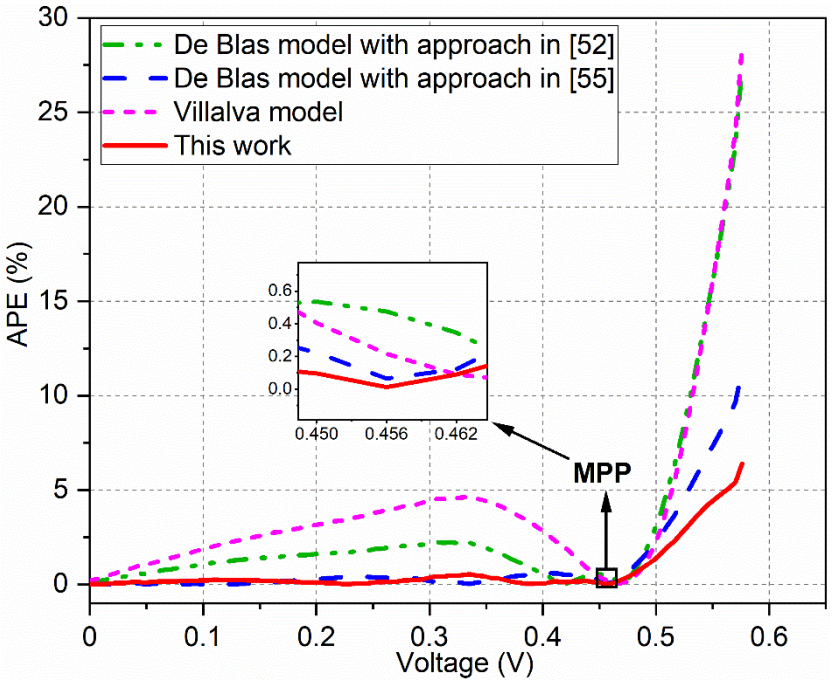

Figure 4.5. APE at each point (except the open circuit voltage point) between experimental and calculated I-V curves at an irradiance of 1000 W/m² and a cell temperature of 25 °C applied to the mono-Si solar cell.

In addition to accurately calculating the parameters by the method of Phang *et al.* [53], the developed technique also allows to determine and visualise the RMSE between experimental and calculated I-V curves for every pair of points 2 and 3 (see Figures 2.11,

4.1 and 4.3). Thereby allowing the technique to be used in investigating the best locations of those points for any type of solar cells. This is demonstrated in Figure 4.6, which shows a plot in MATLAB for the points pairs' index versus the RMSE for the mono-Si solar cell under an irradiance of 1000 W/m² and at a cell temperature of 25 °C. For this I-V curve, the number of data points used for points 2 and 3 was 48 and 6, respectively. This brings the total number of pairs used to calculate the parameters to 288. The numbering sequence of the pairs in Figure 4.6 follows the explanation given in Section 4.2 and shown in the example of Figure 4.3. Each vertical line (with black square symbols) in Figure 4.6 represents the RMSEs of the calculated I-V curves using one point from point-2 range that is combined with 6 points from point-3 range. The first vertical line in the left-hand side of the graph represents point-2 with the first index near I_{sc}. Whereas the last vertical line in the right-hand side represents point-2 with the nearest voltage to 50% of V_{oc}. The lowest point in each vertical line represents point-3 with the second[2] index near V_{oc}. Whereas the uppermost point represents point-3 with the nearest current to 50% of I_{sc}.

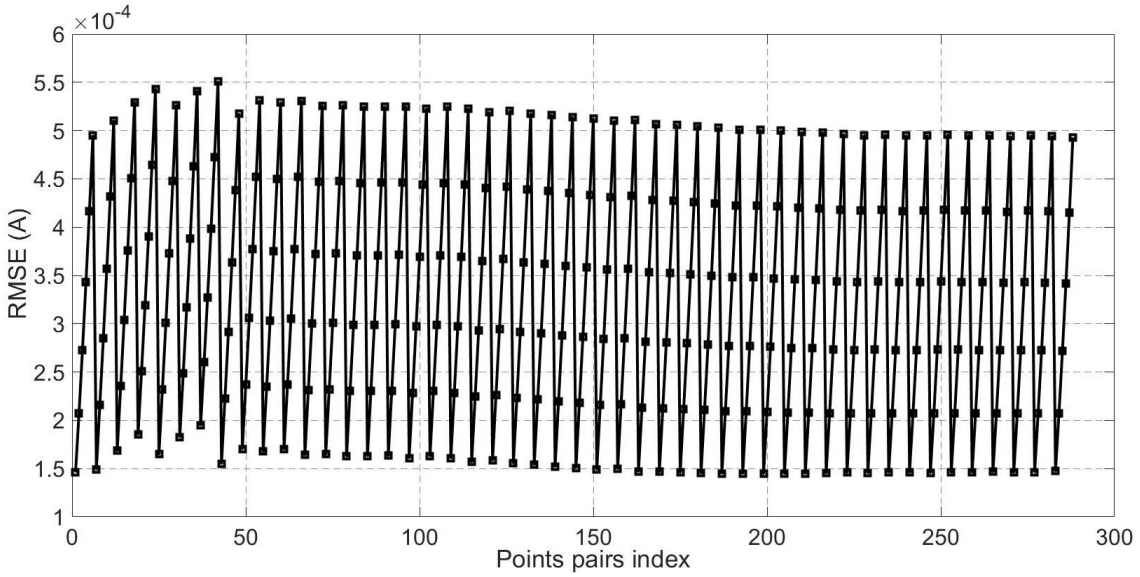

Figure 4.6. I-V curve points 2 and 3 pairs' index versus the RMSE between experimental and calculated I-V curves at an irradiance of 1000 W/m² and a cell temperature of 25 °C applied to the mono-Si solar cell.

An interesting feature can be noticed from Figure 4.6, which is the fact that the accuracy of determining the parameters is greatly affected by the selection of point-3. By contrast, there is only a negligible effect on the accuracy by point-2 selection. Another fact can be

[2] First index near V_{oc} was not used due to the issue of negative or very small R_s value as commented previously at the end of Section 4.2.

deduced is that the closer point-3 to V_{oc} is, the more accurate the parameters extraction will be. This explains why the accuracy of De Blas method with the approach of [55] is similar to that of the developed technique, because in some I-V curves both techniques take the same location for point-3.

The experimental and corresponding calculated I-V curves at two cell temperatures and a constant irradiance of 1000 W/m² are shown in Figure 4.7. Table 4.2 presents the calculated parameters, the RMSE and the MAPE. Similar to the case of two irradiance levels and a fixed temperature shown previously, the proposed technique also provided good performance at low and high temperatures exceeding the accuracy of the other methods as shown in Figure 4.7 and Table 4.2. Furthermore, same findings have also been noticed regarding the large deviation from experimental data resulted from methods of Villalva and De Blas with the approach of [52]. De Blas method with approach of [55], on the other hand, provided a very close accuracy to the developed technique due to the previously mentioned reason of selecting the same point-3 by both techniques. In addition, a high discrepancy in the parameters (except I_{ph}) obtained by different techniques can be observed in Table 4.2. Note that in the case of 20 °C temperature, De Blas method with approach of [55] resulted in a negative value of R_s.

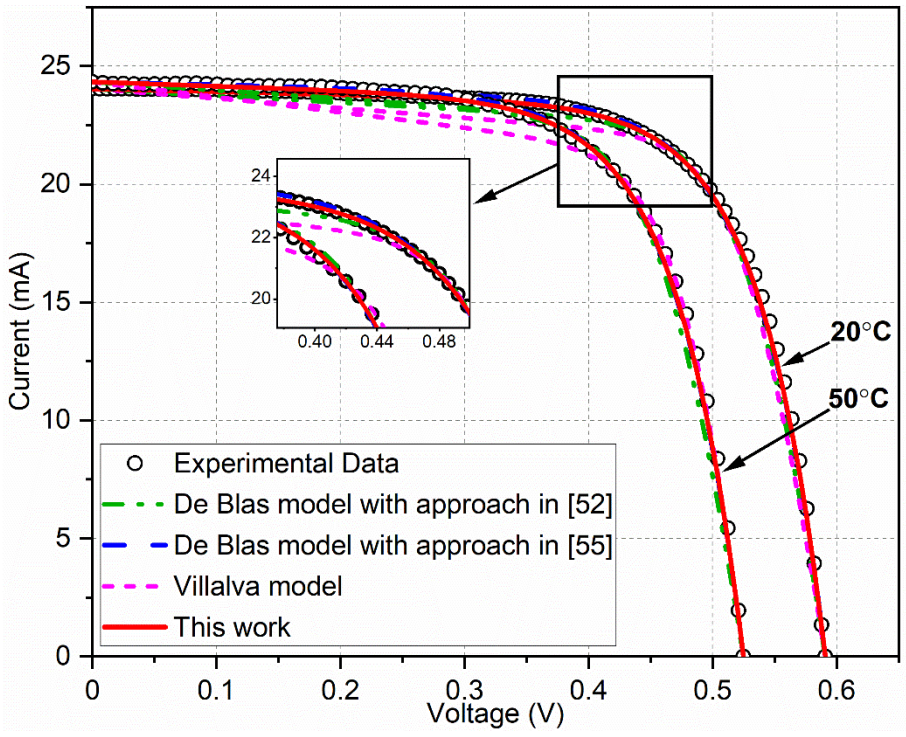

Figure 4.7. Experimental and calculated I-V curves at two cell temperatures and a constant irradiance of 1000 W/m² applied to the mono-Si solar cell.

Table 4.2. Parameters, RMSE and MAPE between experimental and calculated I-V curves at two cell temperatures and a constant irradiance of 1000 W/m² applied to the mono-Si solar cell.

Extraction Method	**Temperature = 20 °C**						
	R_s (Ω)	R_{sh} (kΩ)	n	I_s (μA)	I_{ph} (mA)	RMSE(A)	MAPE (%)
De Blas model with approach in [52]	1.408	0.341	1.260	1.938×10^{-4}	24.144	5.261×10^{-4}	2.755
De Blas model with approach in [55]	-0.020	1.752	2.113	0.370	24.045	2.056×10^{-4}	0.952
Villalva model	1.831	0.241	1	1.518×10^{-6}	24.228	7.221×10^{-4}	3.755
This work	0.084	0.796	1.979	0.172	24.048	1.752×10^{-4}	0.829
	Temperature = 50 °C						
De Blas model with approach in [52]	1.577	0.281	1.101	8.358×10^{-4}	24.469	6.071×10^{-4}	3.190
De Blas model with approach in [55]	0.066	0.909	1.877	1.035	24.334	2.492×10^{-4}	1.213
Villalva model	1.041	0.155	1	1.384×10^{-4}	24.497	7.502×10^{-4}	3.194
This work	0.136	0.573	1.786	0.613	24.339	2.320×10^{-4}	1.201

4.3.1.2. Results of Amorphous Silicon PV Module

In order to validate the developed technique with I-V curves that have a different shape from that of crystalline-Si solar cells, an a-Si PV module with an active area of 28.78 cm² (5.3 cm x 5.43 cm) was used in this work. This SANYO AM-8701 module comprises of 7 series-connected solar cells. According to its data sheet [195], it has a maximum power of 190 mW at STC, corresponding to a current and voltage of respectively 41.2 mA and 4.6 V. In this work, this module used the same experimental test rig of the single solar cells presented in Section 3.3.3. However, the thermocouple used for temperature measurements was attached to the back of the module same as other modules used in this research as explained in Section 3.5.1. In Figure 4.8, a photograph of the module under the characterisation experiment is shown.

The I-V curves of the a-Si module were measured under different operational conditions. For the method of De Blas with approaches of [52] and [55], the adjustments of R_s tolerance and its incremental value was done in the same way as that of the mono-Si cell discussed previously. Villalva method was found to have convergence issues with this shape of I-V curves and so did not provide a solution for the parameters. Therefore, it has been excluded from the results of the a-Si module presented below. Depicted in Figure 4.9 are the I-V curves taken at a constant module temperature of 25 °C and two irradiance levels. The corresponding parameters and errors comparisons are given in Table 4.3.

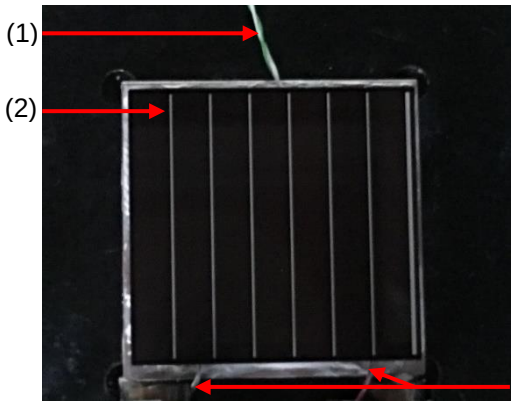

Figure 4.8. The a-Si PV module used in the experiments to validate the parameters extraction technique.

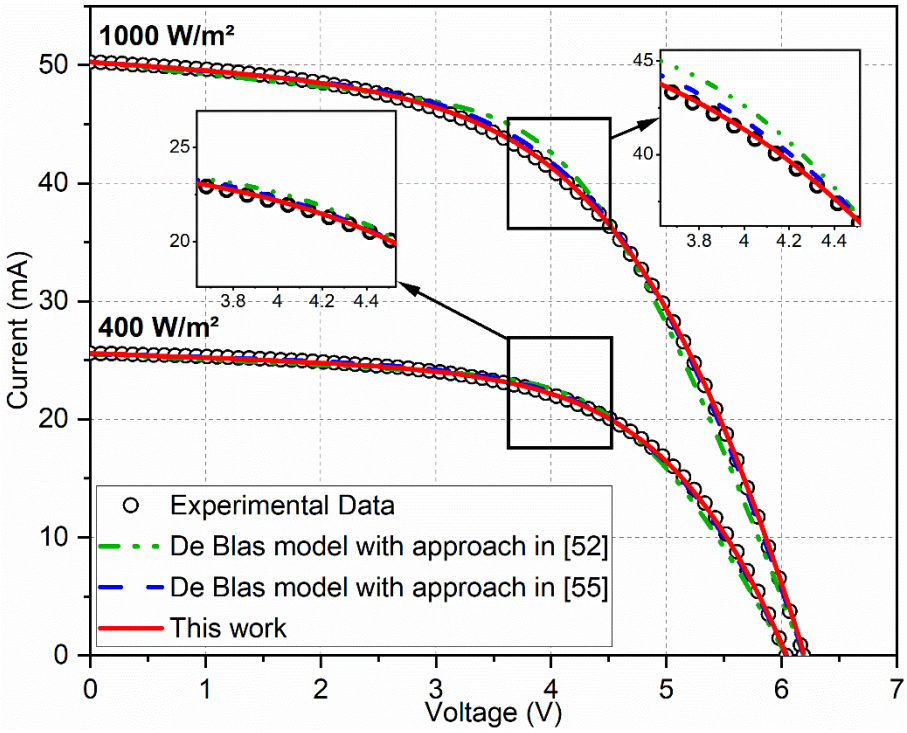

Figure 4.9. Experimental and calculated I-V curves at two irradiance levels and a constant module temperature of 25 °C applied to the a-Si PV module.

Table 4.3. Parameters, RMSE and MAPE between experimental and calculated I-V curves at two irradiance levels and a constant module temperature of 25 °C applied to the a-Si PV module.

Extraction Method	**Irradiance = 1000 W/m²**						
	R_s (Ω)	R_{sh} (kΩ)	n	I_s (μA)	I_{ph} (mA)	RMSE(A)	MAPE (%)
De Blas model with approach in [52]	30.486	0.945	1.975	1.222×10^{-3}	51.889	9.409×10^{-4}	3.308
De Blas model with approach in [55]	18.497	1.486	3.804	5.480	50.888	3.466×10^{-4}	1.043
This work	14.011	1.707	4.622	27.144	50.716	1.082×10^{-4}	0.771
	Irradiance = 400 W/m²						
De Blas model with approach in [52]	37.989	2.134	2.175	4.531×10^{-3}	26.048	5.355×10^{-4}	3.288
De Blas model with approach in [55]	17.088	3.539	3.820	3.634	25.712	2.078×10^{-4}	1.255
This work	13.380	2.936	3.997	5.269	25.712	9.912×10^{-5}	0.528

The above shown results in Figure 4.9 and Table 4.3 reveal that the developed technique is capable of producing accurate parameters for PV devices with a different I-V curve shape from that of crystalline-Si solar cells. The calculated I-V curves nearly coincide with the experimental ones rendering the proposed technique to have the best accuracy among the compared methods. This can also be seen from Table 4.3, showing a very small MAPE, which is less than 1% under both irradiance levels. The RMSE is also very low compared to the other two approaches included in the comparison. Moreover, using De Blas method with the approach of [55] is more accurate than using it with the approach of [52] because the former uses closer point to V_{oc} than the latter as previously stated in the case of the mono-Si cell. In addition, except for I_{ph}, the discrepancy in the parameters calculated by different methods can be clearly perceived from Table 4.3.

The APE at each point on the I-V curves, except the V_{oc} point, is shown for the case of 1000 W/m² and 25 °C in Figure 4.10. Clearly, the proposed technique has better accuracy with a very small APE for voltages up to about 5.5 V. However, the APE becomes larger only near V_{oc}. On the other hand, the other two approached shows a fluctuating APE. At voltages from 0 to about 2.5 V, De Blas method using approach in [55] has similar accuracy to the proposed technique. However, at the MPP, the proposed work performs much better than the other methods as shown in the zoom-in view in Figure 4.10.

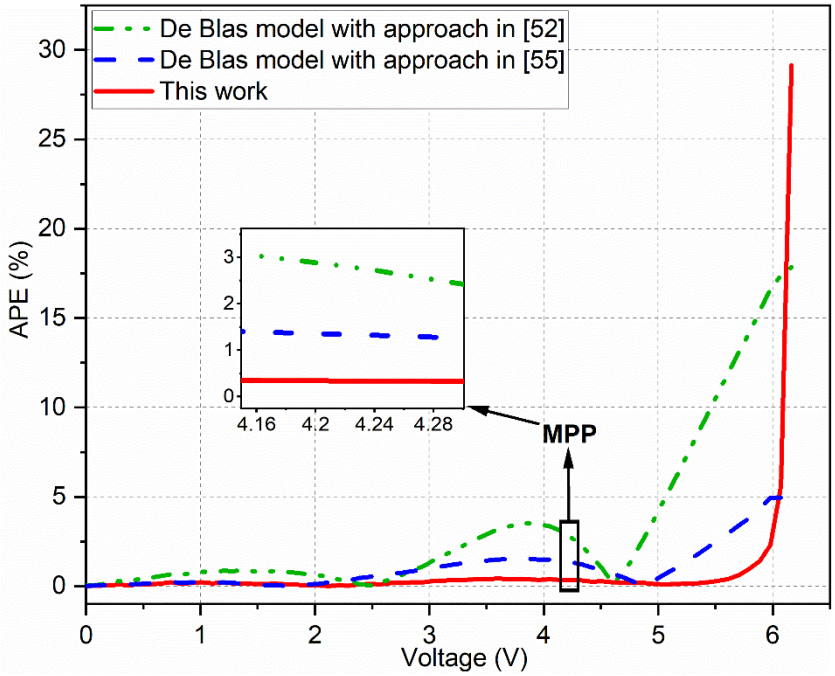

Figure 4.10. APE at each point (except the open circuit voltage point) between experimental and calculated I-V curves at an irradiance of 1000 W/m² and a module temperature of 25 °C applied to the a-Si PV module.

In order to visualise the RMSE for each pair of points used to obtain the slopes of the a-Si module, all the pairs' indices were plotted versus the RMSE of the corresponding I-V curve. This is demonstrated in Figure 4.11 for the case of 1000 W/m² irradiance and 25 °C module temperature. In this case, the number of data points used for point-2 and point-3 was 34 and 10, respectively. Thus, the total number of pairs used was 340 pairs. The numbering sequence of the pairs in Figure 4.11 follows the same procedure as the one of the mono-Si solar cell shown in Figure 4.6 and explained in the previous section.

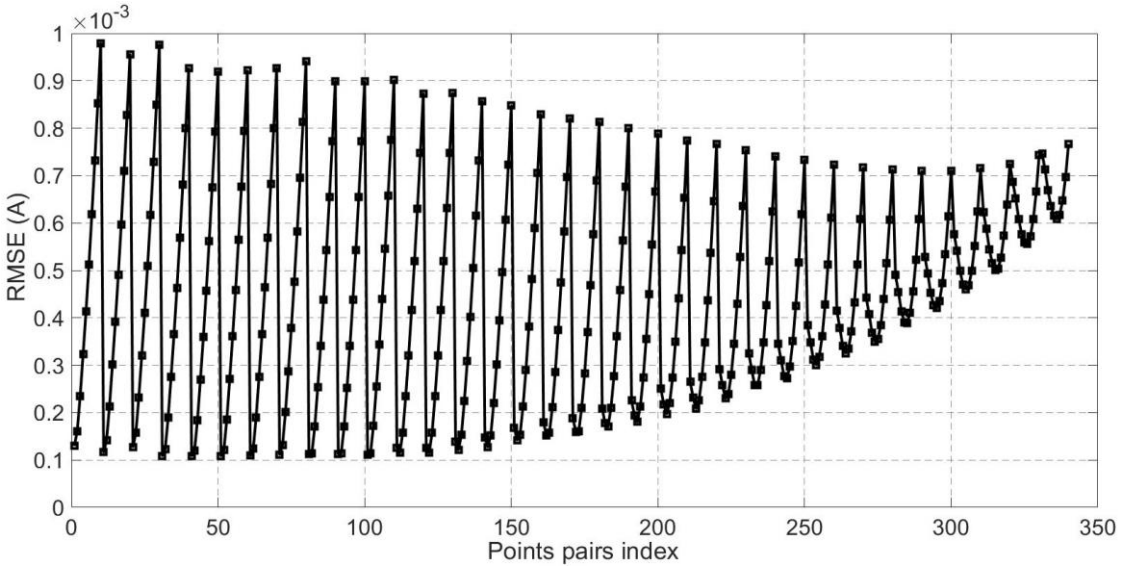

Figure 4.11. I-V curve points 2 and 3 pairs' index versus the RMSE between experimental and calculated I-V curves at an irradiance of 1000 W/m² and a module temperature of 25 °C applied to the a-Si PV module.

Clearly, the behaviour is different from the mono-Si shown in Figure 4.6. Here, the accuracy is better for point-2 when points away from the I_{sc} are used (right-hand side of the graph in Figure 4.11). The accuracy, however, deteriorates as point-2 is closer to I_{sc} (left-hand side of the graph in Figure 4.11). On the other hand, there is a common feature between both devices, which is the fact that the accuracy is better for point-3 having points near the V_{oc} than points that are away from it. This brings a conclusion that the selection of point-3 is much more crucial than that of point-2 for mono-Si solar cells parameters extraction accuracy. Whereas both points 2 and 3 selections are crucial for a-Si modules.

The parameters of the a-Si module were also extracted under two different module temperatures and a constant irradiation of 1000 W/m². The results are given in Figure 4.12 and Table 4.4. Similar to the case of a constant module temperature and two irradiance levels, the technique developed in this work achieved the best agreement between the theoretical and experimental data under the two module temperatures with a MAPE of less than 1%. The other two approaches, on the other hand, provided poorer performances with a MAPE of about 3% and 1% for De Blas model with approaches of [52] and [55], respectively. Further, similar to all previous results of the mono-Si cell and a-Si module, the results in Table 4.4 indicate a high discrepancy in the calculated parameters by different techniques, although this is not the case for I_{ph}.

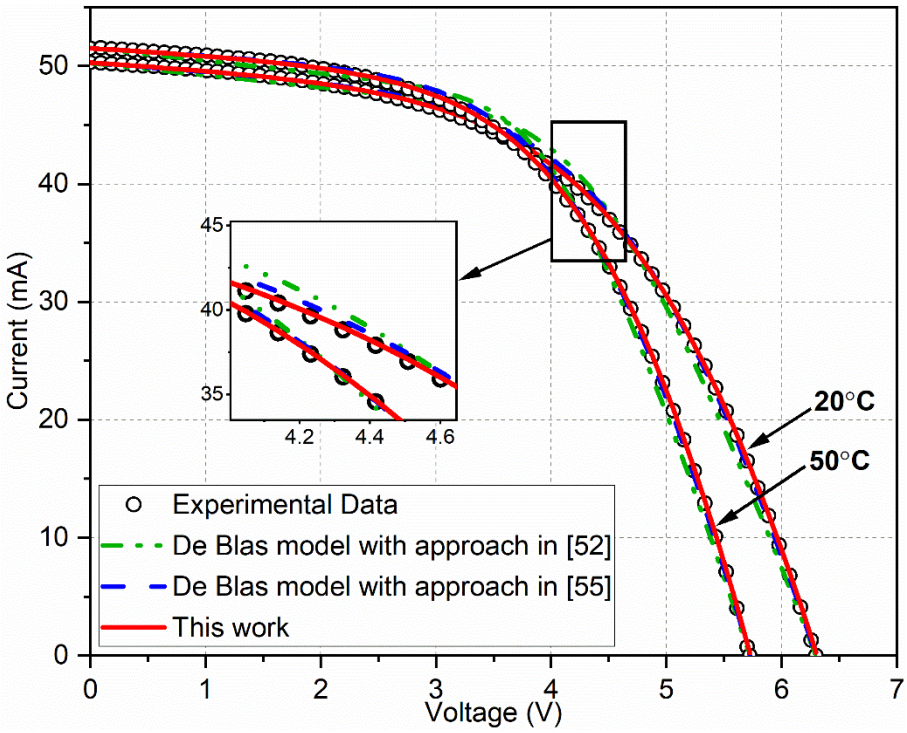

Figure 4.12. Experimental and calculated I-V curves at two module temperatures and a constant irradiance of 1000 W/m² applied to the a-Si PV module.

Table 4.4. Parameters, RMSE and MAPE between experimental and calculated I-V curves at two module temperatures and a constant irradiance of 1000 W/m² applied to the a-Si PV module.

Extraction Method	**Temperature = 20 °C**						
	R_s (Ω)	R_{sh} (kΩ)	n	I_s (μA)	I_{ph} (mA)	RMSE(A)	MAPE (%)
De Blas model with approach in [52]	31.157	0.952	2.076	1.601×10^{-3}	51.932	9.452×10^{-4}	3.309
De Blas model with approach in [55]	19.296	1.383	3.881	4.802	50.983	3.628×10^{-4}	1.091
This work	14.229	1.723	4.872	31.150	50.742	1.107×10^{-4}	0.601
	Temperature = 50 °C						
De Blas model with approach in [52]	27.223	0.900	1.510	1.671×10^{-4}	53.074	8.714×10^{-4}	3
De Blas model with approach in [55]	17.962	1.605	2.891	1.877	52.090	3.731×10^{-4}	1.068
This work	14.211	1.682	3.470	10.138	51.971	1.241×10^{-4}	0.865

4.3.2. Computational Time Evaluation

The time taken for the developed technique to compute the equivalent circuit parameters was determined and compared with the other methods. Indicatively, it is presented here for the mono-Si solar cell and the a-Si PV module under the case of 1000 W/m² irradiance and 25 °C device temperature. All techniques were run on a computer that has a RAM of

8 gigabyte and a core-i5 processor. The time was obtained using the MATLAB tic-toc command and shown in Table 4.5.

It can be seen that the two approaches used with De Blas method took almost the same time for both PV devices. On the other hand, the proposed technique resulted in a longer time of approximately 0.08 and 0.09 second, respectively for the mono-Si solar cell and the a-Si PV module. The time taken for Villalva method, however, is very high compared with the other methods due to employing an iterative-numerical solution. Although the time taken by the proposed technique is longer than that taken by De Blas method, it is still very short when compared with Villalva method and when considering the large number of processed I-V curves, which are respectively 288 and 340 for the mono-Si solar cell and the a-Si PV module. The time taken to calculate the parameters is well below 0.1 second for both PV devices because of the simplicity of the added iterative program to the analytical method of Phang *et al*. [53].

Table 4.5. Time taken by the different methods to compute the five parameters at an irradiance of 1000 W/m² and a device temperature of 25 °C applied to both PV devices.

Extraction method	Computational time (seconds)	
	Mono-Si cell	a-Si module
De Blas model with approach in [52]	0.0124	0.0130
De Blas model with approach in [55]	0.0121	0.0124
Villalva model	16.8328	/
This work	0.0770	0.0872

4.3.3. Repeatability Tests of the Technique

In order to confirm that the parameters extracted by the developed technique are reliable and repeatable, three experimental sets were carried out. They will be called here-in: the best scenario, the medium scenario and the worst scenario. The best scenario experiments were performed on the 0.78 cm² mono-Si solar cell used in the previous sections. Whereas the medium and worst scenarios were performed on another solar cell from the same manufacturing batch and with the same active area. All I-V curve measurements were taken under an irradiance of 1000 W/m² and at a cell temperature of 25 °C.

These three experiments will be also useful in the other investigations of this research as they will demonstrate if the technique is capable of producing different parameters at different experimental cases, which are switching the light source ON and OFF, re-positioning the cell on the test rig and re-soldering its contacts. Furthermore, they will allow to perceive and compare the RSD errors of parameters caused by the different experimental cases.

4.3.3.1. Best Repeatability-Scenario

The best scenario is assessing the repeatability of the technique applied to four I-V curves taken in sequence at one set of measurements[3] under the same irradiance and temperature conditions, and without re-positioning the cell or re-soldering its contacts. The mean value of each parameter and the RSD were then calculated in Microsoft Excel (Equations (3.4) and (3.5)). Moreover, the experimental and theoretical I-V curves of each test were compared in terms of the RMSE and MAPE. Table 4.6 shows the parameters' values for each test along with the mean and RSD.

Table 4.6. The best repeatability-scenario parameters of four I-V curves including the mean and RSD.

Parameter	Test 1	Test 2	Test 3	Test 4	Mean	RSD (%)
R_s (Ω)	0.33	0.31	0.31	0.32	0.32	±3
R_{sh} (kΩ)	0.65	0.67	0.67	0.71	0.68	±3
n	1.963	1.964	1.967	1.969	1.965	±0.1
I_s (μA)	0.240	0.241	0.245	0.248	0.243	±1.4
I_{ph} (mA)	23.745	23.739	23.736	23.739	23.740	±0.01

As shown in Table 4.6, the parameters' values are close to each other with a considerably small RSD. The largest RSD was recorded for R_{sh} and R_s with ±3% each. I_s has also a noticeable error of ±1.4%. This might be attributed to the fact that these parameters are very sensitive to measurement noise and small distortions in the I-V curve, especially R_s and R_{sh} as their extraction is based on the slopes. However, the error does not exceed ±3% for all parameters which confirms that the calculations using the developed technique produce repeatable parameters of I-V measurements at the best scenario. The

[3] One set of measurements are measurements taken in sequence while the light source and all test equipment are still turned ON.

accuracy of the technique can be seen in Figure 4.13, which shows a good agreement between experimental and calculated I-V curves of the four tests. This consistency is also depicted by the small RMSE and MAPE in Table 4.7. The accuracy is almost the same in all tests with the MAPE does not exceed 1.2%.

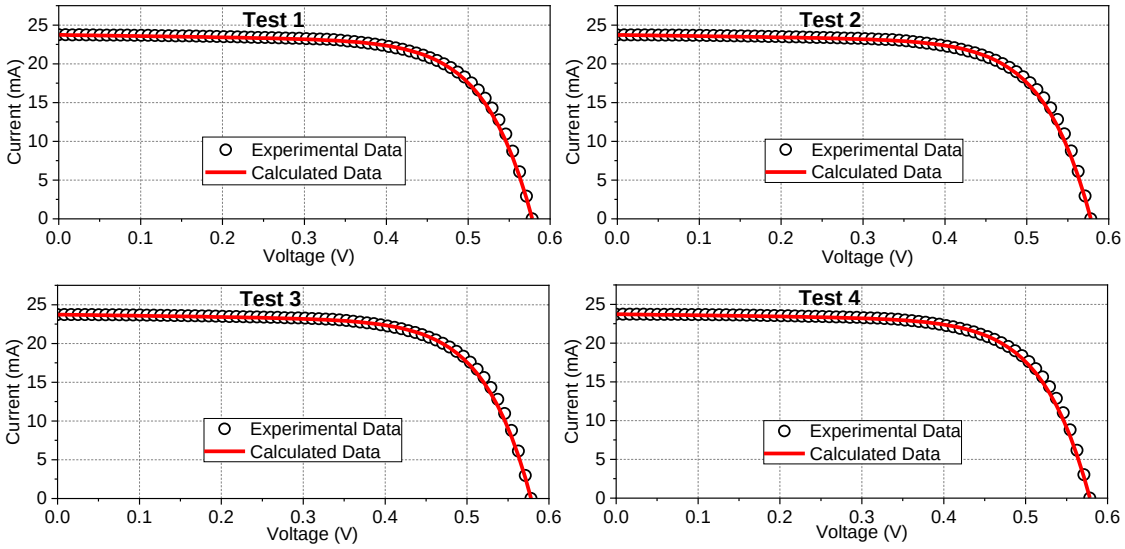

Figure 4.13. Experimental and calculated I-V curves of the four tests of the best repeatability-scenario.

Table 4.7. The RMSE and MAPE between the experimental and calculated I-V curves of the four tests of the best repeatability-scenario.

Test No.	RMSE (A)	MAPE (%)
1	2.634×10^{-4}	1.173
2	2.619×10^{-4}	1.171
3	2.621×10^{-4}	1.181
4	2.690×10^{-4}	1.193

4.3.3.2. Medium Repeatability Scenario

The medium scenario is assessing the technique repeatability in calculating the parameters of four I-V tests under the same irradiance and temperature conditions, but when re-positioning the cell on the test rig. Those tests were performed on a cell from the same batch as the one used in the best scenario tests. For each test, the cell was taken out and then placed again on the heat exchanger. In addition, all experimental equipment were switched OFF and then ON again. Table 4.8 presents the parameters of the four tests under this condition alongside with the mean and RSD.

Table 4.8. The medium repeatability-scenario parameters of four I-V curves including the mean and RSD.

Parameter	Test 1	Test 2	Test 3	Test 4	Mean	RSD (%)
R_s (Ω)	0.58	0.43	0.37	0.34	0.43	±21
R_{sh} (kΩ)	0.51	0.62	0.60	0.74	0.62	±13
n	1.6	2.3	2.2	2.6	2.2	±17
I_s (μA)	0.02	1.14	1.02	4.28	1.61	±99
I_{ph} (mA)	24.7	24.8	24.6	25.1	24.8	±0.7

As shown in Table 4.8, all parameters showed larger RSD than those of the best repeatability scenario shown in Table 4.6. It can be deduced from these results that re-positioning the cell and switching the test equipment OFF and ON can significantly affect the repeatability of the parameters. These results confirm that the technique is capable of detecting this effect.

Figure 4.14 illustrates a comparison between experimental and calculated I-V curves of the four tests. It can be observed that the curvature of the I-V curve near the MPP is slightly changed due to re-positioning the cell and switching the set-up OFF and ON. This change is adequately detected by the technique as shown by the consistency between the experimental and calculated I-V curves in Figure 4.14. This agreement is also shown by the RMSE and MAPE in Table 4.9. The MAPE of all tests is only around 1%.

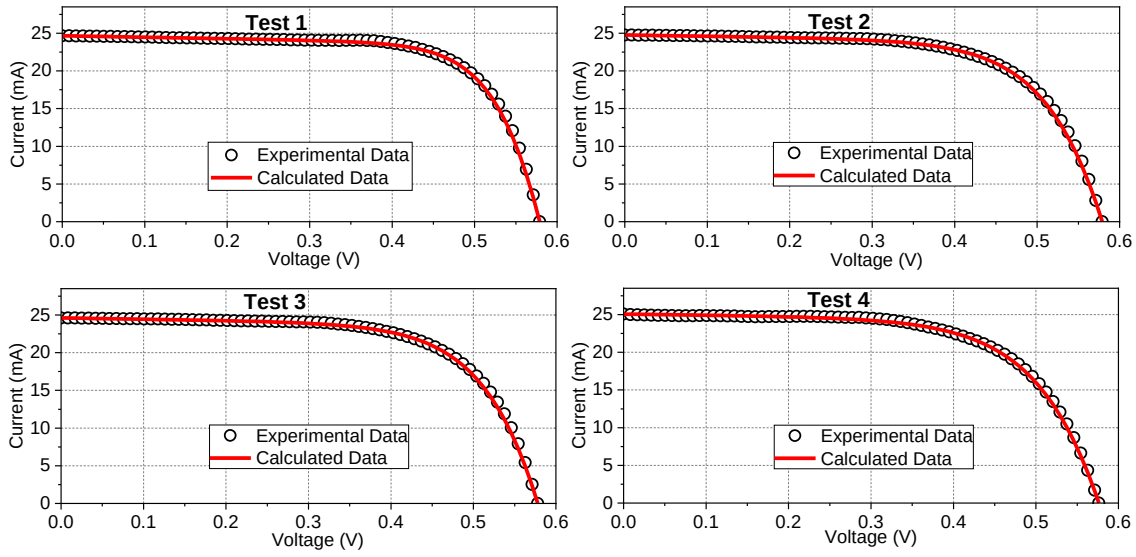

Figure 4.14. Experimental and calculated I-V curves of the four tests of the medium repeatability-scenario.

Table 4.9. The RMSE and MAPE between the experimental and calculated I-V curves of the four tests of the medium repeatability-scenario.

Test No.	RMSE (A)	MAPE (%)
1	2.364×10^{-4}	0.953
2	2.184×10^{-4}	1.000
3	2.247×10^{-4}	1.011
4	1.885×10^{-4}	1.019

4.3.3.3. Worst Repeatability Scenario

This scenario constitutes the worst case, which is re-soldering the cell's contacts before each test in addition to re-positioning the cell and switching all test equipment OFF and ON. The cell used in the medium scenario tests was also used here. As explained previously in Section 3.3.2, to create the cell negative front contact, a ribbon wire was soldered along the front busbar to draw current from the cell. For the back positive contact, the copper part of the PCB was soldered to the back contact sheet of the cell. Before each test, the set-up equipment was switched OFF and the cell front and back contacts were re-soldered. It is to be noted here that to avoid cell damage, soldering of the back contact for each test was done only by heating the cell on the hotplate until the soldering flux melted and then leaving the cell to cool down. For each test, I-V curve measurement was taken and then the technique repeatability and accuracy were obtained. Table 4.10 demonstrates the changes in parameters during the four tests depicted by the RSD.

Table 4.10. The worst repeatability-scenario parameters of four I-V curves including the mean and RSD.

Parameter	Test 1	Test 2	Test 3	Test 4	Mean	RSD (%)
R_s (Ω)	0.6	0.5	0.6	0.1	0.4	±51
R_{sh} (kΩ)	0.51	0.49	0.47	0.45	0.48	±5
n	1.6	1.7	1.6	2.0	1.7	±11
I_s (μA)	0.02	0.04	0.01	0.42	0.12	±138
I_{ph} (mA)	24.7	24.7	25.2	24.3	24.7	±1.3

The deviation between most of the parameters became noticeably high in this scenario, which is expected because re-soldering the contacts could greatly affect the parameters, especially R_s. By contrast, R_{sh} was not significantly affected by re-soldering the cell's contacts. It is evident from these results that the technique is still able to detect changes

in parameters caused by re-soldering. Moreover, the slight change in I-V curve shape due to re-soldering the contacts is also accurately represented by the technique as shown by the agreement between experimental and calculated I-V curves in Figure 4.15. Table 4.11. provides the RMSE and MAPE, which is in the vicinity of only 1% for all tests.

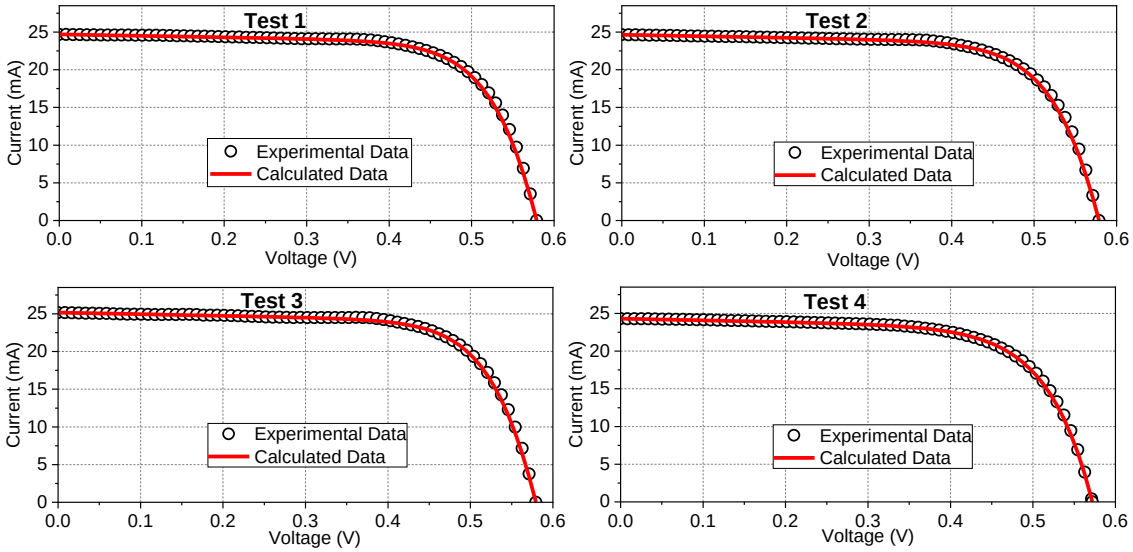

Figure 4.15. Experimental and calculated I-V curves of the four tests of the worst repeatability-scenario.

Table 4.11. The RMSE and MAPE between the experimental and calculated I-V curves of the four tests of the worst repeatability-scenario.

Test No.	RMSE (A)	MAPE (%)
1	2.405×10^{-4}	1.016
2	2.375×10^{-4}	0.972
3	2.312×10^{-4}	0.957
4	1.539×10^{-4}	0.890

4.4. Summary

It has been proved in this chapter that the analytical parameters extraction methods, which are known to be less accurate than iterative and iterative-numerical methods, can actually become more accurate if the suitable points used to calculate the slopes are properly selected. The accuracy of the simple analytical method of Phang *et al.* [53] was improved by adding a simple iterative process that optimises the selection of the points to determine the slopes based on the minimum RMSE. The developed technique is based on entering the points between the vicinity of I_{sc} and 50% of V_{oc} and the points between the vicinity of V_{oc} and 50% of I_{sc}. Thereby testing nearly all possibilities to calculate the slopes and

then selecting the parameters that best fits the theoretical I-V curve with the experimental one. Therefore, for any I-V curve, there is only one pair of points (see Figure 4.3) that result in parameters which provide the best fit between theoretical and experimental I-V curves.

The developed technique was validated using two PV devices with different I-V curve shapes under different operational conditions and the results were compared with an iterative and an iterative-numerical methods from the literature. The findings revealed that the proposed technique has superior accuracy. Despite the increased computational time due to adding the designed program, the technique still features a high level of accuracy with a low level of complexity. There are no convergence issues associated with the technique, which are common in iterative and iterative-numerical methods. Furthermore, the technique presented here can be utilised as a tool to investigate the optimum points' locations for slopes calculations of any type of PV devices, thereby allowing to develop new empirical equations for the slopes in order to calculate the parameters from data sheet information only. The technique can also be successfully utilised with any other parameters extraction method that rely on the slopes.

The findings of this work also imply that the five-parameter model could be sufficiently accurate for characterising PV devices if the precise parameters are extracted. Hence, the results confirm the known fact that this model compromises accuracy and simplicity. Moreover, the parameters calculated by the developed technique are repeatable when calculating them from I-V curves measured in sequence at one set of measurements as shown in the best scenario. In addition, when switching the test equipment OFF and ON, re-positioning the cell and re-soldering its contacts, the changes in parameters caused are adequately detected by the technique. Therefore, the extracted parameters are most likely close to the true physical values. Thus, all further investigations in this research that incorporate calculating the parameters will mainly depend on the five-parameter model and the developed technique.

Chapter 5: Influence of Shading on Solar Cell Parameters and Modelling Accuracy Improvement of PV Modules under Partial Shading

5.1. Introduction

This chapter presents a systematic investigation about partial shading effect on solar cells and its modelling. A literature survey, presented in Section 2.9.2 reveals that there is a lack of complete experimental study that investigates the variations of solar cells' equivalent circuit parameters with shading and hence these variations are not usually taken into account when modelling larger PV systems. In this work, the influence of shading on a mono-Si solar cell equivalent circuit parameters was firstly explored. Then, the influence of shading on the performance parameters was also investigated in order to provide sufficient knowledge about the shading impact. After that, equations that represent the variations of equivalent circuit parameters with shading were developed and tested by modelling a single mono-Si solar cell under different shading percentages. Before implementing the single solar cell model, the effects of partial shading of a solar cell and the equivalent irradiance reduction values incident on its surface had been experimentally compared. The goal was to ensure that it is reasonably correct to enter partial shading in the model as its corresponding irradiance value.

The improvement in accuracy in the single cell model imposed by incorporating the variations of equivalent circuit parameters with shading was found to be poor. Subsequently, the single solar cell model was extended to model a mono-Si PV module taking into account the variations of parameters with shading. It was found that this resulted in a substantial improvement in modelling accuracy at the reverse bias region of the output characteristics when shading a single cell in the module. Thereafter, modelling accuracy was optimised in terms of parameters change with shading by testing improvement in accuracy caused by considering each parameter change in the model independently. This allowed to specify the most important parameter, which was found to be the shunt resistance, whose change with shading needs to be considered in the model in order to achieve high precision in modelling the reverse bias region of the output

characteristics under single-cell shading. Hence, this chapter finally suggests accounting for the variations of the photo-generated current and the shunt resistance of solar cells when modelling partially shaded PV modules.

5.2. Experimental Investigation of Shading Effect on Parameters

The 0.78 cm² active area solar cell, which is shown in Figure 3.12 (c) and has performance parameters presented in Table 3.5, was used in the partial shading effect investigation. As this chapter will investigate different solar cells, this cell will be called solar cell 1 in this chapter. The shading was applied using the objects fabricated by 3D printing technology as explained in Section 3.8. Furthermore, three shading percentages were studied in this work, which are 25, 50 and 75% from the total cell area in addition to the no shading case.

In order to be confident with the results, two main experiments were carried-out over two days, with one experiment per day. Each one of the two experiments involved three I-V curves measured in sequence at one set of measurements under each shading percentage. All shading experiments were carried-out under an irradiance of 1000 W/m² and at a cell temperature of 25 °C. It is to be noted that only opaque partial shading was investigated in this work because opaque partial shading and reducing the light uniformly over the whole cell area have the same effect on solar cells as will be shown later in Section 5.3. A photograph of the solar cell under the 50% shading experiment is given in Figure 5.1.

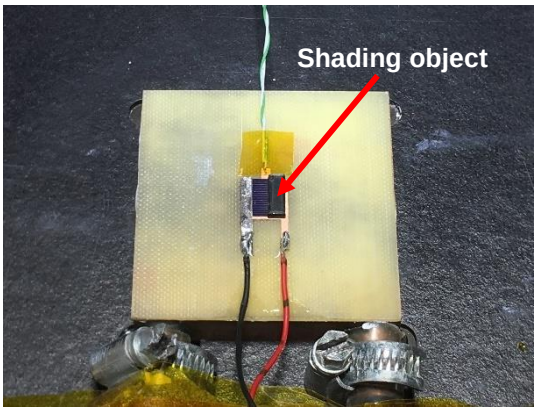

Figure 5.1. The mono-Si solar cell 1 (area = 0.78 cm²) under the light source and 50% shading. (This solar cell was used in investigating the influence of partial shading experiments).

For each one of the two main experiments, once the average I-V curve of the three measurements was obtained at each shading percentage, the performance parameters were firstly extracted from it. While P_{max}, I_{sc} and V_{oc} were directly extracted from the

average experimental I-V curve, R_{ch}, FF and efficiency were determined using equation (2.10), (2.11) and (2.12), respectively. Note that for efficiency calculations of the partially shaded solar cell, the total active area (excluding busbar) was used and not the unshaded area only. Subsequently, the five equivalent circuit parameters were calculated using the technique developed in Chapter 4. In order to avoid negative or very small values of R_s in some I-V curves, the starting point for the range of point-3, which is the range between the vicinity of V_{oc} and 50% of I_{sc} (see Figures 2.11 and 4.3), was the point that has the third index near V_{oc} as previously mentioned at the end of Section 4.2. This approach was applied to all cells investigated in this chapter.

In order to ensure precision in the calculated equivalent circuit parameters, the calculated I-V curves from the parameters were compared with the corresponding experimental ones as shown in Figures 5.2 (a) and (b) for the two main shading experiments, respectively. The MAPE between the experimental and calculated I-V curve for each case is indicated on the curves. As shown, there is a good consistency between the experimental and calculated I-V curves with a MAPE of less than 2% in all cases. This indicates a high precision in calculating the parameters. The Figures also show the significant deterioration occurred to the solar cell performance because of partial shading.

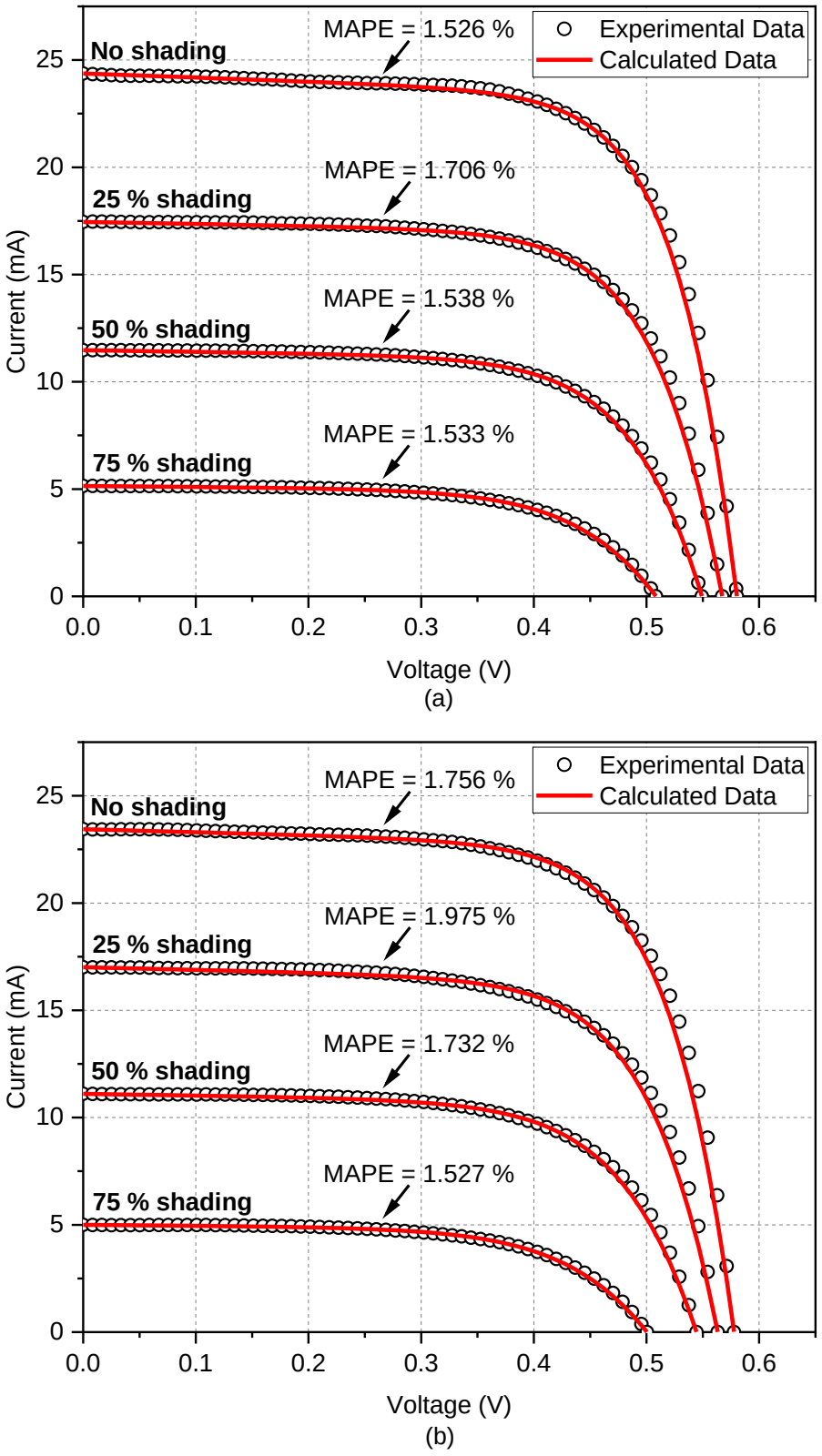

Figure 5.2. Experimental and calculated I-V curves of solar cell 1 under different shading percentages: (a) first experiment and (b) second experiment. (The MAPE between experimental and calculated currents of each curve is indicated. Each experimental I-V curve is the average of three I-V curves taken at one set of measurements. All measurements were taken under a light irradiance of 1000 W/m² and at a cell temperature of 25 °C).

Figures 5.3 (a) to (e) show the variations of equivalent circuit parameters with shading, while Figures 5.4 (a) to (f) show the variations of the performance parameters. The parameters are plotted against the shading factor (α), which is a measure of the extend of opaque shading on the cell surface, that is the faction of the shaded area to the total cell active area [117]. If the total cell active area is A_a and the shaded area is A_{sh}, then the shading factor is calculated from [117]:

$$\alpha = \left(\frac{A_{sh}}{A_a}\right) \tag{5.1}$$

In other words, α will always take a value between 0 and 1, $\alpha = 0$ implies that the cell is fully illuminated, whereas $\alpha = 1$ implies that the cell is fully shaded. For instance, if the cell is 25% shaded, then α will be equal to 0.25. Note that as I-V curves of the cell under partial shading were taken at a fixed cell temperature of 25 °C measured by using the thermocouple, the variation of this temperature because of covering part of the cell when applying shading has been assumed negligible.

Each parameter in Figures 5.3 (a) to (e) and 5.4 (a) to (f) was calculated by averaging the two values from both experiments. The error bars indicate the measurement error, which was taken as the RSD of each parameter calculated from 12 I-V curve measurements taken at STC over three days, with four measurements obtained per day, during which the testing facility was shut down after each day testing. Apart from very few occasions, the error bars of parameters variations with shading do not overlap, indicating that these variations are greater than the error and hence they occurred due to shading. It is to be noted that there was indeed an inevitable error in parameters caused by the small misalignment when placing the shading objects on the cell. This error was not included in Figures 5.3 (a) to (e) and 5.4 (a) to (f) in order to solely present experimental measurement errors and for the sake of brevity. However, this error will be taken into account when implementing the variations of equivalent circuit parameters in the single cell and PV module models in Sections 5.4.2 and 5.5.3.

Besides the variations of the parameters with shading, Figures 5.3 (a) to (e) and 5.4 (a) to (f) also depict the fitting line or curve, fitting equations and the coefficient of determination (R^2). All fitting equations provide the best fit with the parameters data with R^2 equal to 1, except I_{ph}, P_{max}, I_{sc} and efficiency equations, which were fitted to a linear dependency on shading with a very high R^2 as shown in Figures 5.3 (e), 5.4 (a), 5.4 (b)

and 5.4 (e), respectively. The fitting equations of the equivalent circuit parameters in Figures 5.3 (a) to (e) will be used later in Section 5.4.1 to develop empirical equations that govern the variations of those parameters with shading.

As shown in Figures 5.3 (a) and (b), R_s and R_{sh} have a similar trend as both exhibited an increase with shading. The behaviour of R_s under increase of shading agrees to some extend with the work published in [117], albeit with a sharper upward trend in the present work. This might be attributed to the fact that the authors in [117] used a different approach for parameters extraction from the one used in the present work. In addition, the authors did not mention whether the used cell was a mono-Si, same as the one used in the present work, or a poly-Si. Similarly, the rate of R_s increase in the present work is higher than that observed in [130], in which the investigations were carried-out for 27 poly-Si and mono-Si PV modules under changing the irradiance. On the other hand, the work of [132] also shows a similar response for R_s of a mono-Si cell to that of the present work, although it was studied in [132] under reduced irradiance levels and not shading. The response of R_{sh} to shading in the present work is in a good overall agreement with the works of [40], [130], [138] that evaluated the variation in R_{sh} of PV modules with reducing the irradiance. However, R_{sh} response of the present work is different from the one shown in [132], despite the fact that both cells are of the same type. This might be postulated to the difference in experimental equipment used.

The behaviour of the ideality factor n shown in Figure 5.3 (c) exhibits a nearly linear increase with shading. This parameter stays within its bounds for crystalline-Si solar cells (between 1 and 2) for shading percentage up to 25%, but it exceeds this limit for shading percentage greater than 30%. The I_s variation witnessed by Figure 5.3 (d) is similar to that of R_s and R_{sh}. Both n and I_s also exhibited an increase with decreasing the irradiance of a mono-Si cell in [132], but the trends are different from the ones observed in present work. This may also be attributed to the different experimental equipment and different parameters extraction approaches used. Further, those two parameters do not show a defined trend for PV modules when changing the irradiance in [130]. The I_{ph} response depicted in Figure 5.3 (e) seems to follow the well-known dependency of this parameter on irradiance shown by Equation (2.17).

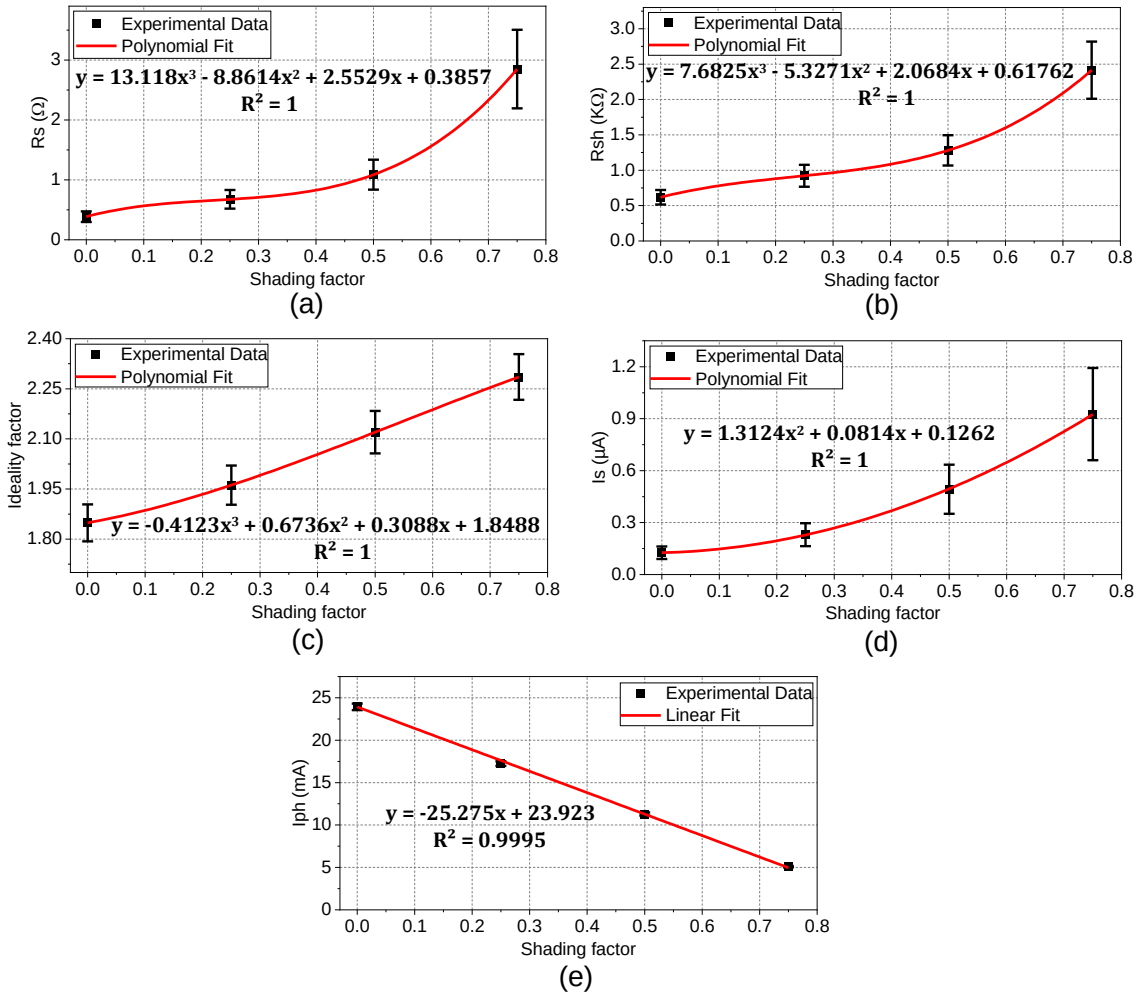

Figure 5.3. Shading effect on solar cell 1 equivalent circuit parameters: (a) series resistance, (b) shunt resistance, (c) ideality factor, (d) reverse saturation current and (e) photo-generated current. (Each parameter value was calculated by averaging two values extracted from two I-V curves, with each I-V curve is the average of three curves taken at one set of measurements. The error bars indicate the RSD of each parameter calculated from 12 I-V curve measurements taken without shading at STC over three days, with four measurements obtained per day).

The P_{max} and I_{sc} shown respectively in Figures 5.4 (a) and (b) declined almost linearly with the increase in shading in a similar behaviour to that of I_{ph} given in Figure 5.3 (e) and almost consistent with the results in [110]. The V_{oc} decreased with the increase of shading in a good agreement with its behaviour in [110] as shown in Figure 5.4 (c). Similarly, the FF given in Figure 5.4 (d) also followed a very similar trend to V_{oc}. The efficiency, on the other hand, was reduced nearly linearly by shading increase as Figure 5.4 (e) illustrates following the same response of P_{max}. Finally, shown in Figure 5.4 (f) is the response of R_{ch} to shading revealing a gradual increase similar to that of R_s and R_{sh}.

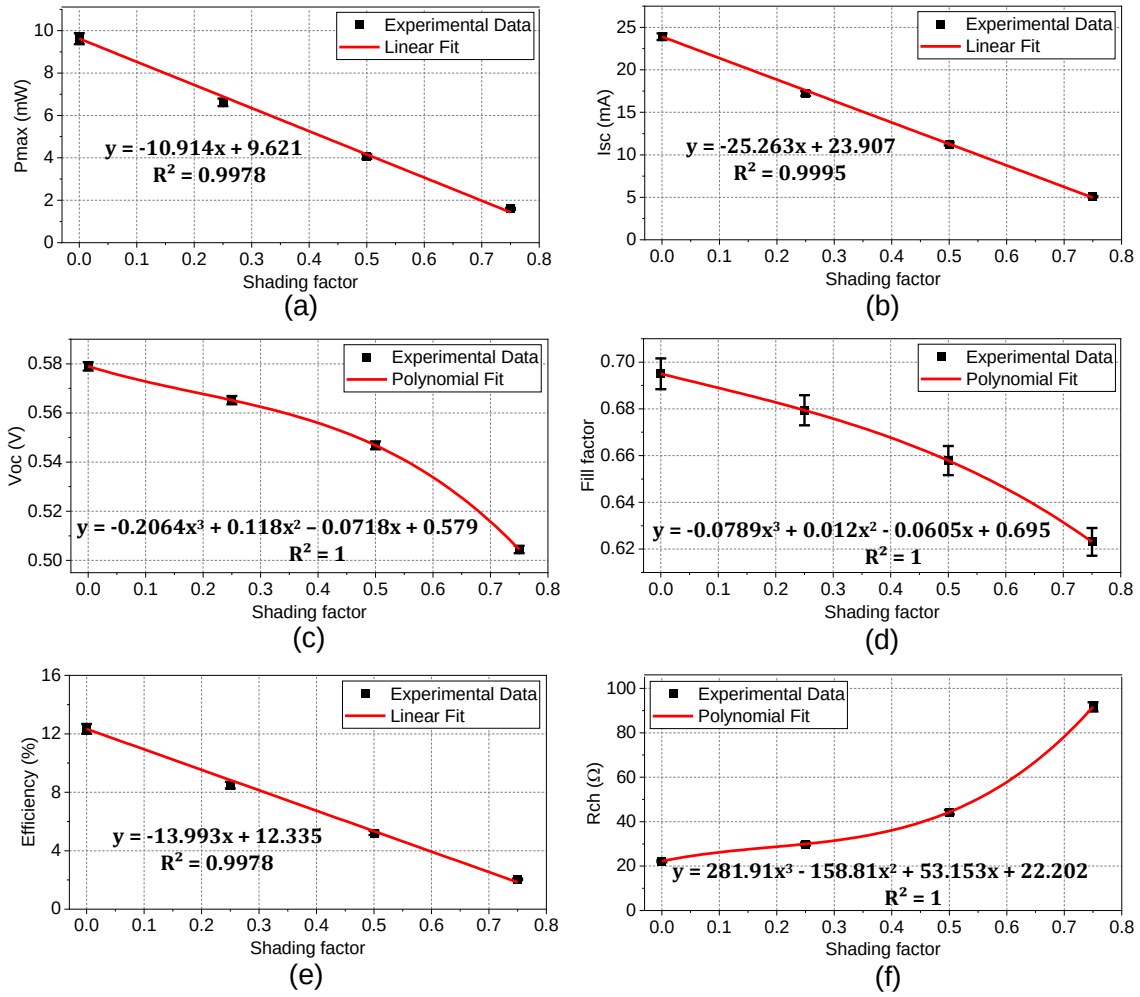

Figure 5.4. Shading effect on solar cell 1 performance parameters: (a) maximum power, (b) short circuit current, (c) open circuit voltage, (d) fill factor, (e) efficiency and (f) characteristics resistance. (Each parameter value was calculated by averaging two values extracted from two I-V curves, with each I-V curve is the average of three curves taken at one set of measurements. The error bars indicate the RSD of each parameter calculated from 12 I-V curve measurements taken without shading at STC over three days, with four measurements obtained per day).

5.3. Comparing Shading with Irradiance Reduction

Before modelling a solar cell under partial shading, it is imperative to ensure that opaque partial shading has the same influence as that of reducing light to the same amount of irradiance the shading would cause. This is because Equation (5.1) implies that entering α in the model as a measure of the degree of shading is in fact equivalent to entering a reduced light with the same intensity. For instance, if the cell receives an irradiance of 1000 W/m² and it is 25% shaded by an opaque object, then α will be equal to 0.25. This is equivalent to receiving 750 W/m², which is a reduction in irradiance by 25%. This assumption was widely used in the literature [107], [109], [110], [115]–[118], [125],

albeit without an experimental study to confirm this fact as previously discussed in Section 2.9.2.

In this investigation, a mono-Si solar cell shown in Figure 5.5 with an active area of 0.8 cm² (1 cm x 0.8 cm) was used and will be called solar cell 2. First, the cell's I-V curve was measured under STC 12 times over three days in order to obtain its equivalent circuit parameters and performance parameters in addition to calculating the RSD, which will be used as an indicator of the measurement error to plot the error bars of parameters. Table 5.1 presents all the parameters of the cell at STC and the RSD. Second, the cell was characterised under two shading percentages of 25 and 50% and two corresponding irradiance levels of 750 and 500 W/m², respectively, at a cell temperature of 25 °C. The irradiance was adjusted using the knob of the 6000 EB electronic ballast and measured using the reference cell 200R as explained in Section 3.2. For each shading and irradiance reduction case, the I-V curve measurement was repeated three times at one set of measurements and the average I-V curve was obtained. Subsequently, the equivalent circuit parameters and performance parameters were calculated for each averaged I-V curve and compared.

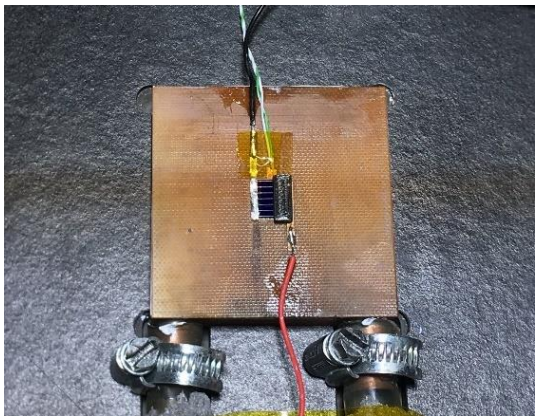

Figure 5.5. The mono-Si solar cell 2 (area = 0.8 cm²) under the light source and 50% shading. (This solar cell was used in comparing shading with irradiance reduction experiments).

Table 5.1. Equivalent circuit parameters and performance parameters of the solar cell 2 shown in Figure 5.5 extracted under STC. (Each parameter value was calculated by averaging 12 values from 12 I-V curve measurements taken over three days, with four measurements obtained per day. The relative standard deviation of each parameter is also shown).

Parameter at STC	Mean value	Relative Standard Deviation (%)
R_s (Ω)	1.2	±20
R_{sh} (kΩ)	0.53	±11
n	0.94	±5.7
I_s (nA)	4×10^{-4}	±142
I_{ph} (mA)	27.7	±1.7
P_{max} (mW)	13.1	±1
I_{sc} (mA)	27.6	±1.7
V_{oc} (V)	0.6218	±0.05
FF	0.763	±0.8
Efficiency (%)	16.4	±1
R_{ch} (Ω)	20.0	±3

Shown in Figures 5.6 (a) and (b) are the I-V and P-V curves at the two shading proportions and two irradiance levels in addition to the no shading case at STC. The I-V and P-V curves of partial shading are well matched with those of decreasing irradiance, implying that both cases cause the same influence on the characteristics of solar cells. This agreement can also be revealed from Table 5.2, which depicts the RMSE and MAPE between the currents of both I-V curves. The RMSE and MAPE were calculated using Equations (4.8) and (4.9), respectively. The errors are significantly small with a MAPE of only about 0.8 and 0.4% for the 25 and 50% shading cases, respectively.

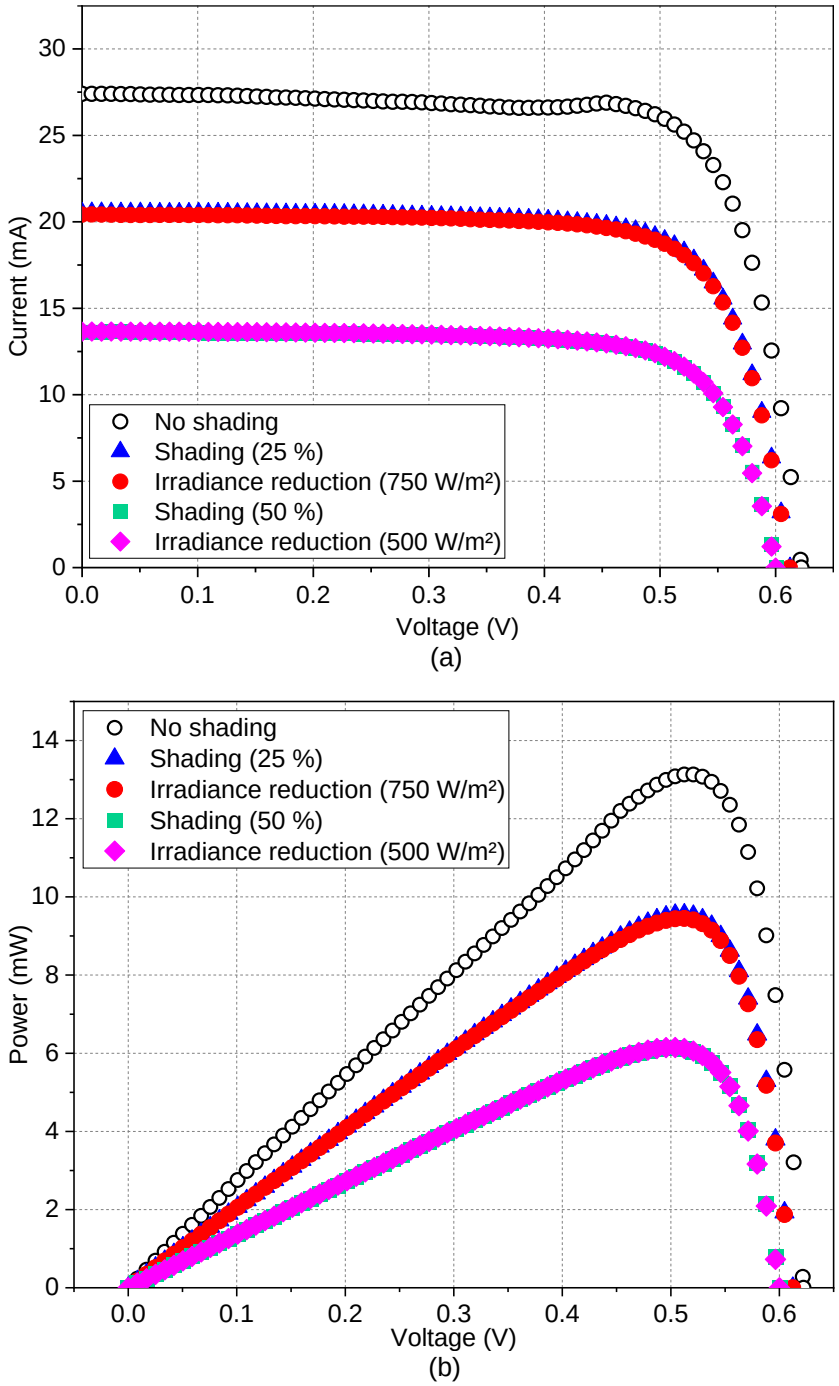

Figure 5.6. Experimental I-V and P-V curves of partial shading and irradiance reduction cases applied to solar cell 2: (a) I-V curves and (b) P-V curves. (Each I-V and P-V curve is the average of three curves taken at one set of measurements. All measurements were taken at a cell temperature of 25 °C).

Table 5.2. The RMSE and MAPE between partial shading and irradiance reduction I-V curves of solar cell 2.

Shaded area percentage (%)	Irradiance (W/m²)	RMSE (A)	MAPE (%)
25	750	1.513×10^{-4}	0.843
50	500	3.761×10^{-5}	0.380

A comparison between the obtained equivalent circuit parameters and performance parameters of partial shading with those of irradiance reduction is depicted in Figures 5.7 (a) to (k). The parameters of both cases agreed well as illustrated by the overlapped error bars in all cases. Even if they are plotted without error bars, the difference between most parameters is still negligible demonstrating that partial shading and decreasing light intensity have almost identical impact.

In terms of parameters variations with shading, an in-depth look into the behaviour of the performance parameters in Figures 5.7 (f) to (k) indicates similar responses to those of cell 1 used for shading effect investigations in Figures 5.4 (a) to (f). On the contrary, apart from I_{ph}, all other equivalent circuit parameters in Figures 5.7 (a) to (d) have overlapped error bars between 25 and 50% shading cases, thus implying that their variations with shading are different from cell 1 equivalent circuit parameters in Figures 5.3 (a) to (d). This might be attributed to the fact that solar cells 1 and 2 were supplied from different batches with a different contact fingers number and hence a different manufacturing technology (see Figures 5.1 and 5.5).

The above-detailed investigation of comparing reduced irradiance with partial shading was carried-out on another solar cell from the same batch of solar cell 2 and the results are given in Appendix B. The results also indicate an agreement between the I-V and P-V of reducing irradiance with those of partial shading and overlapped error bars of all parameters verifying thus the findings of this section.

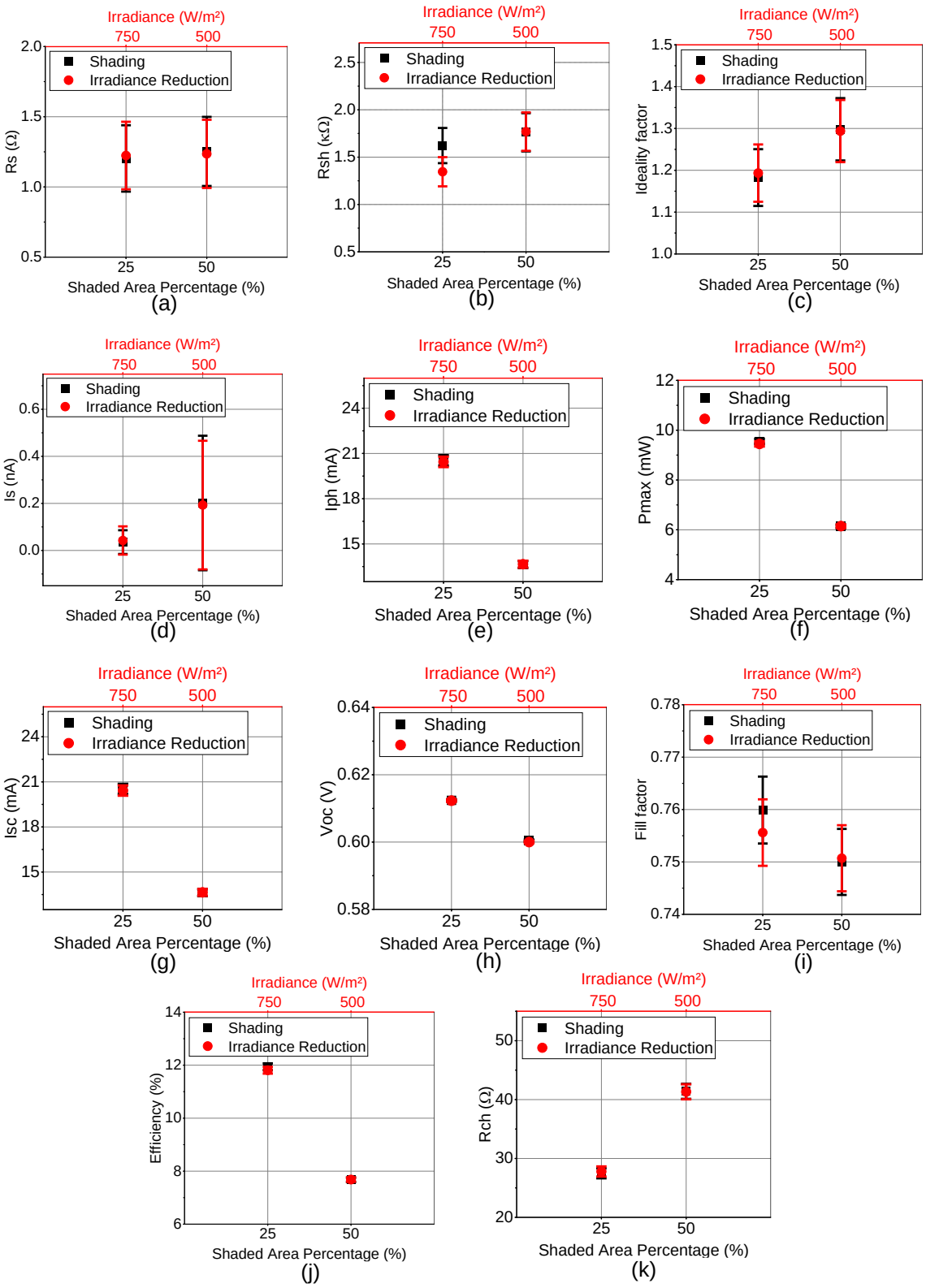

Figure 5.7. Influences of partial shading and irradiance reduction on solar cell 2 equivalent circuit parameters and performance parameters: (a) series resistance, (b) shunt resistance, (c) ideality factor, (d) reverse saturation current, (e) photo-generated current, (f) maximum power, (g) short circuit current, (h) open circuit voltage, (i) fill factor, (j) efficiency and (k) characteristics resistance. (Each parameter value was calculated from the average I-V curve of three curves taken at one set of measurements. The error bars indicate the RSD of each parameter calculated from 12 I-V curve measurements taken without shading at STC over three days, with four measurements obtained per day).

5.4. Considering Variations of Parameters with Shading in a Single Cell Model

This section presents incorporating the variations of the solar cell equivalent circuit parameters shown previously in Figures 5.3 (a) to (e) in modelling single solar cells operating under partial shading to investigate any improvement in accuracy achieved when considering these changes in the model.

5.4.1. Single Cell Modelling Procedure

Normally, a solar cell I-V characteristics can be obtained by solving Equation (2.3) using the five equivalent circuit parameters. However, the parameters need to be adapted from STC to the actual operating irradiance and temperature conditions. When shading occurs, the irradiance received by the cell reduces according to the degree of shading as shown in the previous sections. The reduced irradiance is then entered in the cell model to adapt I_{ph} to the shading condition as shown for instance in [117]. However, in the present section, all equivalent circuit parameters will be adapted to the shading conditions in the model following their behaviour under shading given in Figures 5.3 (a) to (e).

The curve fitting equations that describe the variations of parameters with shading are shown in Figures 5.3 (a) to (e). Nevertheless, these equations explain only the variations of parameters for this case and cannot be directly generalised to any other solar cell. In order to further explain this, take the case of R_s, which is shown in Figure 5.3 (a) and has the following best fit third-degree polynomial equation, as an example:

$$y = 13.118x^3 - 8.8614x^2 + 2.5529x + 0.3857 \quad (5.2)$$

where $x = \alpha$ and $y = R_s$. Thus Equation (5.2) can be written as:

$$R_s = 13.118\alpha^3 - 8.8614\alpha^2 + 2.5529\alpha + 0.3857 \quad (5.3)$$

This equation was obtained by adding a trend line in Microsoft Excel that provides the best fit and then adding R_s at no shading condition ($R_{s,nsh}$) as an intercept, which is 0.3857 **Ω**, as shown by the last term of the above equation. Since the developed equation must determine the new R_s value given $R_{s,nsh}$ and α, Equation (5.3) is not adequate when using it with other solar cells because $R_{s,nsh}$ in the last term will always be added to a fixed value, which is the other three terms in the right-hand side of the equation

$(13.118\alpha^3 - 8.8614\alpha^2 + 2.5529\alpha)$. As $R_{s,nsh}$ is different from one cell to another, this will result in a different trend for the change of R_s with shading to the one given in Figure 5.3 (a).

In order to alleviate this issue, $R_{s,nsh}$ must be included in the above mentioned three terms at the right-hand side of Equation (5.3). This can be done by multiplying and dividing the right and left-hand sides of the equation by $R_{s,nsh}$. Thus Equation (5.3) now becomes:

$$\left(\frac{R_s}{R_{s,nsh}}\right)R_{s,nsh} = \left(\frac{13.118}{R_{s,nsh}}\right)R_{s,nsh}\alpha^3 - \left(\frac{8.8614}{R_{s,nsh}}\right)R_{s,nsh}\alpha^2 + \left(\frac{2.5529}{R_{s,nsh}}\right)R_{s,nsh}\alpha + \left(\frac{R_{s,nsh}}{R_{s,nsh}}\right)R_{s,nsh} \quad (5.4)$$

The values in the first three terms of the right-hand side can now be divided by the $R_{s,nsh}$ value of 0.3857 **Ω**. This yields a generalised equation that describes the variation of R_s with shading for any solar cell:

$$R_s = (34.0109R_{s,nsh}\alpha^3) - (22.9749R_{s,nsh}\alpha^2) + (6.6189R_{s,nsh}\alpha) + R_{s,nsh} \quad (5.5)$$

Equation (5.5) implies that $R_{s,nsh}$ is incorporated in all right-hand side terms. This equation can be applied to any other solar cell and will result in the same trend as that given in Figure 5.3 (a) for the investigated cell. The equations of R_{sh}, n and I_s were developed in the same way using their fitting equations indicated respectively on Figures 5.3 (b), (c) and (d), yielding:

$$R_{sh} = (12.4389R_{sh,nsh}\alpha^3) - (8.6252R_{sh,nsh}\alpha^2) + (3.349R_{sh,nsh}\alpha) + R_{sh,nsh} \quad (5.6)$$

$$n = (-0.223n_{nsh}\alpha^3) + (0.3643n_{nsh}\alpha^2) + (0.167n_{nsh}\alpha) + n_{nsh} \quad (5.7)$$

$$I_s = (10.3994I_{s,nsh}\alpha^2) + (0.645I_{s,nsh}\alpha) + I_{s,nsh} \quad (5.8)$$

As previously mentioned in Section 2.9.2, the parameters with the sub-script nsh represent the values under no shading condition. Note that Equation (5.8) of I_s is a second-degree polynomial equation, but was developed in the same way as the third-degree ones. Regarding I_{ph}, it was found from Figure 5.3 (e) that it is nearly linearly proportional to α and hence to the irradiance received by the cell with an R^2 value of 0.9995. Therefore, from the well-known Equation (2.17) and assuming a constant cell temperature at STC,

I_{ph} change with shading can be expressed by the following equation, which was also presented in [117]:

$$I_{ph} = I_{ph,nsh} * (1 - \alpha) \tag{5.9}$$

It is to be noted that (G/G_{ref}) in Equation (2.17) was replaced by $(1 - \alpha)$ in Equation (5.9), thereby implying the fact that partial shading has identical effect on solar cells as that of irradiance reduction, which was already proved experimentally in Section 5.3. Assume for instance that the cell is working under STC (G_{ref}=1000 W/m²) and it is 75% shaded by an opaque object. Thus, the STC irradiance is reduced by 75% resulting in an actual irradiance (G) of 250 W/m². From Equation (5.1), $(1 - \alpha)$ will be equal to 0.25, which is the same value of (G/G_{ref}).

Note that Equations (5.5) to (5.9) do not consider the temperature variations of the cell because of shading. In other words, the cell temperature was assumed constant with shading as previously mentioned in Section 5.2. This assumption was also adopted in many publications [110], [111], [116], [117].

A flow chart depicting the single cell modelling procedure under partial shading is given in Figure 5.8. The reference five parameters at STC, the irradiance, the cell temperature and the shading percentage are first entered. The model starts by checking whether the cell is working under STC or not. If it is not working under STC, the parameters need to be adapted to the actual irradiance and temperature conditions in order to get the no shading condition parameters, which then need to be used in Equations (5.5) to (5.9) (with the sub-script nsh). This can be done either using Equations (2.13) to (2.17) from the literature or using the new Equations (5.5) to (5.9) proposed in this work, but replacing α by $(1 - G/G_{ref})$ in addition to incorporating the temperature effects on R_s, I_s and I_{ph} from Equations (2.13) and (2.15) to (2.17). However, all experiments using the single cell shading research of this work were performed under STC. Hence, the reference parameters at STC will be equal to the no shading condition parameters.

The second step is to check whether the cell is shaded or not. If it is not shaded, the theoretical I-V curve is calculated using the five parameters from Equation (2.3). However, if it is shaded, then the model will invoke the following steps in sequence:

- The shading factor is calculated from Equation (5.1).

- The five parameters at no shading condition are adapted to the shading condition using Equations (5.5) to (5.9).
- The theoretical I-V curve is calculated from Equation (2.3) using the adapted five parameters.

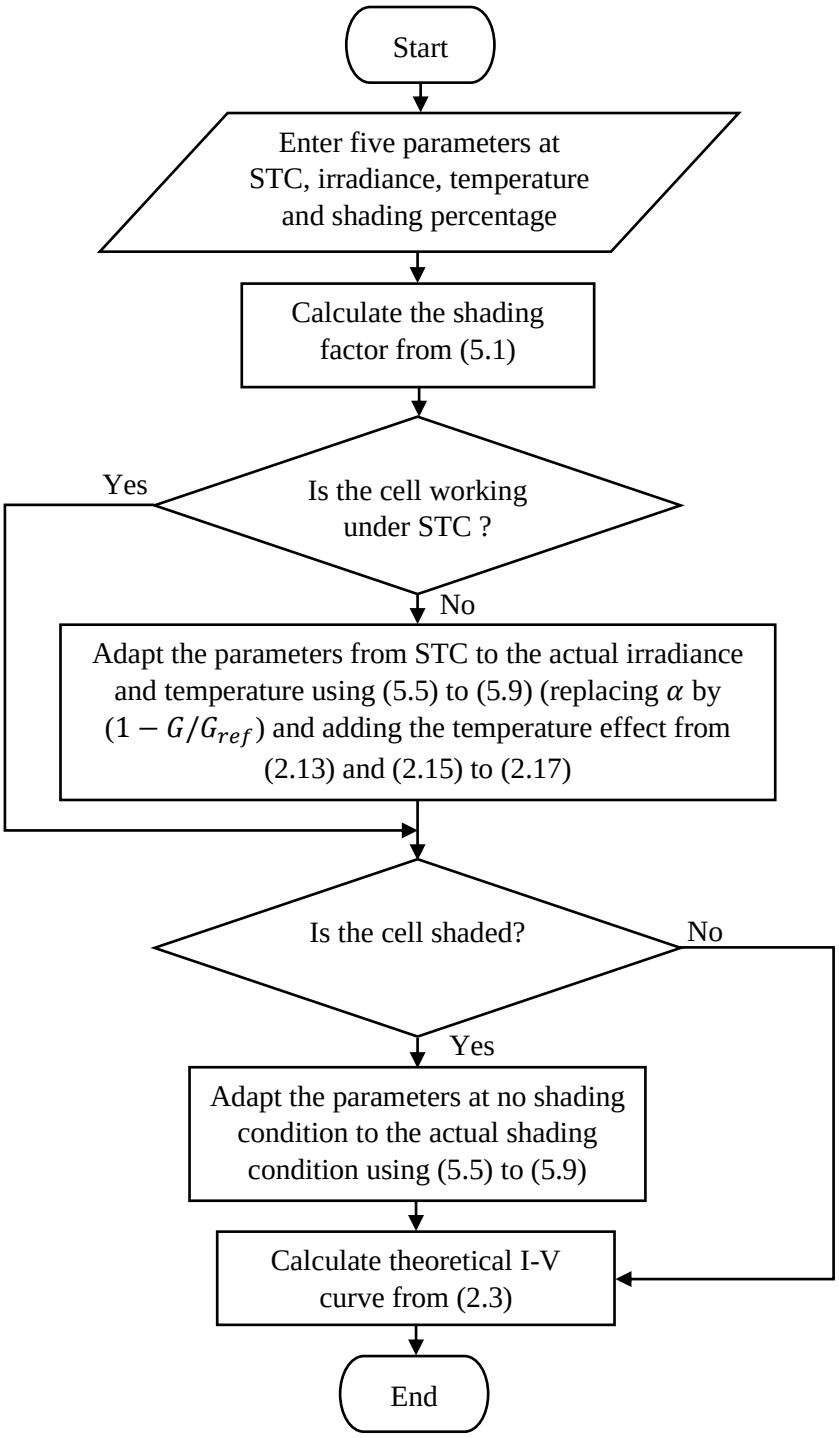

Figure 5.8. The flow chart of the single cell modelling procedure used.

5.4.2. Variations of Parameters with Shading

The next step was to investigate the accuracy of the single cell model when incorporating the variations of the parameters with shading through comparison with experimental data. A mono-Si solar cell, which will be called solar cell 3 and has a different manufacturing technology from that of solar cell 1 shown in Figure 5.1, was characterised under STC with shading percentages of 0, 25, 50 and 75% by taking three I-V curves at one set of measurements for each case. The cell has an active area of 0.8 cm² (1 cm x 0.8 cm) and its photograph under 50% shading is given in Figure 5.9. First, the five parameters of the cell were calculated at STC from the average I-V curve of the three measurements. The parameters are presented in Table 5.3 and a comparison between the experimental and calculated I-V curves is given in Figure 5.10 illustrating a good agreement with a MAPE of 1.339% and thereby a high accuracy in the calculated parameters. From the average I-V curve at STC, the P_{max}, I_{sc} and V_{oc} were found to be 10.45 mW, 27.79 mA and 0.5768 V, respectively.

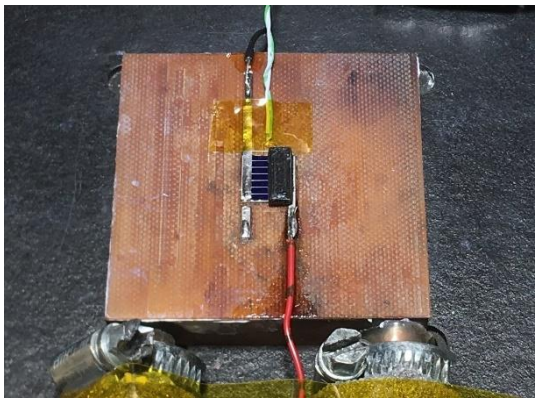

Figure 5.9. The mono-Si solar cell 3 (area = 0.8 cm²) under the light source and 50% shading. (This solar cell was used in single cell modelling experiments).

Table 5.3. Equivalent circuit parameters of the mono-Si solar cell 3 shown in Figure 5.9 extracted under STC. (These parameters were used as a reference to obtain the variations in parameters with shading. The parameters were obtained from the average I-V curve of three curves taken at one set of measurements).

Parameter at STC	Value
R_s (Ω)	0.80
R_{sh} (kΩ)	0.36
n	2.05
I_s (μA)	0.47
I_{ph} (mA)	27.85

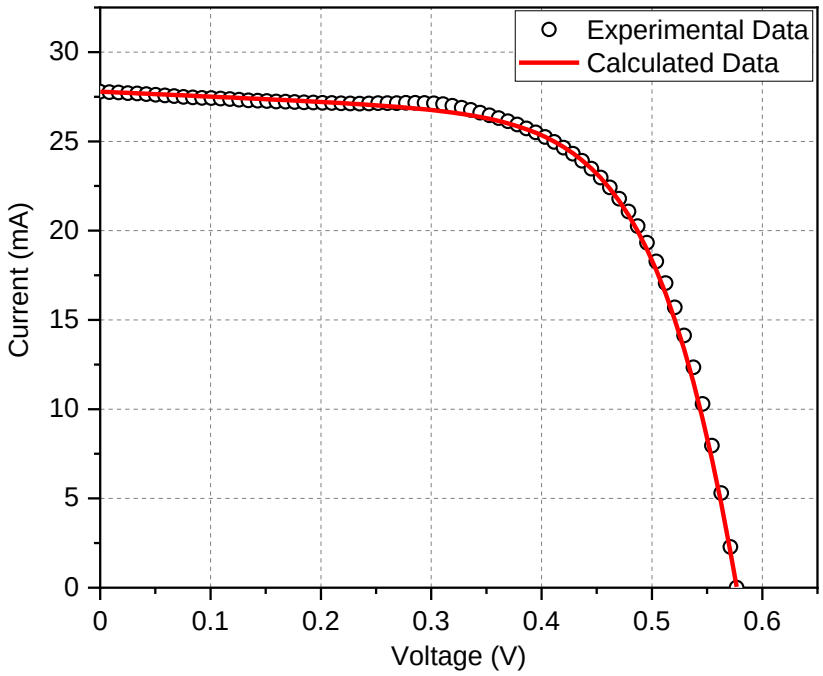

Figure 5.10. Experimental and calculated I-V curves of solar cell 3 at no shading condition. (The calculated I-V curve was produced by the extracted parameters under STC shown in Table 5.3. The experimental I-V curve is the average of three I-V curves taken at one set of measurements under STC. The MAPE between both I-V curves in the Figure is 1.339%).

Second, the single cell model illustrated in Figure 5.8 was invoked in MATLAB to predict the theoretical I-V curves of the three shading percentages incorporating the variations of all parameters with shading given by Equations (5.5) to (5.9). Finally, to assess the validity of those equations, the results were compared with experimental data and with another theoretical I-V curve produced from the model that takes into account only the variation of I_{ph} with shading from Equation (5.9). The approach of taking into account only I_{ph} variation with shading is the commonly used approach as discussed previously in Section 2.9.2. The MATLAB program code of the single cell model for this solar cell is available in Appendix C.

The experimental and theoretical I-V and P-V curves using both modelling approaches are depicted in Figures 5.11 (a) and (b), respectively, including the no shading characteristics at STC. The model using the developed equations of the parameters variations with shading is slightly better in describing the experimental data. In addition, the approach of I_{ph} overestimates the MPP as shown by the zoom-in views in the Figures. Nevertheless, it can be observed that the improvement in accuracy of using the developed equations over the only I_{ph} approach is not significant.

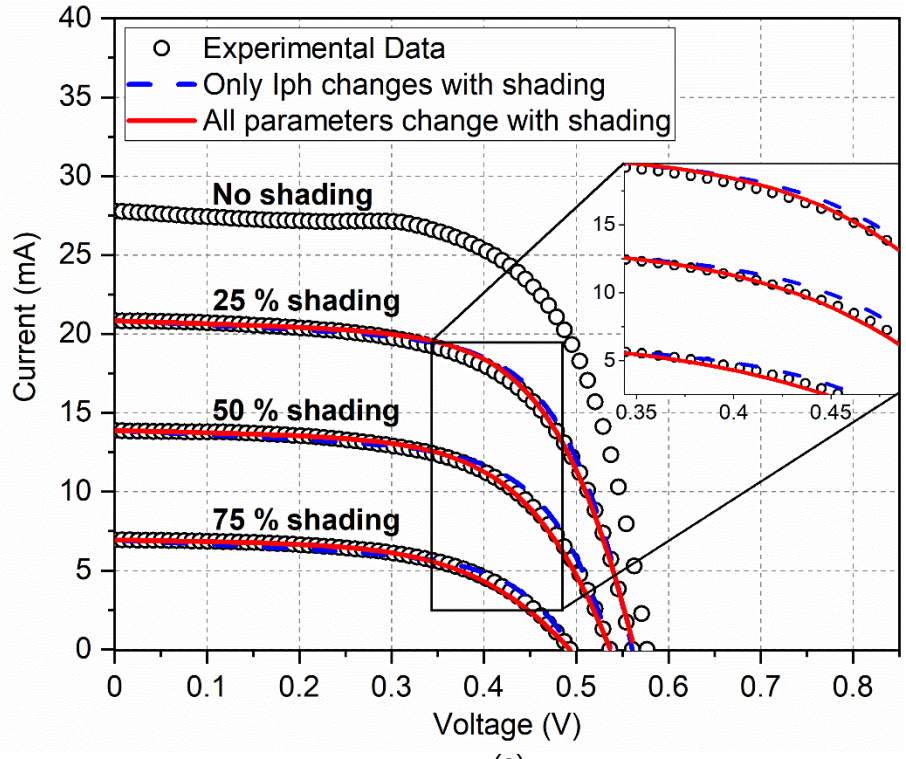

(a)

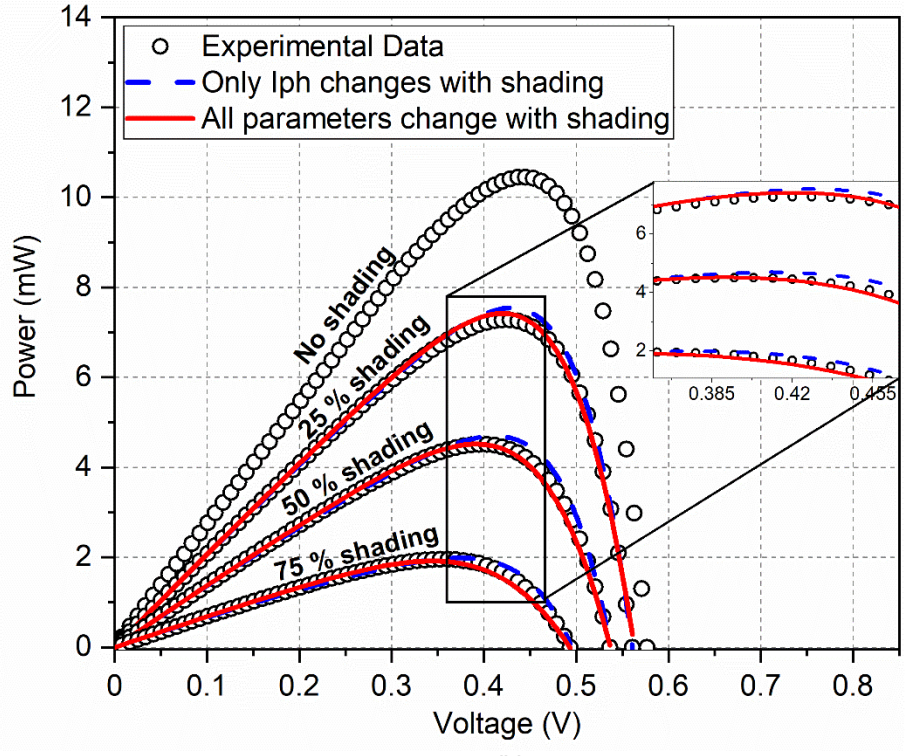

(b)

Figure 5.11. Experimental and modelled I-V and P-V curves of solar cell 3 under different shading percentages produced by the model considering the variation of only the photo-generated current and the variations of all the equivalent circuit parameters with shading: (a) I-V curves and (b) P-V curves. (Each experimental I-V and P-V curve is the average of three curves taken at one set of measurements. All measurements were taken under a light irradiance of 1000 W/m² and at a cell temperature of 25 °C).

This small improvement may even vanish if one takes into account the error bars of the parameters variations with shading in Figures 5.3 (a) to (d) and the inevitable error of placing the shading object. This is presented in Appendix D, in which the modelled output characteristics considering parameters variations with shading are plotted alongside with the modelled characteristics gained from the upper and lower bounds of R_s, R_{sh}, n and I_s resulted from the errors. The modelled characteristics from the only I_{ph} approach was also plotted to assess whether the accuracy improvement imposed by Equations (5.5) to (5.8) is still valid regardless of the errors. Note that I_{ph} was considered unaffected by the errors because its well-known linear dependency on irradiance was used instead of the obtained experimental change in Figure 5.3 (e), which contains the error bars.

The error of placing the shading objects on the cell was assumed to be ±0.2 mm based on a sensible judgment. For obtaining the total upper and lower bounds of R_s, R_{sh}, n and I_s, the ±0.2 mm was first added to / subtracted from the shaded area and then α was calculated from Equation (5.1) for the upper and lower bounds. Subsequently, the upper and lower shading object error bounds of parameters were calculated from Equations (5.5) to (5.8) using the upper and lower bounds of α, respectively. Finally, those bounds were added to the ±RSD of the error bars shown in Figures 5.3 (a) to (d) resulting in the total upper and lower bounds of parameters. Thus, in addition to the modelled characteristics obtained from the mean parameters, two other modelled characteristics were obtained, one from the total upper bound of parameters (+RSD and shading object error), whereas the other one from the total lower bound (-RSD and shading object error).

The modelled characteristics of those three cases and that of the only I_{ph} approach are depicted in Appendix Figures D1 (a) and (b) for 25, 50 and 75% shading. It can be observed that there are noticeable deviations in the I-V and P-V curves caused by the errors. The I-V and P-V curves resulted from the errors nearly overlap with those obtained from the only I_{ph} approach. The errors thus diminish the small improvement in accuracy gained by the developed equations shown in Figures 5.11 (a) and (b).

Therefore, it can be said that the developed equations do not provide appreciable improvement in accuracy over the only I_{ph} approach when modelling a single solar cell. While this may be attributed to the different manufacturing technology of cell 3 from that of cell 1 used to develop Equations (5.5) to (5.8), it will be more interesting to investigate

the validity of the equations for modelling PV modules. This is because PV modules constitute the commercially available unit in PV systems.

5.5. Considering Variations of Parameters with Shading in a PV Module Model

As mentioned previously in Section 2.4, solar cells do not provide a useful amount of power and hence they are usually connected in series to create PV modules. It is anticipated that partial shading effect on a PV module is different from that on a single cell because in a PV module, the effect on a single cell will interact with the unshaded cells connected with it. It is thus important to investigate the inclusion of a single cell partial shading effect in a PV module model under partial shading. In the present section, the variations of single solar cell parameters with shading described by Equation (5.5) to (5.9) were applied to modelling a PV module consisting of several solar cell models.

5.5.1. PV Module Modelling Procedure

The PV module model was built following a procedure used in many publications [108], [110], [111], [116]–[118]. This modelling procedure is based on calculating the voltage of each single cell according to its shading state and then summing-up all the voltages at each current value using a piecewise approach to create the I-V curve of the entire module. The flow chart of the PV module modelling procedure used is shown in Figure 5.12. In order to simply illustrate the voltage calculations, a configuration of a PV module consists of s number of cell-strings and each cell-string consists of c number of cells connected in series is presented in Figure 5.13 as an example adopted from [111]. The cell-strings are numbered (1, 2, … s) and the cells are numbered (1, 2, … c).

Firstly, the irradiance and temperature of the PV module in addition to the shaded area percentage of each cell are entered in the model. Secondly, the reference parameters at STC of the entire module are entered and hence their values for each cell can be calculated by dividing R_s and R_{sh} by the number of cells connected in series [35].

Thirdly, the single solar cell model presented in the previous section is invoked (see Figure 5.8) taking into account the variations of parameters with shading given in Equation (5.5) to (5.9), but without calculating I-V curves of the cells because this will be done in the next step.

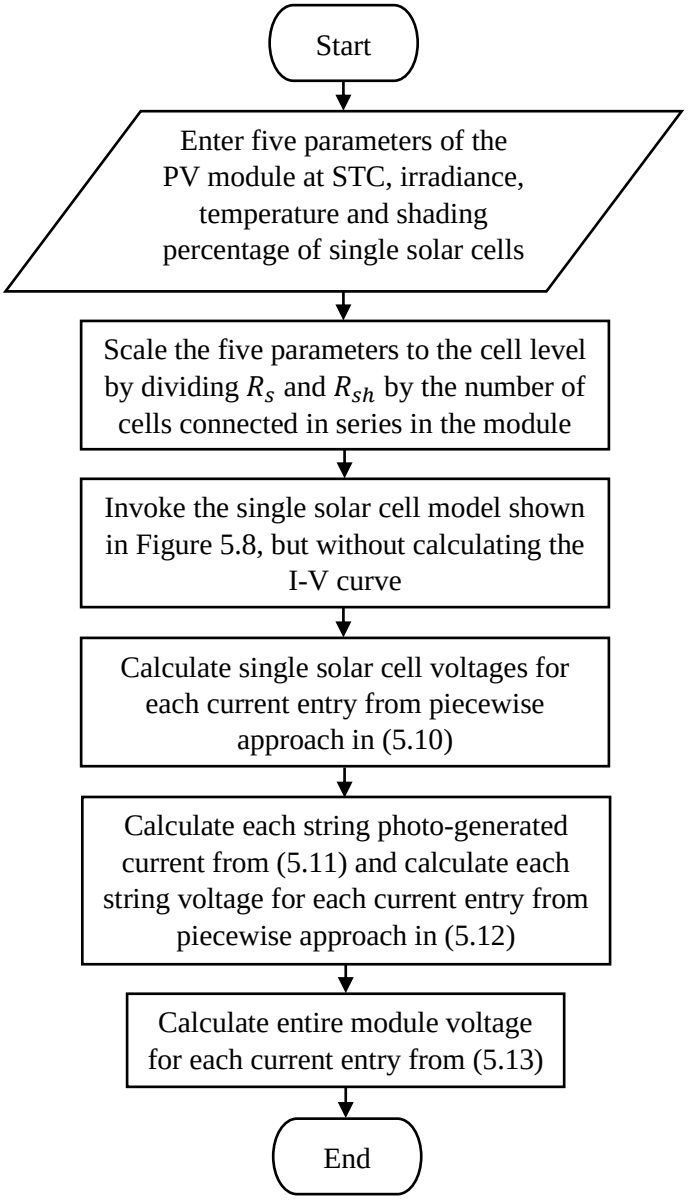

Figure 5.12. The flow chart of the PV module modelling procedure used.

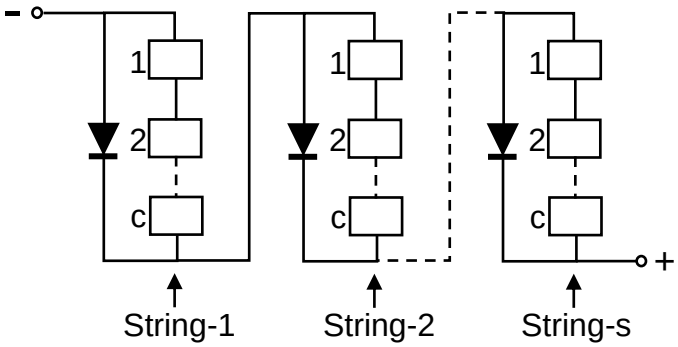

Figure 5.13. A configuration of a PV module consists of series-connected solar cells and cell-strings. (Adapted from [111]).

A piecewise approach presented in [111], [117] is used to calculate the voltage of each cell (V_{cell}) in the module according to its photo-generated current ($I_{ph,cell}$) from:

$$V_{cell} = \begin{cases} solve\ for\ V_{cell}: \left[0 = I_{ph,cell} - I_s\left(exp\left(\frac{IR_s+V_{cell}}{V_{th}.n}\right) - 1\right) - \frac{IR_s+V_{cell}}{R_{sh}} - I\right] & if\ \ 0 \le I \le I_{ph,cell} \\ \left[-\left(R_{sh}\left(I - I_{ph,cell}\right)\right)\right] - IR_s & if\ \ I > I_{ph,cell} \end{cases} \tag{5.10}$$

Note that the works of [111], [117] used the four-parameter model, which is represented by Equation (2.5) with a neglected R_{sh}, to calculate the direct bias voltage from the upper part of Equation (5.10). However, they included R_{sh} when calculating the reverse bias voltage from the lower part of the equation. By contrast, the five-parameter model was used in the present work, thereby using R_{sh} in both parts of the equation.

Equation (5.10) calculates the voltage for each current entry point (I) and implies that if $0 \le I \le I_{ph,cell}$, the cell is in normal operation and the voltage is calculated by solving Equation (2.3) using the Newton Raphson method. By contrast, if $I > I_{ph,cell}$, the cell is shaded and carries a current larger than its maximum current and thereby will be reverse biased by the unshaded cells. The voltage in this case is obtained from the current flowing in reverse bias through R_{sh} and R_s [111].

Once the individual cells voltages are calculated at each current value, another piecewise approach is used to sum-up the voltages of individual cells according to the state of bypass diodes, which is governed by the shading condition. The photo-generated current of each cell-string ($I_{ph,st}$) is first obtained as the minimum current of individual cells in the respective cell-string because of the current limitation by the shaded cell [1]. Thus, it can be expressed as [118]:

$$I_{ph,st} = \min\left(I_{ph,cell}\right) \tag{5.11}$$

Referring to Figure 5.13, the voltage of each cell-string (V_{st}) is then obtained following the piecewise approach of [111] depending on its $I_{ph,st}$ from:

$$V_{st} = \begin{cases} \sum_{i=1}^{c} V_{cell,i} & if \;\; 0 \leq I \leq I_{ph,st} \\ \sum_{i=1}^{c} V_{cell,i} & if \;\; \left(I > I_{ph,st}\right) and \left(\sum_{i=1}^{c} V_{cell,i} \geq -V_D\right) \\ -V_D & if \;\; \left(I > I_{ph,st}\right) and \left(\sum_{i=1}^{c} V_{cell,i} < -V_D\right) \end{cases} \quad (5.12)$$

where V_D is the forward voltage drop of the bypass diode. Equation (5.12) determines a cell-string voltage for each current entry point and it implies that if $0 \leq I \leq I_{ph,st}$, all the cells in the cell-string are in normal operation and hence the total cell-string voltage is the summation of individual cells voltages. On the other hand, if $I > I_{ph,st}$, the cell-string containing the shaded cell will be either bridged by the bypass diode or not, depending on the amount of reverse bias. If the summation of cells' voltages is $\geq -V_D$, the bypass diode will not conduct. However, if the summation of cells' voltages is $< -V_D$, the bypass diode conducts and bridges the cell-string. In this case, the cell-string voltage will be equal to $-V_D$ and hence it will no longer contribute to the module produced power [111]. In fact, this piecewise approach will result in I-V and P-V curves with respectively multiple steps and peaks [111] similar to those shown previously in Figures 2.14 (a) and (b) for a module with two cell-strings.

Finally, as shown in Figure 5.13, the PV module's voltage (V_{mo}) can be obtained by summing up the cell-strings' voltages at each current [111], [117]:

$$V_{mo} = \sum_{j=1}^{s} V_{st,j} \quad (5.13)$$

5.5.2. Variations of Parameters with Shading

It will be interesting now to see whether taking into account the variations of parameters with shading will lead to any accuracy improvement in the PV module model. This needs the model to be designed for a specific real PV module and compared against experimental data. The mono-Si 10 W PV module shown previously in Figures 3.14 (a) to (c) was used in this research. The module was first prepared in terms of bypass diode soldering, temperature measurement and water cooling as presented in Sections 3.4.1, 3.5.1 and 3.5.2, respectively. The configuration of the 36 solar cells in addition to the two bypass diodes was previously depicted in Figure 2.13. In Figure 5.14 below, the PV module is shown while it is under the light source and a single cell is being shaded by 50%. The two fans shown in the figure were added to improve the efficiency of cooling

so that the module's temperature can be maintained at 25 °C for a sufficient time to take the I-V curve measurements.

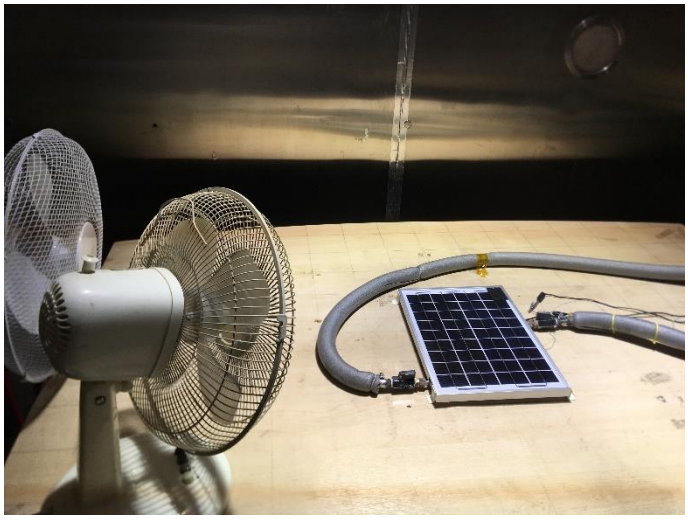

Figure 5.14. The mono-Si 10 W PV module under the light source and 50% shading of one cell. (This module was used in all PV module's modelling experiments).

The P_{max}, I_{sc} and V_{oc} at STC given in the module data sheet are 10 W, 0.61 A and 21.88 V, respectively [194]. Whereas the ones extracted using the experimental set-up form averaging three I-V curves taken at one set of measurements are respectively 9.77 W, 0.516 A and 23.643 V. Note that those measurements were carried-out under a light irradiance of 1000 W/m² measured at the centre of the module[4] and at a module temperature of 25 °C.

The equivalent circuit parameters of the module were obtained from the average I-V curve of the above mentioned three measurements and presented in Table 5.4. It is to be noted that when using the technique presented in Chapter 4, the starting point for point-3 was the first index near V_{oc} (see Figures 2.11 and 4.3) because R_s of the PV module is quite large compared with that of single solar cells. Hence, no negative R_s value is obtained when using points very near to V_{oc}.

The calculated I-V curve from the module's parameters of Table 5.4 is plotted against the experimental one in Figure 5.15 revealing a very good match with a MAPE of only 0.501%. Subsequently, the module's parameters were scaled down to each individual cell

[4] The average irradiance incident on the module (size 34 cm x 24 cm) was estimated as 890 W/m² from the 40 cm x 40 cm area spatial non-uniformity presented in Figure 3.7.

by dividing R_s and R_{sh} by the number of cells. The parameters of individual cells are also presented in Table 5.4.

Table 5.4. Equivalent circuit parameters of the 10 W PV module shown in Figure 5.14 extracted under a light irradiance of 1000 W/m² measured at the centre point of the module and at a module temperature of 25 °C. The parameters of individual cells were used as a reference to obtain the variations in parameters with shading. The module's parameters were obtained from the average I-V curve of three curves taken at one set of measurements).

Parameter[5]	Value for the PV module	Value for the single cell
R_s (Ω)	3.05	0.085
R_{sh} (kΩ)	4.5	0.125
n	0.74	0.74
I_s (nA)	6×10^{-7}	6×10^{-7}
I_{ph} (A)	0.516	0.516

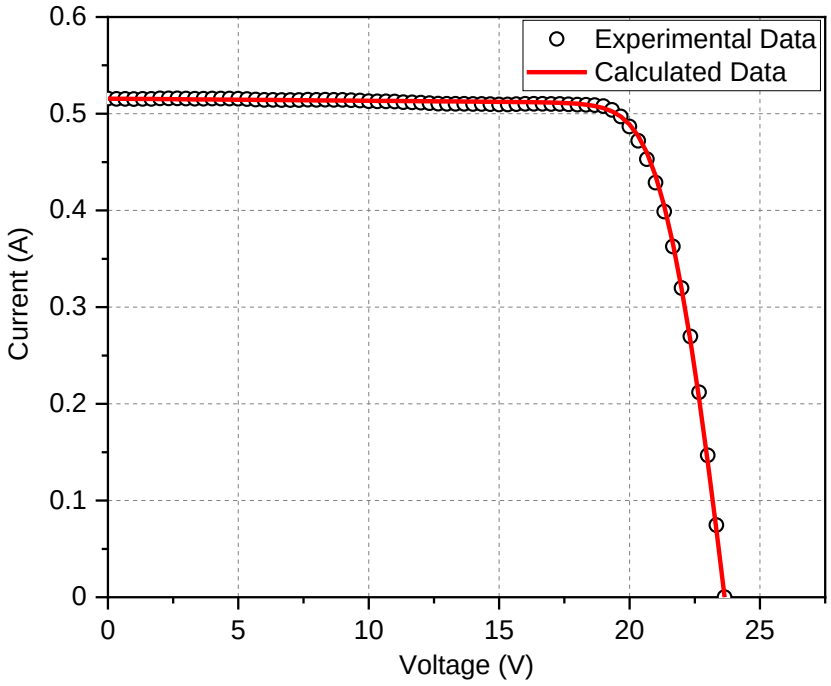

Figure 5.15. Experimental and calculated I-V curves of the 10 W module at no shading condition. (The calculated I-V curve was produced by the extracted parameters shown in Table 5.4. The experimental I-V curve is the average of three I-V curves taken at one set of measurements under a light irradiance of 1000 W/m² measured at the centre point of the module and at a module temperature of 25 °C. The MAPE between both I-V curves in the Figure is 0.501%).

[5] The calculated I_{ph} of this PV module (0.516 A) equals to the measured I_{sc} up to the third decimal place. The reason is that this PV module is very efficient with a high R_{sh}, which causes the current flows through R_{sh} to be negligible. However, they are equal only up to the third decimal place.

Once the parameters of individual cells were acquired at the reference condition, the program code of the model was written in MATLAB, as given in Appendix E, for this PV module allowing to apply any shading percentage to any cell and to consider any parameter as fixed or variable with shading. Although the forward voltage drop (V_D) of the used bypass diodes (IN5819) varies with current and temperature, a fixed value of 0.4 V was used in this work as it provided a good fit with experimental data. The module voltage was calculated from the current as previously discussed in Section 5.5.1, which was entered in the model as a range from 0 to I_{sc} at no shading, thereby allowing the model to predict the output characteristics without using experimental data.

A shading case of a single cell by 75% was selected as a study case to investigate the improvement in accuracy gained by accounting for the variations of parameters with shading. The I-V curve of the module was measured three times at one set of measurements while a single cell in cell-string 2 (see Figure 2.13) is 75% shaded by carefully applying the foam adhesive tape. The measurements were taken at a light irradiance of 1000 W/m² measured at the centre point of the module and at a module temperature of 25 °C. Note that the light non-uniformity causes cells to produce different currents when individually shaded by the same percentage (see Figure 6.2). Hence, the solar cell used in the investigations of this chapter was selected in a way so that when it is 75%, it produces a current equals approximately a quarter of the module's I_{sc} without shading. The slopes' shape of I-V curves does not significantly change when shading cells with different light intensity and hence non-uniformity has no effect on the reliability of results as previously commented in Section 3.2.2.1.

Once the experimental data was obtained, the model code was then adjusted to this shading case and the parameters of the shaded cell variations with shading were changed in the model in the following steps:

- Considering that only I_{ph} changes with shading as per Equation (5.9).
- Considering that only I_{ph} and R_s change with shading as per Equations (5.9) and (5.5), respectively.
- Considering that only I_{ph} and R_{sh} change with shading as per Equations (5.9) and (5.6), respectively.
- Considering that only I_{ph} and n change with shading as per Equations (5.9) and (5.7), respectively.

- Considering that only I_{ph} and I_s change with shading as per Equations (5.9) and (5.8), respectively.
- Considering that all equivalent circuit parameters change with shading as per Equations (5.5) to (5.9).

The I_{ph} was included in all cases because it inherently depends on shading as previously stated, hence it needs always to be variable with it. It was thus used with all other parameters in turn in addition to using all of them in one time. The theoretical I-V and P-V curves obtained from the model implementing the above variations of parameters are plotted against the experimental data in Figures 5.16 (a) and (b), respectively, in addition to the no shading characteristics.

As can be seen, only two cases provided the best fit with experimental data, which are considering the variation of all parameters with shading (dotted black line) and considering the variation of I_{ph} and R_{sh} (solid red line). By contrast, in the other cases, all the I-V and P-V curves nearly overlapped and resulted in a poorer fit with experimental data in the part of the characteristics at which the shaded cell is reverse biased (between 11 V and 23 V), which is between region 1 MPP and the point at which the bypass diode conducts (see Figures 2.14 (a) and (b)).

Therefore, it was shown from those results that the variations of equivalent circuit parameters with shading have noticeable influence on the modelling accuracy of a PV module even though they have no effect on the modelling accuracy of a single cell (see Section 5.4.2). This implies that the series connection of solar cells influences the behaviour of the shaded cell. Furthermore, it was shown from the results that in addition to I_{ph}, R_{sh} is a very important parameter that affects the modelling accuracy in the part of the I-V curve at which the shaded cell is reverse biased. This confirms the fact that there is a strong correlation between R_{sh} and the behaviour of PV modules with shaded cells under reverse bias [98], [128]. Since considering the variations of R_s, n and I_s with shading did not lead to any improvement in accuracy, it has been proposed in this work to use only the variations of I_{ph} and R_{sh} of individual cells with shading represented respectively by Equations (5.9) and (5.6) in modelling partially shaded PV modules. The next section presents an experimental validation for this approach.

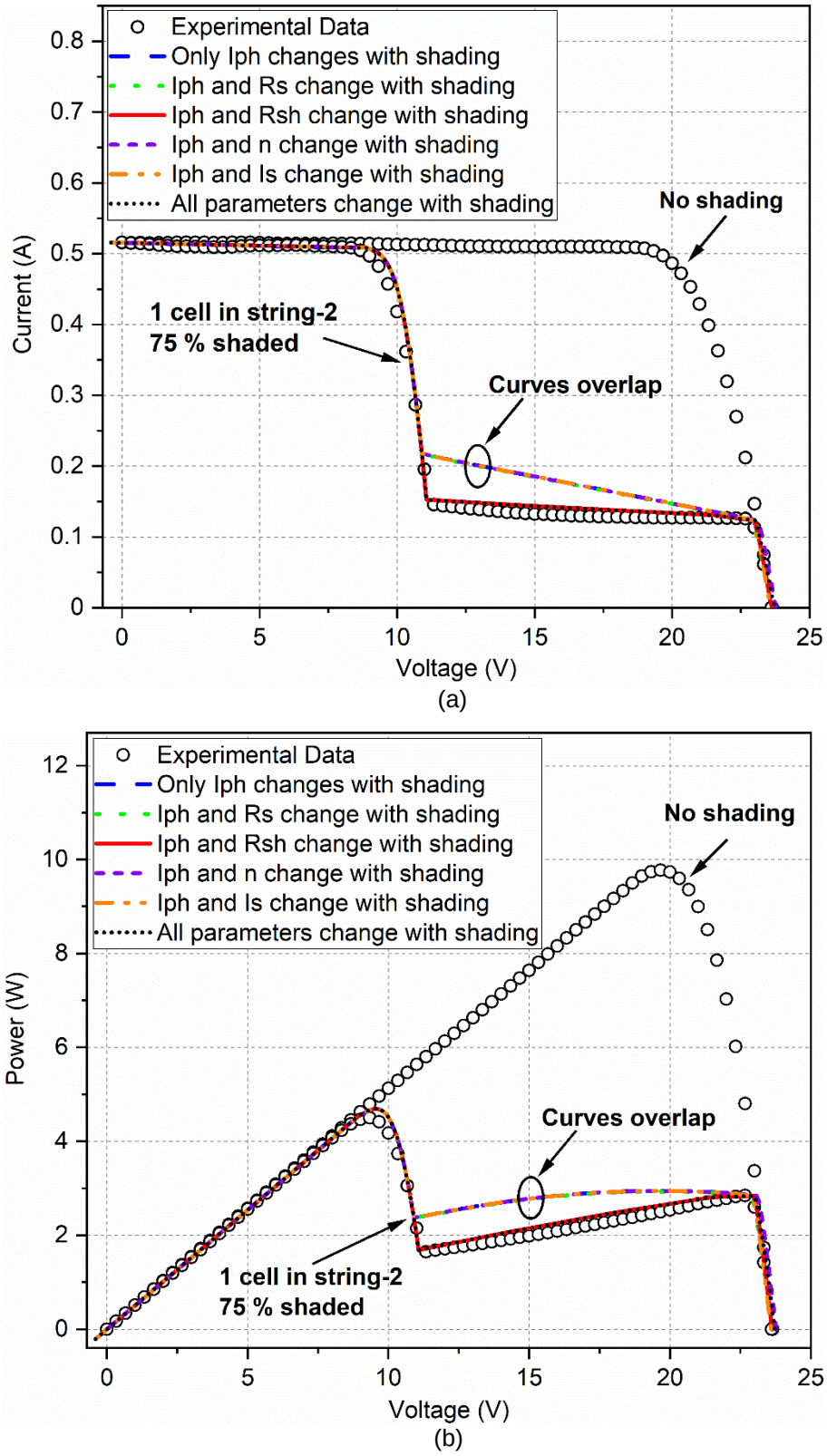

Figure 5.16. Experimental I-V and P-V curves of the 10 W PV module at no shading and 75% shading of one solar cell in addition to the modelled I-V and P-V curves considering different variations of the shaded cell parameters with shading: (a) I-V curves and (b) P-V curves. (Each experimental I-V and P-V curve is the average of three curves taken at one set of measurements. All measurements were taken under a light irradiance of 1000 W/m² measured at the centre point of the module and at a module temperature of 25 °C).

5.5.3. Variation of the Shunt Resistance with Shading

In order to validate the approach of involving the variation of R_{sh} in the PV module's model, six shading cases were applied to the 10 W PV module and the I-V curves were measured three times at one set of measurements for each case. Table 5.5 shows the shading cases and the condition of each cell-string. The shading cases 1 to 4 represent increasing the shading proportion on a single cell from 25 to 100% in a step of 25%. Whereas cases 5 and 6 constitute increasing the number of shaded cells, being 2 and 4 cells, respectively. All experiments were performed under a light irradiance of 1000 W/m² measured at the centre point of the module and at a module temperature of 25 °C. The model was invoked to represent those six cases. The proposed consideration of the variations of I_{ph} and R_{sh} with shading was compared with the well-known approach of considering that only I_{ph} changes with shading in terms of the accurate representation of experimental data.

Table 5.5. The shading cases of the 10 W PV module that has 36 cells connected in series and divided into two cell-strings. (All experiments were carried-out under a light irradiance of 1000 W/m² measured at the centre point of the module and at a module temperature of 25 °C).

Shading Case	Condition of cell-string 1	Condition of cell-string 2
1	No shading	1 cell 25% shading
2	No shading	1 cell 50% shading
3	No shading	1 cell 75% shading
4	No shading	1 cell 100% shading
5	No shading	2 cells 50% shading
6	No shading	4 cells 50% shading

In Figures 5.17 (a) and (b), the experimental and modelled I-V and P-V of cases 1 to 4 are shown alongside with the no shading experimental characteristics. Clearly, the results indicate that incorporating the variations of both I_{ph} and R_{sh} of the shaded cell produced closest results to experimental data in the region when the shaded cell is reverse biased. The only I_{ph} change approach exhibited much larger deviation from experimental data in this region. In addition, this deviation becomes larger when increasing the shading percentage. Nevertheless, other areas on the I-V and P-V curves including both region 1 and 2 MPPs did not show appreciable difference between both approaches as both of them

overlapped. This implies that the proposed change of R_{sh} is useful in improving the model accuracy only in the region of the reverse bias.

It is to be noted that previous works by other researchers have shown that the reverse bias characteristics of shaded solar cells within PV modules can be accurately modelled by adding the avalanche breakdown term to the model [12], [97], [100], [105], [116], [123] as discussed in Section 2.9.2. However, the advantage of considering the variation of R_{sh} is the fact that it does not need the inclusion of the avalanche breakdown term, which requires the determination of additional unknown parameters. Note that a very recent study [120] has reached to similar findings of Figure 5.17 (a) and (b) regarding the accuracy improvement at the reverse bias region imposed by a high R_{sh} value of the shaded solar cell. However, the change of R_{sh} of the shaded cell with shading in [120] was not obtained from partial shading experiments of a single solar cell (see literature review in Section 2.9.2) as it is the case in the present work. In addition, the study of [120] did not investigate the effect of changing the other parameters (R_s, n and I_s) on the model accuracy (Figure 5.16) and also did not investigate the single cell model (Figure 5.11).

Further experiments were conducted by increasing the number of 50% shaded cells represented by cases 5 and 6. The output characteristics of both modelling approaches and experimental data of those two cases are witnessed by Figures 5.18 (a) to (d). Case 5 is shown in Figures 5.18 (a) and (b), whereas case 6 is shown in Figures 5.18 (c) and (d). Although the improvement in accuracy achieved by the proposed approach can still be clearly noticed in case 5, the improvement in case 6 has nearly vanished. The reason can be deduced from comparing cases 2, 5 and 6 (see Figures 5.17 (a) and (b) and 5.18 (a) to (d)), which is the fact that the only I_{ph} change approach gets closer to experimental data at the reverse bias region as the number of shaded cells increases. Hence, the accuracy becomes close to the proposed approach. This may be attributed to the fact that the only I_{ph} change approach is capable of detecting the lowering in slope of the reverse bias region when increasing the number of shaded cells, which occurs due to shifting the breakdown voltage to higher negative voltages [97]. This behaviour was reported experimentally in [97] and by simulation in [97], [98], [116].

In addition, except the reverse bias region, regions including the MPPs exhibited overlapped I-V and P-V curves of both approaches. Thereby confirming that the proposed approach can only enhance the model accuracy in this region.

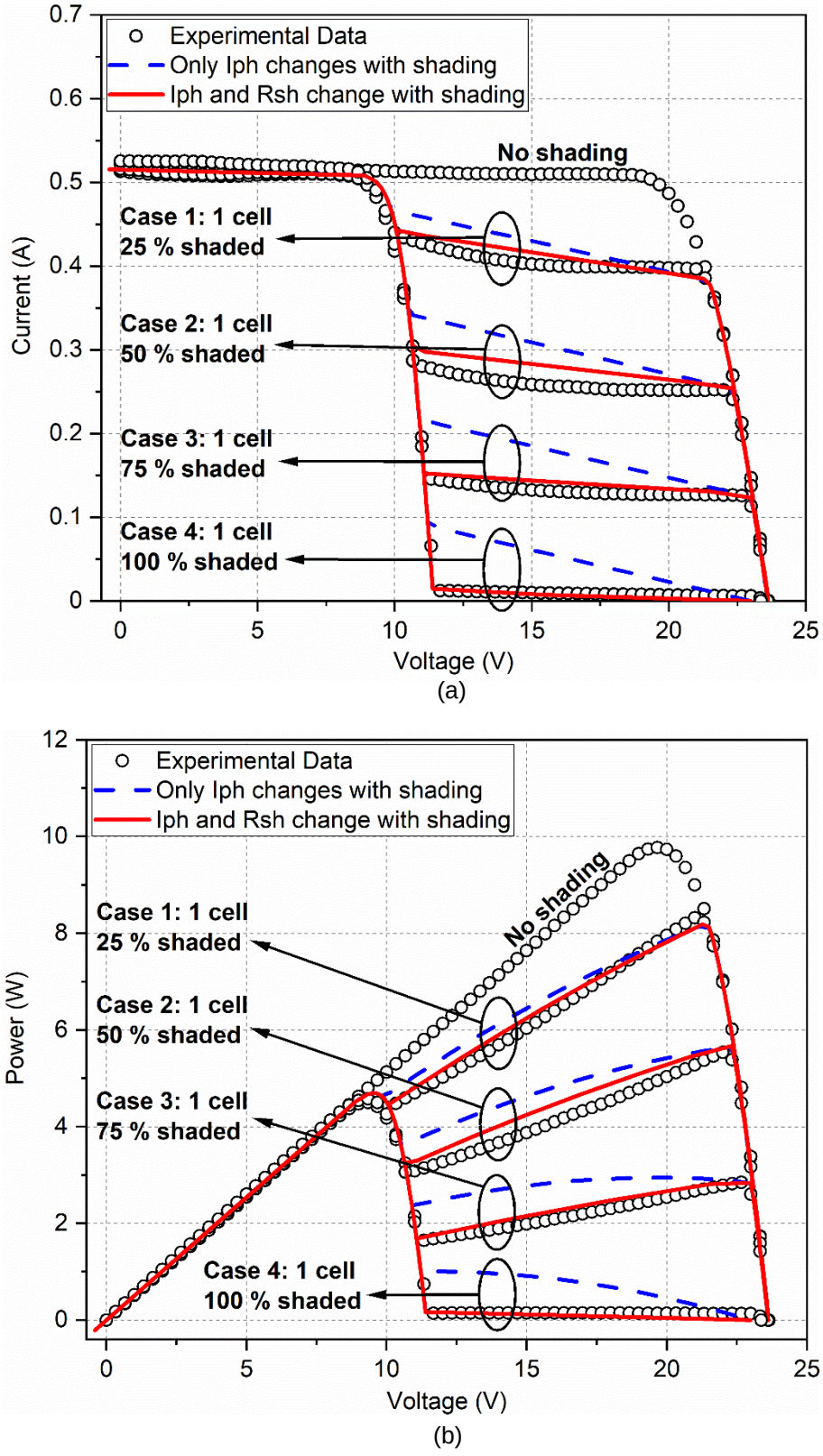

Figure 5.17. Experimental and modelled I-V and P-V curves of the 10 W PV module under shading of a single cell with different percentages (case 1 to 4): (a) I-V curves and (b) P-V curves. (Each experimental I-V and P-V curve is the average of three curves taken at one set of measurements. All measurements were taken under a light irradiance of 1000 W/m² measured at the centre point of the module and at a module temperature of 25 °C).

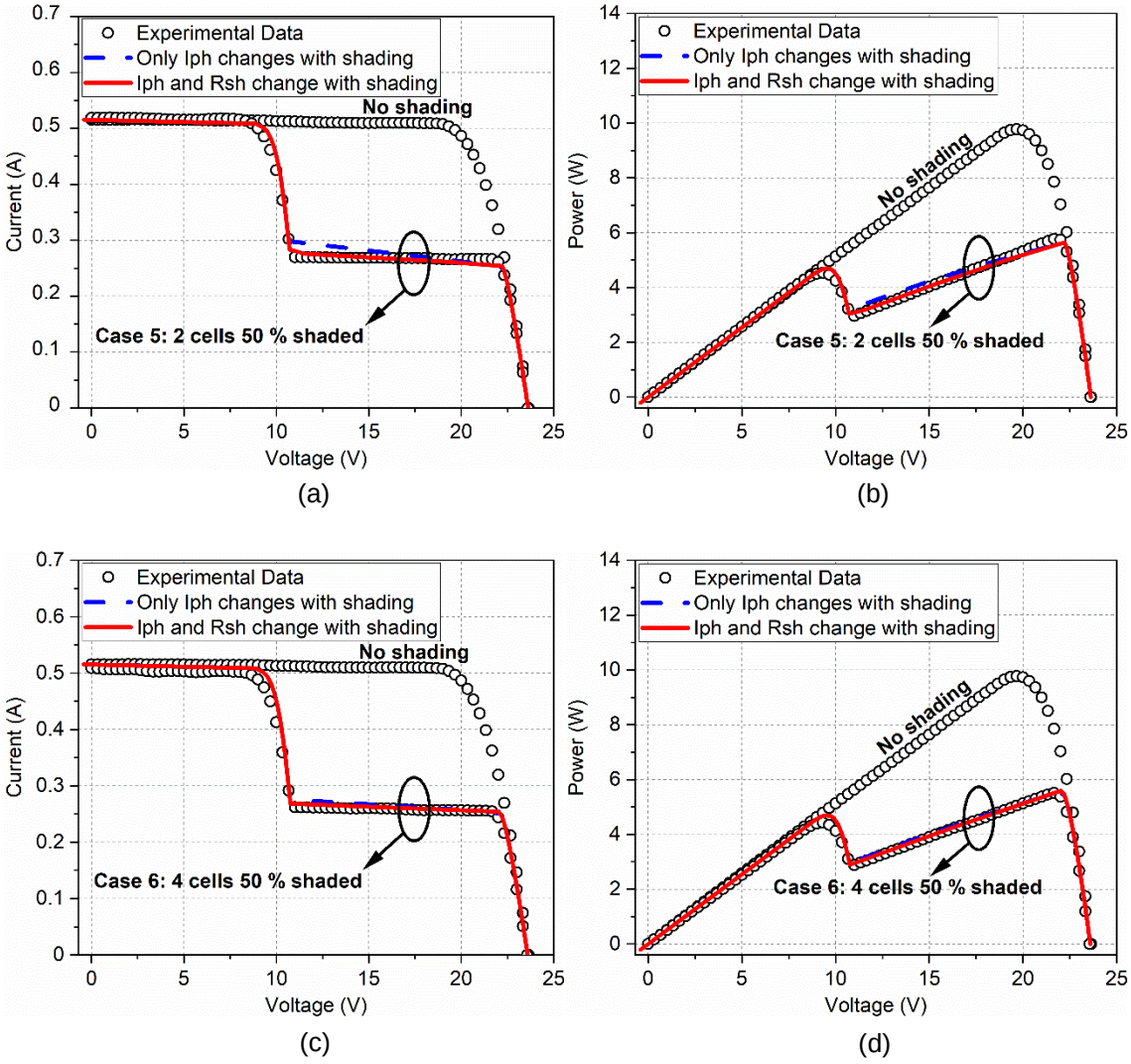

Figure 5.18. Experimental and modelled I-V and P-V curves of the 10 W PV module when increasing the number of shaded cells in string-2 (case 5 and 6): (a) case 5 I-V curve, (b) case 5 P-V curve, (c) case 6 I-V curve and (d) case 6 P-V curve. (Each experimental I-V and P-V curve is the average of three curves taken at one set of measurements. All measurements were taken under a light irradiance of 1000 W/m² measured at the centre point of the module and at a module temperature of 25 °C).

In order to ensure that the error bars of R_{sh} in Figure 5.3 (b) and the shading object error of ±0.2 mm do not deteriorate the proposed approach's improved accuracy, an error assessment was carried-out and presented in Appendix F similar to the one of the single cell model in Section 5.4.2 and Appendix D. First, the modelled output characteristics were obtained using the changes of I_{ph} and R_{sh} with shading and using the only I_{ph} change approach. Second, the upper and lower bounds of R_{sh} were determined from the ±RSD of the error bar in Figure 5.3 (b) and the ±0.2 mm shading object error following the procedure explained in Section 5.4.2. Finally, the modelled output characteristics obtained from the mean R_{sh} value, upper and lower bounds were calculated and plotted

alongside with the only I_{ph} change approach to see whether they overlap or not. The results of cases 1 to 4 are given in Appendix Figures F1 (a) and (b). The results of case 5 are depicted in Appendix Figures F2 (a) and (b), and the results of case 6 are given in Appendix Figures F3 (a) and (b). This error assessment indicates that the errors do not compromise the accuracy improvement achieved from the proposed approach. Thus, the observations and conclusions drawn from Figures 5.17 and 5.18 are valid.

5.6. Summary

Partial shading impact on solar cells was investigated and presented in this chapter in addition to proposing new equations that govern the variations of equivalent circuit parameters with shading. The variations of most equivalent circuit parameters and performance parameters with shading were found to be in a good agreement with previous works in the literature, although the present work constitutes the first study that investigated all of them to the best of the author's knowledge. Furthermore, in order to allow for entering partial shading in a single cell mathematical model as its corresponding irradiance value, it was compared with irradiance reduction in terms of their effects on solar cells' parameters and characteristics. It was observed that both phenomena have almost identical effects.

The proposed equations that explain the variations of the parameters with shading were entered in a single cell model and compared with the commonly used approach, which claims that only I_{ph} changes with shading. The results showed, for the first time, that the improvement in accuracy gained by considering that all parameters change with shading is not significant and less than the measurement error of the experimental set-up and the shading object placement error.

On the other hand, there was a substantial improvement in accuracy over the only I_{ph} approach when modelling PV modules in the region of the characteristics at which the shaded cell is reverse biased. In-depth further experimental and theoretical investigations of the influence of the parameters' variations on the PV module's modelling accuracy revealed that the achieved improvement in accuracy was because of R_{sh}. The other parameters, namely R_s, n and I_s, did not improve the model accuracy when their variations with shading were considered. To the best of the author's knowledge, those findings were not previously reported in the literature. It can thus be claimed that in

addition to I_{ph}, R_{sh} is also a very important parameter that can affect the model accuracy in the reverse bias region. Hence, a modelling approach was proposed in this work, which constitutes taking into account the variations of both I_{ph} and R_{sh} of single cells with shading when modelling PV modules.

The proposed approach was validated experimentally using different shading scenarios and compared with the approach of changing only $I_{ph}$with shading. The results revealed a much higher accuracy for the proposed approach at the reverse bias region when shading a single cell with different percentages. In addition, the improvement is still valid regardless of the measurement error and the shading object placement error considered in the proposed R_{sh} equation. However, this improvement holds for a single cell or two cells shading as it was noticed that it started to diminish when increasing the number of shaded cells. Moreover, the accuracy improvement was only observed in the reverse bias region and there was no improvement in other regions, including the MPPs.

Nonetheless, it can be concluded that the proposed approach can still be used as an accurate tool to simulate the behaviour of PV modules in the reverse bias region under single cell shading without the need to use the avalanche breakdown term, which requires additional parameters that are not readily available (see Section 2.9.2). Single cell shading could occur for instance due to soiling accumulation and plant leaves fall on PV modules [212]. Further, the proposed approach can also be utilised in PV technology research, when accurate representation of the reverse biased solar cell within PV modules is required. Even though the conclusions were drawn from a small 10 W PV module that is intended to be used for battery charging, they might be applied to other large scale modules as well, which needs further research and investigations. Despite the great improvement in accuracy for modelling the reverse bias characteristics under single cell shading due to the concept of an increased R_{sh} with shading, Equation (5.6) still needs to be used with caution as it was developed from only one solar cell.

Chapter 6: Correlation Between Broken Contact Fingers and I-V Characteristics of Partially Shaded PV Modules

6.1. Introduction

This chapter presents a new observation deduced from partial shading of individual solar cells within PV modules. It was noticed that broken contact fingers of a partially shaded cell have an influence on the shape of the I-V curve at the region at which the shaded cell is reverse biased, particularly at the region 1 MPP (see Figure 2.14 (a)). As previously discussed in the literature review in Section 2.10, broken contact fingers are common in PV systems and their current detection techniques are mostly based on complex imaging systems. However, although EL imaging has recently proved to be a cost-effective and valuable tool for inspecting PV modules, it would be useful to investigate the possibility of having an alternative technique that can be used under day light.

In the present work, partial shading of individual cells within a mono-Si PV module was applied and the I-V curves of the module were subsequently measured. A noticeable deformation of the normal shape of the I-V curve at region 1 MPP when shading one of the cells was correlated with broken contact fingers by imaging the cell using ordinary imaging, microscopic imaging and microscopic inspection. Different methods were utilised for validation of this correlation. First, the effect of increasing the number of broken contact fingers on a single mono-Si solar cell's I-V curve and fill factor (FF) was explored and found to have a similar behaviour to the deformed I-V curve of the module, which is a reduction in FF. Second, thermal images of the module were captured. It was interestingly found, however, that they were not capable of detecting the broken contact fingers due to the non-uniformity of the light source. That is to say that hot spots because of light non-uniformity overcame those because of broken contact fingers and hence prevented their appearance.

Third, another attempt to validate the observations from the I-V curve was capturing EL images. It was found that EL imaging successfully detected the cell with broken contact fingers, thereby confirming the correlation between the module's I-V curves under single cell partial shading and broken contact fingers. Fourth, the correlation was further

validated using an in-house assembled mono-Si PV module when intentionally breaking the contact fingers of one cell and correlate the module's I-V curves when shading this cell with its EL images. These observations have made the concept of detecting broken contact fingers using individual cell partial shading under day light feasible.

6.2. I-V Characteristics of a PV Module under Individual Cell Partial Shading

As partial shading of individual cells within PV modules can provide a wealth information about the health of the cells as previously discussed in Section 2.10.4, it was applied in this research to the mono-Si 10 W PV module used in previous investigations of Section 5.5 and shown in Figures 3.14 (a) to (c). The performance parameters at STC were previously mentioned in Section 5.5.2. The 36 cells of this module were numbered as shown in Figure 6.1 in order to easily follow the results of individual cell shading. This module was subjected to an individual cell shading experiment under an irradiance of 1000 W/m² measured at the centre point of the module and at a module temperature of 40 °C. The cells were individually shaded by 50% covering their left-hand side using the adhesive foam tape and the module's I-V curve was subsequently measured three times at one set of measurements for each cell shading.

Note that the shape of the reverse bias region on a PV module's I-V curve is almost the same for a single cell's small and large area shading as shown by the experimental I-V curves in Figure 5.17 (a) and also shown by [123], [139]. Therefore, 50% shading was selected in the present work as it is easy to implement due to the fact that the cells' areas of this module are divided by the busbars into two equal parts.

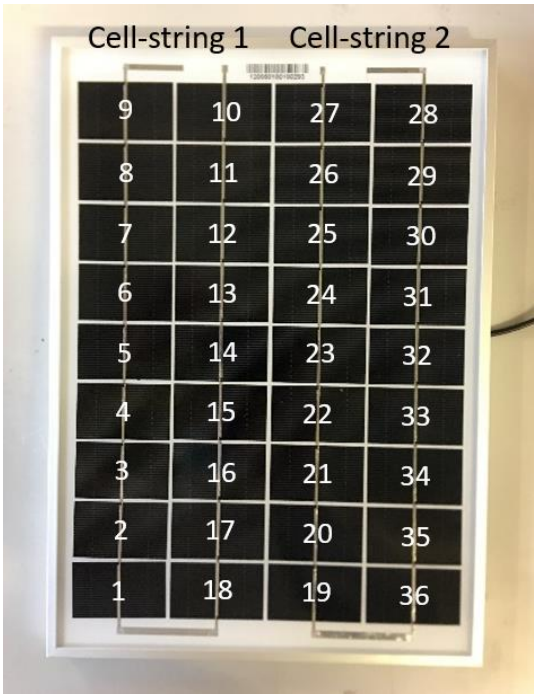

Figure 6.1. Cells numbering of the 10 W PV module used in the investigation of individual cell shading.

In Figure 6.2, the I-V curves when shading individual cells are plotted in addition to the no shading I-V curve. It can be observed from this figure that there are three cells that produce remarkably different module's I-V curves from the other cells at the reverse bias region (between about 10 and 21 V). Cells 3 and 4 showed noticeably higher slopes, which can be postulated to low R_{sh} defects as shown by [128], [172], [174].

Another I-V curve that has a different shape from the rest and indicated in red colour in Figure 6.2, is the one obtained when shading cell 24. This I-V curve is clearly different because of its convex knee at region 1 MPP. This interesting behaviour under single cell partial shading has not been reported before. Thus, further investigations were needed in order to identify the main cause as will be presented later in this chapter.

The discrepancy in I-V curves at the reverse bias region is attributed to the non-uniformity of the light source. As the module current at this region is almost completely limited by the shaded cell current [1], the non-uniformity caused unshaded parts of the cells to produce different currents resulting in the discrepancy seen in Figure 6.2. Despite the non-uniformity of light source, the unique I-V curve behaviour at region 1 MPP when partially shading cell 24 can still be clearly perceived.

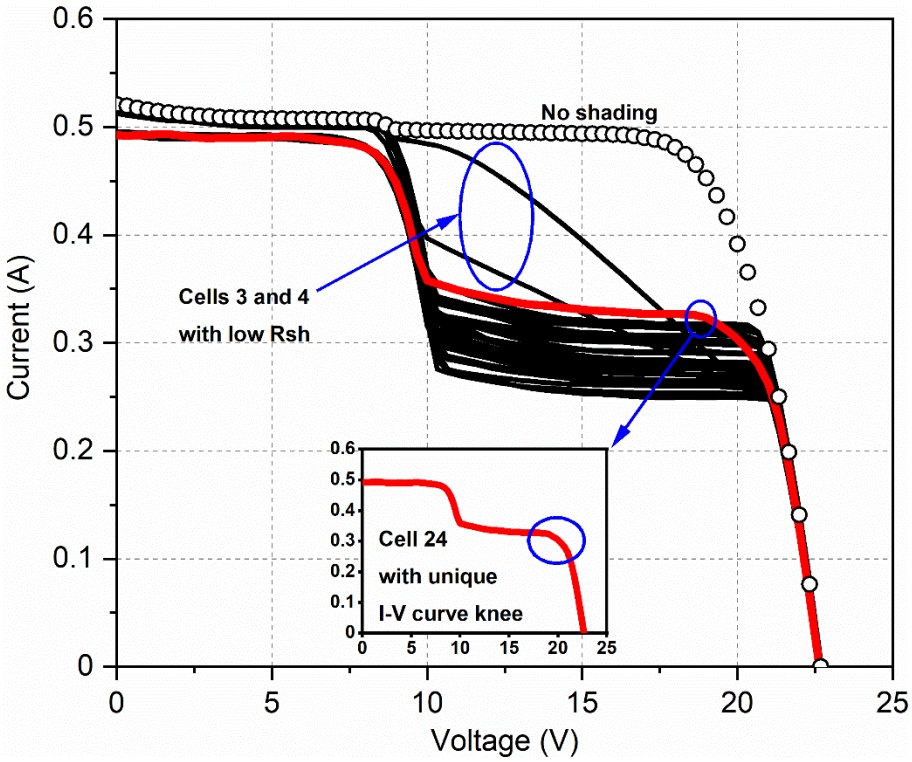

Figure 6.2. Experimental I-V curves of the 10 W PV module at no shading and when shading each cell by 50%. (Each I-V curve is the average of three curves taken at one set of measurements. All measurements were taken under a light irradiance of 1000 W/m² measured at the centre point of the module and at a module temperature of 40 °C).

In order in ensure repeatability of the module's I-V curve resulted from 50% shading of cell 24, the I-V curve measurement was repeated 12 times divided into three different days with four measurements in each day. The testing facility was shut down after each testing day. Those shading experiments were implemented for the left and right-hand sides shading of the cell at an irradiance of 1000 W/m² measured at the centre point of the module and at a module temperature of 40 °C. The results are depicted in Figure 6.3, in which the average I-V curves from the 12 measurements are plotted for the left and right-hand sides shading. The error bars represent the standard deviation (SD) of the currents at the voltage of region 1 MPP knee of the I-V curve resulted from shading the right-hand side of the cell. The results show that the difference between the I-V curves is much greater than the error bars, which validates the repeatability of the unique convex I-V curve knee when shading the left-hand side of cell 24.

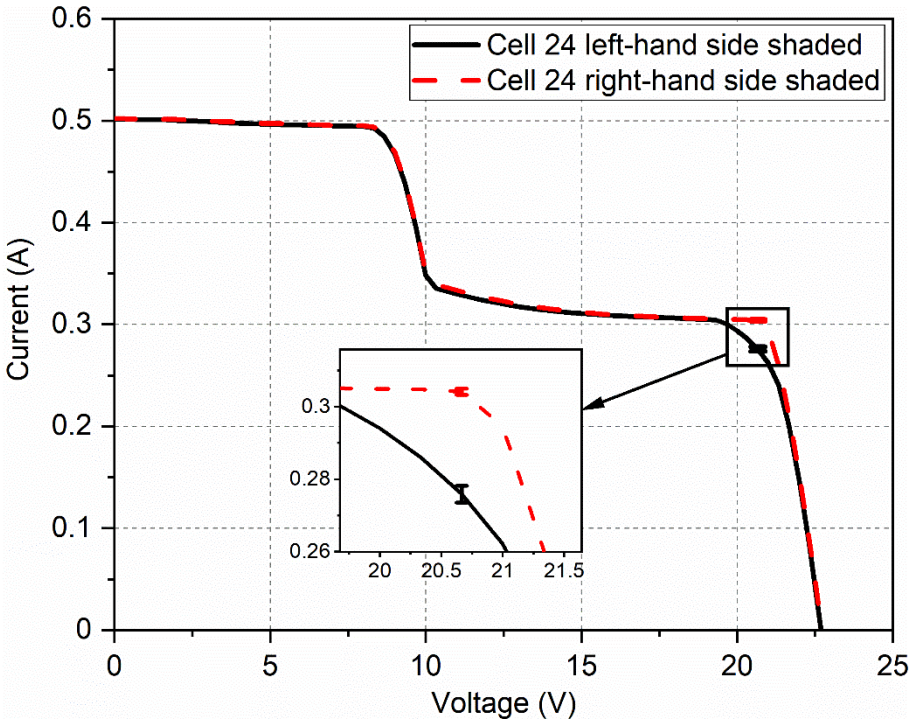

Figure 6.3. Comparison between Experimental I-V curves of the 10 W PV module when shading left and right-hand sides of cell 24. (Each I-V curve is the average of 12 measurements taken over three days, with four measurements obtained per day. The error bars represent the standard deviation of the currents at the voltage of region 1 MPP knee of the right-hand side shading I-V curve. All measurements were taken under a light irradiance of 1000 W/m² measured at the centre point of the module and at a module temperature of 40 °C).

6.3. Inspection of the Solar Cell that Provided a Convex I-V Curve Knee

In order to identify the reason for the convex I-V curve knee resulting from shading cell 24 in the previous section, the cell was inspected and imaged. A close image of the cell was captured using a 12 megapixels camera and given in Figure 6.4 (a) showing a crack at the right-hand side of the cell, marked with the red circle (cannot be clearly seen in the figure). This crack was nearly impossible to be detected by naked eyes. In order to obtain more informative images, the cell was inspected and imaged using a microscope. Figure 6.4 (b) shows an image captured using a 10 megapixels microscopic camera [213] mounted on a microscope model SZ from Olympus [214]. This image clearly shows the crack nearly perpendicular to the contact fingers. In order to investigate whether this crack breaks the contact fingers or not, a zoomed image of the top two contact fingers was captured and depicted in Figure 6.4 (c). This image shows that this crack breaks the contact fingers. A visual inspection using the microscope has also revealed that the crack breaks all the nine contact fingers affected.

Therefore, this interesting observation has confirmed that the deformed convex knee of region 1 MPP in Figure 6.2 when shading cell 24 is most likely due to broken contact fingers. These results confirm that there is a correlation between broken contact fingers of a solar cell and the I-V curve's shape of the module under partial shading of the cell. Thus, it is feasible to identify the cells with broken contact fingers from module's I-V curves under cell partial shading.

It is to be noted that a similar convex knee due to cracks was recently reported in [179], but it was obtained without single cell shading. That is to say that the cracked cell in [179] governs the shape of the I-V curve without shading. Thus, this convex knee will not appear if more serious faults exist in the same cell-string that contains the cracked cell. On the other hand, applying single cell partial shading forces the shaded cell to govern the I-V curve's shape [139] and thus this knee will be presented even if other faults exist.

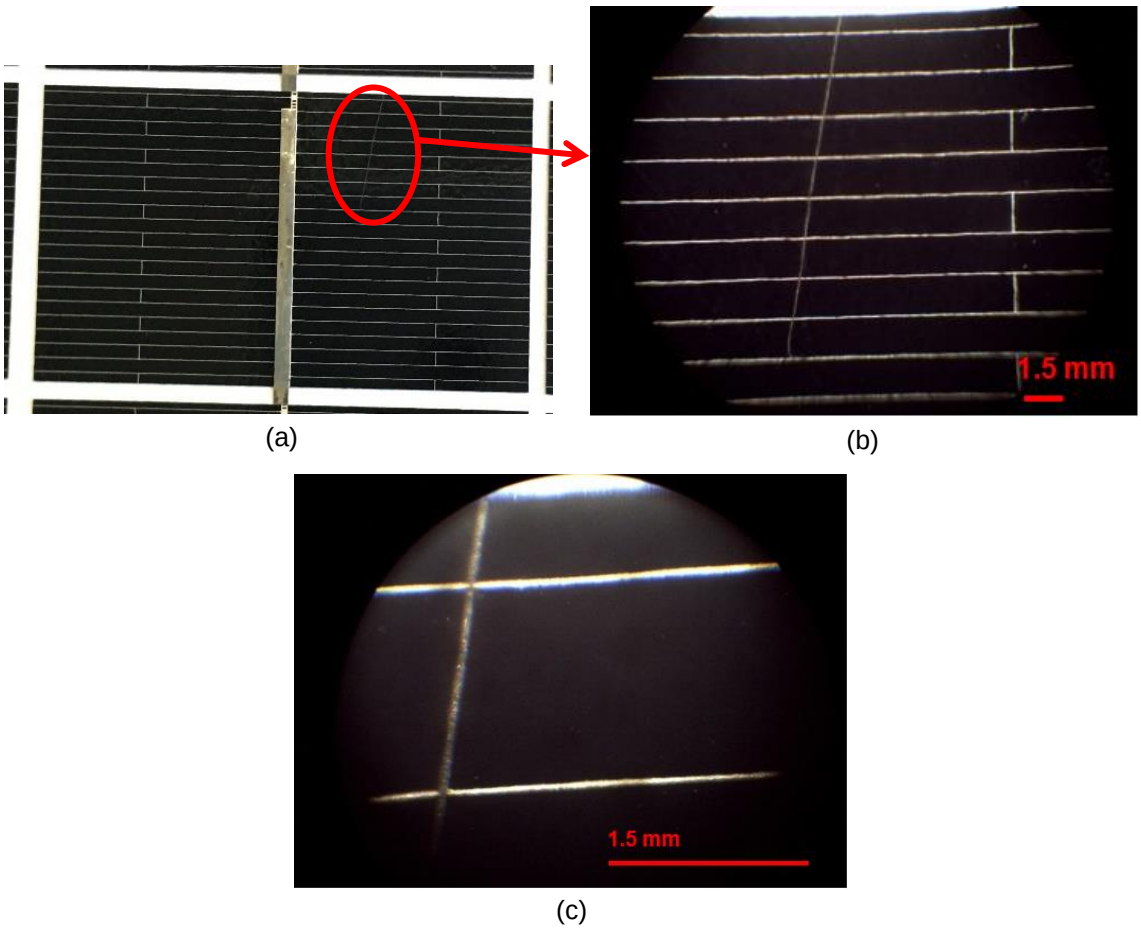

Figure 6.4. Images of the surface of cell 24 which caused the module to have a convex I-V curve knee shown in Figure 6.2: (a) an ordinary image, (b) a microscopic image shows a crack runs through the contact fingers and (c) a zoomed microscopic image at the top of the crack shows that the contact fingers are broken. (Total cell area in (a) is 15 cm² (3 cm x 5 cm)).

6.4. Validation of the Correlation

This section presents different investigations performed to validate the correlation between the characteristics of the PV module under individual cell partial shading and broken contact fingers. First, the influence of increasing the number of broken contact fingers on a single solar cell's I-V curve and FF will be discussed. Second, attempts to validate the correlation by thermal imaging and EL imaging of the 10 W module will be explained. Finally, the correlation is validated using a small module prepared in the laboratory.

6.4.1. Effect of Broken Contact Fingers on the I-V Characteristics and Fill factor a Single Solar Cell

As shown in Figure 6.2, the unique feature of the module's I-V curve when shading cell 24, which has broken contact fingers, is its reduced FF at region 1 represented by the convex knee. Thus, the first step towards validation of this correlation was to study the influence of broken contact fingers on a single solar cell's I-V curve and FF. The used mono-Si solar cell has an active area of 6.25 cm² (2.5 cm x 2.5 cm) and it was prepared following the procedure explained in Section 3.3. The cell has a P_{max}, I_{sc} and V_{oc} of 100.4 mW, 0.213 A and 0.6260 V, respectively at STC, determined from the average of three I-V curves taken at one set of measurements. In addition, it has 16 contact fingers attached to a single busbar as depicted in Figure 6.5, which shows the cell connected with the test rig under the light source.

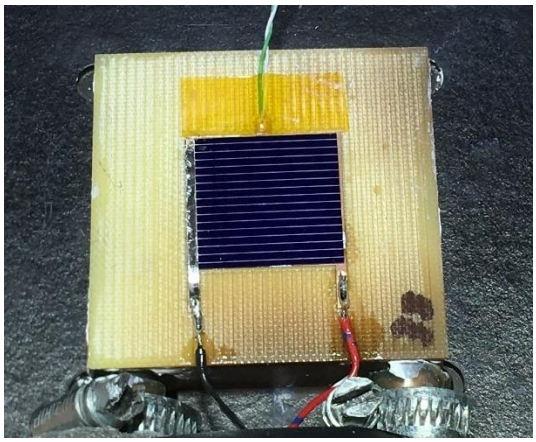

Figure 6.5. The mono-Si solar cell (area = 6.25 cm²) under the light source. (This solar cell was used in investigating the influence of broken contact fingers experiments).

First, an EL image of the cell was captured without any broken contact fingers. The EL imaging experimental set-up was presented previously in Section 3.10. Second, the I-V curve was measured 12 times over three different days with four measurements per day, during which all test equipment and light source were switched OFF after each four measurements. These two steps were repeated, but after cutting 6, 11 and the total 16 contact fingers using a knife and a metal ruler, thereby gradually increasing the number of broken contact fingers. All I-V curve measurements were taken under STC.

The El imaging was used at each stage of cutting the contact fingers in order to ensure that they were broken and not only scratched. The broken contact fingers will make part of the cell area to appear remarkably darker in the EL images due to current flow interruption [14]. The ordinary images and EL images of the cell under the four steps of breaking the contact fingers are demonstrated in Figures 6.6 (a) to (d). The upper and lower photographs of the figure show the ordinary images and EL images, respectively. The disconnected areas due to breaking 6, 11 and 16 contact fingers were approximately 17, 33 and 50% from the total cell area, respectively.

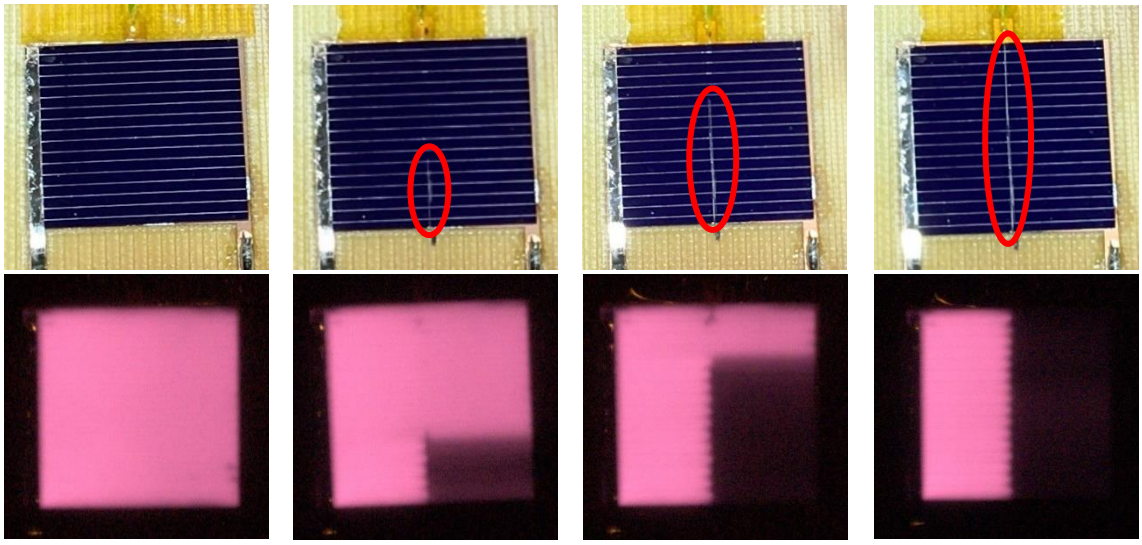

Figure 6.6. Ordinary images and EL images of gradually breaking the solar cell contact fingers: ((top) ordinary images and (bottom) EL images): (a) no broken contact fingers, (b) 6 broken contact fingers, (c) 11 broken contact fingers and (d) 16 broken contact fingers.

The I-V curves at each step of damaging the contact fingers obtained from averaging the 12 measurements are plotted in Figure 6.7 in addition to the error bars added at some points representing the SD of the current. Although I_{sc} and V_{oc} were not greatly affected,

a significant reduction in the P_{max} and FF can be clearly perceived. The I-V curve's knee at the MPP becomes less sharp with increasing the number of broken contact fingers.

The reduction of FF can be seen in Figure 6.8, which depicts its variation with increasing the number of broken contact fingers. The FF was 0.748 at no broken contact fingers and decreased to 0.471 when breaking the 16 contact fingers. This decrease is attributed to the poor electrical contact due to damaging the contact fingers and can be correlated with the increase in the size of the dark part of the EL images in Figures 6.6 (b) to (d).

Comparing Figure 6.7 with the behaviour of the 10 W PV module when partially shading cell 24 in Figure 6.2 reveals that both I-V curves exhibit distorted I-V curve knees with decreased FFs due to damaged contact fingers. Therefore, those results confirm that the change of the I-V curve's shape in Figure 6.2 was due to a reduction in FF of cell 24 caused by damaged contact fingers.

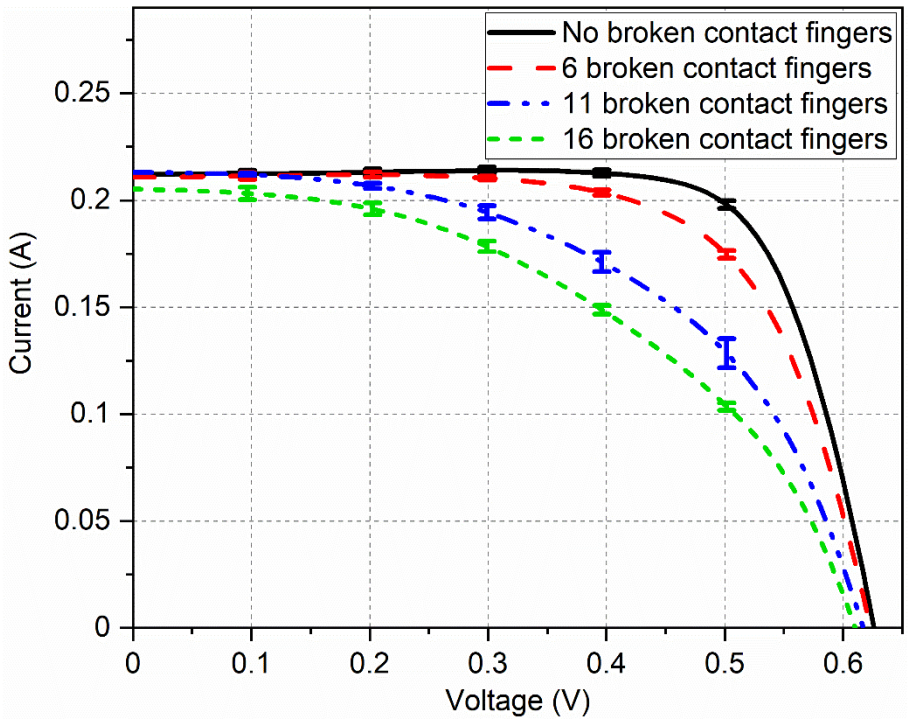

Figure 6.7. Effect of broken contact fingers on the I-V curve of the solar cell. (Each I-V curve is the average of 12 measurements taken at STC over three days, with four measurements obtained per day. The error bars represent the standard deviation of the current at some points).

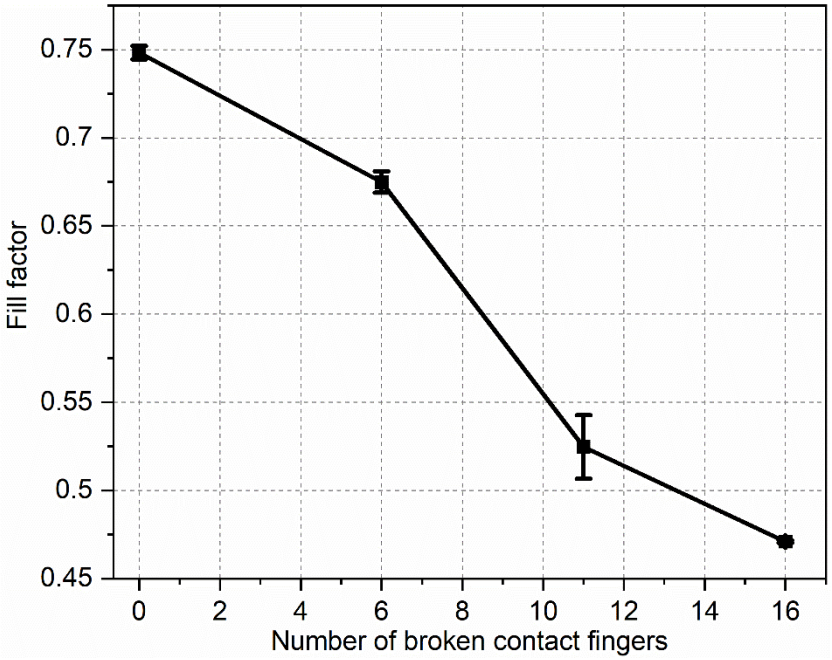

Figure 6.8. Effect of broken contact fingers on the fill factor of the solar cell. (Each fill factor value was calculated by averaging 12 values from 12 I-V curve measurements taken at STC over three days, with four measurements obtained per day. The error bars represent the standard deviation).

6.4.2. Possibility of Validating the Correlation Using Thermal Imaging

Thermal imaging was tested in this work for the detection of broken contact fingers in cell 24 to validate the observed correlation. In thermal imaging, broken cells appear as hot spots as shown by [150]. In the present work, the 10 W PV module was placed under the light source without the cooling system in order to allow heating of the defected cells. Moreover, the module was short circuited in order to capture the thermal images under this condition [1]. Subsequently, a thermal image depicted in Figure 6.9 (a) was captured using the FLIR C2 thermal camera as explained in Section 3.9. The image shows that cell 24 did not exhibit a hot spot. However, other two cells showed hot spots with remarkably higher temperatures, which are cells 5 and 20.

In order to identify the reason why cell 24 did not have a hot spot although its contact fingers are broken, an irradiance mapping on the individual cells was performed. The reference cell 200R was placed on the individual cells and three measurements of irradiance were recorded for each cell while it was measured as 1000 W/m² at the centre point of the module. The averaged irradiance values are presented in Figure 6.9 (b), showing that the cells 5 and 20 that had hot spots also received the minimum irradiances in their respective cell-strings (marked in red font in the figure). This can also be

perceived from Figure 6.10, in which the cells numbers are plotted versus the irradiance and temperature values. The temperatures of cells in Figure 6.10 are the averaged values from three thermal images. It can be seen from this figure that cell 5 had the highest temperature in cell-string 1 and also received the minimum irradiance among all 18 cells in this cell-string. Similarly, cell 20 also had the highest temperature in cell-string 2 and received the minimum irradiance in this cell-string.

Thus, for this experimental case, the broken contact fingers could not be detected using thermal imaging because of the irradiance non-uniformity. In other words, irradiance non-uniformity had more severe effect on solar cells heating than broken contact fingers. Thus, the cells with minimum irradiance in their respective cell-string were the weakest cells. This explains the reason for the appearance of the hot spot on cell 20 in cell-string 2 instead of the defected cell 24 as shown in Figure 6.9 (a). Thermal imaging generally results in hot spots' creation on the weakest cells due to the fact that they work as a load when they are reverse biased [1]. As a matter of fact, the non-uniformity also prevented the appearance of hot spots on cells 3 and 4, which exhibited a module's I-V curves in Figure 6.2 that are correlated with low R_{sh} defects, which are known to cause hot spots [11], [128], [175].

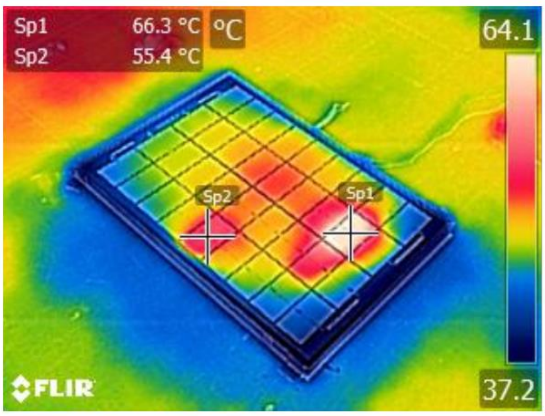

(a)

Cell-string 1		Cell-string 2	
737	747	846	835
704	845	895	864
687	857	973	932
670	838	989	945
644	803	943	909
662	760	860	858
667	716	777	833
710	714	722	732
757	740	728	737

(b)

Figure 6.9. Thermal image and irradiance mapping of the 10 W PV module: (a) thermal image shows the temperature distribution on the cells and (b) irradiance mapping of the cells in W/m². (Each irradiance measurement is the average of three measurements).

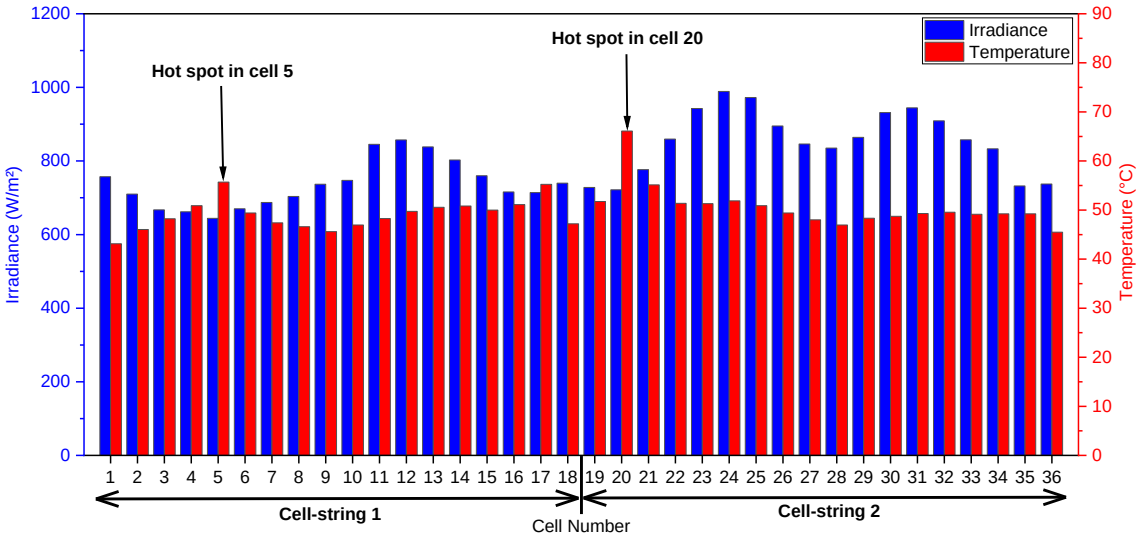

Figure 6.10. Relationship between temperature and irradiance of all cells in the 10 W PV module. (Each irradiance and temperature measurement is the average of three measurements).

6.4.3. Validation of the Correlation Using EL Imaging

EL imaging was used to inspect the 10 W module using the set-up presented in Section 3.10. The EL image is shown in Figure 6.11, revealing that cell 24 has a clear dark region at the top right-hand side corner. This region coincides with the region of damaged contact fingers shown in Figures 6.4 (a) and (b). This EL image confirms that the convex knee of the module's I-V curve when cell 24 is partially shaded shown in Figure 6.2 is due to broken contact fingers of this cell. Therefore, this EL investigation has provided further evidence that it is possible to identify the cells with damaged contact fingers through partial shading of solar cells in PV modules.

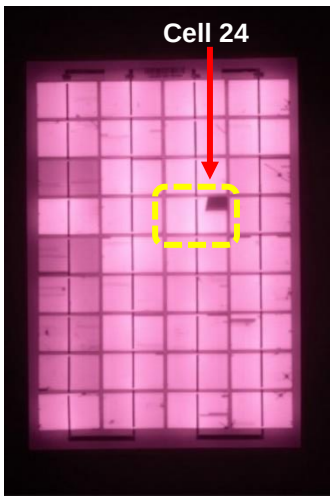

Figure 6.11. EL image of the 10 W PV module shows that cell 24 has broken contact fingers that disconnect a part of the cell area.

6.4.4. Validation of the Correlation Using an In-house Made PV Module

The last validation method used was investigating the influence of broken contact fingers on the I-V curves of another module when shading the affected cell. The in-house made PV module assembled in the laboratory as discussed in Section 3.4.2 was used for this purpose. Under an irradiance of 1000 W/m² measured at the centre point of the module and at a module temperature of 25 °C, this module has a P_{max}, I_{sc} and V_{oc} of respectively 1.0381 W, 0.2038 A and 7.06 V, obtained from the average I-V curve of three curves taken at one set of measurements. In Figure 6.12 (a) a schematic of the configuration of the 12 solar cells and two bypass diodes is shown. Figure 6.12 (b) shows a photograph of the module illustrating the cells' numbering.

First, every cell in the module was shaded by 50% covering its left and right-hand sides, respectively, in order to inspect them by observing the module's I-V curve when they are shaded. Thereby ensuring that they did not have broken contact fingers that deform the module's I-V curve at region 1. The used shading object was fabricated using the 3D printing technology discussed in Section 3.8. A photograph of the module taken while it was under single cell shading experiments is given in Figure 6.13.

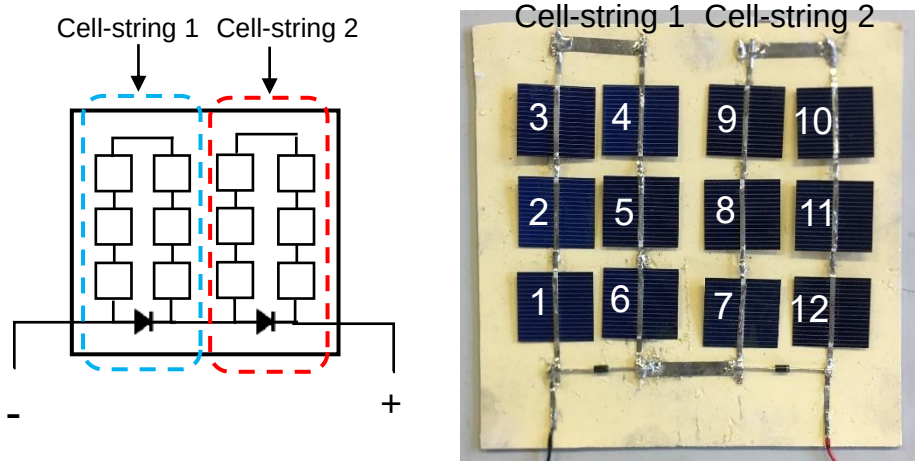

Figure 6.12. The in-house assembled PV module: (a) a schematic diagram of cells and bypass diodes configuration and (b) a photograph showing the cells' numbering.

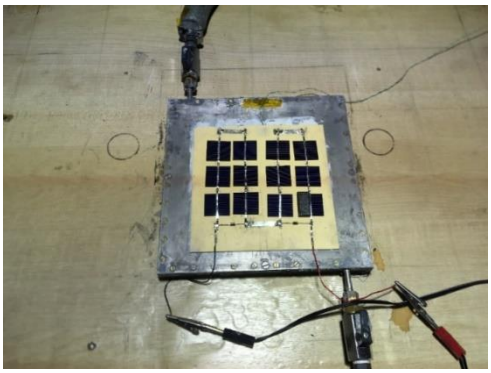

Figure 6.13. The in-house assembled PV module under the light source and 50% shading of one cell. (This PV module was used for validation of the correlation between broken contact fingers and I-V curve under partial shading of solar cells).

The I-V curves of the module when shading the left and right-hand sides of the cells are respectively shown in Figures 6.14 (a) and (b) including the I-V curve at no shading. Each I-V curve in the figure is the average of three curves taken at one set of measurements under a light irradiance of 1000 W/m² measured at the centre point of the module and at a module temperature of 25 °C. It can be seen that there is not any I-V curve that exhibited a unique shape at region 1 MPP. It is to be noted that the step seen in the I-V curve of the no shading condition (at about 3 V) is attributed to the conduction of the bypass diode due to imperfections in soldering the cells, which caused a mismatch. Moreover, the discrepancy in the I-V curves at the reverse bias region (between about 3.1 and 6.5 V) is due to the non-uniformity of irradiance incident on the cells as it is the case with the 10 W PV module explained in Section 6.2 and shown in Figure 6.2.

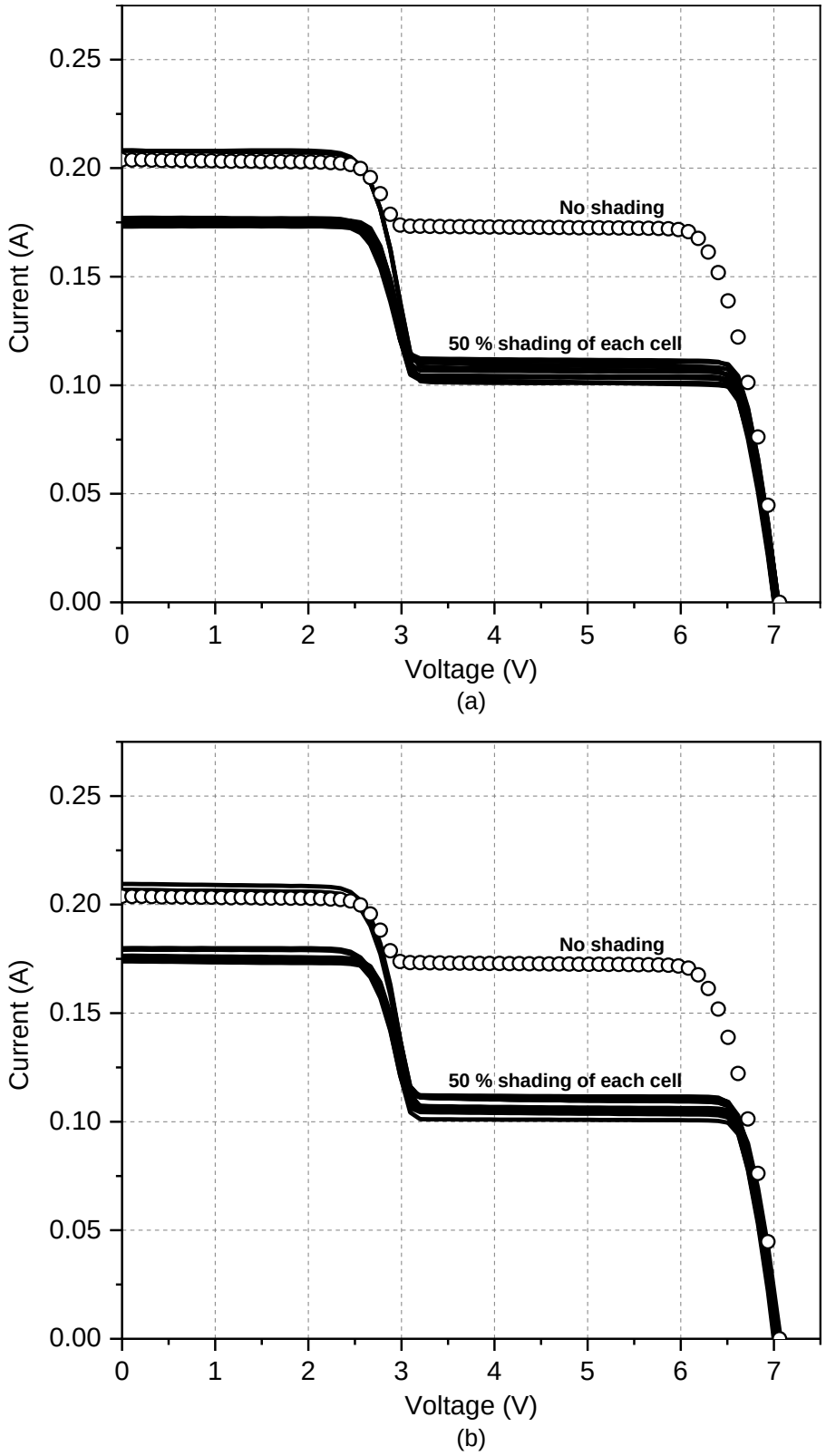

Figure 6.14. Inspection of the in-house assembled PV module through I-V curves under 50% shading of left and right-hand sides of individual cells: (a) left-hand side and (b) right-hand side. (Each I-V curve is the average of three curves taken at one set of measurements. All measurements were taken under a light irradiance of 1000 W/m² measured at the centre point of the module and at a module temperature of 25 °C).

Second, the next step was to investigate the module's behaviour when intentionally breaking the contact fingers of one cell. Cell 12 was selected for this purpose due to its location at the module's corner, which made it simple to perform the experiments. The 16 contact fingers of this cell were cut using a knife and a metal ruler in two steps, which involved cutting 9 and the total 16 contact fingers.

The module's EL image was captured with no broken contact fingers and after each step of breaking them. The ordinary images of cell 12 at each breaking step and the corresponding EL images of the module are depicted in Figures 6.15 (a) to (c). Cutting the cell's contact fingers took place near its busbar as shown in the figures, thus disconnecting approximately a quarter of the cell area when 9 contact fingers are broken and disconnecting about half of it when the total 16 are broken.

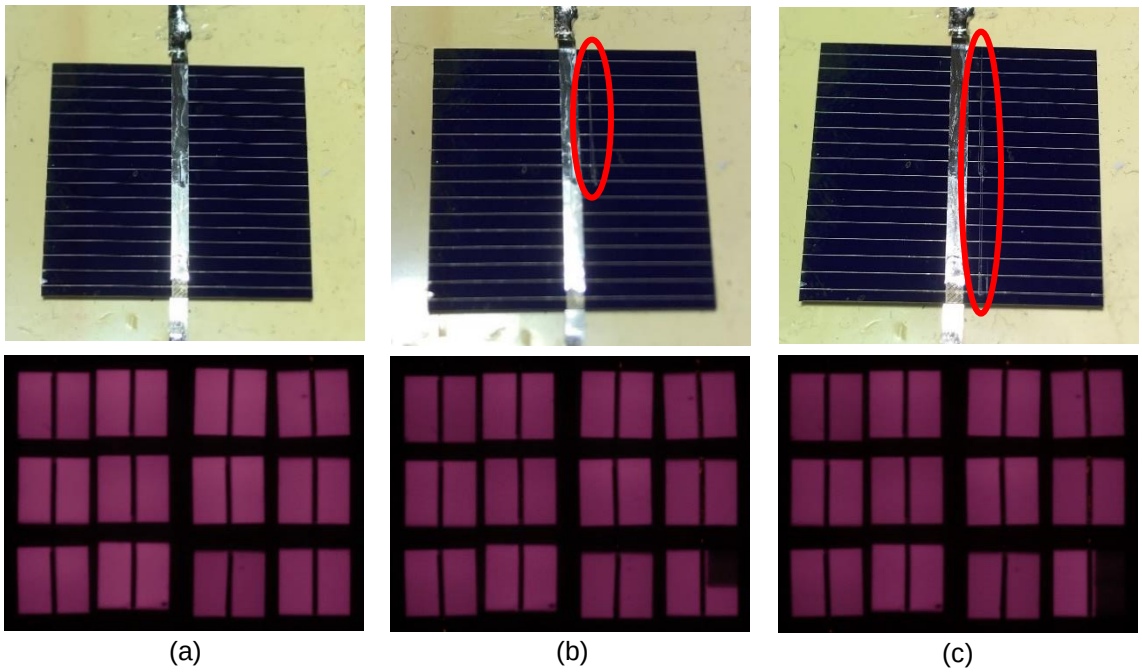

Figure 6.15. Ordinary images and EL images of gradually breaking cell 12 contact fingers in the in-house assembled PV module: ((top) ordinary images of cell 12 and (bottom) EL images of the module): (a) no broken contact fingers, (b) 9 broken contact fingers and (c) 16 broken contact fingers.

Furthermore, without breaking the contact fingers and for each step of breaking them, the I-V curve of the module with 50% shading of cell 12 was measured 12 times over three days, with four measurements taken in each day. The testing facility was switched OFF after each set of four measurements per day. All measurements were taken under a light irradiance of 1000 W/m² measured at the centre point of the module and at a module

temperature of 25 °C. The averaged I-V curves of the 12 measurements for each case are plotted in Figure 6.16 including error bars, which demonstrate the SD of the current at the vicinity of region 1 MPP. The I-V curves and their zoom-in view in the figure show that the slope near region 1 MPP gradually increases when breaking more contact fingers. The variations occurred to the I-V curve are much greater than the error bars, which indicates that breaking the cell contact fingers causes a deformation near region 1 MPP and hence a reduction in the FF of region 1. This can be attributed to a reduction in the FF of the affected cell in a good agreement with the single cell investigation in Figure 6.7.

Although the signature of broken contact fingers on this module's I-V curve is quite different from the one obtained from the 10 W module when shading cell 24 in Figure 6.2, both curves exhibit a reduction in FF of region 1. Therefore, the experimental study of this section has further confirmed that cell partial shading in PV modules can provide an indication of broken contact fingers associated with a particular cell.

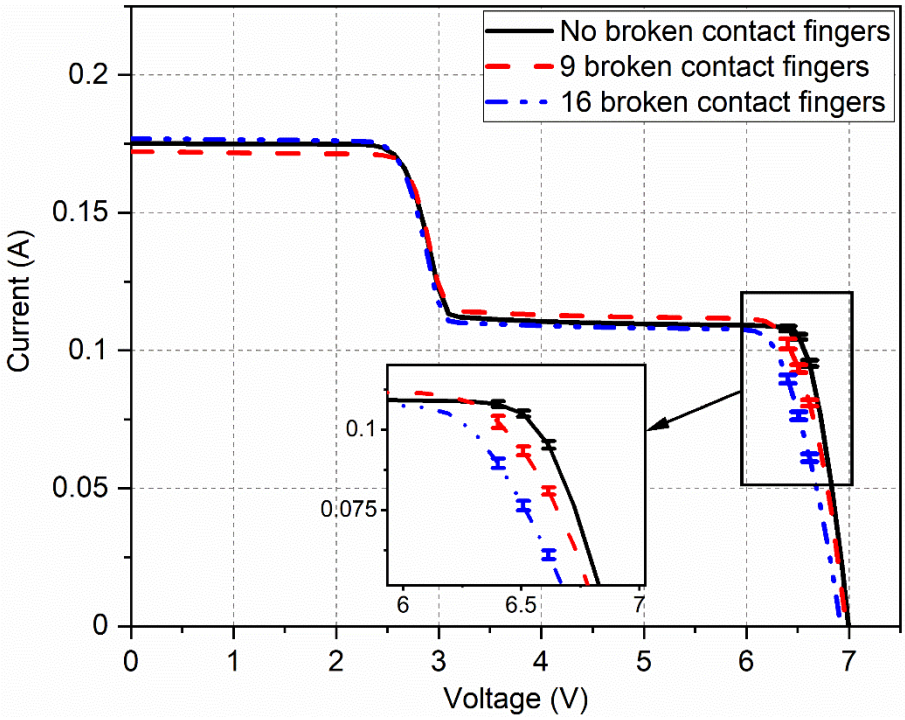

Figure 6.16. Experimental I-V curves of the in-house assembled PV module under 50% shading of cell 12 and with increasing its broken contact fingers. (Each I-V curve is the average of 12 measurements taken over three days, with four measurements obtained per day. The error bars represent the standard deviation of the current at some points near region 1 MPP. All measurements were taken under a light irradiance of 1000 W/m² measured at the centre point of the module and at a module temperature of 25 °C).

6.5. Summary

A new observation of the behaviour of PV modules with partially shaded individual solar cells has led to proving the possibility of detecting cells with broken contact fingers through I-V curves. When partially shading individual cells in a mono-Si PV module, it was found that shading a particular cell caused the module to exhibit an I-V curve with a convex MPP knee. This cell was subsequently imaged by ordinary imaging and microscopic imaging, and inspected under a microscope. The images revealed that this cell has broken contact fingers, thereby confirming the correlation between the module's I-V characteristics under single cell partial shading and broken contact fingers.

This correlation was first validated by investigating the behaviour of a single mono-Si solar cell under broken contact fingers. It was found that breaking the cell contact fingers caused a noticeable decline in its FF, in a good agreement with the behaviour of the PV module when partially shading the affected cell. Then, an attempt to validate the correlation was made using thermal imaging of the PV module, but unfortunately, it was not capable of detecting the cell with broken contact fingers due to irradiance non-uniformity of the light source. It was shown in this experimental investigation that the cells exhibited hot spots in the thermal image were actually receiving the minimum irradiance in their respective cell-strings. In this particular experimental case, the cell received the minimum irradiance was weaker than the cell affected by broken contact fingers in terms of power production, thereby being the weakest cell in the cell-string. Hence, the hot spots appeared on the weakest cell and not on the cell that has broken contact fingers. It can be thus concluded that for the light source used in this work, thermal imaging was not adequate for detecting the cells with broken contact fingers.

Another validation method used in this work was EL imaging. The captured EL image of the module clearly showed that the cell has broken contact fingers that disconnect a part of its area. Moreover, the last validation method was investigating the behaviour of another mono-Si PV module assembled in-house when partially shading a cell affected by broken contact fingers. Although the shape of the resulted module's I-V curve at region 1 MPP was quite different from that of the other module that was originally used to develop the correlation, both I-V curves showed a deformation represented by a reduction of the FF of region 1.

Therefore, it can be concluded from the work presented in this chapter that it is possible to detect damage of the contact fingers of solar cells through I-V curves of partially shaded PV modules. It is to be noted that the work presented in this chapter is a proof of concept only and not a technique for detecting broken contact fingers. This is because defects within a solar cell other than broken contact fingers, such as a high series resistance, may also cause a deformation in region 1 MPP. Hence, further research is indeed required to differentiate the signature of broken contact fingers on I-V curve from those of other defects. The change in region 1 FF or region 1 MPP due to broken contact fingers may then be used to develop a detection technique that can be used under day light.

Chapter 7: Conclusions and Future Work Recommendations

7.1. Introduction

This research work has provided a detailed experimental and theoretical characterisation of solar cells and modules working under partial shading conditions. The aim and objectives of this thesis outlined in Chapter 1 have been successfully achieved. Performance testing of the light source was implemented, and samples of PV devices were prepared in addition to building the experimental set-ups for their characterisation. Furthermore, a technique to improve the accuracy of solar cells parameters extraction from experimental I-V curves was proposed and tested in order to be used in other investigations within this research.

A systematic study of partial shading started by investigating the variations of a solar cell equivalent circuit parameters and performance parameters with shading. Partial shading was then compared with reducing the irradiance in terms of their influence on all solar cell parameters. Subsequently, the variations of the single cell equivalent circuit parameters with shading were used in modelling a solar cell and a PV module, thereby investigating any possible improvements in accuracy gained by considering those variations. Finally, single cell shading within PV modules proved to be useful in detecting broken contact fingers.

In the remainder of this chapter, main conclusions of the findings explored in this research and how they have contributed to the existing knowledge are firstly presented followed by suggestions for future research avenues built upon those findings.

7.2. Conclusions

The main conclusions of this research can be listed for each topic as follows:

1. **Light source testing, solar cells and modules samples and complete I-V curve measurement set-up**

The light source qualification testing in this work according to the E927-10 standards confirmed that it was sufficiently reliable for the purpose of this research with a

classification of Class BCA for solar cells characterisation. The prepared solar cells and modules samples and their test rig including the water cooling was successfully used in this work to perform controlled experiments. Using a PCB as a support for solar cells was found to be a convenient way for soldering the contacts and terminals. In addition, it provided a mechanical support for solar cells and simplified their interface with the cooling system. Similarly, using thermal interface for the in-house assembled PV module has proved to be a valuable solution for supporting the cells and for cooling purpose. The complete characterisation experimental set-up repeatability in terms of producing I-V curves and performance parameters of multiple measurements was found to be reasonably good. The RSD of the measured currents from 12 I-V curves obtained over three different days was found to be about 5%, whereas the RSDs of the corresponding performance parameters did not exceed ±3%.

2. Proposed parameters extraction technique

A simple and fast technique for improving the accuracy of solar cells parameters extraction using the slopes of illuminated I-V curves was proposed and combined with an analytical method from the literature. The technique is based on selecting the points to calculate the slopes that provide the most accurate values of the parameters based on fitting the calculated I-V curve with experimental data. The combined final technique was tested on a mono-Si solar cell and an a-Si PV module and has proved to be very accurate and outperformed other iterative and iterative-numerical benchmark methods from the literature. It can thus be concluded that the accuracy of analytical methods can actually exceed that of iterative and iterative-numerical methods, which are known to be more accurate.

Furthermore, the developed technique can be easily used with any parameters extraction method that depends on the slopes, thereby improving its accuracy. The technique has no convergence issues and hence can be used as a tool to investigate best locations of points for calculating the slopes for any shape of I-V curves, thereby allowing to empirically calculate the slopes for any type of solar cells when the I-V curve data is not available. The single diode five-parameter model was found to be sufficiently accurate for representing real solar cells when the accurate equivalent circuit parameters are extracted. Moreover, the technique was found to have a reasonably good repeatability with the RSDs of the extracted equivalent circuit parameters from four subsequent I-V curve

measurements did not exceed ±3%. It has also a capability to detect the variations in parameters caused by switching the experimental set-up equipment OFF and ON, re-positioning the cell and re-soldering the contacts. Thus, the developed technique was successfully used in all investigations of this research with the MAPE between experimental and calculated I-V curves of less than 2% in all I-V curves presented in this thesis.

3. Influence of shading on solar cells parameters and modelling accuracy improvement of PV modules under partial shading

A concise and complete experimental investigation on the effect of partial shading on solar cells was carried out. This study covered all equivalent circuit parameters and performance parameters. The results revealed that the variations of most parameters with shading are in a good agreement with other works. Furthermore, for the variations of equivalent circuit parameters to be used in modelling PV devices under partial shading, it was imperative to compare the influence of shading on solar cells with that of reducing the irradiance. The results implied that there is no appreciable difference between them with a MAPE between partial shading I-V curves and the corresponding irradiance reduction ones of less than 1% in all cases. Thus, this allowed to confidently enter opaque partial shading as its corresponding reduction of irradiance in the models.

The variations of equivalent circuit parameters with shading were incorporated in modelling a single solar cell and a PV module working under partial shading in order to improve modelling accuracy. The single cell model accuracy did not show a pronounced improvement in accuracy when including the variations of parameters. On the contrary, the PV module model exhibited a high accuracy improvement in the region on the output characteristics at which the shaded cell is reverse biased. Subsequently, the parameter variation that was responsible for this improvement was identified. It is concluded that in addition the inherent variation of the I_{ph} with shading, R_{sh} variation is also of great importance for accurately modelling the region at which the shaded cell is reverse biased.

Therefore, it has been proposed in this work, to use the variations of I_{ph} and R_{sh} of a single cell with shading when modelling partially shaded PV modules instead of using the avalanche breakdown term. However, the improvement in accuracy gained by this approach in modelling the reverse bias region holds only under one or two cell shading.

Although it is still accurate when increasing the number of shaded cells, its accuracy becomes close to that of considering only the inherent variation of I_{ph} with shading. Nevertheless, the approach is still useful when accurate modelling of the reverse bias region under single cell shading is required. Due to considering the variation of R_{sh}, it does not need the inclusion of the avalanche breakdown term to accurately model the reverse bias region. Furthermore, one of the main conclusions of this research is the fact that single cell shading in a PV module exhibits unique characteristics that requires to be treated carefully to achieve accurate modelling. To the best of the author' knowledge, such a systematic study on the effect of parameters change on modelling accuracy has not been previously reported.

4. Correlation between broken contact fingers and I-V characteristics of partially shaded PV modules

It has been found in this research that it is possible to detect damage of the contact fingers of solar cells through I-V curves of partially shaded PV modules. During individual cell partial shading of a PV module, it was found that the module exhibited a convex I-V curve MPP knee when a particular cell was partially shaded. Further investigations and validations correlated this behaviour with broken contact fingers of the cell. Studying the effect of broken contact fingers on a single cell behaviour indicated a reduction in FF, which is a similar response to that of the PV module when shading the affected cell.

Furthermore, it was found that when light non-uniformity exceeds a certain limit, thermal imaging will not be adequate for detecting the cells with broken contact fingers within PV modules. EL imaging, on the other hand, can effectively detect them and hence it was used to validate the observed correlation. Moreover, the correlation was validated by investigating the effect of broken contact fingers on the I-V curves of an in-house assembled PV module. When breaking the contact fingers of one cell in this module, the module's I-V curve showed a reduction in region 1 FF, which is a similar behaviour to that of the other module used originally to observe the correlation.

It can be concluded that partial shading of individual cells is a valuable tool for studying their health state including the detection of broken contact fingers. This work has confirmed the possibility of identifying the cells with broken contact fingers using I-V curve measurements under day light.

7.3. Recommendations for Future Work

Based on the conclusions drawn from this study, recommendations for further research in the future may be summarised for some topics as follows:

1. Proposed parameters extraction technique

It will be useful to use the developed equivalent circuit parameters extraction technique presented in Chapter 4 for establishing a correlation between main performance parameters, which are short circuit current, open circuit voltage and maximum power, and points used to calculate the slopes of I-V curves for different technologies of PV devices. This may be achieved by extracting the equivalent circuit parameters using the technique for many I-V curves of each technology and then establishing empirical equations to calculate the slopes using only the main performance parameters available in data sheets. This might help in accurate determination of the equivalent circuit parameters when the I-V curve data is not available.

2. Influence of shading on solar cells parameters and modelling accuracy improvement of PV Modules under partial shading

- It will be beneficial to perform further tests to validate the variation of R_{sh} with shading represented by Equation (5.6) on a number of solar cells and modules of different technologies. This is because although it has provided accurate modelling in this work, it was actually derived from only one mono-Si solar cell.
- The systematic investigation of determining the variations of equivalent circuit parameters with shading and model accuracy improvement should be implemented on solar cells and modules of different technologies that are commercially available, such as poly-Si and CIGS solar cells. This may be useful in providing a substantial improvement in their modelling accuracy under partial shading.
- It is recommended to assess the accuracy of the proposed modelling approach, which considers the variations of both I_{ph} and R_{sh} with shading in the model, on utility scale PV modules. This is because it was only tested on a small 10 W PV module in this research due to experimental limitations.

3. Correlation between broken contact fingers and I-V characteristics of partially shaded PV modules

- In the investigation of the broken contact fingers effect on the I-V curve of a solar cell presented in Figure 6.7, it was noticed that the I_{sc} was insignificantly affected by increasing the disconnected cell area. Although the reduction in the FF because of increasing the disconnected area has already proved the correlation between broken contact fingers and I-V characteristics of partially shaded PV modules, it may be interesting to find-out the cause for the insignificant reduction in the I_{sc} despite disconnecting about half of the cell area.
- The signature that broken contact fingers cause on the I-V curve of PV modules under single cell partial shading needs to be differentiated from those of other faults. A complete study should investigate signatures of different faults under individual cell partial shading. The concept of broken contact fingers detection can then be implemented in a technique using for instance a microcontroller and an automatic single cell partial shading system for PV modules.
- It will be useful to validate the new observed correlation in this work between the I-V curve under single cell partial shading and broken contact fingers on utility scale PV modules and on other PV modules of different technologies.

References

[1] K. Mertens, *Photovoltaics Fundamentals, Technology and Practice*. Chichester, United Kingdom: Wiley, 2014.

[2] V. Quaschning, *Understanding Renewable Energy Systems, Technology and Practice*, 1st ed. London, United Kingdom: Earthscan, 2005.

[3] Y. Abdelilah *et al.*, "Renewables 2022 analysis and forecasts to 2027," 2023. Accessed: Jan. 11, 2023. [Online]. Available: https://iea.blob.core.windows.net/assets/ada7af90-e280-46c4-a577-df2e4fb44254/Renewables2022.pdf

[4] G. Masson and I. Kaizuka, "Trends in photovoltaic applications 2022," 2022. Accessed: Oct. 06, 2022. [Online]. Available: https://iea-pvps.org/wp-content/uploads/2022/09/PVPS_Trend_Report_2022.pdf

[5] E. I. Batzelis, P. S. Georgilakis, and S. A. Papathanassiou, "Energy models for photovoltaic systems under partial shading conditions: A comprehensive review," *IET Renewable Power Generation*, vol. 9, no. 4, pp. 340–349, May 2015, doi: 10.1049/iet-rpg.2014.0207.

[6] D. Picault, B. Raison, S. Bacha, J. de la Casa, and J. Aguilera, "Forecasting photovoltaic array power production subject to mismatch losses," *Solar Energy*, vol. 84, no. 7, pp. 1301–1309, Jul. 2010, doi: 10.1016/j.solener.2010.04.009.

[7] A. Dolara, G. C. Lazaroiu, S. Leva, and G. Manzolini, "Experimental investigation of partial shading scenarios on PV (photovoltaic) modules," *Energy*, vol. 55, pp. 466–475, Jun. 2013, doi: 10.1016/j.energy.2013.04.009.

[8] M. Dhimish, V. Holmes, P. Mather, and M. Sibley, "Novel hot spot mitigation technique to enhance photovoltaic solar panels output power performance," *Solar Energy Materials and Solar Cells*, vol. 179, pp. 72–79, Jun. 2018, doi: 10.1016/j.solmat.2018.02.019.

[9] K. Ishaque, Z. Salam, and Syafaruddin, "A comprehensive MATLAB Simulink PV system simulator with partial shading capability based on two-diode model," *Solar Energy*, vol. 85, no. 9, pp. 2217–2227, Sep. 2011, doi: 10.1016/j.solener.2011.06.008.

[10] S. M. Hashemzadeh, "A new model-based technique for fast and accurate tracking of global maximum power point in photovoltaic arrays under partial shading conditions," *Renew Energy*, vol. 139, pp. 1061–1076, Aug. 2019, doi: 10.1016/j.renene.2019.03.019.

[11] Y. Wang, K. Itako, T. Kudoh, K. Koh, and Q. Ge, "Voltage-based hot-spot detection method for photovoltaic string using a projector," *Energies (Basel)*, vol. 10, no. 2, pp. 1–14, Feb. 2017, doi: 10.3390/en10020230.

[12] J. W. Bishop, "Computer simulation of the effects of electrical mismatches in photovoltaic cell interconnection circuits," *Solar Cells*, vol. 25, no. 1, pp. 73–89, Oct. 1988, doi: 10.1016/0379-6787(88)90059-2.

[13] S. Kajari-Schröder, I. Kunze, U. Eitner, and M. Köntges, "Spatial and orientational distribution of cracks in crystalline photovoltaic modules generated by mechanical load tests," *Solar Energy Materials and Solar Cells*, vol. 95, no. 11, pp. 3054–3059, Nov. 2011, doi: 10.1016/j.solmat.2011.06.032.

[14] P. Chaturvedi, B. Hoex, and T. M. Walsh, "Broken metal fingers in silicon wafer solar cells and PV modules," *Solar Energy Materials and Solar Cells*, vol. 108, pp. 78–81, Jan. 2013, doi: 10.1016/j.solmat.2012.09.013.

[15] S. K. Tippabhotla *et al.*, "From cells to laminate: probing and modeling residual stress evolution in thin silicon photovoltaic modules using synchrotron X-ray micro-diffraction experiments and finite element simulations," *Progress in Photovoltaics: Research and Applications*, vol. 25, no. 9, pp. 791–809, Sep. 2017, doi: 10.1002/pip.2891.

[16] M. Köntges, M. Siebert, A. Morlier, R. Illing, N. Bessing, and F. Wegert, "Impact of transportation on silicon wafer-based photovoltaic modules," *Progress in Photovoltaics: Research and Applications*, vol. 24, no. 8, pp. 1085–1095, Aug. 2016, doi: 10.1002/pip.2768.

[17] M. Köntges, S. Kajari-Schröder, and I. Kunze, "Crack statistic for wafer-based silicon solar cell modules in the field measured by UV fluorescence," *IEEE J Photovolt*, vol. 3, no. 1, pp. 95–101, Jan. 2013, doi: 10.1109/JPHOTOV.2012.2208941.

[18] *Crystalline Silicon Terrestrial Photovoltaic (PV) Modules – Design Qualification and Type Approval*, IEC 61215, Geneva, Switzerland, Apr. 2005. [Online]. Available: https://solargostaran.com/files/standards/IEC/IEC%2061215-2005.pdf

[19] M. Köntges, I. Kunze, S. Kajari-Schröder, X. Breitenmoser, and B. Bjørneklett, "The risk of power loss in crystalline silicon based photovoltaic modules due to micro-cracks," *Solar Energy Materials and Solar Cells*, vol. 95, no. 4, pp. 1131–1137, Apr. 2011, doi: 10.1016/j.solmat.2010.10.034.

[20] R. A. Messenger and J. Ventre, *Photovoltaic Systems Engineering*, 3rd ed. Boca Raton, FL, USA: CRC Press LLC, 2010.

[21] S. Peake, Ed., *Renewable energy - power for a sustainable future*, 4th ed. Oxford, United Kingdom: Oxford University Press, 2018.

[22] M. Raugei and P. Frankl, “Life cycle impacts and costs of photovoltaic systems: Current state of the art and future outlooks,” *Energy*, vol. 34, no. 3, pp. 392–399, 2009, doi: 10.1016/j.energy.2009.01.001.

[23] “Best Research-Cell Efficiency Chart,” NREL.gov. https://www.nrel.gov/pv/cell-efficiency.html (accessed Jan. 11, 2023).

[24] S. Thomas and A. Tankappan, Eds., *Perovskite photovoltaics: Basic to advanced concepts and implementation*. London, United Kingdom: Academic Press, an imprint of Elsevier, 2018.

[25] D. Bonnet and P. Meyers, “Cadmium-telluride-Material for thin film solar cells,” *J Mater Res*, vol. 13, no. 10, pp. 2740–2753, Oct. 1998, doi: 10.1557/JMR.1998.0376.

[26] A. Abbas *et al.*, “The effect of cadmium chloride treatment on close-spaced sublimated cadmium telluride thin-film solar cells,” *IEEE J Photovolt*, vol. 3, no. 4, pp. 1361–1366, Oct. 2013, doi: 10.1109/JPHOTOV.2013.2264995.

[27] J. Ramanujam and U. P. Singh, “Copper indium gallium selenide based solar cells - A review,” *Energy and Environmental Science*, vol. 10, no. 6. Royal Society of Chemistry, pp. 1306–1319, Jun. 01, 2017. doi: 10.1039/c7ee00826k.

[28] C. A. Andrei, *Towards Efficient Photovoltaic Devices: Key Facts and Experiments on Dye Sensitised Solar Cells*. Newcastle upon Tyne, United Kingdom: Cambridge Scholars Publishing, 2017.

[29] Y. Kusumawati, A. S. Hutama, D. V. Wellia, and R. Subagyo, “Natural resources for dye-sensitized solar cells,” *Heliyon*, vol. 7, no. 12, pp. 1–33, Dec. 2021, doi: 10.1016/j.heliyon.2021.e08436.

[30] J. H. Im, C. R. Lee, J. W. Lee, S. W. Park, and N. G. Park, “6.5% efficient perovskite quantum-dot-sensitized solar cell,” *Nanoscale*, vol. 3, no. 10, pp. 4088–4093, Oct. 2011, doi: 10.1039/c1nr10867k.

[31] M. H. Kang, T. Cheon, and H. Kim, “Fully vacuum-free large-area organic solar cell fabrication from polymer top electrode,” *Solid State Electron*, vol. 186, pp. 1–6, Dec. 2021, doi: 10.1016/j.sse.2021.108192.

[32] M. Petrović, V. Chellappan, and S. Ramakrishna, “Perovskites: Solar cells & engineering applications - materials and device developments,” *Solar Energy*, vol. 122, pp. 678–699, Dec. 2015, doi: 10.1016/j.solener.2015.09.041.

[33] M. C. Eze *et al.*, “Optimum silver contact sputtering parameters for efficient perovskite solar cell fabrication,” *Solar Energy Materials and Solar Cells*, vol. 230, pp. 1–8, Sep. 2021, doi: 10.1016/j.solmat.2021.111185.

[34] J. A. Duffie and W. A. Beckman, *Solar Engineering of Thermal Processes*, 4th ed. Hoboken, NJ, USA: Wiley, 2013.

[35] H. Tian, F. Mancilla-David, K. Ellis, E. Muljadi, and P. Jenkins, "A cell-to-module-to-array detailed model for photovoltaic panels," *Solar Energy*, vol. 86, no. 9, pp. 2695–2706, Sep. 2012, doi: 10.1016/j.solener.2012.06.004.

[36] V. Lo Brano, A. Orioli, G. Ciulla, and A. Di Gangi, "An improved five-parameter model for photovoltaic modules," *Solar Energy Materials and Solar Cells*, vol. 94, no. 8, pp. 1358–1370, Aug. 2010, doi: 10.1016/j.solmat.2010.04.003.

[37] M. G. Villalva, J. R. Gazoli, and E. R. Filho, "Comprehensive approach to modeling and simulation of photovoltaic arrays," *IEEE Trans Power Electron*, vol. 24, no. 5, pp. 1198–1208, May 2009, doi: 10.1109/TPEL.2009.2013862.

[38] S. R. Wenham, M. A. Green, M. E. Watt, R. P. Corkish, and A. B. Sproul, *Applied Photovoltaics*, 3rd ed. Oxford, United Kingdom: Earthscan, 2011.

[39] A. N. Celik and N. Acikgoz, "Modelling and experimental verification of the operating current of mono-crystalline photovoltaic modules using four- and five-parameter models," *Appl Energy*, vol. 84, no. 1, pp. 1–15, Jan. 2007, doi: 10.1016/j.apenergy.2006.04.007.

[40] W. De Soto, S. A. Klein, and W. A. Beckman, "Improvement and validation of a model for photovoltaic array performance," *Solar Energy*, vol. 80, no. 1, pp. 78–88, Jan. 2006, doi: 10.1016/j.solener.2005.06.010.

[41] Q. Kou, S. A. Klein, and W. A. Beckman, "A method for estimating the long-term performance of direct-coupled PV pumping systems," *Solar Energy*, vol. 64, no. 1–3, pp. 33–40, Sep. 1998, doi: 10.1016/S0038-092X(98)00049-8.

[42] K. Ishaque, Z. Salam, H. Taheri, and Syafaruddin, "Modeling and simulation of photovoltaic (PV) system during partial shading based on a two-diode model," *Simul Model Pract Theory*, vol. 19, no. 7, pp. 1613–1626, Aug. 2011, doi: 10.1016/j.simpat.2011.04.005.

[43] K. Nishioka, N. Sakitani, Y. Uraoka, and T. Fuyuki, "Analysis of multicrystalline silicon solar cells by modified 3-diode equivalent circuit model taking leakage current through periphery into consideration," *Solar Energy Materials and Solar Cells*, vol. 91, no. 13, pp. 1222–1227, Aug. 2007, doi: 10.1016/j.solmat.2007.04.009.

[44] Y. Mahmoud and E. F. El-Saadany, "A photovoltaic model with reduced computational time," *IEEE Transactions on Industrial Electronics*, vol. 62, no. 6, pp. 3534–3544, Jun. 2015, doi: 10.1109/TIE.2014.2375275.

[45] A. Hadj Arab, F. Chenlo, and M. Benghanem, "Loss-of-load probability of photovoltaic water pumping systems," *Solar Energy*, vol. 76, no. 6, pp. 713–723, 2004, doi: 10.1016/j.solener.2004.01.006.

[46] D. Sera, R. Teodorescu, and P. Rodriguez, "Photovoltaic module diagnostics by series resistance monitoring and temperature and rated power estimation," in *2008*

34th Annual Conference of IEEE Industrial Electronics, Orlando, FL, USA: IEEE, Nov. 2008, pp. 2195–2199. doi: 10.1109/IECON.2008.4758297.

[47] J. Bai, S. Liu, Y. Hao, Z. Zhang, M. Jiang, and Y. Zhang, "Development of a new compound method to extract the five parameters of PV modules," *Energy Convers Manag*, vol. 79, pp. 294–303, Mar. 2014, doi: 10.1016/j.enconman.2013.12.041.

[48] A. Laudani, F. Mancilla-David, F. Riganti-Fulginei, and A. Salvini, "Reduced-form of the photovoltaic five-parameter model for efficient computation of parameters," *Solar Energy*, vol. 97, pp. 122–127, Nov. 2013, doi: 10.1016/j.solener.2013.07.031.

[49] E. Batzelis, "Non-iterative methods for the extraction of the single-diode model parameters of photovoltaic modules: A review and comparative assessment," *Energies (Basel)*, vol. 12, no. 3, pp. 14–28, Feb. 2019, doi: 10.3390/en12030358.

[50] M. Wolf and H. Rauschenbach, "Series resistance effects on solar cell measurements," *Advanced Energy Conversion*, vol. 3, no. 2, pp. 455–479, Jun. 1963, doi: 10.1016/0365-1789(63)90063-8.

[51] P. A. Kumari and P. Geethanjali, "Parameter estimation for photovoltaic system under normal and partial shading conditions: A survey," *Renewable and Sustainable Energy Reviews*, vol. 84, pp. 1–11, Mar. 2018, doi: 10.1016/j.rser.2017.10.051.

[52] M. S. Benghanem and S. N. Alamri, "Modeling of photovoltaic module and experimental determination of serial resistance," *Journal of Taibah University for Science*, vol. 2, no. 1, pp. 94–105, 2009, doi: 10.1016/s1658-3655(12)60012-0.

[53] J. C. H. Phang, D. S. H. Chan, and J. R. Phillips, "Accurate analytical method for the extraction of solar cell model parameters," *Electron Lett*, vol. 20, no. 10, pp. 406–408, May 1984, doi: 10.1049/el:19840281.

[54] F. Khan, S. H. Baek, Y. Park, and J. H. Kim, "Extraction of diode parameters of silicon solar cells under high illumination conditions," *Energy Convers Manag*, vol. 76, pp. 421–429, Dec. 2013, doi: 10.1016/j.enconman.2013.07.054.

[55] A. Orioli and A. Di Gangi, "A procedure to calculate the five-parameter model of crystalline silicon photovoltaic modules on the basis of the tabular performance data," *Appl Energy*, vol. 102, pp. 1160–1177, Feb. 2013, doi: 10.1016/j.apenergy.2012.06.036.

[56] O. Mares, M. Paulescu, and V. Badescu, "A simple but accurate procedure for solving the five-parameter model," *Energy Convers Manag*, vol. 105, pp. 139–148, Nov. 2015, doi: 10.1016/j.enconman.2015.07.046.

[57] A. Senturk and R. Eke, "A new method to simulate photovoltaic performance of crystalline silicon photovoltaic modules based on datasheet values," *Renew Energy*, vol. 103, pp. 58–69, Apr. 2017, doi: 10.1016/j.renene.2016.11.025.

[58] J. Cubas, S. Pindado, and M. Victoria, "On the analytical approach for modeling photovoltaic systems behavior," *J Power Sources*, vol. 247, pp. 467–474, Feb. 2014, doi: 10.1016/j.jpowsour.2013.09.008.

[59] F. J. Toledo and J. M. Blanes, "Geometric properties of the single-diode photovoltaic model and a new very simple method for parameters extraction," *Renew Energy*, vol. 72, pp. 125–133, Dec. 2014, doi: 10.1016/j.renene.2014.06.032.

[60] H. Saleem and S. Karmalkar, "An analytical method to extract the physical parameters of a solar cell from four points on the illuminated J-V curve," *IEEE Electron Device Letters*, vol. 30, no. 4, pp. 349–352, Apr. 2009, doi: 10.1109/LED.2009.2013882.

[61] E. I. Batzelis and S. A. Papathanassiou, "A Method for the Analytical Extraction of the Single-Diode PV Model Parameters," *IEEE Trans Sustain Energy*, vol. 7, no. 2, pp. 504–512, Apr. 2016, doi: 10.1109/TSTE.2015.2503435.

[62] A. Jain and A. Kapoor, "Exact analytical solutions of the parameters of real solar cells using Lambert W-function," *Solar Energy Materials and Solar Cells*, vol. 81, no. 2, pp. 269–277, Feb. 2004, doi: 10.1016/j.solmat.2003.11.018.

[63] A. Ortiz-Conde, F. J. García Sánchez, and J. Muci, "New method to extract the model parameters of solar cells from the explicit analytic solutions of their illuminated I-V characteristics," *Solar Energy Materials and Solar Cells*, vol. 90, no. 3, pp. 352–361, Feb. 2006, doi: 10.1016/j.solmat.2005.04.023.

[64] J. Cubas, S. Pindado, and C. de Manuel, "Explicit expressions for solar panel equivalent circuit parameters based on analytical formulation and the lambert W-function," *Energies (Basel)*, vol. 7, no. 7, pp. 4098–4115, Jul. 2014, doi: 10.3390/en7074098.

[65] J. Accarino, G. Petrone, C. A. Ramos-Paja, and G. Spagnuolo, "Symbolic algebra for the calculation of the series and parallel resistances in PV module model," in *2013 International Conference on Clean Electrical Power (ICCEP)*, Alghero, Italy: IEEE, Jun. 2013, pp. 62–66. doi: 10.1109/ICCEP.2013.6586967.

[66] L. Peng, Y. Sun, Z. Meng, Y. Wang, and Y. Xu, "A new method for determining the characteristics of solar cells," *J Power Sources*, vol. 227, pp. 131–136, Apr. 2013, doi: 10.1016/j.jpowsour.2012.07.061.

[67] M. Hejri, H. Mokhtari, M. R. Azizian, and L. Söder, "An analytical-numerical approach for parameter determination of a five-parameter single-diode model of photovoltaic cells and modules," *International Journal of Sustainable Energy*, vol. 35, no. 4, pp. 396–410, 2016, doi: 10.1080/14786451.2013.863886.

[68] M. Kumar and A. Kumar, "An efficient parameters extraction technique of photovoltaic models for performance assessment," *Solar Energy*, vol. 158, pp. 192–206, Dec. 2017, doi: 10.1016/j.solener.2017.09.046.

[69] A. Elkholy and A. A. Abou El-Ela, "Optimal parameters estimation and modelling of photovoltaic modules using analytical method," *Heliyon*, vol. 5, no. 7, pp. 1–14, Jul. 2019, doi: 10.1016/j.heliyon.2019.e02137.

[70] F. J. Toledo and J. M. Blanes, "Analytical and quasi-explicit four arbitrary point method for extraction of solar cell single-diode model parameters," *Renew Energy*, vol. 92, pp. 346–356, Jul. 2016, doi: 10.1016/j.renene.2016.02.012.

[71] D. Sera, R. Teodorescu, and P. Rodriguez, "PV panel model based on datasheet values," in *2007 IEEE International Symposium on Industrial Electronics*, Vigo: IEEE, Jun. 2007, pp. 2392–2396. doi: 10.1109/ISIE.2007.4374981.

[72] M. A. de Blas, J. L. Torres, E. Prieto, and A. García, "Selecting a suitable model for characterizing photovoltaic devices," *Renew Energy*, vol. 25, no. 3, pp. 371–380, Mar. 2002, doi: 10.1016/S0960-1481(01)00056-8.

[73] C. Carrero, D. Ramírez, J. Rodríguez, and C. A. Platero, "Accurate and fast convergence method for parameter estimation of PV generators based on three main points of the I-V curve," *Renew Energy*, vol. 36, no. 11, pp. 2972–2977, Nov. 2011, doi: 10.1016/j.renene.2011.04.001.

[74] H. Can and D. Ickilli, "Parameter estimation in modeling of photovoltaic panels based on datasheet values," *J Sol Energy Eng*, vol. 136, no. 2, pp. 1–6, May 2014, doi: 10.1115/1.4024923.

[75] G. Ciulla, V. Lo Brano, V. Di Dio, and G. Cipriani, "A comparison of different one-diode models for the representation of I-V characteristic of a PV cell," *Renewable and Sustainable Energy Reviews*, vol. 32, pp. 684–696, Apr. 2014, doi: 10.1016/j.rser.2014.01.027.

[76] M. G. Villalva, "Modeling and Simulation of Photovoltaic Arrays," sites.google.com. https://sites.google.com/site/mvillalva/pvmodel (accessed Feb. 16, 2022).

[77] G. Wang *et al.*, "An iterative approach for modeling photovoltaic modules without implicit equations," *Appl Energy*, vol. 202, pp. 189–198, Sep. 2017, doi: 10.1016/j.apenergy.2017.05.149.

[78] K. I. Ishibashi, Y. Kimura, and M. Niwano, "An extensively valid and stable method for derivation of all parameters of a solar cell from a single current-voltage characteristic," *J Appl Phys*, vol. 103, no. 9, pp. 1–6, May 2008, doi: 10.1063/1.2895396.

[79] M. Diantoro, T. Suprayogi, A. Hidayat, A. Taufiq, A. Fuad, and R. Suryana, "Shockley's equation fit analyses for solar cell parameters from I-V curves," *International Journal of Photoenergy*, vol. 2018, pp. 1–7, 2018, doi: 10.1155/2018/9214820.

[80] N. Nehaoua, Y. Chergui, and D. E. Mekki, "Determination of organic solar cell parameters based on single or multiple pin structures," *Vacuum*, vol. 84, no. 2, pp. 326–329, Sep. 2009, doi: 10.1016/j.vacuum.2009.07.006.

[81] Y. Chaibi, M. Salhi, A. El-jouni, and A. Essadki, "A new method to extract the equivalent circuit parameters of a photovoltaic panel," *Solar Energy*, vol. 163, pp. 376–386, Mar. 2018, doi: 10.1016/j.solener.2018.02.017.

[82] M. Ye, X. Wang, and Y. Xu, "Parameter extraction of solar cells using particle swarm optimization," *J Appl Phys*, vol. 105, no. 9, pp. 1–8, May 2009, doi: 10.1063/1.3122082.

[83] M. Zagrouba, A. Sellami, M. Bouaïcha, and M. Ksouri, "Identification of PV solar cells and modules parameters using the genetic algorithms: Application to maximum power extraction," *Solar Energy*, vol. 84, no. 5, pp. 860–866, May 2010, doi: 10.1016/j.solener.2010.02.012.

[84] K. Ishaque and Z. Salam, "An improved modeling method to determine the model parameters of photovoltaic (PV) modules using differential evolution (DE)," *Solar Energy*, vol. 85, no. 9, pp. 2349–2359, Sep. 2011, doi: 10.1016/j.solener.2011.06.025.

[85] K. M. El-Naggar, M. R. AlRashidi, M. F. AlHajri, and A. K. Al-Othman, "Simulated Annealing algorithm for photovoltaic parameters identification," *Solar Energy*, vol. 86, no. 1, pp. 266–274, Jan. 2012, doi: 10.1016/j.solener.2011.09.032.

[86] M. F. AlHajri, K. M. El-Naggar, M. R. AlRashidi, and A. K. Al-Othman, "Optimal extraction of solar cell parameters using pattern search," *Renew Energy*, vol. 44, pp. 238–245, Aug. 2012, doi: 10.1016/j.renene.2012.01.082.

[87] D. Oliva, E. Cuevas, and G. Pajares, "Parameter identification of solar cells using artificial bee colony optimization," *Energy*, vol. 72, pp. 93–102, Aug. 2014, doi: 10.1016/j.energy.2014.05.011.

[88] E. E. Ali, M. A. El-Hameed, A. A. El-Fergany, and M. M. El-Arini, "Parameter extraction of photovoltaic generating units using multi-verse optimizer," *Sustainable Energy Technologies and Assessments*, vol. 17, pp. 68–76, Oct. 2016, doi: 10.1016/j.seta.2016.08.004.

[89] S. Li *et al.*, "Parameter extraction of photovoltaic models using an improved teaching-learning-based optimization," *Energy Convers Manag*, vol. 186, pp. 293–305, Apr. 2019, doi: 10.1016/j.enconman.2019.02.048.

[90] X. Chen, B. Xu, C. Mei, Y. Ding, and K. Li, "Teaching–learning–based artificial bee colony for solar photovoltaic parameter estimation," *Appl Energy*, vol. 212, pp. 1578–1588, Feb. 2018, doi: 10.1016/j.apenergy.2017.12.115.

[91] V. J. Chin and Z. Salam, "A new three-point-based approach for the parameter extraction of photovoltaic cells," *Appl Energy*, vol. 237, pp. 519–533, Mar. 2019, doi: 10.1016/j.apenergy.2019.01.009.

[92] C. Olalla, C. Deline, and D. Maksimovic, "Performance of mismatched PV systems with submodule integrated converters," *IEEE J Photovolt*, vol. 4, no. 1, pp. 396–404, Jan. 2014, doi: 10.1109/JPHOTOV.2013.2281878.

[93] S. Silvestre, A. Boronat, and A. Chouder, "Study of bypass diodes configuration on PV modules," *Appl Energy*, vol. 86, no. 9, pp. 1632–1640, Sep. 2009, doi: 10.1016/j.apenergy.2009.01.020.

[94] E. V. Paraskevadaki and S. A. Papathanassiou, "Evaluation of MPP voltage and power of mc-Si PV modules in partial shading conditions," *IEEE Transactions on Energy Conversion*, vol. 26, no. 3, pp. 923–932, Sep. 2011, doi: 10.1109/TEC.2011.2126021.

[95] H. Patel and V. Agarwal, "Maximum power point tracking scheme for PV systems operating under partially shaded conditions," *IEEE Transactions on Industrial Electronics*, vol. 55, no. 4, pp. 1689–1698, Apr. 2008, doi: 10.1109/TIE.2008.917118.

[96] M. K. Al-Smadi and Y. Mahmoud, "Analysis of photovoltaic systems power losses in partial shading conditions," in *IECON 2018 - 44th Annual Conference of the IEEE Industrial Electronics Society*, Washington, DC, USA: IEEE, Oct. 2018, pp. 1699–1704. doi: 10.1109/IECON.2018.8591806.

[97] H. Kawamura *et al.*, "Simulation of I-V characteristics of a PV module with shaded PV cells," *Solar Energy Materials and Solar Cells*, vol. 75, no. 3–4, pp. 613–621, Feb. 2003, doi: 10.1016/S0927-0248(02)00134-4.

[98] M. C. Alonso-García, J. M. Ruiz, and W. Herrmann, "Computer simulation of shading effects in photovoltaic arrays," *Renew Energy*, vol. 31, no. 12, pp. 1986–1993, Oct. 2006, doi: 10.1016/j.renene.2005.09.030.

[99] E. Karatepe, M. Boztepe, and M. Çolak, "Development of a suitable model for characterizing photovoltaic arrays with shaded solar cells," *Solar Energy*, vol. 81, no. 8, pp. 977–992, Aug. 2007, doi: 10.1016/j.solener.2006.12.001.

[100] S. Silvestre and A. Chouder, "Effects of shadowing on photovoltaic module performance," *Progress in Photovoltaics: Research and Applications*, vol. 16, no. 2, pp. 141–149, Mar. 2008, doi: 10.1002/pip.780.

[101] H. Patel and V. Agarwal, "MATLAB-based modeling to study the effects of partial shading on PV array characteristics," *IEEE Transactions on Energy Conversion*, vol. 23, no. 1, pp. 302–310, Mar. 2008, doi: 10.1109/TEC.2007.914308.

[102] Y. J. Wang and P. C. Hsu, "Analytical modelling of partial shading and different orientation of photovoltaic modules," *IET Renewable Power Generation*, vol. 4, no. 3, pp. 272–282, May 2010, doi: 10.1049/iet-rpg.2009.0157.

[103] S. Moballegh and J. Jiang, "Partial shading modeling of photovoltaic system with experimental validations," in *2011 IEEE Power and Energy Society General Meeting*, Detroit, MI: IEEE, Jul. 2011, pp. 1–9. doi: 10.1109/PES.2011.6039281.

[104] M. Seyedmahmoudian, S. Mekhilef, R. Rahmani, R. Yusof, and E. T. Renani, "Analytical modeling of partially shaded photovoltaic systems," *Energies (Basel)*, vol. 6, no. 1, pp. 128–144, Jan. 2013, doi: 10.3390/en6010128.

[105] T. H. Jung, J. W. Ko, G. H. Kang, and H. K. Ahn, "Output characteristics of PV module considering partially reverse biased conditions," *Solar Energy*, vol. 92, pp. 214–220, Jun. 2013, doi: 10.1016/j.solener.2013.03.015.

[106] M. L. Orozco-gutierrez, J. M. Ramirez-scarpetta, G. Spagnuolo, and C. A. Ramos-paja, "A technique for mismatched PV array simulation," *Renew. Energy*, vol. 55, pp. 417–427, Jul. 2013, doi: 10.1016/j.renene.2013.01.009.

[107] C. Olalla, D. Clement, D. Maksimovic, and C. Deline, "A cell-level photovoltaic model for high-granularity simulations," in *2013 15th European Conference on Power Electronics and Applications (EPE)*, Lille: IEEE, Sep. 2013, pp. 1–10. doi: 10.1109/EPE.2013.6631946.

[108] E. I. Batzelis, I. A. Routsolias, and S. A. Papathanassiou, "An explicit PV string model based on the Lambert W function and simplified MPP expressions for operation under partial shading," *IEEE Trans Sustain Energy*, vol. 5, no. 1, pp. 301–312, Jan. 2014, doi: 10.1109/TSTE.2013.2282168.

[109] E. Díaz-Dorado, J. Cidrás, and C. Carrillo, "Discrete I-V model for partially shaded PV-arrays," *Solar Energy*, vol. 103, pp. 96–107, May 2014, doi: 10.1016/j.solener.2014.01.037.

[110] Y. Wang, G. Pei, and L. Zhang, "Effects of frame shadow on the PV character of a photovoltaic/thermal system," *Appl Energy*, vol. 130, pp. 326–332, Oct. 2014, doi: 10.1016/j.apenergy.2014.05.054.

[111] J. Bai, Y. Cao, Y. Hao, Z. Zhang, S. Liu, and F. Cao, "Characteristic output of PV systems under partial shading or mismatch conditions," *Solar Energy*, vol. 112, pp. 41–54, Feb. 2015, doi: 10.1016/j.solener.2014.09.048.

[112] G. N. Psarros, E. I. Batzelis, and S. A. Papathanassiou, "Partial shading analysis of multistring PV arrays and derivation of simplified MPP expressions," *IEEE Trans Sustain Energy*, vol. 6, no. 2, pp. 499–508, Apr. 2015, doi: 10.1109/TSTE.2015.2389715.

[113] V. d'Alessandro, F. Di Napoli, P. Guerriero, and S. Daliento, "An automated high-granularity tool for a fast evaluation of the yield of PV plants accounting for

shading effects," *Renew Energy*, vol. 83, pp. 294–304, Nov. 2015, doi: 10.1016/j.renene.2015.04.041.

[114] X. Qing, H. Sun, X. Feng, and C. Y. Chung, "Submodule-based modeling and simulation of a series-parallel photovoltaic array under mismatch conditions," *IEEE J Photovolt*, vol. 7, no. 6, pp. 1731–1739, Nov. 2017, doi: 10.1109/JPHOTOV.2017.2746265.

[115] J. P. N. Torres, S. K. Nashih, C. A. F. Fernandes, and J. C. Leite, "The effect of shading on photovoltaic solar panels," *Energy Systems*, vol. 9, no. 1, pp. 195–208, Feb. 2018, doi: 10.1007/s12667-016-0225-5.

[116] A. G. Galeano, M. Bressan, F. J. Vargas, and C. Alonso, "Shading ratio impact on photovoltaic modules and correlation with shading patterns," *Energies (Basel)*, vol. 11, no. 4, pp. 1–26, Apr. 2018, doi: 10.3390/en11040852.

[117] L. Zhu, Q. Li, M. Chen, K. Cao, and Y. Sun, "A simplified mathematical model for power output predicting of Building Integrated Photovoltaic under partial shading conditions," *Energy Convers Manag*, vol. 180, pp. 831–843, Jan. 2019, doi: 10.1016/j.enconman.2018.11.036.

[118] P. Bharadwaj and V. John, "Subcell modeling of partially shaded photovoltaic modules," *IEEE Trans Ind Appl*, vol. 55, no. 3, pp. 3046–3054, May 2019, doi: 10.1109/TIA.2019.2899813.

[119] J. D. Bastidas-Rodriguez, J. M. Cruz-Duarte, and R. Correa, "Mismatched series-parallel photovoltaic generator modeling: An implicit current-voltage approach," *IEEE J Photovolt*, vol. 9, no. 3, pp. 768–774, May 2019, doi: 10.1109/JPHOTOV.2019.2898208.

[120] Y. Shen *et al.*, "Modeling of photovoltaic modules under common shading conditions," *Energy*, vol. 256, pp. 1–15, Oct. 2022, doi: 10.1016/j.energy.2022.124618.

[121] E. D. Chepp, F. P. Gasparin, and A. Krenzinger, "Improvements in methods for analysis of partially shaded PV modules," *Renew Energy*, vol. 200, pp. 900–910, Nov. 2022, doi: 10.1016/j.renene.2022.10.035.

[122] K. Ding, X. Bian, H. Liu, and T. Peng, "A MATLAB-simulink-based PV module model and its application under conditions of nonuniform irradiance," *IEEE Transactions on Energy Conversion*, vol. 27, no. 4, pp. 864–872, Dec. 2012, doi: 10.1109/TEC.2012.2216529.

[123] V. Quaschning and R. Hanitsch, "Numerical simulation of current-voltage characteristics of photovoltaic systems with shaded solar cells," *Solar Energy*, vol. 56, no. 6, pp. 513–520, Jun. 1996, doi: 10.1016/0038-092X(96)00006-0.

[124] A. Zegaoui *et al.*, "Photovoltaic cell/panel/array characterizations and modeling considering both reverse and direct modes," *Energy Procedia*, vol. 6, pp. 695–703, 2011, doi: 10.1016/j.egypro.2011.05.079.

[125] M. C. Di Vincenzo and D. Infield, "Detailed PV array model for non-uniform irradiance and its validation against experimental data," *Solar Energy*, vol. 97, pp. 314–331, Nov. 2013, doi: 10.1016/j.solener.2013.08.030.

[126] M. Kermadi, V. J. Chin, S. Mekhilef, and Z. Salam, "A fast and accurate generalized analytical approach for PV arrays modeling under partial shading conditions," *Solar Energy*, vol. 208, pp. 753–765, Sep. 2020, doi: 10.1016/j.solener.2020.07.077.

[127] W. Kreft, E. Przenzak, and M. Filipowicz, "Photovoltaic chain operation analysis in condition of partial shading for systems with and without bypass diodes," *Optik (Stuttg)*, vol. 247, pp. 1–10, Dec. 2021, doi: 10.1016/j.ijleo.2021.167840.

[128] E. L. Meyer and E. E. van Dyk, "The effect of reduced shunt resistance and shading on photovoltaic module performance," in *Conference Record of the Thirty-first IEEE Photovoltaic Specialists Conference*, Lake Buena Vista, FL, USA: IEEE, Jan. 2005, pp. 1331–1334. doi: 10.1109/pvsc.2005.1488387.

[129] M. C. Alonso-García and J. M. Ruíz, "Analysis and modelling the reverse characteristic of photovoltaic cells," *Solar Energy Materials and Solar Cells*, vol. 90, no. 7–8, pp. 1105–1120, May 2006, doi: 10.1016/j.solmat.2005.06.006.

[130] C. S. Ruschel, F. P. Gasparin, and A. Krenzinger, "Experimental analysis of the single diode model parameters dependence on irradiance and temperature," *Solar Energy*, vol. 217, pp. 134–144, Mar. 2021, doi: 10.1016/j.solener.2021.01.067.

[131] M. Sabry and A. E. Ghitas, "Effect of edge shading on the performance of silicon solar cell," *Vacuum*, vol. 80, no. 5, pp. 444–450, Jan. 2006, doi: 10.1016/j.vacuum.2005.07.012.

[132] F. Khan, S. N. Singh, and M. Husain, "Effect of illumination intensity on cell parameters of a silicon solar cell," *Solar Energy Materials and Solar Cells*, vol. 94, no. 9, pp. 1473–1476, Sep. 2010, doi: 10.1016/j.solmat.2010.03.018.

[133] A. E. Ghitas and M. Sabry, "A study of the effect of shadowing location and area on the Si solar cell electrical parameters," *Vacuum*, vol. 81, no. 4, pp. 475–478, Nov. 2006, doi: 10.1016/j.vacuum.2006.07.001.

[134] B. Swatowska and T. Stapiński, "Influence of external conditions on parameters of silicon solar cells," *Materiały Elektroniczne*, vol. 38, no. 1, pp. 13–16, 2010.

[135] B. Swatowska and P. Panek, "The impact of shading on solar cell electrical parameters," *Optica Applicata*, vol. 47, no. 2, pp. 319–323, 2017, doi: 10.5277/oa170214.

[136] W. B. Xiao, F. Y. Hu, H. M. Zhang, and H. M. Wu, "Experimental investigation of the effects of partial shading on photovoltaic cells' electrical parameters," *International Journal of Photoenergy*, vol. 2015, pp. 1–7, 2015, doi: 10.1155/2015/191603.

[137] S. Silvestre and A. Chouder, "Shading effects in characteristic parameters of PV modules," in *2007 Spanish Conference on Electron Devices*, Madrid, Spain: IEEE, Jan. 2007, pp. 116–118. doi: 10.1109/SCED.2007.384007.

[138] C. S. Ruschel, F. P. Gasparin, E. R. Costa, and A. Krenzinger, "Assessment of PV modules shunt resistance dependence on solar irradiance," *Solar Energy*, vol. 133, pp. 35–43, Aug. 2016, doi: 10.1016/j.solener.2016.03.047.

[139] W. Herrmann, W. Wiesner, and W. Vaassen, "Hot spot investigations on PV modules - new concepts for a test standard and consequences for module design with respect to bypass diodes," in *Conference Record of the Twenty Sixth IEEE Photovoltaic Specialists Conference*, Anaheim, CA, USA: IEEE, Sep. 1997, pp. 1129–1132. doi: 10.1109/pvsc.1997.654287.

[140] S. Kajari-Schröder, I. Kunze, and M. Köntges, "Criticality of cracks in PV modules," *Energy Procedia*, vol. 27, pp. 658–663, 2012, doi: 10.1016/j.egypro.2012.07.125.

[141] P. A. Wang, "Industrial challenges for thin wafer manufacturing," in *IEEE 4th World Conference on Photovoltaic Energy Conversion, WCPEC-4*, Waikoloa, HI: IEEE Computer Society, May 2006, pp. 1179–1182. doi: 10.1109/WCPEC.2006.279391.

[142] L. Papargyri *et al.*, "Modelling and experimental investigations of microcracks in crystalline silicon photovoltaics: A review," *Renew Energy*, vol. 145, pp. 2387–2408, Jan. 2020, doi: 10.1016/j.renene.2019.07.138.

[143] M. Dhimish, V. Holmes, B. Mehrdadi, and M. Dales, "The impact of cracks on photovoltaic power performance," *Journal of Science: Advanced Materials and Devices*, vol. 2, no. 2, pp. 199–209, Jun. 2017, doi: 10.1016/j.jsamd.2017.05.005.

[144] Y. C. Chiou, J. Z. Liu, and Y. T. Liang, "Micro crack detection of multi-crystalline silicon solar wafer using machine vision techniques," *Sensor Review*, vol. 31, no. 2, pp. 154–165, Apr. 2011, doi: 10.1108/02602281111110013.

[145] M. Abdelhamid, R. Singh, and M. Omar, "Review of microcrack detection techniques for silicon solar cells," *IEEE J Photovolt*, vol. 4, no. 1, pp. 514–524, Jan. 2014, doi: 10.1109/JPHOTOV.2013.2285622.

[146] A. Morlier, F. Haase, and M. Köntges, "Impact of cracks in multicrystalline silicon solar cells on PV module power -A simulation study based on field data," *IEEE J Photovolt*, vol. 5, no. 6, pp. 1735–1741, Nov. 2015, doi: 10.1109/JPHOTOV.2015.2471076.

[147] P. Grunow, P. Clemens, V. Hoffmann, B. Litzenburger, and L. Podlowski, "Influence of micro cracks in multi-crystalline silicon solar cells on the reliability of PV modules," in *20th European Photovoltaic Solar Energy Conference*, Barcelona, Jun. 2005, pp. 2380–2383.

[148] M. Dhimish, "Micro cracks distribution and power degradation of polycrystalline solar cells wafer: Observations constructed from the analysis of 4000 samples," *Renew Energy*, vol. 145, pp. 466–477, Jan. 2020, doi: 10.1016/j.renene.2019.06.057.

[149] M. Dhimish, V. d'Alessandro, and S. Daliento, "Investigating the impact of cracks on solar cells performance: Analysis based on nonuniform and uniform crack distributions," *IEEE Trans Industr Inform*, vol. 18, no. 3, pp. 1684–1693, Mar. 2022, doi: 10.1109/TII.2021.3088721.

[150] A. Dolara, G. C. Lazaroiu, S. Leva, G. Manzolini, and L. Votta, "Snail trails and cell microcrack impact on PV module maximum power and energy production," *IEEE J Photovolt*, vol. 6, no. 5, pp. 1269–1277, Sep. 2016, doi: 10.1109/JPHOTOV.2016.2576682.

[151] M. Dhimish, V. Holmes, M. Dales, and B. Mehrdadi, "Effect of micro cracks on photovoltaic output power: Case study based on real time long term data measurements," *Micro Nano Lett*, vol. 12, no. 10, pp. 803–807, Oct. 2017, doi: 10.1049/mnl.2017.0205.

[152] B. Su, H. Chen, P. Chen, G. Bian, K. Liu, and W. Liu, "Deep learning-based solar-cell manufacturing defect detection with complementary attention network," *IEEE Trans Industr Inform*, vol. 17, no. 6, pp. 4084–4095, Jun. 2021, doi: 10.1109/TII.2020.3008021.

[153] W. Muehleisen *et al.*, "Outdoor detection and visualization of hailstorm damages of photovoltaic plants," *Renew Energy*, vol. 118, pp. 138–145, Apr. 2018, doi: 10.1016/j.renene.2017.11.010.

[154] T. Fuyuki, H. Kondo, T. Yamazaki, Y. Takahashi, and Y. Uraoka, "Photographic surveying of minority carrier diffusion length in polycrystalline silicon solar cells by electroluminescence," *Appl Phys Lett*, vol. 86, no. 26, pp. 1–3, Jun. 2005, doi: 10.1063/1.1978979.

[155] T. Fuyuki and A. Kitiyanan, "Photographic diagnosis of crystalline silicon solar cells utilizing electroluminescence," *Appl Phys A Mater Sci Process*, vol. 96, no. 1, pp. 189–196, Jul. 2009, doi: 10.1007/s00339-008-4986-0.

[156] L. Stoicescu, M. Reuter, and J. H. Werner, "DaySy: Luminescence imaging of PV modules in daylight," in *29th European Photovoltaic Solar Energy Conference and Exhibition*, Sep. 2014, pp. 2553–2554.

[157] M. Frazão, J. A. Silva, K. Lobato, and J. M. Serra, "Electroluminescence of silicon solar cells using a consumer grade digital camera," *Measurement (Lond)*, vol. 99, pp. 7–12, Mar. 2017, doi: 10.1016/j.measurement.2016.12.017.

[158] S. Deitsch *et al.*, "Automatic classification of defective photovoltaic module cells in electroluminescence images," *Solar Energy*, vol. 185, pp. 455–468, Jun. 2019, doi: 10.1016/j.solener.2019.02.067.

[159] M. Dhimish, V. Holmes, and P. Mather, "Novel photovoltaic micro crack detection technique," *IEEE Transactions on Device and Materials Reliability*, vol. 19, no. 2, pp. 304–312, Jun. 2019, doi: 10.1109/TDMR.2019.2907019.

[160] M. Dhimish and P. Mather, "Ultrafast high-resolution solar cell cracks detection process," *IEEE Trans Industr Inform*, vol. 16, no. 7, pp. 4769–4777, Jul. 2020, doi: 10.1109/TII.2019.2946210.

[161] G. Alves Dos Reis Benatto *et al.*, "Drone-based daylight electroluminescence imaging of PV modules," *IEEE J Photovolt*, vol. 10, no. 3, pp. 872–877, May 2020, doi: 10.1109/JPHOTOV.2020.2978068.

[162] H. R. Parikh *et al.*, "Solar cell cracks and finger failure detection using statistical parameters of electroluminescence images and machine learning," *Applied Sciences (Switzerland)*, vol. 10, no. 24, pp. 1–14, Dec. 2020, doi: 10.3390/app10248834.

[163] T. Trupke, R. A. Bardos, M. C. Schubert, and W. Warta, "Photoluminescence imaging of silicon wafers," *Appl Phys Lett*, vol. 89, no. 4, pp. 044107-1–044107-3, Jul. 2006, doi: 10.1063/1.2234747.

[164] R. Bhoopathy, O. Kunz, M. Juhl, T. Trupke, and Z. Hameiri, "Outdoor photoluminescence imaging of photovoltaic modules with sunlight excitation," *Progress in Photovoltaics: Research and Applications*, vol. 26, no. 1, pp. 69–73, Jan. 2018, doi: 10.1002/pip.2946.

[165] O. Breitenstein *et al.*, "Can luminescence imaging replace lock-in thermography on solar cells?," *IEEE J Photovolt*, vol. 1, no. 2, pp. 159–167, Dec. 2011, doi: 10.1109/JPHOTOV.2011.2169394.

[166] T. M. Pletzer, J. I. van Mölken, S. Rißland, O. Breitenstein, and J. Knoch, "Influence of cracks on the local current-voltage parameters of silicon solar cells," *Progress in Photovoltaics: Research and Applications*, vol. 23, no. 4, pp. 428–436, Apr. 2015, doi: 10.1002/pip.2443.

[167] S. S. Ko, C. S. Liu, and Y. C. Lin, "Optical inspection system with tunable exposure unit for micro-crack detection in solar wafers," *Optik (Stuttg)*, vol. 124, no. 19, pp. 4030–4035, Oct. 2013, doi: 10.1016/j.ijleo.2012.12.024.

[168] W. Dallas, O. Polupan, and S. Ostapenko, "Resonance ultrasonic vibrations for crack detection in photovoltaic silicon wafers," *Meas Sci Technol*, vol. 18, no. 3, pp. 852–858, Mar. 2007, doi: 10.1088/0957-0233/18/3/038.

[169] T. K. Wen and C. C. Yin, "Crack detection in photovoltaic cells by interferometric analysis of electronic speckle patterns," *Solar Energy Materials and Solar Cells*, vol. 98, pp. 216–223, Mar. 2012, doi: 10.1016/j.solmat.2011.10.034.

[170] S. K. Chakrapani, M. J. Padiyar, and K. Balasubramaniam, "Crack detection in full size Cz-silicon wafers using lamb wave air coupled ultrasonic testing (LAC-UT)," *J Nondestr Eval*, vol. 31, no. 1, pp. 46–55, Mar. 2012, doi: 10.1007/s10921-011-0119-3.

[171] C. Hilmersson, D. P. Hess, W. Dallas, and S. Ostapenko, "Crack detection in single-crystalline silicon wafers using impact testing," *Applied Acoustics*, vol. 69, no. 8, pp. 755–760, Aug. 2008, doi: 10.1016/j.apacoust.2007.03.002.

[172] V. d'Alessandro, P. Guerriero, S. Daliento, and M. Gargiulo, "A straightforward method to extract the shunt resistance of photovoltaic cells from current-voltage characteristics of mounted arrays," *Solid State Electron*, vol. 63, no. 1, pp. 130–136, Sep. 2011, doi: 10.1016/j.sse.2011.05.018.

[173] Y. S. Kim, S. M. Kang, B. Johnston, and R. Winston, "A novel method to extract the series resistances of individual cells in a photovoltaic module," *Solar Energy Materials and Solar Cells*, vol. 115, pp. 21–28, Aug. 2013, doi: 10.1016/j.solmat.2013.03.021.

[174] S. Daliento, F. Di Napoli, P. Guerriero, and V. d'Alessandro, "A modified bypass circuit for improved hot spot reliability of solar panels subject to partial shading," *Solar Energy*, vol. 134, pp. 211–218, Sep. 2016, doi: 10.1016/j.solener.2016.05.001.

[175] S. Yang, K. Itako, T. Kudoh, K. Koh, and Q. Ge, "Monitoring and suppression of the typical hot-spot phenomenon resulting from low-resistance defects in a PV string," *IEEE J Photovolt*, vol. 8, no. 6, pp. 1809–1817, Nov. 2018, doi: 10.1109/JPHOTOV.2018.2861734.

[176] G. B. Alers, J. Zhou, C. Deline, P. Hacke, and S. R. Kurtz, "Degradation of individual cells in a module measured with differential IV analysis," *Progress in Photovoltaics: Research and Applications*, vol. 19, no. 8, pp. 977–982, Dec. 2011, doi: 10.1002/pip.1013.

[177] W. Wang, A. C.-F. Liu, H. S.-H. Chung, R. W.-H. Lau, J. Zhang, and A. W.-L. Lo, "Fault diagnosis of photovoltaic panels using dynamic current-voltage characteristics," *IEEE Trans Power Electron*, vol. 31, no. 2, pp. 1588–1599, Feb. 2016, doi: 10.1109/TPEL.2015.2424079.

[178] M. Al-Soeidat, T. Cheng, D. D. C. Lu, and V. G. Agelidis, "Experimental study of static and dynamic behaviours of cracked PV panels," *IET Renewable Power*

Generation, vol. 13, no. 16, pp. 3002–3008, Dec. 2019, doi: 10.1049/iet-rpg.2019.0359.

[179] M. Ma, Z. Zhang, P. Yun, Z. Xie, H. Wang, and W. Ma, "Photovoltaic module current mismatch fault diagnosis based on I-V data," *IEEE J Photovolt*, vol. 11, no. 3, pp. 779–788, May 2021, doi: 10.1109/JPHOTOV.2021.3059425.

[180] Thermotron, "Panel Walk-in Testing Chambers," WP-563-THCM1-5-5-AC, Aug. 2017. https://thermotron.com/wp-content/uploads/2015/08/BC-140-Walk-In-Environmental-Chamber.pdf (accessed May 10, 2022).

[181] ARRI, "ARRISUN Lampheads Technical Data and Manuals," ARRISUN 60, Feb. 2007. https://www.arri.com/en/lighting/daylight/discontinued/arrisun (accessed May 10, 2022).

[182] Philips, "MSR Hot Restrike," MSR 6000 HR UNP data sheet, Aug. 2011. https://www.esvit.cz/upload/files/000007d533/871150020093800.pdf (accessed May 10, 2022).

[183] ARRI, "Standard Ballast Manuals," 6000 EB Electronic Ballast, Mar. 2002. https://www.arri.com/en/lighting/ballasts/discontinued?type=Manuals (accessed May 10, 2022).

[184] *Standard Specification for Solar Simulation for Terrestrial Photovoltaic Testing*, E927-10, West Conshohocken, PA, USA, Jul. 2010. [Online]. Available: https://www.astm.org/e0927-10.html

[185] StellarNet, "Dual-Detector Super Range (DSR) Spectrometer Systems," Dual-DSR Spectrometer Features. https://www.stellarnet.us/stellarnet-downloads/dual-detector-super-range-spectrometers-systems/ (accessed May 10, 2022).

[186] "Reference Air Mass 1.5 Spectra," NREL.gov. https://www.nrel.gov/grid/solar-resource/spectra-am1.5.html (accessed May 10, 2022).

[187] Kipp & Zonen, "Kipp & Zonen Instruction Manual," CM 21 Precision Pyranometer, 2004. https://www.kippzonen.com/Download/52/CM-21-Pyranometer-Manual?ShowInfo=true (accessed May 11, 2022).

[188] SEAWARD, "Solar Survey 100/200R Series," 200R data sheet. https://www.seaward.com/gb/support/download/371 (accessed May 11, 2022).

[189] "High precision solar cell cutting," Solarcapturetechnologies.com. https://www.solarcapturetechnologies.com/solar-cells/ (accessed May 11, 2022).

[190] M. Al-Shidhani, M. Al-Najideen, V. G. Rocha, and G. Min, "Design and testing of 3D printed cross compound parabolic concentrators for LCPV system," in *14th International Conference on Concentrator Photovoltaic Systems (CPV-14)*, American Institute of Physics Inc., Apr. 2018, pp. 020001-1–020001-8. doi: 10.1063/1.5053489.

[191] LPFK Laser & Electronics, "LPFK Laser & Electronics," ProtoMat S100 Manual, Feb. 2006. http://www.lpkfusa.com/downloads/support/docs/man_s100.pdf (accessed May 11, 2022).

[192] RS Components, "Technical data – RS Part number: 8007658," Tin/Lead Solder Wire data sheet. https://docs.rs-online.com/d8b8/0900766b8158654d.pdf (accessed May 11, 2022).

[193] Rs Components, "Thermal Grease," Silicone Thermal Grease, 2.9W/m·K data sheet. https://docs.rs-online.com/1ca0/A700000008000596.pdf (accessed May 11, 2022).

[194] "Betop-camp 10W 12V Solar Battery Charger," Amazon.co.uk. https://www.amazon.co.uk/gp/product/B07H3MQWJY/ref=ppx_yo_dt_b_asin_title_o03_s00?ie=UTF8&psc=1 (accessed May 11, 2022).

[195] RS Components, "Sanyo Amorphous Solar Cell," AM-8701 data sheet, Oct. 2008. https://docs.rs-online.com/4fc2/0900766b80d10e98.pdf (accessed May 11, 2022).

[196] "40 V, 1 A axial Power Schottky Rectifier," St.com. https://www.st.com/en/diodes-and-rectifiers/1n5819.html (accessed May 11, 2022).

[197] RS Components, "Low Drop Power Schottky Rectifier," 1N5819 data sheet. https://docs.rs-online.com/6961/0900766b80da3e32.pdf (accessed May 11, 2022).

[198] RS Components, "Thermally Conductive Gap Filler," Thermal Interface Sheet data sheet. https://docs.rs-online.com/86db/0900766b81587041.pdf (accessed May 11, 2022).

[199] RS Components, "Thermocouples," RS PRO Type K Thermocouple 5m Length data sheet. https://docs.rs-online.com/8d96/A700000007349798.pdf (accessed May 11, 2022).

[200] "TC-08 Data Logger," Picotech.com. https://www.picotech.com/data-logger/tc-08/thermocouple-data-logger (accessed May 11, 2022).

[201] RS Components, "Cloud-connected 8-channel Thermocouple Data Logger," TC-08 data sheet. https://docs.rs-online.com/02ae/A700000008443156.pdf (accessed May 11, 2022).

[202] "Tesa 51408," Tesa.com. https://www.tesa.com/en/industry/tesa-51408.html (accessed May 11, 2022).

[203] RS Components, "Tesa 51408 Product Information," 51408 data sheet, Dec. 2020. https://docs.rs-online.com/3ab3/A700000007387792.pdf (accessed May 11, 2022).

[204] NESLAB Instruments, "GP Series Constant Temperature Bath and Circulator," GP-300 Instruction and Operation Manual, Jul. 1997. https://www.chillercity.com/OPMANUAL/gp.pdf (accessed May 11, 2022).

[205] RS Components, "RS PRO PE Pipe Insulation," RS Stock 485-997 data sheet. https://docs.rs-online.com/656d/0900766b8157f57b.pdf (accessed May 11, 2022).

[206] KEITHLEY, "System SourceMeter Multi-Channel I-V Test Solutions," 2601 Source Meter data sheet, Oct. 2007. https://www.testequipmenthq.com/datasheets/KEITHLEY-2601-Datasheet.pdf (accessed May 11, 2022).

[207] "GPIB Instrument Control Device," NI.com. https://www.ni.com/sic/configurator/configure.action?sfId=NI&wcs_l=en-gb&wcs_k=gpib-instrument-control-device&wcs_s=43190 (accessed May 11, 2022).

[208] "Ultimaker 2 Extended +," 3dgbire.com. https://3dgbire.com/pages/ultimaker-2-extended-plus-tech-specs (accessed May 12, 2022).

[209] FLIR, "FLIR C2 Powerful, compact thermal imaging system," FLIR C2 data sheet, 2014. https://www.flirmedia.com/MMC/THG/Brochures/BLD_008/BLD_008_EN.pdf (accessed May 12, 2022).

[210] "Thermal Imaging Guidebook for Building and Renewable Energy Applications," Flirmedia.com. http://www.flirmedia.com/MMC/THG/Brochures/T820325/T820325_EN.pdf (accessed May 12, 2022).

[211] "D40 Specifications," Imaging.nikon.com. https://imaging.nikon.com/lineup/dslr/d40/spec.htm (accessed May 12, 2022).

[212] M. R. Maghami, H. Hizam, C. Gomes, M. A. Radzi, M. I. Rezadad, and S. Hajighorbani, "Power loss due to soiling on solar panel: A review," *Renewable and Sustainable Energy Reviews*, vol. 59, pp. 1307–1316, Jun. 2016, doi: 10.1016/j.rser.2016.01.044.

[213] Motic, "Moticam Series," USB 2.0 & 3.0 Cameras, Moticam 10+, 2018. https://www.moticamseries.com/downloads/30_100_MOTICAM_SERIES_CA_1812_EN.pdf (accessed Aug. 11, 2022).

[214] "SZ Stereo Microscope," olympus-lifescience.com. https://www.olympus-lifescience.com/en/technology/museum/micro/1961/ (accessed Aug. 11, 2022).

Appendix A: Parameter Extraction Technique MATLAB Code

Main Technique Code:

```
%%% Abdulhamid Atia %%%
% This program code is for a technique used to improve the accuracy of an analytical parameters extraction method of solar cells.

% Experimental I-V curve needs to be entered in a note pad file located in the same folder as this program m-file and named (Exp_IV_data). The voltage and current should be entered in (volts) and (Amps), respectively. The first column of the note pad file should be the voltage, whereas the second column should be the current.

clear all
clc
tic % Command used to determine the computational time of the program

%======== Main entries ========

Voc = 0.5802; % Open circuit voltage
Isc = 0.02437290; % Short circuit current
load('Exp_IV_data.txt'); % Enter the name of attached note pad file contains the experimental I-V data
V = Exp_IV_data(:,1)'; % Define voltage vector
I = Exp_IV_data(:,2)'; % Define current vector
Vm = V(find(V.*I==max(V.*I))); % Extract voltage at the MPP
Im = I(find(V.*I==max(V.*I))); % Extract current at the MPP
T = 25+273.15; % Cell temperature in Kelvin
K = 1.3806488E-23; % Boltzmann constant
q = 1.60217657E-19; % Electron charge
Vth = (K*T)/q; % Thermal voltage for a single solar cell
% Ns = 7; % Used in the case of a PV modules (number of cells in series)
%Vth = Ns*(K*T)/q; % Thermal voltage for a PV module
global ErrorRMS MAPE % Define errors

%======== Define currents and voltages used to calculate the slopes ========

%======== Fixed values for V1, I1, V4 and I4 ========

V1 = 0;
I1 = Isc;
V4 = Voc;
I4 = 0;

%======== Points ranges for V2, I2, V3 and I3 ========

% These are the ranges of points used to calculate the slopes. V2 and I2 represent point-2, whereas V3 and I3 represent point-3. The start and end point of each range are determined here for a particular I-V curve and can be changed according to the number of data points of the I-V curve:
V2 = V(2:find(V==Vm)-20); % This range starts from the first point near Isc and ends at 50% of Voc
I2 = I(2:find(I==Im)-20); % This range starts from the first point near Isc and ends at 50% of Voc
V3 = flip(V(find(V==Vm)+10:(end-3))); % This range starts from the third point near Voc and ends at 50% of Isc
```

```
I3 = flip(I(find(I==Im)+10:(end-3))); % This range starts from the third point near Voc and ends at 50% of Isc

%======== Initialise Rsh0 and Rs0 ========

Rsh0 = zeros(1,length(I2)); % Initial value of the shunt resistance
Rs0 = zeros(1,length(I3)); % Initial value of the series resistance

%======== Main routine ========

% This part calculates the five parameters from every pair of points for point 2 and 3:
for i = 1:length(I2)
   Rsh0(i) = (V2(i)-V1)/(I1-I2(i)); % Calculate Rsh0 from the slope at Isc
   for j = 1:length(I3)
      Rs0(j) = (V4-V3(j))/(I3(j)-I4); % Calculate Rs0 from the slope at Voc
      Rsh = Rsh0(i); % Calculate shunt resistance
      n = (Vm+(Im*Rs0(j))-Voc)/(Vth*((log(Isc-(Vm/Rsh)-Im))-(log(Isc-(Voc/Rsh)))+(Im/(Isc-(Voc/Rsh))))); % Calculate ideality factor
      Is = (Isc-(Voc/Rsh))*exp(-Voc/(n*Vth)); % Calculate reverse saturation current
      Rs = Rs0(j)-(((n*Vth)/Is)*exp(-Voc/(n*Vth))); % Calculate series resistance
      Iph = (Isc*(1+(Rs/Rsh)))+(Is*(exp((Isc*Rs)/(n*Vth))-1)); % Calculate photo-generated current
      Newton_Raphson(V,I,Rs,Rsh,n,Is,Iph,Vth,I2(i),I3(j)); % Call the Newton Raphson method m-file
      vec_Rs(j,i) = Rs;
      vec_Rsh(j,i) = Rsh;
      vec_n(j,i) = n;
      vec_Is(j,i) = Is;
      vec_Iph(j,i) = Iph;
   end
end

% Find the index of calculated I-V curve that provides the best fit with experimental data:
indx = find(ErrorRMS(:,3)'==min(ErrorRMS(:,3)'));

%======== Store and display values of the five parameters ========

Rs = vec_Rs(indx);
Rsh = vec_Rsh(indx);
n = vec_n(indx);
Is = vec_Is(indx);
Iph = vec_Iph(indx);
disp(['Rs = ',num2str(vec_Rs(indx))])
disp(['Rsh = ',num2str(vec_Rsh(indx))])
disp(['n = ',num2str(vec_n(indx))])
disp(['Is = ',num2str(vec_Is(indx))])
disp(['Iph = ',num2str(vec_Iph(indx))])

%======== Display values of the currents of points 2 and 3 that provide the best fit parameters ========
%%%%%%%%%% (deactivate if not required) %%%%%%%%%%

disp(['I2 in Amps = ',num2str(ErrorRMS(indx,1))])
disp(['I3 in Amps = ',num2str(ErrorRMS(indx,2))])

%======== Display locations of points 2 and 3 that provide the best fit parameters ========
%%%%%%%%%% (deactivate if not required) %%%%%%%%%%

I2_best = (ErrorRMS(indx,1));
I2_best_ind = find(I2 == I2_best);
V2_best = num2str(V2(I2_best_ind));
I3_best = (ErrorRMS(indx,2));
```

```
I3_best_ind = find(I3 == I3_best);
V3_best = num2str(V3(I3_best_ind));
best_point2 = (str2num(V2_best)*100)/Voc ;
best_point3 = (I3_best*100)/Isc;
disp(['Best location of point 2 (% of Voc) =',num2str(best_point2)])
disp(['Best location of point 3 (% of Isc) =',num2str(best_point3)])

%======== Calculate the best fit I-V curve ========

Vc = V; % Experimental voltage entries
Ic = zeros(1,length(Vc));
for j = 1 : size(Vc,2)
      f(j) = Iph-Is*(exp((Vc(j)+Ic(j)*Rs)/(Vth*n))-1)-(Vc(j)+Ic(j)*Rs)/Rsh-Ic(j);
      while (abs(f(j))>0.000001)
         f(j) = Iph-Is*(exp((Vc(j)+Ic(j)*Rs)/(Vth*n))-1)-(Vc(j)+Ic(j)*Rs)/Rsh-Ic(j);
         dif_f(j) = -Is*Rs/(Vth*n)*exp((Vc(j)+Ic(j)*Rs)/(Vth*n))-Rs/Rsh-1;
         I_(j) = Ic(j)-((f(j))/(dif_f(j)));
         Ic(j) = I_(j); % Calculated current
      end
end

%======== Calculate errors between experimental and best fit I-V curves ========

RMSE_best_fit = sqrt(sum((I-Ic).^2)/length(I)) % Root mean square error of current in Amperes (A)
Iexp = I(1:(end-1)); % Exclude the Voc point from MAPE and APE calculations
Ical = Ic(1:(end-1)); % Exclude the Voc point from MAPE and APE calculations
MAPE_best_fit = sum(abs(Iexp-Ical).*(100./Iexp))/length(Iexp) % Mean absolute percentage error of
current
APE = abs(Iexp-Ical).*(100./Iexp); % Absolute percentage error for each point on the I-V curve

%======== Plot experimental and best fit I-V curves ========

figure (1)
plot(V,I, 'o','LineWidth',2, 'color', 'K')
hold on
plot (V, Ic, '-', 'LineWidth',2, 'color', 'R')
title ('Experimental vs calculated I-V curve');
xlabel('Voltage (V)');
ylabel('Current (A)');
grid on
legend ('Experimental data', 'Calculated data')

%======== Plot the APE between experimental and best fit I-V curves at each point ========
%%%%%%%%%% (deactivate if not required) %%%%%%%%%%

figure (2)
Vexp = V(1:(end-1));
plot(Vexp,APE, '-Ko', 'LineWidth',2)
title ('APE between experimental and calculated I-V curves');
xlabel('Voltage (V)');
ylabel('APE (%)');
grid on

%======== Plot the errors for every pairs of points 2 and 3 ========
%%%%%%%%%% (deactivate if not required) %%%%%%%%%%

figure(3),
plot(1:length(ErrorRMS(:,3)'),ErrorRMS(:,3)','-Ks', 'LineWidth',2)
xlabel('Points pairs index')
ylabel('RMSE (A)')
```

```
title('RMSE of I-V Curves for Different pairs of Points')
grid on
figure(4),
plot(1:length(MAPE(:,3)'),MAPE(:,3)','-Ko', 'LineWidth',2)
xlabel('Points pairs index')
ylabel('MAPE (%)')
title('MAPE of I-V Curves for Different pairs of Points')
grid on

toc % Command used to determine the computational time of the program
```

Newton Raphson method Code:

```
% This program is called in the main program of calculating the five parameters. It is used to calculate I-V curves for each pair of points 2 and 3 using the Newton Raphson method.

function [] = Newton_Raphson(V,I,Rs,Rsh,n,Is,Iph,Vth,I2,I3);
global ErrorRMS MAPE

%======== Newton Raphson method code to calculate the I-V curve ========

Vc = V; % Experimental voltage entries
Ic = zeros(1,length(Vc));
for j = 1 : size(Vc,2)
      f(j) = Iph-Is*(exp((Vc(j)+Ic(j)*Rs)/(Vth*n))-1)-(Vc(j)+Ic(j)*Rs)/Rsh-Ic(j);
      while (abs(f(j))>0.000001)
         f(j) = Iph-Is*(exp((Vc(j)+Ic(j)*Rs)/(Vth*n))-1)-(Vc(j)+Ic(j)*Rs)/Rsh-Ic(j);
         dif_f(j) = -Is*Rs/(Vth*n)*exp((Vc(j)+Ic(j)*Rs)/(Vth*n))-Rs/Rsh-1;
         I_(j) = Ic(j)-((f(j))/(dif_f(j)));
         Ic(j) = I_(j); % Calculated current
      end
end

%======== Error Calculations for every calculated I-V curve ========

ErrorRMS = [ErrorRMS; I2 I3 sqrt(sum(abs(I-Ic).^2)/length(I))]; % Root mean square error of current in Amperes (A)
Iexp = I(1:(end-1)); % Exclude the Voc point from MAPE calculations
Ical = Ic(1:(end-1)); % Exclude the Voc point from MAPE calculations
MAPE = [MAPE; I2 I3 sum(abs(Iexp-Ical).*(100./Iexp))/length(Iexp)]; % Mean absolute percentage error of current
end
```

Appendix B: Comparing Shading with Irradiance Reduction Using Another Solar Cell

This appendix presents an experiment to study the difference between partial shading and irradiance reduction effects applied to another solar cell from the same patch of cell 2 shown in Figure 5.5 and investigated in section 5.3.

Appendix Table B.1. Equivalent circuit parameters and performance parameters of the other solar cell used to compare shading with irradiance reduction. (This cell is from the same batch of cell 2 shown in Figure 5.5. The parameters were extracted under STC. Each parameter value was calculated by averaging 12 values from 12 I-V curve measurements taken over three days, with four measurements obtained per day. The relative standard deviation of each parameter is also shown).

Parameter at STC	Mean	Relative Standard Deviation (%)
R_s (Ω)	1.19	±5
R_{sh} (kΩ)	0.51	±10.7
n	0.95	±7
I_s (nA)	7.3×10^{-4}	±116
I_{ph} (mA)	28.8	±2.95
P_{max} (mW)	13.6	±4.3
I_{sc} (mA)	28.7	±2.95
V_{oc} (V)	0.622	±0.42
FF	0.76	±1
Efficiency (%)	17.0	±4
R_{ch} (Ω)	19.4	±3.5

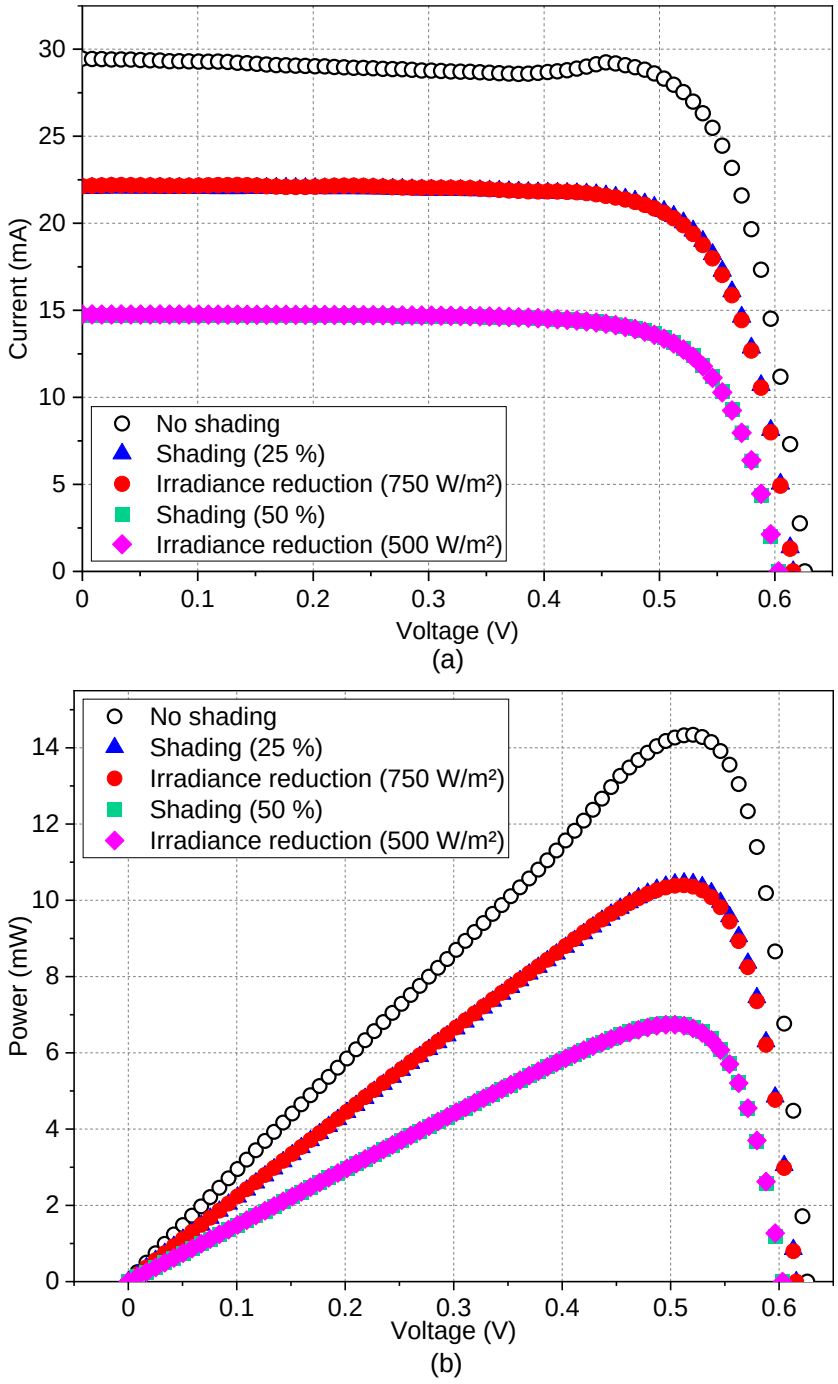

Appendix Figure B.1. Experimental I-V and P-V curves of partial shading and irradiance reduction cases applied to the solar cell, which is from the same batch of cell 2 shown in Figure 5.5: (a) I-V and (b) P-V curves. (Each I-V and P-V curve is the average of three curves taken at one set of measurements. All measurements were taken at a cell temperature of 25 °C).

Appendix Table B.2. The RMSE and MAPE between partial shading and irradiance reduction I-V curves of the solar cell, which is from the same batch of cell 2 shown in Figure 5.5.

Shaded area percentage (%)	Irradiance (W/m²)	RMSE (A)	MAPE (%)
25	750	1.247×10^{-4}	0.671
50	500	4.575×10^{-5}	0.386

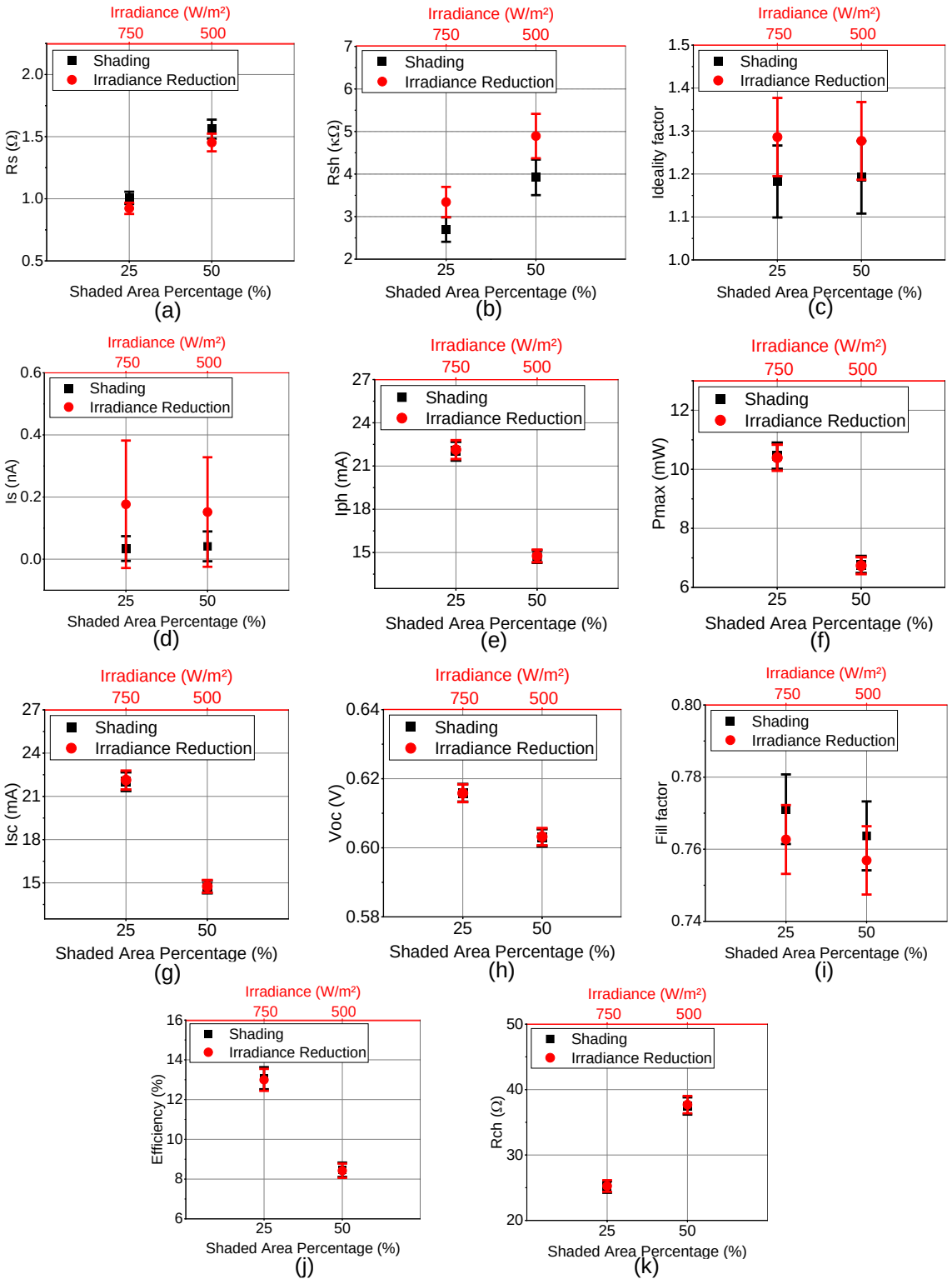

Appendix Figure B.2. Influences of partial shading and irradiance reduction on the equivalent circuit parameters and performance parameters of the solar cell, which is from the same batch of cell 2 shown in Figure 5.5: (a) series resistance, (b) shunt resistance, (c) ideality factor, (d) reverse saturation current, (e) photo-generated current, (f) maximum power, (g) short circuit current, (h) open circuit voltage, (i) fill factor, (j) efficiency and (k) characteristics resistance. (Each parameter value was calculated from the average I-V curve of three curves taken at one set of measurements. The error bars indicate the RSD of each parameter calculated from 12 I-V curve measurements taken without shading at STC over three days, with four measurements obtained per day).

Appendix C: Single Solar Cell Model MATLAB Code

```
%%% Abdulhamid Atia %%%
% This program code is for a single solar cell model works under partial shading. This program calculates model parameters when part of the solar cell is shaded and produces the modelled I-V and P-V curves.

% In order to compare the model with experimental data, experimental I-V curve needs to be entered in a note pad file located in the same folder as this program m-file and named (Cell_Exp_IV_data).

clear all
clc

%======== Main entries ========

Sh_per = 25; % Shading percentage
AT = 0.00008; % Total cell area
A2 = (AT*Sh_per)/100;  % Shaded area
Alfa = A2/AT; % Calculate shading factor
G1 = 1000; % Unshaded part irradiance
G2 = 0; % Shaded part irradiance
T = 25+273.15; % Cell temperature in Kelvin
G_ref = 1000; % Reference irradiance
T_ref = 25+273.15; % Reference temperature
k = 1.3806488E-23; % Boltzmann constant
q = 1.60217657E-19; % Electron charge
Vth = (k*T)/q; % Thermal voltage
Eg_ref = 1.12; % Bandgap of silicon at STC
load('Cell_Exp_IV_data.txt'); % Enter the name of attached note pad file contains the experimental I-V data
V = Cell_Exp_IV_data(:,1)'; % Define voltage vector
I = Cell_Exp_IV_data(:,2)'; % Define current vector

%======== Equivalent circuit parameters at STC ========

Rs_ref = 0.8025; % Series resistance at STC
Rsh_ref = 364.6488; % Shunt resistance at STC
n_ref = 2.0544; % Ideality factor at STC
Is_ref = 0.47046e-06; % Reverse saturation current at STC
Iph_ref = 0.0278468; % Photo-generated current at STC

%======== Temperature coefficient of the current ========

Ki = (0.0398/100)*Iph_ref; % Obtained from data sheet of commercial mono-Si solar cells

%======== Check if the cell is working under STC or not ========

% If the cell is working under STC, parameters under no shading will be equal to the STC parameters:
if G1 == G_ref && T == T_ref
Iph_nsh = Iph_ref;
Rs_nsh = Rs_ref;
Rsh_nsh = Rsh_ref;
Is_nsh = Is_ref;
n_nsh = n_ref;
```

```
% If the cell is not working under STC, adapt the STC parameters to the actual irradiance and temperature
in order to determine the parameters under no shading. All parameters equations are included here. If
some parameters are required to be set fixed with irradiance and temperature, they should be made equal
to their values under STC:
else
Rs_nsh = ((34.0109*Rs_ref*(1-(G1/G_ref))^3)-(22.9749*Rs_ref*(1-(G1/G_ref))^2)+(6.6189*Rs_ref*(1-
(G1/G_ref)))+Rs_ref)*(T/T_ref);
Rsh_nsh = (12.4389*Rsh_ref*(1-(G1/G_ref))^3)-(8.6252*Rsh_ref*(1-
(G1/G_ref))^2)+(3.3490*Rsh_ref*(1-(G1/G_ref)))+Rsh_ref;
n_nsh = (-0.2230*n_ref*(1-(G1/G_ref))^3)+(0.3643*n_ref*(1-(G1/G_ref))^2)+(0.1670*n_ref*(1-
(G1/G_ref)))+n_ref;
Eg = Eg_ref*(1-0.0002677*(T-T_ref));
Is_nsh = ((10.3994*Is_ref*(1-(G1/G_ref))^2)+(0.6450*Is_ref*(1-
(G1/G_ref)))+Is_ref)*((T/T_ref)^3*exp((Eg/k)*(1/T_ref-1/T)));
Iph_nsh = (Iph_ref+(Ki*(T-T_ref)))*(1-(1-(G1/G_ref)));
end

%======== Calculate the variations of the parameters with shading ========

% All parameters equations are included here. If some parameters are required to be set fixed with
shading, they should be made equal to their values under no shading:
Rs = (34.0109*Rs_nsh*Alfa^3)-(22.9749*Rs_nsh*Alfa^2)+(6.6189*Rs_nsh*Alfa)+Rs_nsh;
Rsh = (12.4389*Rsh_nsh*Alfa^3)-(8.6252*Rsh_nsh*Alfa^2)+(3.3490*Rsh_nsh*Alfa)+Rsh_nsh;
n = (-0.2230*n_nsh*Alfa^3)+(0.3643*n_nsh*Alfa^2)+(0.1670*n_nsh*Alfa)+n_nsh;
Is = (10.3994*Is_nsh*Alfa^2)+(0.6450*Is_nsh*Alfa)+Is_nsh;
Iph = Iph_nsh*(1-Alfa);

%======== Calculate the modelled I-V curve ========

Vc = V; % Experimental voltage entries
Ic = zeros(1,length(Vc));
for j = 1 : size(Vc,2)
      f(j) = Iph-Is*(exp((Vc(j)+Ic(j)*Rs)/(Vth*n))-1)-(Vc(j)+Ic(j)*Rs)/Rsh-Ic(j);
      while (abs(f(j))>0.000001)
         f(j) = Iph-Is*(exp((Vc(j)+Ic(j)*Rs)/(Vth*n))-1)-(Vc(j)+Ic(j)*Rs)/Rsh-Ic(j);
         dif_f(j) = -Is*Rs/(Vth*n)*exp((Vc(j)+Ic(j)*Rs)/(Vth*n))-Rs/Rsh-1;
         I_(j) = Ic(j)-((f(j))/(dif_f(j)));
         Ic(j) = I_(j); % Calculated current
      end
end

%======== Calculate errors between experimental and modelled I-V curves ========

RMSE = sqrt(sum((I-Ic).^2)/length(I)) % Root mean square error of current in Amperes (A)
Iexp = I(1:(end-1)); % Exclude the Voc point from MAPE calculation
Ical = Ic(1:(end-1)); % Exclude the Voc point from MAPE calculation
MAPE = sum(abs(Iexp-Ical).*(100./Iexp))/length(Iexp) % Mean absolute percentage error of current

%======== Plot experimental and modelled I-V and P-V curves ========

figure (1)
plot(V,I, 'o','LineWidth',2, 'color', 'K')
hold on
plot (V, Ic, '-', 'LineWidth',2, 'color', 'R')
title ('Experimental vs modelled I-V curve');
xlabel('Voltage (V)');
ylabel('Current (A)');
grid on
legend ('Experimental data', 'Model')
Pe = V.*I; % Experimental power
```

```
Pc = V.*Ic; % Calculated power
figure (2)
plot(V,Pe, 'o','LineWidth',2, 'color', 'K')
hold on
plot (V, Pc, '-', 'LineWidth',2, 'color', 'R')
title ('Experimental vs modelled P-V curve');
xlabel('Voltage (V)');
ylabel('Power (W)');
grid on
legend ('Experimental data', 'Model')
```

Appendix D: Assessment of the Influence of Measurement Error and Shading Object Placement Error on the Single Solar Cell Model

This appendix presents an assessment of the single cell model accuracy (when all parameters change with shading in the model) considering the ±RSD of R_s, R_{sh}, n and I_s shown respectively by the error bars in Figures 5.3 (a) to (d) and considering the error due to placing the shading object within ±0.2 mm (refer to Section 5.4.2).

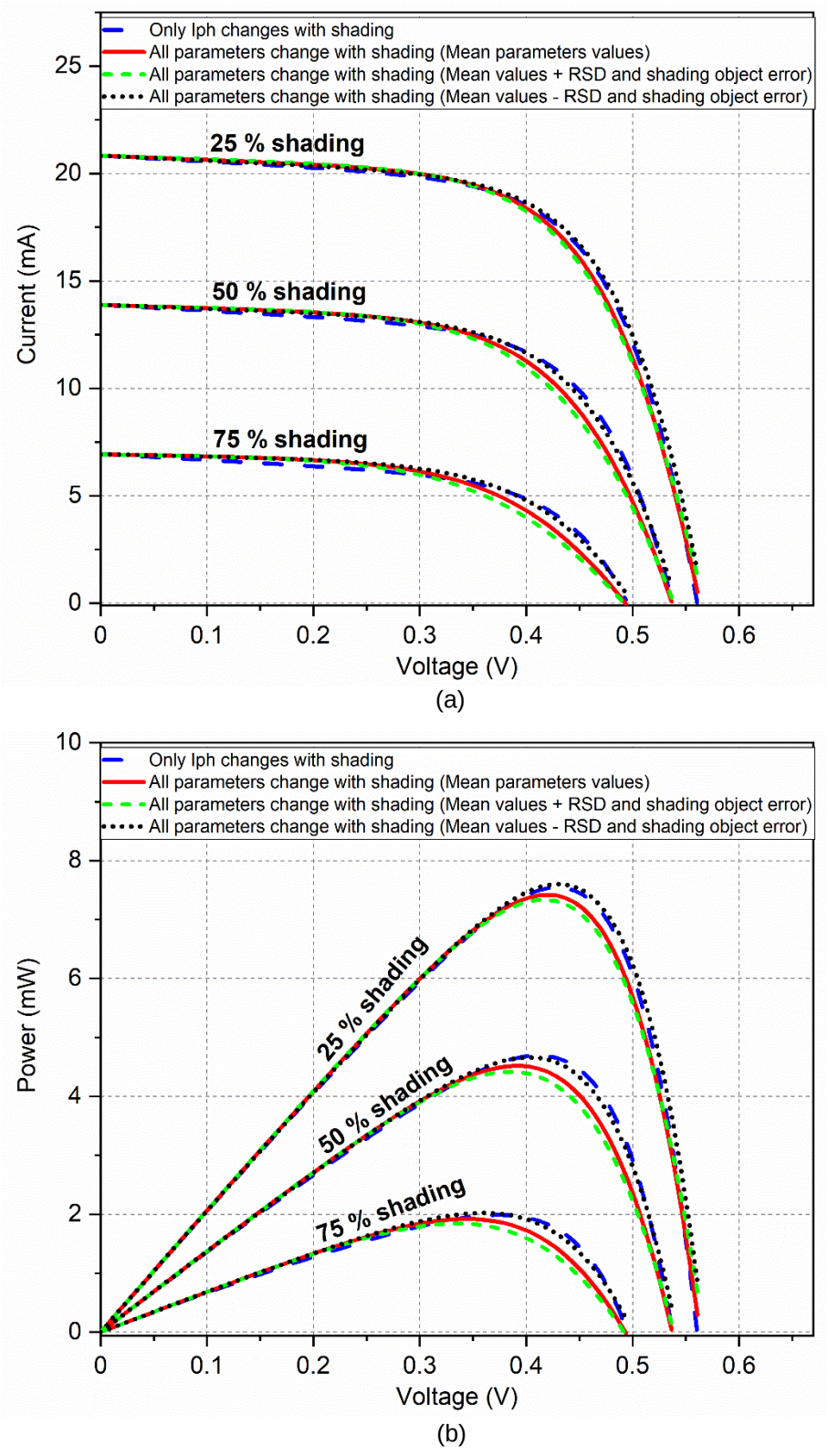

Appendix Figure D.1. Assessing the influence of shading object placement error (±0.2 mm) and relative standard deviation of the series resistance, shunt resistance, ideality factor and reverse saturation current on the improvement in modelling accuracy of solar cell 3 when considering that all cell parameters change with shading: (a) I-V curves and (b) P-V curves. (The experimental data is not included here to avoid crowd of plots).

Appendix E: PV Module Model MATLAB Code

```
%%% Abdulhamid Atia %%%
% This program code is for a PV module model works under partial shading. This program calculates
model parameters of individual solar cells considering their shading cases and produces the modelled I-V
and P-V curves. This program is written here for a 10 W mono-crystalline PV module with 36 series-
connected solar cells and two bypass diodes. In order to compare model with experimental data,
experimental I-V curve needs to be entered in a note pad file located in the same folder as this program
m-file and named (Module_Exp_IV_data).

clear all
clc

%======== Main entries ========

BP_Diodes = 1; % Is the module equipped with bypass diodes ? Enter 1 if yes and 0 if no.
G_ref = 1000; % Reference irradiance
T_ref = 25+273.15; % Reference temperature
T = 25+273.15;  % Module temperature in Kelvin
k = 1.3806488E-23; % Boltzmann constant
q = 1.60217657E-19; % Electron charge
Vth = (k*T)/q; % Thermal voltage
Eg_ref = 1.12; % Bandgap of silicon at STC
VD = 0.4; % Forward voltage drop of the bypass diode
I = flip(0:0.007261788732394:0.515587); % Enter current data for voltage calculation
load('Module_Exp_IV_data.txt'); % Enter the name of attached note pad file contains the experimental I-
V data
V_exp = Module_Exp_IV_data(:,1)'; % Define voltage vector
I_exp = Module_Exp_IV_data(:,2)'; % Define current vector

%======== Equivalent circuit parameters of solar cells at STC ========
% Note: For the used PV module in this work, those parameters were extracted under a light irradiance of
1000 W/m² measured at the centre point of the module and at a module temperature of 25 °C.

Rs_ref = 0.0848; % Series resistance at STC
Rsh_ref = 126.2497; % Shunt resistance at STC
n_ref = 0.74245; % Ideality factor at STC
Is_ref = 5.696E-16; % Reverse saturation current at STC
Iph_ref = 0.51593; % Photo-generated current at STC

%======== Temperature coefficient of the current ========

Ki = (0.0398/100)*Iph_ref; % Obtained from data sheet of commercial mono-Si solar cells

%======== Adapt the parameters of every single cell from STC to the actual irradiance, temperature
and partial shading ========

%======== Cell 1_1 ========

Sh_per1_1 = 25; % Shading percentage
AT1_1 = 0.0015; % Total cell area
A1_1_2 = (AT1_1*Sh_per1_1)/100; % Shaded area
Alfa1_1 = A1_1_2/AT1_1; % Calculate shading factor
G1_1_1 = 1000; % Unshaded part irradiance
G1_1_2 = 0; % Shaded part irradiance
```

```
%======== Check if cell 1_1 is working under STC or not ========

% If the cell is working under STC, parameters under no shading (with sub-script 'nsh') will be equal to
the STC parameters:
if G1_1_1 == G_ref && T == T_ref
Iph_nsh1_1 = Iph_ref;
Rs_nsh1_1 = Rs_ref;
Rsh_nsh1_1 = Rsh_ref;
Is_nsh1_1 = Is_ref;
n_nsh1_1 = n_ref;

% If the cell is not working under STC, adapt the STC parameters to the actual irradiance and temperature
in order to determine the parameters under no shading. All parameters equations are included here. If
some parameters are required to be set fixed with irradiance and temperature, they should be made equal
to their values under STC:
else
Rs_nsh1_1 = ((34.0109*Rs_ref*(1-(G1_1_1/G_ref))^3)-(22.9749*Rs_ref*(1-
(G1_1_1/G_ref))^2)+(6.6189*Rs_ref*(1-(G1_1_1/G_ref)))+Rs_ref)*(T/T_ref);
Rsh_nsh1_1 = (12.4389*Rsh_ref*(1-(G1_1_1/G_ref))^3)-(8.6252*Rsh_ref*(1-
(G1_1_1/G_ref))^2)+(3.3490*Rsh_ref*(1-(G1_1_1/G_ref)))+Rsh_ref;
n_nsh1_1 = (-0.2230*n_ref*(1-(G1_1_1/G_ref))^3)+(0.3643*n_ref*(1-
(G1_1_1/G_ref))^2)+(0.1670*n_ref*(1-(G1_1_1/G_ref)))+n_ref;
Eg = Eg_ref*(1-0.0002677*(T-T_ref));
Is_nsh1_1 = ((10.3994*Is_ref*(1-(G1_1_1/G_ref))^2)+(0.6450*Is_ref*(1-
(G1_1_1/G_ref)))+Is_ref)*((T/T_ref)^3*exp((Eg/k)*(1/T_ref-1/T)));
Iph_nsh1_1 = (Iph_ref+(Ki*(T-T_ref)))*(1-(1-(G1_1_1/G_ref)));
end

%======== Calculate the variations of the parameters of cell 1_1 with shading ========

% If the cell is shaded, calculate the variations of the parameters with shading. All parameters equations
are included here. If some parameters are required to be set fixed with shading, they should be made
equal to their values under no shading:
if Alfa1_1 > 0
Rs1_1 = (34.0109*Rs_nsh1_1*Alfa1_1^3)-
(22.9749*Rs_nsh1_1*Alfa1_1^2)+(6.6189*Rs_nsh1_1*Alfa1_1)+Rs_nsh1_1;
Rsh1_1 = (12.4389*Rsh_nsh1_1*Alfa1_1^3)-
(8.6252*Rsh_nsh1_1*Alfa1_1^2)+(3.3490*Rsh_nsh1_1*Alfa1_1)+Rsh_nsh1_1;
n1_1 = (-0.2230*n_nsh1_1*Alfa1_1^3) + (0.3643*n_nsh1_1*Alfa1_1^2)+
(0.1670*n_nsh1_1*Alfa1_1)+n_nsh1_1;
Is1_1 = (10.3994*Is_nsh1_1*Alfa1_1^2)+(0.6450*Is_nsh1_1*Alfa1_1)+Is_nsh1_1;
Iph1_1 = Iph_nsh1_1*(1-Alfa1_1);

% If the cell is not shaded, the cell parameters will be equal to the parameters under no shading:
else
Rs1_1 = Rs_nsh1_1;
Rsh1_1 =  Rsh_nsh1_1;
Iph1_1 = Iph_nsh1_1;
n1_1 =  n_nsh1_1;
Is1_1 = Is_nsh1_1;
end

%======== Cell 1_2 ========

Sh_per1_2 = 0; % Shading percentage
AT1_2 = 0.0015; % Total cell area
A1_2_2 = (AT1_2*Sh_per1_2)/100; % Shaded area
Alfa1_2 = A1_2_2/AT1_2; % Calculate shading factor
G1_2_1 = 1000; % Unshaded part irradiance
```

```
G1_2_2 = 0; % Shaded part irradiance

%======== Check if cell 1_2 is working under STC or not ========

% If the cell is working under STC, parameters under no shading (with sub-script 'nsh') will be equal to
the STC parameters:
if G1_2_1 == G_ref && T == T_ref
Iph_nsh1_2 = Iph_ref;
Rs_nsh1_2 = Rs_ref;
Rsh_nsh1_2 = Rsh_ref;
Is_nsh1_2 = Is_ref;
n_nsh1_2 = n_ref;

% If the cell is not working under STC, adapt the STC parameters to the actual irradiance and temperature
in order to determine the parameters under no shading. All parameters equations are included here. If
some parameters are required to be set fixed with irradiance and temperature, they should be made equal
to their values under STC:
else
Rs_nsh1_2 = ((34.0109*Rs_ref*(1-(G1_2_1/G_ref))^3)-(22.9749*Rs_ref*(1-
(G1_2_1/G_ref))^2)+(6.6189*Rs_ref*(1-(G1_2_1/G_ref)))+Rs_ref)*(T/T_ref);
Rsh_nsh1_2 = (12.4389*Rsh_ref*(1-(G1_2_1/G_ref))^3)-(8.6252*Rsh_ref*(1-
(G1_2_1/G_ref))^2)+(3.3490*Rsh_ref*(1-(G1_2_1/G_ref)))+Rsh_ref;
n_nsh1_2 = (-0.2230*n_ref*(1-(G1_2_1/G_ref))^3)+(0.3643*n_ref*(1-
(G1_2_1/G_ref))^2)+(0.1670*n_ref*(1-(G1_2_1/G_ref)))+n_ref;
Eg = Eg_ref*(1-0.0002677*(T-T_ref));
Is_nsh1_2 = ((10.3994*Is_ref*(1-(G1_2_1/G_ref))^2)+(0.6450*Is_ref*(1-
(G1_2_1/G_ref)))+Is_ref)*((T/T_ref)^3*exp((Eg/k)*(1/T_ref-1/T)));
Iph_nsh1_2 = (Iph_ref+(Ki*(T-T_ref)))*(1-(1-(G1_2_1/G_ref)));
end

%======== Calculate the variations of the parameters of cell 1_2 with shading ========

% If the cell is shaded, calculate the variations of the parameters with shading. All parameters equations
are included here. If some parameters are required to be set fixed with shading, they should be made
equal to their values under no shading:
if Alfa1_2 > 0
Rs1_2 = (34.0109*Rs_nsh1_2*Alfa1_2^3)-
(22.9749*Rs_nsh1_2*Alfa1_2^2)+(6.6189*Rs_nsh1_2*Alfa1_2)+Rs_nsh1_2;
Rsh1_2 = (12.4389*Rsh_nsh1_2*Alfa1_2^3)-
(8.6252*Rsh_nsh1_2*Alfa1_2^2)+(3.3490*Rsh_nsh1_2*Alfa1_2)+Rsh_nsh1_2;
n1_2 = (-0.2230*n_nsh1_2*Alfa1_2^3) + (0.3643*n_nsh1_2*Alfa1_2^2)+
(0.1670*n_nsh1_2*Alfa1_2)+n_nsh1_2;
Is1_2 = (10.3994*Is_nsh1_2*Alfa1_2^2)+(0.6450*Is_nsh1_2*Alfa1_2)+Is_nsh1_2;
Iph1_2 = Iph_nsh1_2*(1-Alfa1_2);

% If the cell is not shaded, the cell parameters will be equal to the parameters under no shading:
else
Rs1_2 = Rs_nsh1_2;
Rsh1_2 =  Rsh_nsh1_2;
Iph1_2 = Iph_nsh1_2;
n1_2 =  n_nsh1_2;
Is1_2 = Is_nsh1_2;
end

%======== Cell 1_3 ========

Sh_per1_3 = 0; % Shading percentage
AT1_3 = 0.0015; % Total cell area
A1_3_2 = (AT1_3*Sh_per1_3)/100; % Shaded area
Alfa1_3 = A1_3_2/AT1_3; % Calculate shading factor
```

```
G1_3_1 = 1000; % Unshaded part irradiance
G1_3_2 = 0; % Shaded part irradiance

%======== Check if cell 1_3 is working under STC or not ========

% If the cell is working under STC, parameters under no shading (with sub-script 'nsh') will be equal to
the STC parameters:
if G1_3_1 == G_ref && T == T_ref
Iph_nsh1_3 = Iph_ref;
Rs_nsh1_3 = Rs_ref;
Rsh_nsh1_3 = Rsh_ref;
Is_nsh1_3 = Is_ref;
n_nsh1_3 = n_ref;

% If the cell is not working under STC, adapt the STC parameters to the actual irradiance and temperature
in order to determine the parameters under no shading. All parameters equations are included here. If
some parameters are required to be set fixed with irradiance and temperature, they should be made equal
to their values under STC:
else
Rs_nsh1_3 = ((34.0109*Rs_ref*(1-(G1_3_1/G_ref))^3)-(22.9749*Rs_ref*(1-
(G1_3_1/G_ref))^2)+(6.6189*Rs_ref*(1-(G1_3_1/G_ref)))+Rs_ref)*(T/T_ref);
Rsh_nsh1_3 = (12.4389*Rsh_ref*(1-(G1_3_1/G_ref))^3)-(8.6252*Rsh_ref*(1-
(G1_3_1/G_ref))^2)+(3.3490*Rsh_ref*(1-(G1_3_1/G_ref)))+Rsh_ref;
n_nsh1_3 = (-0.2230*n_ref*(1-(G1_3_1/G_ref))^3)+(0.3643*n_ref*(1-
(G1_3_1/G_ref))^2)+(0.1670*n_ref*(1-(G1_3_1/G_ref)))+n_ref;
Eg = Eg_ref*(1-0.0002677*(T-T_ref));
Is_nsh1_3 = ((10.3994*Is_ref*(1-(G1_3_1/G_ref))^2)+(0.6450*Is_ref*(1-
(G1_3_1/G_ref)))+Is_ref)*((T/T_ref)^3*exp((Eg/k)*(1/T_ref-1/T)));
Iph_nsh1_3 = (Iph_ref+(Ki*(T-T_ref)))*(1-(1-(G1_3_1/G_ref)));
end

%======== Calculate the variations of the parameters of cell 1_3 with shading ========

% If the cell is shaded, calculate the variations of the parameters with shading. All parameters equations
are included here. If some parameters are required to be set fixed with shading, they should be made
equal to their values under no shading:
if Alfa1_3 > 0
Rs1_3 = (34.0109*Rs_nsh1_3*Alfa1_3^3)-
(22.9749*Rs_nsh1_3*Alfa1_3^2)+(6.6189*Rs_nsh1_3*Alfa1_3)+Rs_nsh1_3;
Rsh1_3 = (12.4389*Rsh_nsh1_3*Alfa1_3^3)-
(8.6252*Rsh_nsh1_3*Alfa1_3^2)+(3.3490*Rsh_nsh1_3*Alfa1_3)+Rsh_nsh1_3;
n1_3 = (-0.2230*n_nsh1_3*Alfa1_3^3) + (0.3643*n_nsh1_3*Alfa1_3^2)+
(0.1670*n_nsh1_3*Alfa1_3)+n_nsh1_3;
Is1_3 = (10.3994*Is_nsh1_3*Alfa1_3^2)+(0.6450*Is_nsh1_3*Alfa1_3)+Is_nsh1_3;
Iph1_3 = Iph_nsh1_3*(1-Alfa1_3);

% If the cell is not shaded, the cell parameters will be equal to the parameters under no shading:
else
Rs1_3 = Rs_nsh1_3;
Rsh1_3 =  Rsh_nsh1_3;
Iph1_3 = Iph_nsh1_3;
n1_3 =  n_nsh1_3;
Is1_3 = Is_nsh1_3;
end

%======== Cell 1_4 ========

Sh_per1_4 = 0; % Shading percentage
AT1_4 = 0.0015; % Total cell area
A1_4_2 = (AT1_4*Sh_per1_4)/100; % Shaded area
```

```
Alfa1_4 = A1_4_2/AT1_4; % Calculate shading factor
G1_4_1 = 1000; % Unshaded part irradiance
G1_4_2 = 0; % Shaded part irradiance

%======== Check if cell 1_4 is working under STC or not ========

% If the cell is working under STC, parameters under no shading (with sub-script 'nsh') will be equal to
the STC parameters:
if G1_4_1 == G_ref && T == T_ref
Iph_nsh1_4 = Iph_ref;
Rs_nsh1_4 = Rs_ref;
Rsh_nsh1_4 = Rsh_ref;
Is_nsh1_4 = Is_ref;
n_nsh1_4 = n_ref;

% If the cell is not working under STC, adapt the STC parameters to the actual irradiance and temperature
in order to determine the parameters under no shading. All parameters equations are included here. If
some parameters are required to be set fixed with irradiance and temperature, they should be made equal
to their values under STC:
else
Rs_nsh1_4 = ((34.0109*Rs_ref*(1-(G1_4_1/G_ref))^3)-(22.9749*Rs_ref*(1-
(G1_4_1/G_ref))^2)+(6.6189*Rs_ref*(1-(G1_4_1/G_ref)))+Rs_ref)*(T/T_ref);
Rsh_nsh1_4 = (12.4389*Rsh_ref*(1-(G1_4_1/G_ref))^3)-(8.6252*Rsh_ref*(1-
(G1_4_1/G_ref))^2)+(3.3490*Rsh_ref*(1-(G1_4_1/G_ref)))+Rsh_ref;
n_nsh1_4 = (-0.2230*n_ref*(1-(G1_4_1/G_ref))^3)+(0.3643*n_ref*(1-
(G1_4_1/G_ref))^2)+(0.1670*n_ref*(1-(G1_4_1/G_ref)))+n_ref;
Eg = Eg_ref*(1-0.0002677*(T-T_ref));
Is_nsh1_4 = ((10.3994*Is_ref*(1-(G1_4_1/G_ref))^2)+(0.6450*Is_ref*(1-
(G1_4_1/G_ref)))+Is_ref)*((T/T_ref)^3*exp((Eg/k)*(1/T_ref-1/T)));
Iph_nsh1_4 = (Iph_ref+(Ki*(T-T_ref)))*(1-(1-(G1_4_1/G_ref)));
end

%======== Calculate the variations of the parameters of cell 1_4 with shading ========

% If the cell is shaded, calculate the variations of the parameters with shading. All parameters equations
are included here. If some parameters are required to be set fixed with shading, they should be made
equal to their values under no shading:
if Alfa1_4 > 0
Rs1_4 = (34.0109*Rs_nsh1_4*Alfa1_4^3)-
(22.9749*Rs_nsh1_4*Alfa1_4^2)+(6.6189*Rs_nsh1_4*Alfa1_4)+Rs_nsh1_4;
Rsh1_4 = (12.4389*Rsh_nsh1_4*Alfa1_4^3)-
(8.6252*Rsh_nsh1_4*Alfa1_4^2)+(3.3490*Rsh_nsh1_4*Alfa1_4)+Rsh_nsh1_4;
n1_4 = (-0.2230*n_nsh1_4*Alfa1_4^3) + (0.3643*n_nsh1_4*Alfa1_4^2)+
(0.1670*n_nsh1_4*Alfa1_4)+n_nsh1_4;
Is1_4 = (10.3994*Is_nsh1_4*Alfa1_4^2)+(0.6450*Is_nsh1_4*Alfa1_4)+Is_nsh1_4;
Iph1_4 = Iph_nsh1_4*(1-Alfa1_4);

% If the cell is not shaded, the cell parameters will be equal to the parameters under no shading:
else
Rs1_4 = Rs_nsh1_4;
Rsh1_4 =  Rsh_nsh1_4;
Iph1_4 = Iph_nsh1_4;
n1_4 =  n_nsh1_4;
Is1_4 = Is_nsh1_4;
end

%======== Cell 1_5 ========

Sh_per1_5 = 0; % Shading percentage
AT1_5 = 0.0015; % Total cell area
```

```
A1_5_2 = (AT1_5*Sh_per1_5)/100; % Shaded area
Alfa1_5 = A1_5_2/AT1_5; % Calculate shading factor
G1_5_1 = 1000; % Unshaded part irradiance
G1_5_2 = 0; % Shaded part irradiance

%======== Check if cell 1_5 is working under STC or not ========

% If the cell is working under STC, parameters under no shading (with sub-script 'nsh') will be equal to
the STC parameters:
if G1_5_1 == G_ref && T == T_ref
Iph_nsh1_5 = Iph_ref;
Rs_nsh1_5 = Rs_ref;
Rsh_nsh1_5 = Rsh_ref;
Is_nsh1_5 = Is_ref;
n_nsh1_5 = n_ref;

% If the cell is not working under STC, adapt the STC parameters to the actual irradiance and temperature
in order to determine the parameters under no shading. All parameters equations are included here. If
some parameters are required to be set fixed with irradiance and temperature, they should be made equal
to their values under STC:
else
Rs_nsh1_5 = ((34.0109*Rs_ref*(1-(G1_5_1/G_ref))^3)-(22.9749*Rs_ref*(1-
(G1_5_1/G_ref))^2)+(6.6189*Rs_ref*(1-(G1_5_1/G_ref)))+Rs_ref)*(T/T_ref);
Rsh_nsh1_5 = (12.4389*Rsh_ref*(1-(G1_5_1/G_ref))^3)-(8.6252*Rsh_ref*(1-
(G1_5_1/G_ref))^2)+(3.3490*Rsh_ref*(1-(G1_5_1/G_ref)))+Rsh_ref;
n_nsh1_5 = (-0.2230*n_ref*(1-(G1_5_1/G_ref))^3)+(0.3643*n_ref*(1-
(G1_5_1/G_ref))^2)+(0.1670*n_ref*(1-(G1_5_1/G_ref)))+n_ref;
Eg = Eg_ref*(1-0.0002677*(T-T_ref));
Is_nsh1_5 = ((10.3994*Is_ref*(1-(G1_5_1/G_ref))^2)+(0.6450*Is_ref*(1-
(G1_5_1/G_ref)))+Is_ref)*((T/T_ref)^3*exp((Eg/k)*(1/T_ref-1/T)));
Iph_nsh1_5 = (Iph_ref+(Ki*(T-T_ref)))*(1-(1-(G1_5_1/G_ref)));
end

%======== Calculate the variations of the parameters of cell 1_5 with shading ========

% If the cell is shaded, calculate the variations of the parameters with shading. All parameters equations
are included here. If some parameters are required to be set fixed with shading, they should be made
equal to their values under no shading:
if Alfa1_5 > 0
Rs1_5 = (34.0109*Rs_nsh1_5*Alfa1_5^3)-
(22.9749*Rs_nsh1_5*Alfa1_5^2)+(6.6189*Rs_nsh1_5*Alfa1_5)+Rs_nsh1_5;
Rsh1_5 = (12.4389*Rsh_nsh1_5*Alfa1_5^3)-
(8.6252*Rsh_nsh1_5*Alfa1_5^2)+(3.3490*Rsh_nsh1_5*Alfa1_5)+Rsh_nsh1_5;
n1_5 = (-0.2230*n_nsh1_5*Alfa1_5^3) + (0.3643*n_nsh1_5*Alfa1_5^2)+
(0.1670*n_nsh1_5*Alfa1_5)+n_nsh1_5;
Is1_5 = (10.3994*Is_nsh1_5*Alfa1_5^2)+(0.6450*Is_nsh1_5*Alfa1_5)+Is_nsh1_5;
Iph1_5 = Iph_nsh1_5*(1-Alfa1_5);

% If the cell is not shaded, the cell parameters will be equal to the parameters under no shading:
else
Rs1_5 = Rs_nsh1_5;
Rsh1_5 =  Rsh_nsh1_5;
Iph1_5 = Iph_nsh1_5;
n1_5 =  n_nsh1_5;
Is1_5 = Is_nsh1_5;
end


%======== Cell 1_6 ========
```

```
Sh_per1_6 = 0; % Shading percentage
AT1_6 = 0.0015; % Total cell area
A1_6_2 = (AT1_6*Sh_per1_6)/100; % Shaded area
Alfa1_6 = A1_6_2/AT1_6; % Calculate shading factor
G1_6_1 = 1000; % Unshaded part irradiance
G1_6_2 = 0; % Shaded part irradiance

%======== Check if cell 1_6 is working under STC or not ========

% If the cell is working under STC, parameters under no shading (with sub-script 'nsh') will be equal to
the STC parameters:
if G1_6_1 == G_ref && T == T_ref
Iph_nsh1_6 = Iph_ref;
Rs_nsh1_6 = Rs_ref;
Rsh_nsh1_6 = Rsh_ref;
Is_nsh1_6 = Is_ref;
n_nsh1_6 = n_ref;

% If the cell is not working under STC, adapt the STC parameters to the actual irradiance and temperature
in order to determine the parameters under no shading. All parameters equations are included here. If
some parameters are required to be set fixed with irradiance and temperature, they should be made equal
to their values under STC:
else
Rs_nsh1_6 = ((34.0109*Rs_ref*(1-(G1_6_1/G_ref))^3)-(22.9749*Rs_ref*(1-
(G1_6_1/G_ref))^2)+(6.6189*Rs_ref*(1-(G1_6_1/G_ref)))+Rs_ref)*(T/T_ref);
Rsh_nsh1_6 = (12.4389*Rsh_ref*(1-(G1_6_1/G_ref))^3)-(8.6252*Rsh_ref*(1-
(G1_6_1/G_ref))^2)+(3.3490*Rsh_ref*(1-(G1_6_1/G_ref)))+Rsh_ref;
n_nsh1_6 = (-0.2230*n_ref*(1-(G1_6_1/G_ref))^3)+(0.3643*n_ref*(1-
(G1_6_1/G_ref))^2)+(0.1670*n_ref*(1-(G1_6_1/G_ref)))+n_ref;
Eg = Eg_ref*(1-0.0002677*(T-T_ref));
Is_nsh1_6 = ((10.3994*Is_ref*(1-(G1_6_1/G_ref))^2)+(0.6450*Is_ref*(1-
(G1_6_1/G_ref)))+Is_ref)*((T/T_ref)^3*exp((Eg/k)*(1/T_ref-1/T)));
Iph_nsh1_6 = (Iph_ref+(Ki*(T-T_ref)))*(1-(1-(G1_6_1/G_ref)));
end

%======== Calculate the variations of the parameters of cell 1_6 with shading ========

% If the cell is shaded, calculate the variations of the parameters with shading. All parameters equations
are included here. If some parameters are required to be set fixed with shading, they should be made
equal to their values under no shading:
if Alfa1_6 > 0
Rs1_6 = (34.0109*Rs_nsh1_6*Alfa1_6^3)-
(22.9749*Rs_nsh1_6*Alfa1_6^2)+(6.6189*Rs_nsh1_6*Alfa1_6)+Rs_nsh1_6;
Rsh1_6 = (12.4389*Rsh_nsh1_6*Alfa1_6^3)-
(8.6252*Rsh_nsh1_6*Alfa1_6^2)+(3.3490*Rsh_nsh1_6*Alfa1_6)+Rsh_nsh1_6;
n1_6 = (-0.2230*n_nsh1_6*Alfa1_6^3) + (0.3643*n_nsh1_6*Alfa1_6^2)+
(0.1670*n_nsh1_6*Alfa1_6)+n_nsh1_6;
Is1_6 = (10.3994*Is_nsh1_6*Alfa1_6^2)+(0.6450*Is_nsh1_6*Alfa1_6)+Is_nsh1_6;
Iph1_6 = Iph_nsh1_6*(1-Alfa1_6);

% If the cell is not shaded, the cell parameters will be equal to the parameters under no shading:
else
Rs1_6 = Rs_nsh1_6;
Rsh1_6 =  Rsh_nsh1_6;
Iph1_6 = Iph_nsh1_6;
n1_6 =  n_nsh1_6;
Is1_6 = Is_nsh1_6;
end

%======== Cell 1_7 ========
```

```
Sh_per1_7 = 0; % Shading percentage
AT1_7 = 0.0015; % Total cell area
A1_7_2 = (AT1_7*Sh_per1_7)/100; % Shaded area
Alfa1_7 = A1_7_2/AT1_7; % Calculate shading factor
G1_7_1 = 1000; % Unshaded part irradiance
G1_7_2 = 0; % Shaded part irradiance

%======== Check if cell 1_7 is working under STC or not ========

% If the cell is working under STC, parameters under no shading (with sub-script 'nsh') will be equal to
the STC parameters:
if G1_7_1 == G_ref && T == T_ref
Iph_nsh1_7 = Iph_ref;
Rs_nsh1_7 = Rs_ref;
Rsh_nsh1_7 = Rsh_ref;
Is_nsh1_7 = Is_ref;
n_nsh1_7 = n_ref;

% If the cell is not working under STC, adapt the STC parameters to the actual irradiance and temperature
in order to determine the parameters under no shading. All parameters equations are included here. If
some parameters are required to be set fixed with irradiance and temperature, they should be made equal
to their values under STC:
else
Rs_nsh1_7 = ((34.0109*Rs_ref*(1-(G1_7_1/G_ref))^3)-(22.9749*Rs_ref*(1-
(G1_7_1/G_ref))^2)+(6.6189*Rs_ref*(1-(G1_7_1/G_ref)))+Rs_ref)*(T/T_ref);
Rsh_nsh1_7 = (12.4389*Rsh_ref*(1-(G1_7_1/G_ref))^3)-(8.6252*Rsh_ref*(1-
(G1_7_1/G_ref))^2)+(3.3490*Rsh_ref*(1-(G1_7_1/G_ref)))+Rsh_ref;
n_nsh1_7 = (-0.2230*n_ref*(1-(G1_7_1/G_ref))^3)+(0.3643*n_ref*(1-
(G1_7_1/G_ref))^2)+(0.1670*n_ref*(1-(G1_7_1/G_ref)))+n_ref;
Eg = Eg_ref*(1-0.0002677*(T-T_ref));
Is_nsh1_7 = ((10.3994*Is_ref*(1-(G1_7_1/G_ref))^2)+(0.6450*Is_ref*(1-
(G1_7_1/G_ref)))+Is_ref)*((T/T_ref)^3*exp((Eg/k)*(1/T_ref-1/T)));
Iph_nsh1_7 = (Iph_ref+(Ki*(T-T_ref)))*(1-(1-(G1_7_1/G_ref)));
end

%======== Calculate the variations of the parameters of cell 1_7 with shading ========

% If the cell is shaded, calculate the variations of the parameters with shading. All parameters equations
are included here. If some parameters are required to be set fixed with shading, they should be made
equal to their values under no shading:
if Alfa1_7 > 0
Rs1_7 = (34.0109*Rs_nsh1_7*Alfa1_7^3)-
(22.9749*Rs_nsh1_7*Alfa1_7^2)+(6.6189*Rs_nsh1_7*Alfa1_7)+Rs_nsh1_7;
Rsh1_7 = (12.4389*Rsh_nsh1_7*Alfa1_7^3)-
(8.6252*Rsh_nsh1_7*Alfa1_7^2)+(3.3490*Rsh_nsh1_7*Alfa1_7)+Rsh_nsh1_7;
n1_7 = (-0.2230*n_nsh1_7*Alfa1_7^3) + (0.3643*n_nsh1_7*Alfa1_7^2)+
(0.1670*n_nsh1_7*Alfa1_7)+n_nsh1_7;
Is1_7 = (10.3994*Is_nsh1_7*Alfa1_7^2)+(0.6450*Is_nsh1_7*Alfa1_7)+Is_nsh1_7;
Iph1_7 = Iph_nsh1_7*(1-Alfa1_7);

% If the cell is not shaded, the cell parameters will be equal to the parameters under no shading:
else
Rs1_7 = Rs_nsh1_7;
Rsh1_7 =  Rsh_nsh1_7;
Iph1_7 = Iph_nsh1_7;
n1_7 =  n_nsh1_7;
Is1_7 = Is_nsh1_7;
end
```

```
%======== Cell 1_8 ========

Sh_per1_8 = 0; % Shading percentage
AT1_8 = 0.0015; % Total cell area
A1_8_2 = (AT1_8*Sh_per1_8)/100; % Shaded area
Alfa1_8 = A1_8_2/AT1_8; % Calculate shading factor
G1_8_1 = 1000; % Unshaded part irradiance
G1_8_2 = 0; % Shaded part irradiance

%======== Check if cell 1_8 is working under STC or not ========

% If the cell is working under STC, parameters under no shading (with sub-script 'nsh') will be equal to
the STC parameters:
if G1_8_1 == G_ref && T == T_ref
Iph_nsh1_8 = Iph_ref;
Rs_nsh1_8 = Rs_ref;
Rsh_nsh1_8 = Rsh_ref;
Is_nsh1_8 = Is_ref;
n_nsh1_8 = n_ref;

% If the cell is not working under STC, adapt the STC parameters to the actual irradiance and temperature
in order to determine the parameters under no shading. All parameters equations are included here. If
some parameters are required to be set fixed with irradiance and temperature, they should be made equal
to their values under STC:
else
Rs_nsh1_8 = ((34.0109*Rs_ref*(1-(G1_8_1/G_ref))^3)-(22.9749*Rs_ref*(1-
(G1_8_1/G_ref))^2)+(6.6189*Rs_ref*(1-(G1_8_1/G_ref)))+Rs_ref)*(T/T_ref);
Rsh_nsh1_8 = (12.4389*Rsh_ref*(1-(G1_8_1/G_ref))^3)-(8.6252*Rsh_ref*(1-
(G1_8_1/G_ref))^2)+(3.3490*Rsh_ref*(1-(G1_8_1/G_ref)))+Rsh_ref;
n_nsh1_8 = (-0.2230*n_ref*(1-(G1_8_1/G_ref))^3)+(0.3643*n_ref*(1-
(G1_8_1/G_ref))^2)+(0.1670*n_ref*(1-(G1_8_1/G_ref)))+n_ref;
Eg = Eg_ref*(1-0.0002677*(T-T_ref));
Is_nsh1_8 = ((10.3994*Is_ref*(1-(G1_8_1/G_ref))^2)+(0.6450*Is_ref*(1-
(G1_8_1/G_ref)))+Is_ref)*((T/T_ref)^3*exp((Eg/k)*(1/T_ref-1/T)));
Iph_nsh1_8 = (Iph_ref+(Ki*(T-T_ref)))*(1-(1-(G1_8_1/G_ref)));
end

%======== Calculate the variations of the parameters of cell 1_8 with shading ========

% If the cell is shaded, calculate the variations of the parameters with shading. All parameters equations
are included here. If some parameters are required to be set fixed with shading, they should be made
equal to their values under no shading:
if Alfa1_8 > 0
Rs1_8 = (34.0109*Rs_nsh1_8*Alfa1_8^3)-
(22.9749*Rs_nsh1_8*Alfa1_8^2)+(6.6189*Rs_nsh1_8*Alfa1_8)+Rs_nsh1_8;
Rsh1_8 = (12.4389*Rsh_nsh1_8*Alfa1_8^3)-
(8.6252*Rsh_nsh1_8*Alfa1_8^2)+(3.3490*Rsh_nsh1_8*Alfa1_8)+Rsh_nsh1_8;
n1_8 = (-0.2230*n_nsh1_8*Alfa1_8^3) + (0.3643*n_nsh1_8*Alfa1_8^2)+
(0.1670*n_nsh1_8*Alfa1_8)+n_nsh1_8;
Is1_8 = (10.3994*Is_nsh1_8*Alfa1_8^2)+(0.6450*Is_nsh1_8*Alfa1_8)+Is_nsh1_8;
Iph1_8 = Iph_nsh1_8*(1-Alfa1_8);

% If the cell is not shaded, the cell parameters will be equal to the parameters under no shading:
else
Rs1_8 = Rs_nsh1_8;
Rsh1_8 =  Rsh_nsh1_8;
Iph1_8 = Iph_nsh1_8;
n1_8 =  n_nsh1_8;
Is1_8 = Is_nsh1_8;
end
```

```
%======== Cell 1_9 ========

Sh_per1_9 = 0; % Shading percentage
AT1_9 = 0.0015; % Total cell area
A1_9_2 = (AT1_9*Sh_per1_9)/100; % Shaded area
Alfa1_9 = A1_9_2/AT1_9; % Calculate shading factor
G1_9_1 = 1000; % Unshaded part irradiance
G1_9_2 = 0; % Shaded part irradiance

%======== Check if cell 1_9 is working under STC or not ========

% If the cell is working under STC, parameters under no shading (with sub-script 'nsh') will be equal to
the STC parameters:
if G1_9_1 == G_ref && T == T_ref
Iph_nsh1_9 = Iph_ref;
Rs_nsh1_9 = Rs_ref;
Rsh_nsh1_9 = Rsh_ref;
Is_nsh1_9 = Is_ref;
n_nsh1_9 = n_ref;

% If the cell is not working under STC, adapt the STC parameters to the actual irradiance and temperature
in order to determine the parameters under no shading. All parameters equations are included here. If
some parameters are required to be set fixed with irradiance and temperature, they should be made equal
to their values under STC:
else
Rs_nsh1_9 = ((34.0109*Rs_ref*(1-(G1_9_1/G_ref))^3)-(22.9749*Rs_ref*(1-
(G1_9_1/G_ref))^2)+(6.6189*Rs_ref*(1-(G1_9_1/G_ref)))+Rs_ref)*(T/T_ref);
Rsh_nsh1_9 = (12.4389*Rsh_ref*(1-(G1_9_1/G_ref))^3)-(8.6252*Rsh_ref*(1-
(G1_9_1/G_ref))^2)+(3.3490*Rsh_ref*(1-(G1_9_1/G_ref)))+Rsh_ref;
n_nsh1_9 = (-0.2230*n_ref*(1-(G1_9_1/G_ref))^3)+(0.3643*n_ref*(1-
(G1_9_1/G_ref))^2)+(0.1670*n_ref*(1-(G1_9_1/G_ref)))+n_ref;
Eg = Eg_ref*(1-0.0002677*(T-T_ref));
Is_nsh1_9 = ((10.3994*Is_ref*(1-(G1_9_1/G_ref))^2)+(0.6450*Is_ref*(1-
(G1_9_1/G_ref)))+Is_ref)*((T/T_ref)^3*exp((Eg/k)*(1/T_ref-1/T)));
Iph_nsh1_9 = (Iph_ref+(Ki*(T-T_ref)))*(1-(1-(G1_9_1/G_ref)));
end

%======== Calculate the variations of the parameters of cell 1_9 with shading ========

% If the cell is shaded, calculate the variations of the parameters with shading. All parameters equations
are included here. If some parameters are required to be set fixed with shading, they should be made
equal to their values under no shading:
if Alfa1_9 > 0
Rs1_9 = (34.0109*Rs_nsh1_9*Alfa1_9^3)-
(22.9749*Rs_nsh1_9*Alfa1_9^2)+(6.6189*Rs_nsh1_9*Alfa1_9)+Rs_nsh1_9;
Rsh1_9 = (12.4389*Rsh_nsh1_9*Alfa1_9^3)-
(8.6252*Rsh_nsh1_9*Alfa1_9^2)+(3.3490*Rsh_nsh1_9*Alfa1_9)+Rsh_nsh1_9;
n1_9 = (-0.2230*n_nsh1_9*Alfa1_9^3) + (0.3643*n_nsh1_9*Alfa1_9^2)+
(0.1670*n_nsh1_9*Alfa1_9)+n_nsh1_9;
Is1_9 = (10.3994*Is_nsh1_9*Alfa1_9^2)+(0.6450*Is_nsh1_9*Alfa1_9)+Is_nsh1_9;
Iph1_9 = Iph_nsh1_9*(1-Alfa1_9);

% If the cell is not shaded, the cell parameters will be equal to the parameters under no shading:
else
Rs1_9 = Rs_nsh1_9;
Rsh1_9 =  Rsh_nsh1_9;
Iph1_9 = Iph_nsh1_9;
n1_9 =  n_nsh1_9;
Is1_9 = Is_nsh1_9;
```

```
end

%======== Cell 1_10 ========

Sh_per1_10 = 0; % Shading percentage
AT1_10 = 0.0015; % Total cell area
A1_10_2 = (AT1_10*Sh_per1_10)/100; % Shaded area
Alfa1_10 = A1_10_2/AT1_10; % Calculate shading factor
G1_10_1 = 1000; % Unshaded part irradiance
G1_10_2 = 0; % Shaded part irradiance

%======== Check if cell 1_10 is working under STC or not ========

% If the cell is working under STC, parameters under no shading (with sub-script 'nsh') will be equal to
the STC parameters:
if G1_10_1 == G_ref && T == T_ref
Iph_nsh1_10 = Iph_ref;
Rs_nsh1_10 = Rs_ref;
Rsh_nsh1_10 = Rsh_ref;
Is_nsh1_10 = Is_ref;
n_nsh1_10 = n_ref;

% If the cell is not working under STC, adapt the STC parameters to the actual irradiance and temperature
in order to determine the parameters under no shading. All parameters equations are included here. If
some parameters are required to be set fixed with irradiance and temperature, they should be made equal
to their values under STC:
else
Rs_nsh1_10 = ((34.0109*Rs_ref*(1-(G1_10_1/G_ref))^3)-(22.9749*Rs_ref*(1-
(G1_10_1/G_ref))^2)+(6.6189*Rs_ref*(1-(G1_10_1/G_ref)))+Rs_ref)*(T/T_ref);
Rsh_nsh1_10 = (12.4389*Rsh_ref*(1-(G1_10_1/G_ref))^3)-(8.6252*Rsh_ref*(1-
(G1_10_1/G_ref))^2)+(3.3490*Rsh_ref*(1-(G1_10_1/G_ref)))+Rsh_ref;
n_nsh1_10 = (-0.2230*n_ref*(1-(G1_10_1/G_ref))^3)+(0.3643*n_ref*(1-
(G1_10_1/G_ref))^2)+(0.1670*n_ref*(1-(G1_10_1/G_ref)))+n_ref;
Eg = Eg_ref*(1-0.0002677*(T-T_ref));
Is_nsh1_10 = ((10.3994*Is_ref*(1-(G1_10_1/G_ref))^2)+(0.6450*Is_ref*(1-
(G1_10_1/G_ref)))+Is_ref)*((T/T_ref)^3*exp((Eg/k)*(1/T_ref-1/T)));
Iph_nsh1_10 = (Iph_ref+(Ki*(T-T_ref)))*(1-(1-(G1_10_1/G_ref)));
end

%======== Calculate the variations of the parameters of cell 1_10 with shading ========

% If the cell is shaded, calculate the variations of the parameters with shading. All parameters equations
are included here. If some parameters are required to be set fixed with shading, they should be made
equal to their values under no shading:
if Alfa1_10 > 0
Rs1_10 = (34.0109*Rs_nsh1_10*Alfa1_10^3)-
(22.9749*Rs_nsh1_10*Alfa1_10^2)+(6.6189*Rs_nsh1_10*Alfa1_10)+Rs_nsh1_10;
Rsh1_10 = (12.4389*Rsh_nsh1_10*Alfa1_10^3)-
(8.6252*Rsh_nsh1_10*Alfa1_10^2)+(3.3490*Rsh_nsh1_10*Alfa1_10)+Rsh_nsh1_10;
n1_10 = (-0.2230*n_nsh1_10*Alfa1_10^3) + (0.3643*n_nsh1_10*Alfa1_10^2)+
(0.1670*n_nsh1_10*Alfa1_10)+n_nsh1_10;
Is1_10 = (10.3994*Is_nsh1_10*Alfa1_10^2)+(0.6450*Is_nsh1_10*Alfa1_10)+Is_nsh1_10;
Iph1_10 = Iph_nsh1_10*(1-Alfa1_10);

% If the cell is not shaded, the cell parameters will be equal to the parameters under no shading:
else
Rs1_10 = Rs_nsh1_10;
Rsh1_10 =  Rsh_nsh1_10;
Iph1_10 = Iph_nsh1_10;
n1_10 =  n_nsh1_10;
```

```
Is1_10 = Is_nsh1_10;
end

%======== Cell 1_11 ========

Sh_per1_11 = 0; % Shading percentage
AT1_11 = 0.0015; % Total cell area
A1_11_2 = (AT1_11*Sh_per1_11)/100; % Shaded area
Alfa1_11 = A1_11_2/AT1_11; % Calculate shading factor
G1_11_1 = 1000; % Unshaded part irradiance
G1_11_2 = 0; % Shaded part irradiance

%======== Check if cell 1_11 is working under STC or not ========

% If the cell is working under STC, parameters under no shading (with sub-script 'nsh') will be equal to
the STC parameters:
if G1_11_1 == G_ref && T == T_ref
Iph_nsh1_11 = Iph_ref;
Rs_nsh1_11 = Rs_ref;
Rsh_nsh1_11 = Rsh_ref;
Is_nsh1_11 = Is_ref;
n_nsh1_11 = n_ref;

% If the cell is not working under STC, adapt the STC parameters to the actual irradiance and temperature
in order to determine the parameters under no shading. All parameters equations are included here. If
some parameters are required to be set fixed with irradiance and temperature, they should be made equal
to their values under STC:
else
Rs_nsh1_11 = ((34.0109*Rs_ref*(1-(G1_11_1/G_ref))^3)-(22.9749*Rs_ref*(1-
(G1_11_1/G_ref))^2)+(6.6189*Rs_ref*(1-(G1_11_1/G_ref)))+Rs_ref)*(T/T_ref);
Rsh_nsh1_11 = (12.4389*Rsh_ref*(1-(G1_11_1/G_ref))^3)-(8.6252*Rsh_ref*(1-
(G1_11_1/G_ref))^2)+(3.3490*Rsh_ref*(1-(G1_11_1/G_ref)))+Rsh_ref;
n_nsh1_11 = (-0.2230*n_ref*(1-(G1_11_1/G_ref))^3)+(0.3643*n_ref*(1-
(G1_11_1/G_ref))^2)+(0.1670*n_ref*(1-(G1_11_1/G_ref)))+n_ref;
Eg = Eg_ref*(1-0.0002677*(T-T_ref));
Is_nsh1_11 = ((10.3994*Is_ref*(1-(G1_11_1/G_ref))^2)+(0.6450*Is_ref*(1-
(G1_11_1/G_ref)))+Is_ref)*((T/T_ref)^3*exp((Eg/k)*(1/T_ref-1/T)));
Iph_nsh1_11 = (Iph_ref+(Ki*(T-T_ref)))*(1-(1-(G1_11_1/G_ref)));
end

%======== Calculate the variations of the parameters of cell 1_11 with shading ========

% If the cell is shaded, calculate the variations of the parameters with shading. All parameters equations
are included here. If some parameters are required to be set fixed with shading, they should be made
equal to their values under no shading:
if Alfa1_11 > 0
Rs1_11 = (34.0109*Rs_nsh1_11*Alfa1_11^3)-
(22.9749*Rs_nsh1_11*Alfa1_11^2)+(6.6189*Rs_nsh1_11*Alfa1_11)+Rs_nsh1_11;
Rsh1_11 = (12.4389*Rsh_nsh1_11*Alfa1_11^3)-
(8.6252*Rsh_nsh1_11*Alfa1_11^2)+(3.3490*Rsh_nsh1_11*Alfa1_11)+Rsh_nsh1_11;
n1_11 = (-0.2230*n_nsh1_11*Alfa1_11^3) + (0.3643*n_nsh1_11*Alfa1_11^2)+
(0.1670*n_nsh1_11*Alfa1_11)+n_nsh1_11;
Is1_11 = (10.3994*Is_nsh1_11*Alfa1_11^2)+(0.6450*Is_nsh1_11*Alfa1_11)+Is_nsh1_11;
Iph1_11 = Iph_nsh1_11*(1-Alfa1_11);

% If the cell is not shaded, the cell parameters will be equal to the parameters under no shading:
else
Rs1_11 = Rs_nsh1_11;
Rsh1_11 =  Rsh_nsh1_11;
Iph1_11 = Iph_nsh1_11;
```

```
n1_11 =  n_nsh1_11;
Is1_11 = Is_nsh1_11;
end

%======== Cell 1_12 ========

Sh_per1_12 = 0; % Shading percentage
AT1_12 = 0.0015; % Total cell area
A1_12_2 = (AT1_12*Sh_per1_12)/100; % Shaded area
Alfa1_12 = A1_12_2/AT1_12; % Calculate shading factor
G1_12_1 = 1000; % Unshaded part irradiance
G1_12_2 = 0; % Shaded part irradiance

%======== Check if cell 1_12 is working under STC or not ========

% If the cell is working under STC, parameters under no shading (with sub-script 'nsh') will be equal to
the STC parameters:
if G1_12_1 == G_ref && T == T_ref
Iph_nsh1_12 = Iph_ref;
Rs_nsh1_12 = Rs_ref;
Rsh_nsh1_12 = Rsh_ref;
Is_nsh1_12 = Is_ref;
n_nsh1_12 = n_ref;

% If the cell is not working under STC, adapt the STC parameters to the actual irradiance and temperature
in order to determine the parameters under no shading. All parameters equations are included here. If
some parameters are required to be set fixed with irradiance and temperature, they should be made equal
to their values under STC:
else
Rs_nsh1_12 = ((34.0109*Rs_ref*(1-(G1_12_1/G_ref))^3)-(22.9749*Rs_ref*(1-
(G1_12_1/G_ref))^2)+(6.6189*Rs_ref*(1-(G1_12_1/G_ref)))+Rs_ref)*(T/T_ref);
Rsh_nsh1_12 = (12.4389*Rsh_ref*(1-(G1_12_1/G_ref))^3)-(8.6252*Rsh_ref*(1-
(G1_12_1/G_ref))^2)+(3.3490*Rsh_ref*(1-(G1_12_1/G_ref)))+Rsh_ref;
n_nsh1_12 = (-0.2230*n_ref*(1-(G1_12_1/G_ref))^3)+(0.3643*n_ref*(1-
(G1_12_1/G_ref))^2)+(0.1670*n_ref*(1-(G1_12_1/G_ref)))+n_ref;
Eg = Eg_ref*(1-0.0002677*(T-T_ref));
Is_nsh1_12 = ((10.3994*Is_ref*(1-(G1_12_1/G_ref))^2)+(0.6450*Is_ref*(1-
(G1_12_1/G_ref)))+Is_ref)*((T/T_ref)^3*exp((Eg/k)*(1/T_ref-1/T)));
Iph_nsh1_12 = (Iph_ref+(Ki*(T-T_ref)))*(1-(1-(G1_12_1/G_ref)));
end

%======== Calculate the variations of the parameters of cell 1_12 with shading ========

% If the cell is shaded, calculate the variations of the parameters with shading. All parameters equations
are included here. If some parameters are required to be set fixed with shading, they should be made
equal to their values under no shading:
if Alfa1_12 > 0
Rs1_12 = (34.0109*Rs_nsh1_12*Alfa1_12^3)-
(22.9749*Rs_nsh1_12*Alfa1_12^2)+(6.6189*Rs_nsh1_12*Alfa1_12)+Rs_nsh1_12;
Rsh1_12 = (12.4389*Rsh_nsh1_12*Alfa1_12^3)-
(8.6252*Rsh_nsh1_12*Alfa1_12^2)+(3.3490*Rsh_nsh1_12*Alfa1_12)+Rsh_nsh1_12;
n1_12 = (-0.2230*n_nsh1_12*Alfa1_12^3) + (0.3643*n_nsh1_12*Alfa1_12^2)+
(0.1670*n_nsh1_12*Alfa1_12)+n_nsh1_12;
Is1_12 = (10.3994*Is_nsh1_12*Alfa1_12^2)+(0.6450*Is_nsh1_12*Alfa1_12)+Is_nsh1_12;
Iph1_12 = Iph_nsh1_12*(1-Alfa1_12);

% If the cell is not shaded, the cell parameters will be equal to the parameters under no shading:
else
Rs1_12 = Rs_nsh1_12;
Rsh1_12 =  Rsh_nsh1_12;
```

```
Iph1_12 = Iph_nsh1_12;
n1_12 =  n_nsh1_12;
Is1_12 = Is_nsh1_12;
end

%======== Cell 1_13 ========

Sh_per1_13 = 0; % Shading percentage
AT1_13 = 0.0015; % Total cell area
A1_13_2 = (AT1_13*Sh_per1_13)/100; % Shaded area
Alfa1_13 = A1_13_2/AT1_13; % Calculate shading factor
G1_13_1 = 1000; % Unshaded part irradiance
G1_13_2 = 0; % Shaded part irradiance

%======== Check if cell 1_13 is working under STC or not ========

% If the cell is working under STC, parameters under no shading (with sub-script 'nsh') will be equal to
the STC parameters:
if G1_13_1 == G_ref && T == T_ref
Iph_nsh1_13 = Iph_ref;
Rs_nsh1_13 = Rs_ref;
Rsh_nsh1_13 = Rsh_ref;
Is_nsh1_13 = Is_ref;
n_nsh1_13 = n_ref;

% If the cell is not working under STC, adapt the STC parameters to the actual irradiance and temperature
in order to determine the parameters under no shading. All parameters equations are included here. If
some parameters are required to be set fixed with irradiance and temperature, they should be made equal
to their values under STC:
else
Rs_nsh1_13 = ((34.0109*Rs_ref*(1-(G1_13_1/G_ref))^3)-(22.9749*Rs_ref*(1-
(G1_13_1/G_ref))^2)+(6.6189*Rs_ref*(1-(G1_13_1/G_ref)))+Rs_ref)*(T/T_ref);
Rsh_nsh1_13 = (12.4389*Rsh_ref*(1-(G1_13_1/G_ref))^3)-(8.6252*Rsh_ref*(1-
(G1_13_1/G_ref))^2)+(3.3490*Rsh_ref*(1-(G1_13_1/G_ref)))+Rsh_ref;
n_nsh1_13 = (-0.2230*n_ref*(1-(G1_13_1/G_ref))^3)+(0.3643*n_ref*(1-
(G1_13_1/G_ref))^2)+(0.1670*n_ref*(1-(G1_13_1/G_ref)))+n_ref;
Eg = Eg_ref*(1-0.0002677*(T-T_ref));
Is_nsh1_13 = ((10.3994*Is_ref*(1-(G1_13_1/G_ref))^2)+(0.6450*Is_ref*(1-
(G1_13_1/G_ref)))+Is_ref)*((T/T_ref)^3*exp((Eg/k)*(1/T_ref-1/T)));
Iph_nsh1_13 = (Iph_ref+(Ki*(T-T_ref)))*(1-(1-(G1_13_1/G_ref)));
end

%======== Calculate the variations of the parameters of cell 1_13 with shading ========

% If the cell is shaded, calculate the variations of the parameters with shading. All parameters equations
are included here. If some parameters are required to be set fixed with shading, they should be made
equal to their values under no shading:
if Alfa1_13 > 0
Rs1_13 = (34.0109*Rs_nsh1_13*Alfa1_13^3)-
(22.9749*Rs_nsh1_13*Alfa1_13^2)+(6.6189*Rs_nsh1_13*Alfa1_13)+Rs_nsh1_13;
Rsh1_13 = (12.4389*Rsh_nsh1_13*Alfa1_13^3)-
(8.6252*Rsh_nsh1_13*Alfa1_13^2)+(3.3490*Rsh_nsh1_13*Alfa1_13)+Rsh_nsh1_13;
n1_13 = (-0.2230*n_nsh1_13*Alfa1_13^3) + (0.3643*n_nsh1_13*Alfa1_13^2)+
(0.1670*n_nsh1_13*Alfa1_13)+n_nsh1_13;
Is1_13 = (10.3994*Is_nsh1_13*Alfa1_13^2)+(0.6450*Is_nsh1_13*Alfa1_13)+Is_nsh1_13;
Iph1_13 = Iph_nsh1_13*(1-Alfa1_13);

% If the cell is not shaded, the cell parameters will be equal to the parameters under no shading:
else
Rs1_13 = Rs_nsh1_13;
```

```
Rsh1_13 =  Rsh_nsh1_13;
Iph1_13 = Iph_nsh1_13;
n1_13 =  n_nsh1_13;
Is1_13 = Is_nsh1_13;
end

%======== Cell 1_14 ========

Sh_per1_14 = 0; % Shading percentage
AT1_14 = 0.0015; % Total cell area
A1_14_2 = (AT1_14*Sh_per1_14)/100; % Shaded area
Alfa1_14 = A1_14_2/AT1_14; % Calculate shading factor
G1_14_1 = 1000; % Unshaded part irradiance
G1_14_2 = 0; % Shaded part irradiance

%======== Check if cell 1_14 is working under STC or not ========

% If the cell is working under STC, parameters under no shading (with sub-script 'nsh') will be equal to
the STC parameters:
if G1_14_1 == G_ref && T == T_ref
Iph_nsh1_14 = Iph_ref;
Rs_nsh1_14 = Rs_ref;
Rsh_nsh1_14 = Rsh_ref;
Is_nsh1_14 = Is_ref;
n_nsh1_14 = n_ref;

% If the cell is not working under STC, adapt the STC parameters to the actual irradiance and temperature
in order to determine the parameters under no shading. All parameters equations are included here. If
some parameters are required to be set fixed with irradiance and temperature, they should be made equal
to their values under STC:
else
Rs_nsh1_14 = ((34.0109*Rs_ref*(1-(G1_14_1/G_ref))^3)-(22.9749*Rs_ref*(1-
(G1_14_1/G_ref))^2)+(6.6189*Rs_ref*(1-(G1_14_1/G_ref)))+Rs_ref)*(T/T_ref);
Rsh_nsh1_14 = (12.4389*Rsh_ref*(1-(G1_14_1/G_ref))^3)-(8.6252*Rsh_ref*(1-
(G1_14_1/G_ref))^2)+(3.3490*Rsh_ref*(1-(G1_14_1/G_ref)))+Rsh_ref;
n_nsh1_14 = (-0.2230*n_ref*(1-(G1_14_1/G_ref))^3)+(0.3643*n_ref*(1-
(G1_14_1/G_ref))^2)+(0.1670*n_ref*(1-(G1_14_1/G_ref)))+n_ref;
Eg = Eg_ref*(1-0.0002677*(T-T_ref));
Is_nsh1_14 = ((10.3994*Is_ref*(1-(G1_14_1/G_ref))^2)+(0.6450*Is_ref*(1-
(G1_14_1/G_ref)))+Is_ref)*((T/T_ref)^3*exp((Eg/k)*(1/T_ref-1/T)));
Iph_nsh1_14 = (Iph_ref+(Ki*(T-T_ref)))*(1-(1-(G1_14_1/G_ref)));
end

%======== Calculate the variations of the parameters of cell 1_14 with shading ========

% If the cell is shaded, calculate the variations of the parameters with shading. All parameters equations
are included here. If some parameters are required to be set fixed with shading, they should be made
equal to their values under no shading:
if Alfa1_14 > 0
Rs1_14 = (34.0109*Rs_nsh1_14*Alfa1_14^3)-
(22.9749*Rs_nsh1_14*Alfa1_14^2)+(6.6189*Rs_nsh1_14*Alfa1_14)+Rs_nsh1_14;
Rsh1_14 = (12.4389*Rsh_nsh1_14*Alfa1_14^3)-
(8.6252*Rsh_nsh1_14*Alfa1_14^2)+(3.3490*Rsh_nsh1_14*Alfa1_14)+Rsh_nsh1_14;
n1_14 = (-0.2230*n_nsh1_14*Alfa1_14^3) + (0.3643*n_nsh1_14*Alfa1_14^2)+
(0.1670*n_nsh1_14*Alfa1_14)+n_nsh1_14;
Is1_14 = (10.3994*Is_nsh1_14*Alfa1_14^2)+(0.6450*Is_nsh1_14*Alfa1_14)+Is_nsh1_14;
Iph1_14 = Iph_nsh1_14*(1-Alfa1_14);

% If the cell is not shaded, the cell parameters will be equal to the parameters under no shading:
else
```

```
Rs1_14 = Rs_nsh1_14;
Rsh1_14 =  Rsh_nsh1_14;
Iph1_14 = Iph_nsh1_14;
n1_14 =  n_nsh1_14;
Is1_14 = Is_nsh1_14;
end

%======== Cell 1_15 ========

Sh_per1_15 = 0; % Shading percentage
AT1_15 = 0.0015; % Total cell area
A1_15_2 = (AT1_15*Sh_per1_15)/100; % Shaded area
Alfa1_15 = A1_15_2/AT1_15; % Calculate shading factor
G1_15_1 = 1000; % Unshaded part irradiance
G1_15_2 = 0; % Shaded part irradiance

%======== Check if cell 1_15 is working under STC or not ========

% If the cell is working under STC, parameters under no shading (with sub-script 'nsh') will be equal to
the STC parameters:
if G1_15_1 == G_ref && T == T_ref
Iph_nsh1_15 = Iph_ref;
Rs_nsh1_15 = Rs_ref;
Rsh_nsh1_15 = Rsh_ref;
Is_nsh1_15 = Is_ref;
n_nsh1_15 = n_ref;

% If the cell is not working under STC, adapt the STC parameters to the actual irradiance and temperature
in order to determine the parameters under no shading. All parameters equations are included here. If
some parameters are required to be set fixed with irradiance and temperature, they should be made equal
to their values under STC:
else
Rs_nsh1_15 = ((34.0109*Rs_ref*(1-(G1_15_1/G_ref))^3)-(22.9749*Rs_ref*(1-
(G1_15_1/G_ref))^2)+(6.6189*Rs_ref*(1-(G1_15_1/G_ref)))+Rs_ref)*(T/T_ref);
Rsh_nsh1_15 = (12.4389*Rsh_ref*(1-(G1_15_1/G_ref))^3)-(8.6252*Rsh_ref*(1-
(G1_15_1/G_ref))^2)+(3.3490*Rsh_ref*(1-(G1_15_1/G_ref)))+Rsh_ref;
n_nsh1_15 = (-0.2230*n_ref*(1-(G1_15_1/G_ref))^3)+(0.3643*n_ref*(1-
(G1_15_1/G_ref))^2)+(0.1670*n_ref*(1-(G1_15_1/G_ref)))+n_ref;
Eg = Eg_ref*(1-0.0002677*(T-T_ref));
Is_nsh1_15 = ((10.3994*Is_ref*(1-(G1_15_1/G_ref))^2)+(0.6450*Is_ref*(1-
(G1_15_1/G_ref)))+Is_ref)*((T/T_ref)^3*exp((Eg/k)*(1/T_ref-1/T)));
Iph_nsh1_15 = (Iph_ref+(Ki*(T-T_ref)))*(1-(1-(G1_15_1/G_ref)));
end

%======== Calculate the variations of the parameters of cell 1_15 with shading ========

% If the cell is shaded, calculate the variations of the parameters with shading. All parameters equations
are included here. If some parameters are required to be set fixed with shading, they should be made
equal to their values under no shading:
if Alfa1_15 > 0
Rs1_15 = (34.0109*Rs_nsh1_15*Alfa1_15^3)-
(22.9749*Rs_nsh1_15*Alfa1_15^2)+(6.6189*Rs_nsh1_15*Alfa1_15)+Rs_nsh1_15;
Rsh1_15 = (12.4389*Rsh_nsh1_15*Alfa1_15^3)-
(8.6252*Rsh_nsh1_15*Alfa1_15^2)+(3.3490*Rsh_nsh1_15*Alfa1_15)+Rsh_nsh1_15;
n1_15 = (-0.2230*n_nsh1_15*Alfa1_15^3) + (0.3643*n_nsh1_15*Alfa1_15^2)+
(0.1670*n_nsh1_15*Alfa1_15)+n_nsh1_15;
Is1_15 = (10.3994*Is_nsh1_15*Alfa1_15^2)+(0.6450*Is_nsh1_15*Alfa1_15)+Is_nsh1_15;
Iph1_15 = Iph_nsh1_15*(1-Alfa1_15);

% If the cell is not shaded, the cell parameters will be equal to the parameters under no shading:
```

```
else
Rs1_15 = Rs_nsh1_15;
Rsh1_15 =  Rsh_nsh1_15;
Iph1_15 = Iph_nsh1_15;
n1_15 =  n_nsh1_15;
Is1_15 = Is_nsh1_15;
end

%======== Cell 1_16 ========

Sh_per1_16 = 0; % Shading percentage
AT1_16 = 0.0015; % Total cell area
A1_16_2 = (AT1_16*Sh_per1_16)/100; % Shaded area
Alfa1_16 = A1_16_2/AT1_16; % Calculate shading factor
G1_16_1 = 1000; % Unshaded part irradiance
G1_16_2 = 0; % Shaded part irradiance

%======== Check if cell 1_16 is working under STC or not ========

% If the cell is working under STC, parameters under no shading (with sub-script 'nsh') will be equal to
the STC parameters:
if G1_16_1 == G_ref && T == T_ref
Iph_nsh1_16 = Iph_ref;
Rs_nsh1_16 = Rs_ref;
Rsh_nsh1_16 = Rsh_ref;
Is_nsh1_16 = Is_ref;
n_nsh1_16 = n_ref;

% If the cell is not working under STC, adapt the STC parameters to the actual irradiance and temperature
in order to determine the parameters under no shading. All parameters equations are included here. If
some parameters are required to be set fixed with irradiance and temperature, they should be made equal
to their values under STC:
else
Rs_nsh1_16 = ((34.0109*Rs_ref*(1-(G1_16_1/G_ref))^3)-(22.9749*Rs_ref*(1-
(G1_16_1/G_ref))^2)+(6.6189*Rs_ref*(1-(G1_16_1/G_ref)))+Rs_ref)*(T/T_ref);
Rsh_nsh1_16 = (12.4389*Rsh_ref*(1-(G1_16_1/G_ref))^3)-(8.6252*Rsh_ref*(1-
(G1_16_1/G_ref))^2)+(3.3490*Rsh_ref*(1-(G1_16_1/G_ref)))+Rsh_ref;
n_nsh1_16 = (-0.2230*n_ref*(1-(G1_16_1/G_ref))^3)+(0.3643*n_ref*(1-
(G1_16_1/G_ref))^2)+(0.1670*n_ref*(1-(G1_16_1/G_ref)))+n_ref;
Eg = Eg_ref*(1-0.0002677*(T-T_ref));
Is_nsh1_16 = ((10.3994*Is_ref*(1-(G1_16_1/G_ref))^2)+(0.6450*Is_ref*(1-
(G1_16_1/G_ref)))+Is_ref)*((T/T_ref)^3*exp((Eg/k)*(1/T_ref-1/T)));
Iph_nsh1_16 = (Iph_ref+(Ki*(T-T_ref)))*(1-(1-(G1_16_1/G_ref)));
end

%======== Calculate the variations of the parameters of cell 1_16 with shading ========

% If the cell is shaded, calculate the variations of the parameters with shading. All parameters equations
are included here. If some parameters are required to be set fixed with shading, they should be made
equal to their values under no shading:
if Alfa1_16 > 0
Rs1_16 = (34.0109*Rs_nsh1_16*Alfa1_16^3)-
(22.9749*Rs_nsh1_16*Alfa1_16^2)+(6.6189*Rs_nsh1_16*Alfa1_16)+Rs_nsh1_16;
Rsh1_16 = (12.4389*Rsh_nsh1_16*Alfa1_16^3)-
(8.6252*Rsh_nsh1_16*Alfa1_16^2)+(3.3490*Rsh_nsh1_16*Alfa1_16)+Rsh_nsh1_16;
n1_16 = (-0.2230*n_nsh1_16*Alfa1_16^3) + (0.3643*n_nsh1_16*Alfa1_16^2)+
(0.1670*n_nsh1_16*Alfa1_16)+n_nsh1_16;
Is1_16 = (10.3994*Is_nsh1_16*Alfa1_16^2)+(0.6450*Is_nsh1_16*Alfa1_16)+Is_nsh1_16;
Iph1_16 = Iph_nsh1_16*(1-Alfa1_16);
```

```
% If the cell is not shaded, the cell parameters will be equal to the parameters under no shading:
else
Rs1_16 = Rs_nsh1_16;
Rsh1_16 =  Rsh_nsh1_16;
Iph1_16 = Iph_nsh1_16;
n1_16 =  n_nsh1_16;
Is1_16 = Is_nsh1_16;
end

%======== Cell 1_17 ========

Sh_per1_17 = 0; % Shading percentage
AT1_17 = 0.0015; % Total cell area
A1_17_2 = (AT1_17*Sh_per1_17)/100; % Shaded area
Alfa1_17 = A1_17_2/AT1_17; % Calculate shading factor
G1_17_1 = 1000; % Unshaded part irradiance
G1_17_2 = 0; % Shaded part irradiance

%======== Check if cell 1_17 is working under STC or not ========

% If the cell is working under STC, parameters under no shading (with sub-script 'nsh') will be equal to
the STC parameters:
if G1_17_1 == G_ref && T == T_ref
Iph_nsh1_17 = Iph_ref;
Rs_nsh1_17 = Rs_ref;
Rsh_nsh1_17 = Rsh_ref;
Is_nsh1_17 = Is_ref;
n_nsh1_17 = n_ref;

% If the cell is not working under STC, adapt the STC parameters to the actual irradiance and temperature
in order to determine the parameters under no shading. All parameters equations are included here. If
some parameters are required to be set fixed with irradiance and temperature, they should be made equal
to their values under STC:
else
Rs_nsh1_17 = ((34.0109*Rs_ref*(1-(G1_17_1/G_ref))^3)-(22.9749*Rs_ref*(1-
(G1_17_1/G_ref))^2)+(6.6189*Rs_ref*(1-(G1_17_1/G_ref)))+Rs_ref)*(T/T_ref);
Rsh_nsh1_17 = (12.4389*Rsh_ref*(1-(G1_17_1/G_ref))^3)-(8.6252*Rsh_ref*(1-
(G1_17_1/G_ref))^2)+(3.3490*Rsh_ref*(1-(G1_17_1/G_ref)))+Rsh_ref;
n_nsh1_17 = (-0.2230*n_ref*(1-(G1_17_1/G_ref))^3)+(0.3643*n_ref*(1-
(G1_17_1/G_ref))^2)+(0.1670*n_ref*(1-(G1_17_1/G_ref)))+n_ref;
Eg = Eg_ref*(1-0.0002677*(T-T_ref));
Is_nsh1_17 = ((10.3994*Is_ref*(1-(G1_17_1/G_ref))^2)+(0.6450*Is_ref*(1-
(G1_17_1/G_ref)))+Is_ref)*((T/T_ref)^3*exp((Eg/k)*(1/T_ref-1/T)));
Iph_nsh1_17 = (Iph_ref+(Ki*(T-T_ref)))*(1-(1-(G1_17_1/G_ref)));
end

%======== Calculate the variations of the parameters of cell 1_17 with shading ========

% If the cell is shaded, calculate the variations of the parameters with shading. All parameters equations
are included here. If some parameters are required to be set fixed with shading, they should be made
equal to their values under no shading:
if Alfa1_17 > 0
Rs1_17 = (34.0109*Rs_nsh1_17*Alfa1_17^3)-
(22.9749*Rs_nsh1_17*Alfa1_17^2)+(6.6189*Rs_nsh1_17*Alfa1_17)+Rs_nsh1_17;
Rsh1_17 = (12.4389*Rsh_nsh1_17*Alfa1_17^3)-
(8.6252*Rsh_nsh1_17*Alfa1_17^2)+(3.3490*Rsh_nsh1_17*Alfa1_17)+Rsh_nsh1_17;
n1_17 = (-0.2230*n_nsh1_17*Alfa1_17^3) + (0.3643*n_nsh1_17*Alfa1_17^2)+
(0.1670*n_nsh1_17*Alfa1_17)+n_nsh1_17;
Is1_17 = (10.3994*Is_nsh1_17*Alfa1_17^2)+(0.6450*Is_nsh1_17*Alfa1_17)+Is_nsh1_17;
Iph1_17 = Iph_nsh1_17*(1-Alfa1_17);
```

```
% If the cell is not shaded, the cell parameters will be equal to the parameters under no shading:
else
Rs1_17 = Rs_nsh1_17;
Rsh1_17 =  Rsh_nsh1_17;
Iph1_17 = Iph_nsh1_17;
n1_17 =  n_nsh1_17;
Is1_17 = Is_nsh1_17;
end

%======== Cell 1_18 ========

Sh_per1_18 = 0; % Shading percentage
AT1_18 = 0.0015; % Total cell area
A1_18_2 = (AT1_18*Sh_per1_18)/100; % Shaded area
Alfa1_18 = A1_18_2/AT1_18; % Calculate shading factor
G1_18_1 = 1000; % Unshaded part irradiance
G1_18_2 = 0; % Shaded part irradiance

%======== Check if cell 1_18 is working under STC or not ========

% If the cell is working under STC, parameters under no shading (with sub-script 'nsh') will be equal to
the STC parameters:
if G1_18_1 == G_ref && T == T_ref
Iph_nsh1_18 = Iph_ref;
Rs_nsh1_18 = Rs_ref;
Rsh_nsh1_18 = Rsh_ref;
Is_nsh1_18 = Is_ref;
n_nsh1_18 = n_ref;

% If the cell is not working under STC, adapt the STC parameters to the actual irradiance and temperature
in order to determine the parameters under no shading. All parameters equations are included here. If
some parameters are required to be set fixed with irradiance and temperature, they should be made equal
to their values under STC:
else
Rs_nsh1_18 = ((34.0109*Rs_ref*(1-(G1_18_1/G_ref))^3)-(22.9749*Rs_ref*(1-
(G1_18_1/G_ref))^2)+(6.6189*Rs_ref*(1-(G1_18_1/G_ref)))+Rs_ref)*(T/T_ref);
Rsh_nsh1_18 = (12.4389*Rsh_ref*(1-(G1_18_1/G_ref))^3)-(8.6252*Rsh_ref*(1-
(G1_18_1/G_ref))^2)+(3.3490*Rsh_ref*(1-(G1_18_1/G_ref)))+Rsh_ref;
n_nsh1_18 = (-0.2230*n_ref*(1-(G1_18_1/G_ref))^3)+(0.3643*n_ref*(1-
(G1_18_1/G_ref))^2)+(0.1670*n_ref*(1-(G1_18_1/G_ref)))+n_ref;
Eg = Eg_ref*(1-0.0002677*(T-T_ref));
Is_nsh1_18 = ((10.3994*Is_ref*(1-(G1_18_1/G_ref))^2)+(0.6450*Is_ref*(1-
(G1_18_1/G_ref)))+Is_ref)*((T/T_ref)^3*exp((Eg/k)*(1/T_ref-1/T)));
Iph_nsh1_18 = (Iph_ref+(Ki*(T-T_ref)))*(1-(1-(G1_18_1/G_ref)));
end

%======== Calculate the variations of the parameters of cell 1_18 with shading ========

% If the cell is shaded, calculate the variations of the parameters with shading. All parameters equations
are included here. If some parameters are required to be set fixed with shading, they should be made
equal to their values under no shading:
if Alfa1_18 > 0
Rs1_18 = (34.0109*Rs_nsh1_18*Alfa1_18^3)-
(22.9749*Rs_nsh1_18*Alfa1_18^2)+(6.6189*Rs_nsh1_18*Alfa1_18)+Rs_nsh1_18;
Rsh1_18 = (12.4389*Rsh_nsh1_18*Alfa1_18^3)-
(8.6252*Rsh_nsh1_18*Alfa1_18^2)+(3.3490*Rsh_nsh1_18*Alfa1_18)+Rsh_nsh1_18;
n1_18 = (-0.2230*n_nsh1_18*Alfa1_18^3) + (0.3643*n_nsh1_18*Alfa1_18^2)+
(0.1670*n_nsh1_18*Alfa1_18)+n_nsh1_18;
Is1_18 = (10.3994*Is_nsh1_18*Alfa1_18^2)+(0.6450*Is_nsh1_18*Alfa1_18)+Is_nsh1_18;
```

```
Iph1_18 = Iph_nsh1_18*(1-Alfa1_18);

% If the cell is not shaded, the cell parameters will be equal to the parameters under no shading:
else
Rs1_18 = Rs_nsh1_18;
Rsh1_18 =  Rsh_nsh1_18;
Iph1_18 = Iph_nsh1_18;
n1_18 =  n_nsh1_18;
Is1_18 = Is_nsh1_18;
end

%======== Cell 2_1 ========

Sh_per2_1 = 0; % Shading percentage
AT2_1 = 0.0015; % Total cell area
A2_1_2 = (AT2_1*Sh_per2_1)/100; % Shaded area
Alfa2_1 = A2_1_2/AT2_1; % Calculate shading factor
G2_1_1 = 1000; % Unshaded part irradiance
G2_1_2 = 0; % Shaded part irradiance

%======== Check if cell 2_1 is working under STC or not ========

% If the cell is working under STC, parameters under no shading (with sub-script 'nsh') will be equal to
the STC parameters:
if G2_1_1 == G_ref && T == T_ref
Iph_nsh2_1 = Iph_ref;
Rs_nsh2_1 = Rs_ref;
Rsh_nsh2_1 = Rsh_ref;
Is_nsh2_1 = Is_ref;
n_nsh2_1 = n_ref;

% If the cell is not working under STC, adapt the STC parameters to the actual irradiance and temperature
in order to determine the parameters under no shading. All parameters equations are included here. If
some parameters are required to be set fixed with irradiance and temperature, they should be made equal
to their values under STC:
else
Rs_nsh2_1 = ((34.0109*Rs_ref*(1-(G2_1_1/G_ref))^3)-(22.9749*Rs_ref*(1-
(G2_1_1/G_ref))^2)+(6.6189*Rs_ref*(1-(G2_1_1/G_ref)))+Rs_ref)*(T/T_ref);
Rsh_nsh2_1 = (12.4389*Rsh_ref*(1-(G2_1_1/G_ref))^3)-(8.6252*Rsh_ref*(1-
(G2_1_1/G_ref))^2)+(3.3490*Rsh_ref*(1-(G2_1_1/G_ref)))+Rsh_ref;
n_nsh2_1 = (-0.2230*n_ref*(1-(G2_1_1/G_ref))^3)+(0.3643*n_ref*(1-
(G2_1_1/G_ref))^2)+(0.1670*n_ref*(1-(G2_1_1/G_ref)))+n_ref;
Eg = Eg_ref*(1-0.0002677*(T-T_ref));
Is_nsh2_1 = ((10.3994*Is_ref*(1-(G2_1_1/G_ref))^2)+(0.6450*Is_ref*(1-
(G2_1_1/G_ref)))+Is_ref)*((T/T_ref)^3*exp((Eg/k)*(1/T_ref-1/T)));
Iph_nsh2_1 = (Iph_ref+(Ki*(T-T_ref)))*(1-(1-(G2_1_1/G_ref)));
end

%======== Calculate the variations of the parameters of cell 2_1 with shading ========

% If the cell is shaded, calculate the variations of the parameters with shading. All parameters equations
are included here. If some parameters are required to be set fixed with shading, they should be made
equal to their values under no shading:
if Alfa2_1 > 0
Rs2_1 = (34.0109*Rs_nsh2_1*Alfa2_1^3)-
(22.9749*Rs_nsh2_1*Alfa2_1^2)+(6.6189*Rs_nsh2_1*Alfa2_1)+Rs_nsh2_1;
Rsh2_1 = (12.4389*Rsh_nsh2_1*Alfa2_1^3)-
(8.6252*Rsh_nsh2_1*Alfa2_1^2)+(3.3490*Rsh_nsh2_1*Alfa2_1)+Rsh_nsh2_1;
n2_1 = (-0.2230*n_nsh2_1*Alfa2_1^3) + (0.3643*n_nsh2_1*Alfa2_1^2)+
(0.1670*n_nsh2_1*Alfa2_1)+n_nsh2_1;
```

```
Is2_1 = (10.3994*Is_nsh2_1*Alfa2_1^2)+(0.6450*Is_nsh2_1*Alfa2_1)+Is_nsh2_1;
Iph2_1 = Iph_nsh2_1*(1-Alfa2_1);

% If the cell is not shaded, the cell parameters will be equal to the parameters under no shading:
else
Rs2_1 = Rs_nsh2_1;
Rsh2_1 =  Rsh_nsh2_1;
Iph2_1 = Iph_nsh2_1;
n2_1 =  n_nsh2_1;
Is2_1 = Is_nsh2_1;
end

%======== Cell 2_2 ========

Sh_per2_2 = 0; % Shading percentage
AT2_2 = 0.0015; % Total cell area
A2_2_2 = (AT2_2*Sh_per2_2)/100; % Shaded area
Alfa2_2 = A2_2_2/AT2_2; % Calculate shading factor
G2_2_1 = 1000; % Unshaded part irradiance
G2_2_2 = 0; % Shaded part irradiance

%======== Check if cell 2_2 is working under STC or not ========

% If the cell is working under STC, parameters under no shading (with sub-script 'nsh') will be equal to
the STC parameters:
if G2_2_1 == G_ref && T == T_ref
Iph_nsh2_2 = Iph_ref;
Rs_nsh2_2 = Rs_ref;
Rsh_nsh2_2 = Rsh_ref;
Is_nsh2_2 = Is_ref;
n_nsh2_2 = n_ref;

% If the cell is not working under STC, adapt the STC parameters to the actual irradiance and temperature
in order to determine the parameters under no shading. All parameters equations are included here. If
some parameters are required to be set fixed with irradiance and temperature, they should be made equal
to their values under STC:
else
Rs_nsh2_2 = ((34.0109*Rs_ref*(1-(G2_2_1/G_ref))^3)-(22.9749*Rs_ref*(1-
(G2_2_1/G_ref))^2)+(6.6189*Rs_ref*(1-(G2_2_1/G_ref)))+Rs_ref)*(T/T_ref);
Rsh_nsh2_2 = (12.4389*Rsh_ref*(1-(G2_2_1/G_ref))^3)-(8.6252*Rsh_ref*(1-
(G2_2_1/G_ref))^2)+(3.3490*Rsh_ref*(1-(G2_2_1/G_ref)))+Rsh_ref;
n_nsh2_2 = (-0.2230*n_ref*(1-(G2_2_1/G_ref))^3)+(0.3643*n_ref*(1-
(G2_2_1/G_ref))^2)+(0.1670*n_ref*(1-(G2_2_1/G_ref)))+n_ref;
Eg = Eg_ref*(1-0.0002677*(T-T_ref));
Is_nsh2_2 = ((10.3994*Is_ref*(1-(G2_2_1/G_ref))^2)+(0.6450*Is_ref*(1-
(G2_2_1/G_ref)))+Is_ref)*((T/T_ref)^3*exp((Eg/k)*(1/T_ref-1/T)));
Iph_nsh2_2 = (Iph_ref+(Ki*(T-T_ref)))*(1-(1-(G2_2_1/G_ref)));
end

%======== Calculate the variations of the parameters of cell 2_2 with shading ========

% If the cell is shaded, calculate the variations of the parameters with shading. All parameters equations
are included here. If some parameters are required to be set fixed with shading, they should be made
equal to their values under no shading:
if Alfa2_2 > 0
Rs2_2 = (34.0109*Rs_nsh2_2*Alfa2_2^3)-
(22.9749*Rs_nsh2_2*Alfa2_2^2)+(6.6189*Rs_nsh2_2*Alfa2_2)+Rs_nsh2_2;
Rsh2_2 = (12.4389*Rsh_nsh2_2*Alfa2_2^3)-
(8.6252*Rsh_nsh2_2*Alfa2_2^2)+(3.3490*Rsh_nsh2_2*Alfa2_2)+Rsh_nsh2_2;
```

```
n2_2 = (-0.2230*n_nsh2_2*Alfa2_2^3) + (0.3643*n_nsh2_2*Alfa2_2^2)+
(0.1670*n_nsh2_2*Alfa2_2)+n_nsh2_2;
Is2_2 = (10.3994*Is_nsh2_2*Alfa2_2^2)+(0.6450*Is_nsh2_2*Alfa2_2)+Is_nsh2_2;
Iph2_2 = Iph_nsh2_2*(1-Alfa2_2);

% If the cell is not shaded, the cell parameters will be equal to the parameters under no shading:
else
Rs2_2 = Rs_nsh2_2;
Rsh2_2 =  Rsh_nsh2_2;
Iph2_2 = Iph_nsh2_2;
n2_2 =  n_nsh2_2;
Is2_2 = Is_nsh2_2;
end

%======== Cell 2_3 ========

Sh_per2_3 = 0; % Shading percentage
AT2_3 = 0.0015; % Total cell area
A2_3_2 = (AT2_3*Sh_per2_3)/100; % Shaded area
Alfa2_3 = A2_3_2/AT2_3; % Calculate shading factor
G2_3_1 = 1000; % Unshaded part irradiance
G2_3_2 = 0; % Shaded part irradiance

%======== Check if cell 2_3 is working under STC or not ========

% If the cell is working under STC, parameters under no shading (with sub-script 'nsh') will be equal to
the STC parameters:
if G2_3_1 == G_ref && T == T_ref
Iph_nsh2_3 = Iph_ref;
Rs_nsh2_3 = Rs_ref;
Rsh_nsh2_3 = Rsh_ref;
Is_nsh2_3 = Is_ref;
n_nsh2_3 = n_ref;

% If the cell is not working under STC, adapt the STC parameters to the actual irradiance and temperature
in order to determine the parameters under no shading. All parameters equations are included here. If
some parameters are required to be set fixed with irradiance and temperature, they should be made equal
to their values under STC:
else
Rs_nsh2_3 = ((34.0109*Rs_ref*(1-(G2_3_1/G_ref))^3)-(22.9749*Rs_ref*(1-
(G2_3_1/G_ref))^2)+(6.6189*Rs_ref*(1-(G2_3_1/G_ref)))+Rs_ref)*(T/T_ref);
Rsh_nsh2_3 = (12.4389*Rsh_ref*(1-(G2_3_1/G_ref))^3)-(8.6252*Rsh_ref*(1-
(G2_3_1/G_ref))^2)+(3.3490*Rsh_ref*(1-(G2_3_1/G_ref)))+Rsh_ref;
n_nsh2_3 = (-0.2230*n_ref*(1-(G2_3_1/G_ref))^3)+(0.3643*n_ref*(1-
(G2_3_1/G_ref))^2)+(0.1670*n_ref*(1-(G2_3_1/G_ref)))+n_ref;
Eg = Eg_ref*(1-0.0002677*(T-T_ref));
Is_nsh2_3 = ((10.3994*Is_ref*(1-(G2_3_1/G_ref))^2)+(0.6450*Is_ref*(1-
(G2_3_1/G_ref)))+Is_ref)*((T/T_ref)^3*exp((Eg/k)*(1/T_ref-1/T)));
Iph_nsh2_3 = (Iph_ref+(Ki*(T-T_ref)))*(1-(1-(G2_3_1/G_ref)));
end

%======== Calculate the variations of the parameters of cell 2_3 with shading ========

% If the cell is shaded, calculate the variations of the parameters with shading. All parameters equations
are included here. If some parameters are required to be set fixed with shading, they should be made
equal to their values under no shading:
if Alfa2_3 > 0
Rs2_3 = (34.0109*Rs_nsh2_3*Alfa2_3^3)-
(22.9749*Rs_nsh2_3*Alfa2_3^2)+(6.6189*Rs_nsh2_3*Alfa2_3)+Rs_nsh2_3;
```

```
Rsh2_3 = (12.4389*Rsh_nsh2_3*Alfa2_3^3)-
(8.6252*Rsh_nsh2_3*Alfa2_3^2)+(3.3490*Rsh_nsh2_3*Alfa2_3)+Rsh_nsh2_3;
n2_3 = (-0.2230*n_nsh2_3*Alfa2_3^3) + (0.3643*n_nsh2_3*Alfa2_3^2)+
(0.1670*n_nsh2_3*Alfa2_3)+n_nsh2_3;
Is2_3 = (10.3994*Is_nsh2_3*Alfa2_3^2)+(0.6450*Is_nsh2_3*Alfa2_3)+Is_nsh2_3;
Iph2_3 = Iph_nsh2_3*(1-Alfa2_3);

% If the cell is not shaded, the cell parameters will be equal to the parameters under no shading:
else
Rs2_3 = Rs_nsh2_3;
Rsh2_3 =  Rsh_nsh2_3;
Iph2_3 = Iph_nsh2_3;
n2_3 =  n_nsh2_3;
Is2_3 = Is_nsh2_3;
end

%======== Cell 2_4 ========

Sh_per2_4 = 0; % Shading percentage
AT2_4 = 0.0015; % Total cell area
A2_4_2 = (AT2_4*Sh_per2_4)/100; % Shaded area
Alfa2_4 = A2_4_2/AT2_4; % Calculate shading factor
G2_4_1 = 1000; % Unshaded part irradiance
G2_4_2 = 0; % Shaded part irradiance

%======== Check if cell 2_4 is working under STC or not ========

% If the cell is working under STC, parameters under no shading (with sub-script 'nsh') will be equal to
the STC parameters:
if G2_4_1 == G_ref && T == T_ref
Iph_nsh2_4 = Iph_ref;
Rs_nsh2_4 = Rs_ref;
Rsh_nsh2_4 = Rsh_ref;
Is_nsh2_4 = Is_ref;
n_nsh2_4 = n_ref;

% If the cell is not working under STC, adapt the STC parameters to the actual irradiance and temperature
in order to determine the parameters under no shading. All parameters equations are included here. If
some parameters are required to be set fixed with irradiance and temperature, they should be made equal
to their values under STC:
else
Rs_nsh2_4 = ((34.0109*Rs_ref*(1-(G2_4_1/G_ref))^3)-(22.9749*Rs_ref*(1-
(G2_4_1/G_ref))^2)+(6.6189*Rs_ref*(1-(G2_4_1/G_ref)))+Rs_ref)*(T/T_ref);
Rsh_nsh2_4 = (12.4389*Rsh_ref*(1-(G2_4_1/G_ref))^3)-(8.6252*Rsh_ref*(1-
(G2_4_1/G_ref))^2)+(3.3490*Rsh_ref*(1-(G2_4_1/G_ref)))+Rsh_ref;
n_nsh2_4 = (-0.2230*n_ref*(1-(G2_4_1/G_ref))^3)+(0.3643*n_ref*(1-
(G2_4_1/G_ref))^2)+(0.1670*n_ref*(1-(G2_4_1/G_ref)))+n_ref;
Eg = Eg_ref*(1-0.0002677*(T-T_ref));
Is_nsh2_4 = ((10.3994*Is_ref*(1-(G2_4_1/G_ref))^2)+(0.6450*Is_ref*(1-
(G2_4_1/G_ref)))+Is_ref)*((T/T_ref)^3*exp((Eg/k)*(1/T_ref-1/T)));
Iph_nsh2_4 = (Iph_ref+(Ki*(T-T_ref)))*(1-(1-(G2_4_1/G_ref)));
end

%======== Calculate the variations of the parameters of cell 2_4 with shading ========

% If the cell is shaded, calculate the variations of the parameters with shading. All parameters equations
are included here. If some parameters are required to be set fixed with shading, they should be made
equal to their values under no shading:
if Alfa2_4 > 0
```

```
Rs2_4 = (34.0109*Rs_nsh2_4*Alfa2_4^3)-
(22.9749*Rs_nsh2_4*Alfa2_4^2)+(6.6189*Rs_nsh2_4*Alfa2_4)+Rs_nsh2_4;
Rsh2_4 = (12.4389*Rsh_nsh2_4*Alfa2_4^3)-
(8.6252*Rsh_nsh2_4*Alfa2_4^2)+(3.3490*Rsh_nsh2_4*Alfa2_4)+Rsh_nsh2_4;
n2_4 = (-0.2230*n_nsh2_4*Alfa2_4^3) + (0.3643*n_nsh2_4*Alfa2_4^2)+
(0.1670*n_nsh2_4*Alfa2_4)+n_nsh2_4;
Is2_4 = (10.3994*Is_nsh2_4*Alfa2_4^2)+(0.6450*Is_nsh2_4*Alfa2_4)+Is_nsh2_4;
Iph2_4 = Iph_nsh2_4*(1-Alfa2_4);

% If the cell is not shaded, the cell parameters will be equal to the parameters under no shading:
else
Rs2_4 = Rs_nsh2_4;
Rsh2_4 =  Rsh_nsh2_4;
Iph2_4 = Iph_nsh2_4;
n2_4 =  n_nsh2_4;
Is2_4 = Is_nsh2_4;
end

%======== Cell 2_5 ========

Sh_per2_5 = 0; % Shading percentage
AT2_5 = 0.0015; % Total cell area
A2_5_2 = (AT2_5*Sh_per2_5)/100; % Shaded area
Alfa2_5 = A2_5_2/AT2_5; % Calculate shading factor
G2_5_1 = 1000; % Unshaded part irradiance
G2_5_2 = 0; % Shaded part irradiance

%======== Check if cell 2_5 is working under STC or not ========

% If the cell is working under STC, parameters under no shading (with sub-script 'nsh') will be equal to
the STC parameters:
if G2_5_1 == G_ref && T == T_ref
Iph_nsh2_5 = Iph_ref;
Rs_nsh2_5 = Rs_ref;
Rsh_nsh2_5 = Rsh_ref;
Is_nsh2_5 = Is_ref;
n_nsh2_5 = n_ref;

% If the cell is not working under STC, adapt the STC parameters to the actual irradiance and temperature
in order to determine the parameters under no shading. All parameters equations are included here. If
some parameters are required to be set fixed with irradiance and temperature, they should be made equal
to their values under STC:
else
Rs_nsh2_5 = ((34.0109*Rs_ref*(1-(G2_5_1/G_ref))^3)-(22.9749*Rs_ref*(1-
(G2_5_1/G_ref))^2)+(6.6189*Rs_ref*(1-(G2_5_1/G_ref)))+Rs_ref)*(T/T_ref);
Rsh_nsh2_5 = (12.4389*Rsh_ref*(1-(G2_5_1/G_ref))^3)-(8.6252*Rsh_ref*(1-
(G2_5_1/G_ref))^2)+(3.3490*Rsh_ref*(1-(G2_5_1/G_ref)))+Rsh_ref;
n_nsh2_5 = (-0.2230*n_ref*(1-(G2_5_1/G_ref))^3)+(0.3643*n_ref*(1-
(G2_5_1/G_ref))^2)+(0.1670*n_ref*(1-(G2_5_1/G_ref)))+n_ref;
Eg = Eg_ref*(1-0.0002677*(T-T_ref));
Is_nsh2_5 = ((10.3994*Is_ref*(1-(G2_5_1/G_ref))^2)+(0.6450*Is_ref*(1-
(G2_5_1/G_ref)))+Is_ref)*((T/T_ref)^3*exp((Eg/k)*(1/T_ref-1/T)));
Iph_nsh2_5 = (Iph_ref+(Ki*(T-T_ref)))*(1-(1-(G2_5_1/G_ref)));
end

%======== Calculate the variations of the parameters of cell 2_5 with shading ========

% If the cell is shaded, calculate the variations of the parameters with shading. All parameters equations
are included here. If some parameters are required to be set fixed with shading, they should be made
equal to their values under no shading:
```

```
if Alfa2_5 > 0
Rs2_5 = (34.0109*Rs_nsh2_5*Alfa2_5^3)-
(22.9749*Rs_nsh2_5*Alfa2_5^2)+(6.6189*Rs_nsh2_5*Alfa2_5)+Rs_nsh2_5;
Rsh2_5 = (12.4389*Rsh_nsh2_5*Alfa2_5^3)-
(8.6252*Rsh_nsh2_5*Alfa2_5^2)+(3.3490*Rsh_nsh2_5*Alfa2_5)+Rsh_nsh2_5;
n2_5 = (-0.2230*n_nsh2_5*Alfa2_5^3) + (0.3643*n_nsh2_5*Alfa2_5^2)+
(0.1670*n_nsh2_5*Alfa2_5)+n_nsh2_5;
Is2_5 = (10.3994*Is_nsh2_5*Alfa2_5^2)+(0.6450*Is_nsh2_5*Alfa2_5)+Is_nsh2_5;
Iph2_5 = Iph_nsh2_5*(1-Alfa2_5);

% If the cell is not shaded, the cell parameters will be equal to the parameters under no shading:
else
Rs2_5 = Rs_nsh2_5;
Rsh2_5 =  Rsh_nsh2_5;
Iph2_5 = Iph_nsh2_5;
n2_5 =  n_nsh2_5;
Is2_5 = Is_nsh2_5;
end

%======== Cell 2_6 ========

Sh_per2_6 = 0; % Shading percentage
AT2_6 = 0.0015; % Total cell area
A2_6_2 = (AT2_6*Sh_per2_6)/100; % Shaded area
Alfa2_6 = A2_6_2/AT2_6; % Calculate shading factor
G2_6_1 = 1000; % Unshaded part irradiance
G2_6_2 = 0; % Shaded part irradiance

%======== Check if cell 2_6 is working under STC or not ========

% If the cell is working under STC, parameters under no shading (with sub-script 'nsh') will be equal to
the STC parameters:
if G2_6_1 == G_ref && T == T_ref
Iph_nsh2_6 = Iph_ref;
Rs_nsh2_6 = Rs_ref;
Rsh_nsh2_6 = Rsh_ref;
Is_nsh2_6 = Is_ref;
n_nsh2_6 = n_ref;

% If the cell is not working under STC, adapt the STC parameters to the actual irradiance and temperature
in order to determine the parameters under no shading. All parameters equations are included here. If
some parameters are required to be set fixed with irradiance and temperature, they should be made equal
to their values under STC:
else
Rs_nsh2_6 = ((34.0109*Rs_ref*(1-(G2_6_1/G_ref))^3)-(22.9749*Rs_ref*(1-
(G2_6_1/G_ref))^2)+(6.6189*Rs_ref*(1-(G2_6_1/G_ref)))+Rs_ref)*(T/T_ref);
Rsh_nsh2_6 = (12.4389*Rsh_ref*(1-(G2_6_1/G_ref))^3)-(8.6252*Rsh_ref*(1-
(G2_6_1/G_ref))^2)+(3.3490*Rsh_ref*(1-(G2_6_1/G_ref)))+Rsh_ref;
n_nsh2_6 = (-0.2230*n_ref*(1-(G2_6_1/G_ref))^3)+(0.3643*n_ref*(1-
(G2_6_1/G_ref))^2)+(0.1670*n_ref*(1-(G2_6_1/G_ref)))+n_ref;
Eg = Eg_ref*(1-0.0002677*(T-T_ref));
Is_nsh2_6 = ((10.3994*Is_ref*(1-(G2_6_1/G_ref))^2)+(0.6450*Is_ref*(1-
(G2_6_1/G_ref)))+Is_ref)*((T/T_ref)^3*exp((Eg/k)*(1/T_ref-1/T)));
Iph_nsh2_6 = (Iph_ref+(Ki*(T-T_ref)))*(1-(1-(G2_6_1/G_ref)));
end

%======== Calculate the variations of the parameters of cell 2_6 with shading ========
```

```
% If the cell is shaded, calculate the variations of the parameters with shading. All parameters equations
are included here. If some parameters are required to be set fixed with shading, they should be made
equal to their values under no shading:
if Alfa2_6 > 0
Rs2_6 = (34.0109*Rs_nsh2_6*Alfa2_6^3)-
(22.9749*Rs_nsh2_6*Alfa2_6^2)+(6.6189*Rs_nsh2_6*Alfa2_6)+Rs_nsh2_6;
Rsh2_6 = (12.4389*Rsh_nsh2_6*Alfa2_6^3)-
(8.6252*Rsh_nsh2_6*Alfa2_6^2)+(3.3490*Rsh_nsh2_6*Alfa2_6)+Rsh_nsh2_6;
n2_6 = (-0.2230*n_nsh2_6*Alfa2_6^3) + (0.3643*n_nsh2_6*Alfa2_6^2)+
(0.1670*n_nsh2_6*Alfa2_6)+n_nsh2_6;
Is2_6 = (10.3994*Is_nsh2_6*Alfa2_6^2)+(0.6450*Is_nsh2_6*Alfa2_6)+Is_nsh2_6;
Iph2_6 = Iph_nsh2_6*(1-Alfa2_6);

% If the cell is not shaded, the cell parameters will be equal to the parameters under no shading:
else
Rs2_6 = Rs_nsh2_6;
Rsh2_6 =  Rsh_nsh2_6;
Iph2_6 = Iph_nsh2_6;
n2_6 =  n_nsh2_6;
Is2_6 = Is_nsh2_6;
end

%======== Cell 2_7 ========

Sh_per2_7 = 0; % Shading percentage
AT2_7 = 0.0015; % Total cell area
A2_7_2 = (AT2_7*Sh_per2_7)/100; % Shaded area
Alfa2_7 = A2_7_2/AT2_7; % Calculate shading factor
G2_7_1 = 1000; % Unshaded part irradiance
G2_7_2 = 0; % Shaded part irradiance

%======== Check if cell 2_7 is working under STC or not ========

% If the cell is working under STC, parameters under no shading (with sub-script 'nsh') will be equal to
the STC parameters:
if G2_7_1 == G_ref && T == T_ref
Iph_nsh2_7 = Iph_ref;
Rs_nsh2_7 = Rs_ref;
Rsh_nsh2_7 = Rsh_ref;
Is_nsh2_7 = Is_ref;
n_nsh2_7 = n_ref;

% If the cell is not working under STC, adapt the STC parameters to the actual irradiance and temperature
in order to determine the parameters under no shading. All parameters equations are included here. If
some parameters are required to be set fixed with irradiance and temperature, they should be made equal
to their values under STC:
else
Rs_nsh2_7 = ((34.0109*Rs_ref*(1-(G2_7_1/G_ref))^3)-(22.9749*Rs_ref*(1-
(G2_7_1/G_ref))^2)+(6.6189*Rs_ref*(1-(G2_7_1/G_ref)))+Rs_ref)*(T/T_ref);
Rsh_nsh2_7 = (12.4389*Rsh_ref*(1-(G2_7_1/G_ref))^3)-(8.6252*Rsh_ref*(1-
(G2_7_1/G_ref))^2)+(3.3490*Rsh_ref*(1-(G2_7_1/G_ref)))+Rsh_ref;
n_nsh2_7 = (-0.2230*n_ref*(1-(G2_7_1/G_ref))^3)+(0.3643*n_ref*(1-
(G2_7_1/G_ref))^2)+(0.1670*n_ref*(1-(G2_7_1/G_ref)))+n_ref;
Eg = Eg_ref*(1-0.0002677*(T-T_ref));
Is_nsh2_7 = ((10.3994*Is_ref*(1-(G2_7_1/G_ref))^2)+(0.6450*Is_ref*(1-
(G2_7_1/G_ref)))+Is_ref)*((T/T_ref)^3*exp((Eg/k)*(1/T_ref-1/T)));
Iph_nsh2_7 = (Iph_ref+(Ki*(T-T_ref)))*(1-(1-(G2_7_1/G_ref)));
end

%======== Calculate the variations of the parameters of cell 2_7 with shading ========
```

```
% If the cell is shaded, calculate the variations of the parameters with shading. All parameters equations
are included here. If some parameters are required to be set fixed with shading, they should be made
equal to their values under no shading:
if Alfa2_7 > 0
Rs2_7 = (34.0109*Rs_nsh2_7*Alfa2_7^3)-
(22.9749*Rs_nsh2_7*Alfa2_7^2)+(6.6189*Rs_nsh2_7*Alfa2_7)+Rs_nsh2_7;
Rsh2_7 = (12.4389*Rsh_nsh2_7*Alfa2_7^3)-
(8.6252*Rsh_nsh2_7*Alfa2_7^2)+(3.3490*Rsh_nsh2_7*Alfa2_7)+Rsh_nsh2_7;
n2_7 = (-0.2230*n_nsh2_7*Alfa2_7^3) + (0.3643*n_nsh2_7*Alfa2_7^2)+
(0.1670*n_nsh2_7*Alfa2_7)+n_nsh2_7;
Is2_7 = (10.3994*Is_nsh2_7*Alfa2_7^2)+(0.6450*Is_nsh2_7*Alfa2_7)+Is_nsh2_7;
Iph2_7 = Iph_nsh2_7*(1-Alfa2_7);

% If the cell is not shaded, the cell parameters will be equal to the parameters under no shading:
else
Rs2_7 = Rs_nsh2_7;
Rsh2_7 =  Rsh_nsh2_7;
Iph2_7 = Iph_nsh2_7;
n2_7 =  n_nsh2_7;
Is2_7 = Is_nsh2_7;
end

%======== Cell 2_8 ========

Sh_per2_8 = 0; % Shading percentage
AT2_8 = 0.0015; % Total cell area
A2_8_2 = (AT2_8*Sh_per2_8)/100; % Shaded area
Alfa2_8 = A2_8_2/AT2_8; % Calculate shading factor
G2_8_1 = 1000; % Unshaded part irradiance
G2_8_2 = 0; % Shaded part irradiance

%======== Check if cell 2_8 is working under STC or not ========

% If the cell is working under STC, parameters under no shading (with sub-script 'nsh') will be equal to
the STC parameters:
if G2_8_1 == G_ref && T == T_ref
Iph_nsh2_8 = Iph_ref;
Rs_nsh2_8 = Rs_ref;
Rsh_nsh2_8 = Rsh_ref;
Is_nsh2_8 = Is_ref;
n_nsh2_8 = n_ref;

% If the cell is not working under STC, adapt the STC parameters to the actual irradiance and temperature
in order to determine the parameters under no shading. All parameters equations are included here. If
some parameters are required to be set fixed with irradiance and temperature, they should be made equal
to their values under STC:
else
Rs_nsh2_8 = ((34.0109*Rs_ref*(1-(G2_8_1/G_ref))^3)-(22.9749*Rs_ref*(1-
(G2_8_1/G_ref))^2)+(6.6189*Rs_ref*(1-(G2_8_1/G_ref)))+Rs_ref)*(T/T_ref);
Rsh_nsh2_8 = (12.4389*Rsh_ref*(1-(G2_8_1/G_ref))^3)-(8.6252*Rsh_ref*(1-
(G2_8_1/G_ref))^2)+(3.3490*Rsh_ref*(1-(G2_8_1/G_ref)))+Rsh_ref;
n_nsh2_8 = (-0.2230*n_ref*(1-(G2_8_1/G_ref))^3)+(0.3643*n_ref*(1-
(G2_8_1/G_ref))^2)+(0.1670*n_ref*(1-(G2_8_1/G_ref)))+n_ref;
Eg = Eg_ref*(1-0.0002677*(T-T_ref));
Is_nsh2_8 = ((10.3994*Is_ref*(1-(G2_8_1/G_ref))^2)+(0.6450*Is_ref*(1-
(G2_8_1/G_ref)))+Is_ref)*((T/T_ref)^3*exp((Eg/k)*(1/T_ref-1/T)));
Iph_nsh2_8 = (Iph_ref+(Ki*(T-T_ref)))*(1-(1-(G2_8_1/G_ref)));
end
```

```
%======== Calculate the variations of the parameters of cell 2_8 with shading ========

% If the cell is shaded, calculate the variations of the parameters with shading. All parameters equations
are included here. If some parameters are required to be set fixed with shading, they should be made
equal to their values under no shading:
if Alfa2_8 > 0
Rs2_8 = (34.0109*Rs_nsh2_8*Alfa2_8^3)-
(22.9749*Rs_nsh2_8*Alfa2_8^2)+(6.6189*Rs_nsh2_8*Alfa2_8)+Rs_nsh2_8;
Rsh2_8 = (12.4389*Rsh_nsh2_8*Alfa2_8^3)-
(8.6252*Rsh_nsh2_8*Alfa2_8^2)+(3.3490*Rsh_nsh2_8*Alfa2_8)+Rsh_nsh2_8;
n2_8 = (-0.2230*n_nsh2_8*Alfa2_8^3) + (0.3643*n_nsh2_8*Alfa2_8^2)+
(0.1670*n_nsh2_8*Alfa2_8)+n_nsh2_8;
Is2_8 = (10.3994*Is_nsh2_8*Alfa2_8^2)+(0.6450*Is_nsh2_8*Alfa2_8)+Is_nsh2_8;
Iph2_8 = Iph_nsh2_8*(1-Alfa2_8);

% If the cell is not shaded, the cell parameters will be equal to the parameters under no shading:
else
Rs2_8 = Rs_nsh2_8;
Rsh2_8 =  Rsh_nsh2_8;
Iph2_8 = Iph_nsh2_8;
n2_8 =  n_nsh2_8;
Is2_8 = Is_nsh2_8;
end

%======== Cell 2_9 ========

Sh_per2_9 = 0; % Shading percentage
AT2_9 = 0.0015; % Total cell area
A2_9_2 = (AT2_9*Sh_per2_9)/100; % Shaded area
Alfa2_9 = A2_9_2/AT2_9; % Calculate shading factor
G2_9_1 = 1000; % Unshaded part irradiance
G2_9_2 = 0; % Shaded part irradiance

%======== Check if cell 2_9 is working under STC or not ========

% If the cell is working under STC, parameters under no shading (with sub-script 'nsh') will be equal to
the STC parameters:
if G2_9_1 == G_ref && T == T_ref
Iph_nsh2_9 = Iph_ref;
Rs_nsh2_9 = Rs_ref;
Rsh_nsh2_9 = Rsh_ref;
Is_nsh2_9 = Is_ref;
n_nsh2_9 = n_ref;

% If the cell is not working under STC, adapt the STC parameters to the actual irradiance and temperature
in order to determine the parameters under no shading. All parameters equations are included here. If
some parameters are required to be set fixed with irradiance and temperature, they should be made equal
to their values under STC:
else
Rs_nsh2_9 = ((34.0109*Rs_ref*(1-(G2_9_1/G_ref))^3)-(22.9749*Rs_ref*(1-
(G2_9_1/G_ref))^2)+(6.6189*Rs_ref*(1-(G2_9_1/G_ref)))+Rs_ref)*(T/T_ref);
Rsh_nsh2_9 = (12.4389*Rsh_ref*(1-(G2_9_1/G_ref))^3)-(8.6252*Rsh_ref*(1-
(G2_9_1/G_ref))^2)+(3.3490*Rsh_ref*(1-(G2_9_1/G_ref)))+Rsh_ref;
n_nsh2_9 = (-0.2230*n_ref*(1-(G2_9_1/G_ref))^3)+(0.3643*n_ref*(1-
(G2_9_1/G_ref))^2)+(0.1670*n_ref*(1-(G2_9_1/G_ref)))+n_ref;
Eg = Eg_ref*(1-0.0002677*(T-T_ref));
Is_nsh2_9 = ((10.3994*Is_ref*(1-(G2_9_1/G_ref))^2)+(0.6450*Is_ref*(1-
(G2_9_1/G_ref)))+Is_ref)*((T/T_ref)^3*exp((Eg/k)*(1/T_ref-1/T)));
Iph_nsh2_9 = (Iph_ref+(Ki*(T-T_ref)))*(1-(1-(G2_9_1/G_ref)));
end
```

```
%======== Calculate the variations of the parameters of cell 2_9 with shading ========

% If the cell is shaded, calculate the variations of the parameters with shading. All parameters equations
are included here. If some parameters are required to be set fixed with shading, they should be made
equal to their values under no shading:
if Alfa2_9 > 0
Rs2_9 = (34.0109*Rs_nsh2_9*Alfa2_9^3)-
(22.9749*Rs_nsh2_9*Alfa2_9^2)+(6.6189*Rs_nsh2_9*Alfa2_9)+Rs_nsh2_9;
Rsh2_9 = (12.4389*Rsh_nsh2_9*Alfa2_9^3)-
(8.6252*Rsh_nsh2_9*Alfa2_9^2)+(3.3490*Rsh_nsh2_9*Alfa2_9)+Rsh_nsh2_9;
n2_9 = (-0.2230*n_nsh2_9*Alfa2_9^3) + (0.3643*n_nsh2_9*Alfa2_9^2)+
(0.1670*n_nsh2_9*Alfa2_9)+n_nsh2_9;
Is2_9 = (10.3994*Is_nsh2_9*Alfa2_9^2)+(0.6450*Is_nsh2_9*Alfa2_9)+Is_nsh2_9;
Iph2_9 = Iph_nsh2_9*(1-Alfa2_9);

% If the cell is not shaded, the cell parameters will be equal to the parameters under no shading:
else
Rs2_9 = Rs_nsh2_9;
Rsh2_9 =  Rsh_nsh2_9;
Iph2_9 = Iph_nsh2_9;
n2_9 =  n_nsh2_9;
Is2_9 = Is_nsh2_9;
end

%======== Cell 2_10 ========

Sh_per2_10 = 0; % Shading percentage
AT2_10 = 0.0015; % Total cell area
A2_10_2 = (AT2_10*Sh_per2_10)/100; % Shaded area
Alfa2_10 = A2_10_2/AT2_10; % Calculate shading factor
G2_10_1 = 1000; % Unshaded part irradiance
G2_10_2 = 0; % Shaded part irradiance

%======== Check if cell 2_10 is working under STC or not ========

% If the cell is working under STC, parameters under no shading (with sub-script 'nsh') will be equal to
the STC parameters:
if G2_10_1 == G_ref && T == T_ref
Iph_nsh2_10 = Iph_ref;
Rs_nsh2_10 = Rs_ref;
Rsh_nsh2_10 = Rsh_ref;
Is_nsh2_10 = Is_ref;
n_nsh2_10 = n_ref;

% If the cell is not working under STC, adapt the STC parameters to the actual irradiance and temperature
in order to determine the parameters under no shading. All parameters equations are included here. If
some parameters are required to be set fixed with irradiance and temperature, they should be made equal
to their values under STC:
else
Rs_nsh2_10 = ((34.0109*Rs_ref*(1-(G2_10_1/G_ref))^3)-(22.9749*Rs_ref*(1-
(G2_10_1/G_ref))^2)+(6.6189*Rs_ref*(1-(G2_10_1/G_ref)))+Rs_ref)*(T/T_ref);
Rsh_nsh2_10 = (12.4389*Rsh_ref*(1-(G2_10_1/G_ref))^3)-(8.6252*Rsh_ref*(1-
(G2_10_1/G_ref))^2)+(3.3490*Rsh_ref*(1-(G2_10_1/G_ref)))+Rsh_ref;
n_nsh2_10 = (-0.2230*n_ref*(1-(G2_10_1/G_ref))^3)+(0.3643*n_ref*(1-
(G2_10_1/G_ref))^2)+(0.1670*n_ref*(1-(G2_10_1/G_ref)))+n_ref;
Eg = Eg_ref*(1-0.0002677*(T-T_ref));
Is_nsh2_10 = ((10.3994*Is_ref*(1-(G2_10_1/G_ref))^2)+(0.6450*Is_ref*(1-
(G2_10_1/G_ref)))+Is_ref)*((T/T_ref)^3*exp((Eg/k)*(1/T_ref-1/T)));
Iph_nsh2_10 = (Iph_ref+(Ki*(T-T_ref)))*(1-(1-(G2_10_1/G_ref)));
```

```
end

%======== Calculate the variations of the parameters of cell 2_10 with shading ========

% If the cell is shaded, calculate the variations of the parameters with shading. All parameters equations
are included here. If some parameters are required to be set fixed with shading, they should be made
equal to their values under no shading:
if Alfa2_10 > 0
Rs2_10 = (34.0109*Rs_nsh2_10*Alfa2_10^3)-
(22.9749*Rs_nsh2_10*Alfa2_10^2)+(6.6189*Rs_nsh2_10*Alfa2_10)+Rs_nsh2_10;
Rsh2_10 = (12.4389*Rsh_nsh2_10*Alfa2_10^3)-
(8.6252*Rsh_nsh2_10*Alfa2_10^2)+(3.3490*Rsh_nsh2_10*Alfa2_10)+Rsh_nsh2_10;
n2_10 = (-0.2230*n_nsh2_10*Alfa2_10^3) + (0.3643*n_nsh2_10*Alfa2_10^2)+
(0.1670*n_nsh2_10*Alfa2_10)+n_nsh2_10;
Is2_10 = (10.3994*Is_nsh2_10*Alfa2_10^2)+(0.6450*Is_nsh2_10*Alfa2_10)+Is_nsh2_10;
Iph2_10 = Iph_nsh2_10*(1-Alfa2_10);

% If the cell is not shaded, the cell parameters will be equal to the parameters under no shading:
else
Rs2_10 = Rs_nsh2_10;
Rsh2_10 =  Rsh_nsh2_10;
Iph2_10 = Iph_nsh2_10;
n2_10 =  n_nsh2_10;
Is2_10 = Is_nsh2_10;
end

%======== Cell 2_11 ========

Sh_per2_11 = 0; % Shading percentage
AT2_11 = 0.0015; % Total cell area
A2_11_2 = (AT2_11*Sh_per2_11)/100; % Shaded area
Alfa2_11 = A2_11_2/AT2_11; % Calculate shading factor
G2_11_1 = 1000; % Unshaded part irradiance
G2_11_2 = 0; % Shaded part irradiance

%======== Check if cell 2_11 is working under STC or not ========

% If the cell is working under STC, parameters under no shading (with sub-script 'nsh') will be equal to
the STC parameters:
if G2_11_1 == G_ref && T == T_ref
Iph_nsh2_11 = Iph_ref;
Rs_nsh2_11 = Rs_ref;
Rsh_nsh2_11 = Rsh_ref;
Is_nsh2_11 = Is_ref;
n_nsh2_11 = n_ref;

% If the cell is not working under STC, adapt the STC parameters to the actual irradiance and temperature
in order to determine the parameters under no shading. All parameters equations are included here. If
some parameters are required to be set fixed with irradiance and temperature, they should be made equal
to their values under STC:
else
Rs_nsh2_11 = ((34.0109*Rs_ref*(1-(G2_11_1/G_ref))^3)-(22.9749*Rs_ref*(1-
(G2_11_1/G_ref))^2)+(6.6189*Rs_ref*(1-(G2_11_1/G_ref)))+Rs_ref)*(T/T_ref);
Rsh_nsh2_11 = (12.4389*Rsh_ref*(1-(G2_11_1/G_ref))^3)-(8.6252*Rsh_ref*(1-
(G2_11_1/G_ref))^2)+(3.3490*Rsh_ref*(1-(G2_11_1/G_ref)))+Rsh_ref;
n_nsh2_11 = (-0.2230*n_ref*(1-(G2_11_1/G_ref))^3)+(0.3643*n_ref*(1-
(G2_11_1/G_ref))^2)+(0.1670*n_ref*(1-(G2_11_1/G_ref)))+n_ref;
Eg = Eg_ref*(1-0.0002677*(T-T_ref));
Is_nsh2_11 = ((10.3994*Is_ref*(1-(G2_11_1/G_ref))^2)+(0.6450*Is_ref*(1-
(G2_11_1/G_ref)))+Is_ref)*((T/T_ref)^3*exp((Eg/k)*(1/T_ref-1/T)));
```

```
Iph_nsh2_11 = (Iph_ref+(Ki*(T-T_ref)))*(1-(1-(G2_11_1/G_ref)));
end

%======== Calculate the variations of the parameters of cell 2_11 with shading ========

% If the cell is shaded, calculate the variations of the parameters with shading. All parameters equations
are included here. If some parameters are required to be set fixed with shading, they should be made
equal to their values under no shading:
if Alfa2_11 > 0
Rs2_11 = (34.0109*Rs_nsh2_11*Alfa2_11^3)-
(22.9749*Rs_nsh2_11*Alfa2_11^2)+(6.6189*Rs_nsh2_11*Alfa2_11)+Rs_nsh2_11;
Rsh2_11 = (12.4389*Rsh_nsh2_11*Alfa2_11^3)-
(8.6252*Rsh_nsh2_11*Alfa2_11^2)+(3.3490*Rsh_nsh2_11*Alfa2_11)+Rsh_nsh2_11;
n2_11 = (-0.2230*n_nsh2_11*Alfa2_11^3) + (0.3643*n_nsh2_11*Alfa2_11^2)+
(0.1670*n_nsh2_11*Alfa2_11)+n_nsh2_11;
Is2_11 = (10.3994*Is_nsh2_11*Alfa2_11^2)+(0.6450*Is_nsh2_11*Alfa2_11)+Is_nsh2_11;
Iph2_11 = Iph_nsh2_11*(1-Alfa2_11);

% If the cell is not shaded, the cell parameters will be equal to the parameters under no shading:
else
Rs2_11 = Rs_nsh2_11;
Rsh2_11 =  Rsh_nsh2_11;
Iph2_11 = Iph_nsh2_11;
n2_11 =  n_nsh2_11;
Is2_11 = Is_nsh2_11;
end

%======== Cell 2_12 ========

Sh_per2_12 = 0; % Shading percentage
AT2_12 = 0.0015; % Total cell area
A2_12_2 = (AT2_12*Sh_per2_12)/100; % Shaded area
Alfa2_12 = A2_12_2/AT2_12; % Calculate shading factor
G2_12_1 = 1000; % Unshaded part irradiance
G2_12_2 = 0; % Shaded part irradiance

%======== Check if cell 2_12 is working under STC or not ========

% If the cell is working under STC, parameters under no shading (with sub-script 'nsh') will be equal to
the STC parameters:
if G2_12_1 == G_ref && T == T_ref
Iph_nsh2_12 = Iph_ref;
Rs_nsh2_12 = Rs_ref;
Rsh_nsh2_12 = Rsh_ref;
Is_nsh2_12 = Is_ref;
n_nsh2_12 = n_ref;

% If the cell is not working under STC, adapt the STC parameters to the actual irradiance and temperature
in order to determine the parameters under no shading. All parameters equations are included here. If
some parameters are required to be set fixed with irradiance and temperature, they should be made equal
to their values under STC:
else
Rs_nsh2_12 = ((34.0109*Rs_ref*(1-(G2_12_1/G_ref))^3)-(22.9749*Rs_ref*(1-
(G2_12_1/G_ref))^2)+(6.6189*Rs_ref*(1-(G2_12_1/G_ref)))+Rs_ref)*(T/T_ref);
Rsh_nsh2_12 = (12.4389*Rsh_ref*(1-(G2_12_1/G_ref))^3)-(8.6252*Rsh_ref*(1-
(G2_12_1/G_ref))^2)+(3.3490*Rsh_ref*(1-(G2_12_1/G_ref)))+Rsh_ref;
n_nsh2_12 = (-0.2230*n_ref*(1-(G2_12_1/G_ref))^3)+(0.3643*n_ref*(1-
(G2_12_1/G_ref))^2)+(0.1670*n_ref*(1-(G2_12_1/G_ref)))+n_ref;
Eg = Eg_ref*(1-0.0002677*(T-T_ref));
```

```
Is_nsh2_12 = ((10.3994*Is_ref*(1-(G2_12_1/G_ref))^2)+(0.6450*Is_ref*(1-
(G2_12_1/G_ref)))+Is_ref)*((T/T_ref)^3*exp((Eg/k)*(1/T_ref-1/T)));
Iph_nsh2_12 = (Iph_ref+(Ki*(T-T_ref)))*(1-(1-(G2_12_1/G_ref)));
end

%======== Calculate the variations of the parameters of cell 2_12 with shading ========

% If the cell is shaded, calculate the variations of the parameters with shading. All parameters equations
are included here. If some parameters are required to be set fixed with shading, they should be made
equal to their values under no shading:
if Alfa2_12 > 0
Rs2_12 = (34.0109*Rs_nsh2_12*Alfa2_12^3)-
(22.9749*Rs_nsh2_12*Alfa2_12^2)+(6.6189*Rs_nsh2_12*Alfa2_12)+Rs_nsh2_12;
Rsh2_12 = (12.4389*Rsh_nsh2_12*Alfa2_12^3)-
(8.6252*Rsh_nsh2_12*Alfa2_12^2)+(3.3490*Rsh_nsh2_12*Alfa2_12)+Rsh_nsh2_12;
n2_12 = (-0.2230*n_nsh2_12*Alfa2_12^3) + (0.3643*n_nsh2_12*Alfa2_12^2)+
(0.1670*n_nsh2_12*Alfa2_12)+n_nsh2_12;
Is2_12 = (10.3994*Is_nsh2_12*Alfa2_12^2)+(0.6450*Is_nsh2_12*Alfa2_12)+Is_nsh2_12;
Iph2_12 = Iph_nsh2_12*(1-Alfa2_12);

% If the cell is not shaded, the cell parameters will be equal to the parameters under no shading:
else
Rs2_12 = Rs_nsh2_12;
Rsh2_12 =  Rsh_nsh2_12;
Iph2_12 = Iph_nsh2_12;
n2_12 =  n_nsh2_12;
Is2_12 = Is_nsh2_12;
end

%======== Cell 2_13 ========

Sh_per2_13 = 0; % Shading percentage
AT2_13 = 0.0015; % Total cell area
A2_13_2 = (AT2_13*Sh_per2_13)/100; % Shaded area
Alfa2_13 = A2_13_2/AT2_13; % Calculate shading factor
G2_13_1 = 1000; % Unshaded part irradiance
G2_13_2 = 0; % Shaded part irradiance

%======== Check if cell 2_13 is working under STC or not ========

% If the cell is working under STC, parameters under no shading (with sub-script 'nsh') will be equal to
the STC parameters:
if G2_13_1 == G_ref && T == T_ref
Iph_nsh2_13 = Iph_ref;
Rs_nsh2_13 = Rs_ref;
Rsh_nsh2_13 = Rsh_ref;
Is_nsh2_13 = Is_ref;
n_nsh2_13 = n_ref;

% If the cell is not working under STC, adapt the STC parameters to the actual irradiance and temperature
in order to determine the parameters under no shading. All parameters equations are included here. If
some parameters are required to be set fixed with irradiance and temperature, they should be made equal
to their values under STC:
else
Rs_nsh2_13 = ((34.0109*Rs_ref*(1-(G2_13_1/G_ref))^3)-(22.9749*Rs_ref*(1-
(G2_13_1/G_ref))^2)+(6.6189*Rs_ref*(1-(G2_13_1/G_ref)))+Rs_ref)*(T/T_ref);
Rsh_nsh2_13 = (12.4389*Rsh_ref*(1-(G2_13_1/G_ref))^3)-(8.6252*Rsh_ref*(1-
(G2_13_1/G_ref))^2)+(3.3490*Rsh_ref*(1-(G2_13_1/G_ref)))+Rsh_ref;
n_nsh2_13 = (-0.2230*n_ref*(1-(G2_13_1/G_ref))^3)+(0.3643*n_ref*(1-
(G2_13_1/G_ref))^2)+(0.1670*n_ref*(1-(G2_13_1/G_ref)))+n_ref;
```

```
Eg = Eg_ref*(1-0.0002677*(T-T_ref));
Is_nsh2_13 = ((10.3994*Is_ref*(1-(G2_13_1/G_ref))^2)+(0.6450*Is_ref*(1-
(G2_13_1/G_ref)))+Is_ref)*((T/T_ref)^3*exp((Eg/k)*(1/T_ref-1/T)));
Iph_nsh2_13 = (Iph_ref+(Ki*(T-T_ref)))*(1-(1-(G2_13_1/G_ref)));
end

%======== Calculate the variations of the parameters of cell 2_13 with shading ========

% If the cell is shaded, calculate the variations of the parameters with shading. All parameters equations
are included here. If some parameters are required to be set fixed with shading, they should be made
equal to their values under no shading:
if Alfa2_13 > 0
Rs2_13 = (34.0109*Rs_nsh2_13*Alfa2_13^3)-
(22.9749*Rs_nsh2_13*Alfa2_13^2)+(6.6189*Rs_nsh2_13*Alfa2_13)+Rs_nsh2_13;
Rsh2_13 = (12.4389*Rsh_nsh2_13*Alfa2_13^3)-
(8.6252*Rsh_nsh2_13*Alfa2_13^2)+(3.3490*Rsh_nsh2_13*Alfa2_13)+Rsh_nsh2_13;
n2_13 = (-0.2230*n_nsh2_13*Alfa2_13^3) + (0.3643*n_nsh2_13*Alfa2_13^2)+
(0.1670*n_nsh2_13*Alfa2_13)+n_nsh2_13;
Is2_13 = (10.3994*Is_nsh2_13*Alfa2_13^2)+(0.6450*Is_nsh2_13*Alfa2_13)+Is_nsh2_13;
Iph2_13 = Iph_nsh2_13*(1-Alfa2_13);

% If the cell is not shaded, the cell parameters will be equal to the parameters under no shading:
else
Rs2_13 = Rs_nsh2_13;
Rsh2_13 =  Rsh_nsh2_13;
Iph2_13 = Iph_nsh2_13;
n2_13 =  n_nsh2_13;
Is2_13 = Is_nsh2_13;
end

%======== Cell 2_14 ========

Sh_per2_14 = 0; % Shading percentage
AT2_14 = 0.0015; % Total cell area
A2_14_2 = (AT2_14*Sh_per2_14)/100; % Shaded area
Alfa2_14 = A2_14_2/AT2_14; % Calculate shading factor
G2_14_1 = 1000; % Unshaded part irradiance
G2_14_2 = 0; % Shaded part irradiance

%======== Check if cell 2_14 is working under STC or not ========

% If the cell is working under STC, parameters under no shading (with sub-script 'nsh') will be equal to
the STC parameters:
if G2_14_1 == G_ref && T == T_ref
Iph_nsh2_14 = Iph_ref;
Rs_nsh2_14 = Rs_ref;
Rsh_nsh2_14 = Rsh_ref;
Is_nsh2_14 = Is_ref;
n_nsh2_14 = n_ref;

% If the cell is not working under STC, adapt the STC parameters to the actual irradiance and temperature
in order to determine the parameters under no shading. All parameters equations are included here. If
some parameters are required to be set fixed with irradiance and temperature, they should be made equal
to their values under STC:
else
Rs_nsh2_14 = ((34.0109*Rs_ref*(1-(G2_14_1/G_ref))^3)-(22.9749*Rs_ref*(1-
(G2_14_1/G_ref))^2)+(6.6189*Rs_ref*(1-(G2_14_1/G_ref)))+Rs_ref)*(T/T_ref);
Rsh_nsh2_14 = (12.4389*Rsh_ref*(1-(G2_14_1/G_ref))^3)-(8.6252*Rsh_ref*(1-
(G2_14_1/G_ref))^2)+(3.3490*Rsh_ref*(1-(G2_14_1/G_ref)))+Rsh_ref;
```

```
n_nsh2_14 = (-0.2230*n_ref*(1-(G2_14_1/G_ref))^3)+(0.3643*n_ref*(1-
(G2_14_1/G_ref))^2)+(0.1670*n_ref*(1-(G2_14_1/G_ref)))+n_ref;
Eg = Eg_ref*(1-0.0002677*(T-T_ref));
Is_nsh2_14 = ((10.3994*Is_ref*(1-(G2_14_1/G_ref))^2)+(0.6450*Is_ref*(1-
(G2_14_1/G_ref)))+Is_ref)*((T/T_ref)^3*exp((Eg/k)*(1/T_ref-1/T)));
Iph_nsh2_14 = (Iph_ref+(Ki*(T-T_ref)))*(1-(1-(G2_14_1/G_ref)));
end

%======== Calculate the variations of the parameters of cell 2_14 with shading ========

% If the cell is shaded, calculate the variations of the parameters with shading. All parameters equations
are included here. If some parameters are required to be set fixed with shading, they should be made
equal to their values under no shading:
if Alfa2_14 > 0
Rs2_14 = (34.0109*Rs_nsh2_14*Alfa2_14^3)-
(22.9749*Rs_nsh2_14*Alfa2_14^2)+(6.6189*Rs_nsh2_14*Alfa2_14)+Rs_nsh2_14;
Rsh2_14 = (12.4389*Rsh_nsh2_14*Alfa2_14^3)-
(8.6252*Rsh_nsh2_14*Alfa2_14^2)+(3.3490*Rsh_nsh2_14*Alfa2_14)+Rsh_nsh2_14;
n2_14 = (-0.2230*n_nsh2_14*Alfa2_14^3) + (0.3643*n_nsh2_14*Alfa2_14^2)+
(0.1670*n_nsh2_14*Alfa2_14)+n_nsh2_14;
Is2_14 = (10.3994*Is_nsh2_14*Alfa2_14^2)+(0.6450*Is_nsh2_14*Alfa2_14)+Is_nsh2_14;
Iph2_14 = Iph_nsh2_14*(1-Alfa2_14);

% If the cell is not shaded, the cell parameters will be equal to the parameters under no shading:
else
Rs2_14 = Rs_nsh2_14;
Rsh2_14 =  Rsh_nsh2_14;
Iph2_14 = Iph_nsh2_14;
n2_14 =  n_nsh2_14;
Is2_14 = Is_nsh2_14;
end

%======== Cell 2_15 ========

Sh_per2_15 = 0; % Shading percentage
AT2_15 = 0.0015; % Total cell area
A2_15_2 = (AT2_15*Sh_per2_15)/100; % Shaded area
Alfa2_15 = A2_15_2/AT2_15; % Calculate shading factor
G2_15_1 = 1000; % Unshaded part irradiance
G2_15_2 = 0; % Shaded part irradiance

%======== Check if cell 2_15 is working under STC or not ========

% If the cell is working under STC, parameters under no shading (with sub-script 'nsh') will be equal to
the STC parameters:
if G2_15_1 == G_ref && T == T_ref
Iph_nsh2_15 = Iph_ref;
Rs_nsh2_15 = Rs_ref;
Rsh_nsh2_15 = Rsh_ref;
Is_nsh2_15 = Is_ref;
n_nsh2_15 = n_ref;

% If the cell is not working under STC, adapt the STC parameters to the actual irradiance and temperature
in order to determine the parameters under no shading. All parameters equations are included here. If
some parameters are required to be set fixed with irradiance and temperature, they should be made equal
to their values under STC:
else
Rs_nsh2_15 = ((34.0109*Rs_ref*(1-(G2_15_1/G_ref))^3)-(22.9749*Rs_ref*(1-
(G2_15_1/G_ref))^2)+(6.6189*Rs_ref*(1-(G2_15_1/G_ref)))+Rs_ref)*(T/T_ref);
```

```
Rsh_nsh2_15 = (12.4389*Rsh_ref*(1-(G2_15_1/G_ref))^3)-(8.6252*Rsh_ref*(1-
(G2_15_1/G_ref))^2)+(3.3490*Rsh_ref*(1-(G2_15_1/G_ref)))+Rsh_ref;
n_nsh2_15 = (-0.2230*n_ref*(1-(G2_15_1/G_ref))^3)+(0.3643*n_ref*(1-
(G2_15_1/G_ref))^2)+(0.1670*n_ref*(1-(G2_15_1/G_ref)))+n_ref;
Eg = Eg_ref*(1-0.0002677*(T-T_ref));
Is_nsh2_15 = ((10.3994*Is_ref*(1-(G2_15_1/G_ref))^2)+(0.6450*Is_ref*(1-
(G2_15_1/G_ref)))+Is_ref)*((T/T_ref)^3*exp((Eg/k)*(1/T_ref-1/T)));
Iph_nsh2_15 = (Iph_ref+(Ki*(T-T_ref)))*(1-(1-(G2_15_1/G_ref)));
end

%======== Calculate the variations of the parameters of cell 2_15 with shading ========

% If the cell is shaded, calculate the variations of the parameters with shading. All parameters equations
are included here. If some parameters are required to be set fixed with shading, they should be made
equal to their values under no shading:
if Alfa2_15 > 0
Rs2_15 = (34.0109*Rs_nsh2_15*Alfa2_15^3)-
(22.9749*Rs_nsh2_15*Alfa2_15^2)+(6.6189*Rs_nsh2_15*Alfa2_15)+Rs_nsh2_15;
Rsh2_15 = (12.4389*Rsh_nsh2_15*Alfa2_15^3)-
(8.6252*Rsh_nsh2_15*Alfa2_15^2)+(3.3490*Rsh_nsh2_15*Alfa2_15)+Rsh_nsh2_15;
n2_15 = (-0.2230*n_nsh2_15*Alfa2_15^3) + (0.3643*n_nsh2_15*Alfa2_15^2)+
(0.1670*n_nsh2_15*Alfa2_15)+n_nsh2_15;
Is2_15 = (10.3994*Is_nsh2_15*Alfa2_15^2)+(0.6450*Is_nsh2_15*Alfa2_15)+Is_nsh2_15;
Iph2_15 = Iph_nsh2_15*(1-Alfa2_15);

% If the cell is not shaded, the cell parameters will be equal to the parameters under no shading:
else
Rs2_15 = Rs_nsh2_15;
Rsh2_15 =  Rsh_nsh2_15;
Iph2_15 = Iph_nsh2_15;
n2_15 =  n_nsh2_15;
Is2_15 = Is_nsh2_15;
end

%======== Cell 2_16 ========

Sh_per2_16 = 0; % Shading percentage
AT2_16 = 0.0015; % Total cell area
A2_16_2 = (AT2_16*Sh_per2_16)/100; % Shaded area
Alfa2_16 = A2_16_2/AT2_16; % Calculate shading factor
G2_16_1 = 1000; % Unshaded part irradiance
G2_16_2 = 0; % Shaded part irradiance

%======== Check if cell 2_16 is working under STC or not ========

% If the cell is working under STC, parameters under no shading (with sub-script 'nsh') will be equal to
the STC parameters:
if G2_16_1 == G_ref && T == T_ref
Iph_nsh2_16 = Iph_ref;
Rs_nsh2_16 = Rs_ref;
Rsh_nsh2_16 = Rsh_ref;
Is_nsh2_16 = Is_ref;
n_nsh2_16 = n_ref;

% If the cell is not working under STC, adapt the STC parameters to the actual irradiance and temperature
in order to determine the parameters under no shading. All parameters equations are included here. If
some parameters are required to be set fixed with irradiance and temperature, they should be made equal
to their values under STC:
else
```

```
Rs_nsh2_16 = ((34.0109*Rs_ref*(1-(G2_16_1/G_ref))^3)-(22.9749*Rs_ref*(1-
(G2_16_1/G_ref))^2)+(6.6189*Rs_ref*(1-(G2_16_1/G_ref)))+Rs_ref)*(T/T_ref);
Rsh_nsh2_16 = (12.4389*Rsh_ref*(1-(G2_16_1/G_ref))^3)-(8.6252*Rsh_ref*(1-
(G2_16_1/G_ref))^2)+(3.3490*Rsh_ref*(1-(G2_16_1/G_ref)))+Rsh_ref;
n_nsh2_16 = (-0.2230*n_ref*(1-(G2_16_1/G_ref))^3)+(0.3643*n_ref*(1-
(G2_16_1/G_ref))^2)+(0.1670*n_ref*(1-(G2_16_1/G_ref)))+n_ref;
Eg = Eg_ref*(1-0.0002677*(T-T_ref));
Is_nsh2_16 = ((10.3994*Is_ref*(1-(G2_16_1/G_ref))^2)+(0.6450*Is_ref*(1-
(G2_16_1/G_ref)))+Is_ref)*((T/T_ref)^3*exp((Eg/k)*(1/T_ref-1/T)));
Iph_nsh2_16 = (Iph_ref+(Ki*(T-T_ref)))*(1-(1-(G2_16_1/G_ref)));
end

%======== Calculate the variations of the parameters of cell 2_16 with shading ========

% If the cell is shaded, calculate the variations of the parameters with shading. All parameters equations
are included here. If some parameters are required to be set fixed with shading, they should be made
equal to their values under no shading:
if Alfa2_16 > 0
Rs2_16 = (34.0109*Rs_nsh2_16*Alfa2_16^3)-
(22.9749*Rs_nsh2_16*Alfa2_16^2)+(6.6189*Rs_nsh2_16*Alfa2_16)+Rs_nsh2_16;
Rsh2_16 = (12.4389*Rsh_nsh2_16*Alfa2_16^3)-
(8.6252*Rsh_nsh2_16*Alfa2_16^2)+(3.3490*Rsh_nsh2_16*Alfa2_16)+Rsh_nsh2_16;
n2_16 = (-0.2230*n_nsh2_16*Alfa2_16^3) + (0.3643*n_nsh2_16*Alfa2_16^2)+
(0.1670*n_nsh2_16*Alfa2_16)+n_nsh2_16;
Is2_16 = (10.3994*Is_nsh2_16*Alfa2_16^2)+(0.6450*Is_nsh2_16*Alfa2_16)+Is_nsh2_16;
Iph2_16 = Iph_nsh2_16*(1-Alfa2_16);

% If the cell is not shaded, the cell parameters will be equal to the parameters under no shading:
else
Rs2_16 = Rs_nsh2_16;
Rsh2_16 =  Rsh_nsh2_16;
Iph2_16 = Iph_nsh2_16;
n2_16 =  n_nsh2_16;
Is2_16 = Is_nsh2_16;
end

%======== Cell 2_17 ========

Sh_per2_17 = 0; % Shading percentage
AT2_17 = 0.0015; % Total cell area
A2_17_2 = (AT2_17*Sh_per2_17)/100; % Shaded area
Alfa2_17 = A2_17_2/AT2_17; % Calculate shading factor
G2_17_1 = 1000; % Unshaded part irradiance
G2_17_2 = 0; % Shaded part irradiance

%======== Check if cell 2_17 is working under STC or not ========

% If the cell is working under STC, parameters under no shading (with sub-script 'nsh') will be equal to
the STC parameters:
if G2_17_1 == G_ref && T == T_ref
Iph_nsh2_17 = Iph_ref;
Rs_nsh2_17 = Rs_ref;
Rsh_nsh2_17 = Rsh_ref;
Is_nsh2_17 = Is_ref;
n_nsh2_17 = n_ref;

% If the cell is not working under STC, adapt the STC parameters to the actual irradiance and temperature
in order to determine the parameters under no shading. All parameters equations are included here. If
some parameters are required to be set fixed with irradiance and temperature, they should be made equal
to their values under STC:
```

```
else
Rs_nsh2_17 = ((34.0109*Rs_ref*(1-(G2_17_1/G_ref))^3)-(22.9749*Rs_ref*(1-
(G2_17_1/G_ref))^2)+(6.6189*Rs_ref*(1-(G2_17_1/G_ref)))+Rs_ref)*(T/T_ref);
Rsh_nsh2_17 = (12.4389*Rsh_ref*(1-(G2_17_1/G_ref))^3)-(8.6252*Rsh_ref*(1-
(G2_17_1/G_ref))^2)+(3.3490*Rsh_ref*(1-(G2_17_1/G_ref)))+Rsh_ref;
n_nsh2_17 = (-0.2230*n_ref*(1-(G2_17_1/G_ref))^3)+(0.3643*n_ref*(1-
(G2_17_1/G_ref))^2)+(0.1670*n_ref*(1-(G2_17_1/G_ref)))+n_ref;
Eg = Eg_ref*(1-0.0002677*(T-T_ref));
Is_nsh2_17 = ((10.3994*Is_ref*(1-(G2_17_1/G_ref))^2)+(0.6450*Is_ref*(1-
(G2_17_1/G_ref)))+Is_ref)*((T/T_ref)^3*exp((Eg/k)*(1/T_ref-1/T)));
Iph_nsh2_17 = (Iph_ref+(Ki*(T-T_ref)))*(1-(1-(G2_17_1/G_ref)));
end

%======== Calculate the variations of the parameters of cell 2_17 with shading ========

% If the cell is shaded, calculate the variations of the parameters with shading. All parameters equations
are included here. If some parameters are required to be set fixed with shading, they should be made
equal to their values under no shading:
if Alfa2_17 > 0
Rs2_17 = (34.0109*Rs_nsh2_17*Alfa2_17^3)-
(22.9749*Rs_nsh2_17*Alfa2_17^2)+(6.6189*Rs_nsh2_17*Alfa2_17)+Rs_nsh2_17;
Rsh2_17 = (12.4389*Rsh_nsh2_17*Alfa2_17^3)-
(8.6252*Rsh_nsh2_17*Alfa2_17^2)+(3.3490*Rsh_nsh2_17*Alfa2_17)+Rsh_nsh2_17;
n2_17 = (-0.2230*n_nsh2_17*Alfa2_17^3) + (0.3643*n_nsh2_17*Alfa2_17^2)+
(0.1670*n_nsh2_17*Alfa2_17)+n_nsh2_17;
Is2_17 = (10.3994*Is_nsh2_17*Alfa2_17^2)+(0.6450*Is_nsh2_17*Alfa2_17)+Is_nsh2_17;
Iph2_17 = Iph_nsh2_17*(1-Alfa2_17);

% If the cell is not shaded, the cell parameters will be equal to the parameters under no shading:
else
Rs2_17 = Rs_nsh2_17;
Rsh2_17 =  Rsh_nsh2_17;
Iph2_17 = Iph_nsh2_17;
n2_17 =  n_nsh2_17;
Is2_17 = Is_nsh2_17;
end

%======== Cell 2_18 ========

Sh_per2_18 = 0; % Shading percentage
AT2_18 = 0.0015; % Total cell area
A2_18_2 = (AT2_18*Sh_per2_18)/100; % Shaded area
Alfa2_18 = A2_18_2/AT2_18; % Calculate shading factor
G2_18_1 = 1000; % Unshaded part irradiance
G2_18_2 = 0; % Shaded part irradiance

%======== Check if cell 2_18 is working under STC or not ========

% If the cell is working under STC, parameters under no shading (with sub-script 'nsh') will be equal to
the STC parameters:
if G2_18_1 == G_ref && T == T_ref
Iph_nsh2_18 = Iph_ref;
Rs_nsh2_18 = Rs_ref;
Rsh_nsh2_18 = Rsh_ref;
Is_nsh2_18 = Is_ref;
n_nsh2_18 = n_ref;

% If the cell is not working under STC, adapt the STC parameters to the actual irradiance and temperature
in order to determine the parameters under no shading. All parameters equations are included here. If
```

```
some parameters are required to be set fixed with irradiance and temperature, they should be made equal
to their values under STC:
else
Rs_nsh2_18 = ((34.0109*Rs_ref*(1-(G2_18_1/G_ref))^3)-(22.9749*Rs_ref*(1-
(G2_18_1/G_ref))^2)+(6.6189*Rs_ref*(1-(G2_18_1/G_ref)))+Rs_ref)*(T/T_ref);
Rsh_nsh2_18 = (12.4389*Rsh_ref*(1-(G2_18_1/G_ref))^3)-(8.6252*Rsh_ref*(1-
(G2_18_1/G_ref))^2)+(3.3490*Rsh_ref*(1-(G2_18_1/G_ref)))+Rsh_ref;
n_nsh2_18 = (-0.2230*n_ref*(1-(G2_18_1/G_ref))^3)+(0.3643*n_ref*(1-
(G2_18_1/G_ref))^2)+(0.1670*n_ref*(1-(G2_18_1/G_ref)))+n_ref;
Eg = Eg_ref*(1-0.0002677*(T-T_ref));
Is_nsh2_18 = ((10.3994*Is_ref*(1-(G2_18_1/G_ref))^2)+(0.6450*Is_ref*(1-
(G2_18_1/G_ref)))+Is_ref)*((T/T_ref)^3*exp((Eg/k)*(1/T_ref-1/T)));
Iph_nsh2_18 = (Iph_ref+(Ki*(T-T_ref)))*(1-(1-(G2_18_1/G_ref)));
end

%======== Calculate the variations of the parameters of cell 2_18 with shading ========

% If the cell is shaded, calculate the variations of the parameters with shading. All parameters equations
are included here. If some parameters are required to be set fixed with shading, they should be made
equal to their values under no shading:
if Alfa2_18 > 0
Rs2_18 = (34.0109*Rs_nsh2_18*Alfa2_18^3)-
(22.9749*Rs_nsh2_18*Alfa2_18^2)+(6.6189*Rs_nsh2_18*Alfa2_18)+Rs_nsh2_18;
Rsh2_18 = (12.4389*Rsh_nsh2_18*Alfa2_18^3)-
(8.6252*Rsh_nsh2_18*Alfa2_18^2)+(3.3490*Rsh_nsh2_18*Alfa2_18)+Rsh_nsh2_18;
n2_18 = (-0.2230*n_nsh2_18*Alfa2_18^3) + (0.3643*n_nsh2_18*Alfa2_18^2)+
(0.1670*n_nsh2_18*Alfa2_18)+n_nsh2_18;
Is2_18 = (10.3994*Is_nsh2_18*Alfa2_18^2)+(0.6450*Is_nsh2_18*Alfa2_18)+Is_nsh2_18;
Iph2_18 = Iph_nsh2_18*(1-Alfa2_18);

% If the cell is not shaded, the cell parameters will be equal to the parameters under no shading:
else
Rs2_18 = Rs_nsh2_18;
Rsh2_18 =  Rsh_nsh2_18;
Iph2_18 = Iph_nsh2_18;
n2_18 =  n_nsh2_18;
Is2_18 = Is_nsh2_18;
end

%======== Calculating shading factor of cell-strings ========

Alfa1 = (Alfa1_1 + Alfa1_2 + Alfa1_3 + Alfa1_4 + Alfa1_5 + Alfa1_6 + Alfa1_7 + Alfa1_8 + Alfa1_9 +
Alfa1_10 + Alfa1_11 + Alfa1_12 + Alfa1_13 + Alfa1_14+Alfa1_15+Alfa1_16+Alfa1_17+Alfa1_18)/18;
Alfa2 = (Alfa2_1 + Alfa2_2 + Alfa2_3 + Alfa2_4 + Alfa2_5 + Alfa2_6 + Alfa2_7 + Alfa2_8 + Alfa2_9 +
Alfa2_10 + Alfa2_11 + Alfa2_12 + Alfa2_13 + Alfa2_14+Alfa2_15+Alfa2_16+Alfa2_17+Alfa2_18)/18;

%======== Initialise voltages of individual cells ========

V1_1 = ones(1,length(I));
V1_2 = ones(1,length(I));
V1_3 = ones(1,length(I));
V1_4 = ones(1,length(I));
V1_5 = ones(1,length(I));
V1_6 = ones(1,length(I));
V1_7 = ones(1,length(I));
V1_8 = ones(1,length(I));
V1_9 = ones(1,length(I));
V1_10 = ones(1,length(I));
V1_11 = ones(1,length(I));
V1_12 = ones(1,length(I));
```

```
V1_13 = ones(1,length(I));
V1_14 = ones(1,length(I));
V1_15 = ones(1,length(I));
V1_16 = ones(1,length(I));
V1_17 = ones(1,length(I));
V1_18 = ones(1,length(I));

V2_1 = ones(1,length(I));
V2_2 = ones(1,length(I));
V2_3 = ones(1,length(I));
V2_4 = ones(1,length(I));
V2_5 = ones(1,length(I));
V2_6 = ones(1,length(I));
V2_7 = ones(1,length(I));
V2_8 = ones(1,length(I));
V2_9 = ones(1,length(I));
V2_10 = ones(1,length(I));
V2_11 = ones(1,length(I));
V2_12 = ones(1,length(I));
V2_13 = ones(1,length(I));
V2_14 = ones(1,length(I));
V2_15 = ones(1,length(I));
V2_16 = ones(1,length(I));
V2_17 = ones(1,length(I));
V2_18 = ones(1,length(I));

%======== Calculate voltages of individual cells ========

for j = 1 : size(I,2)

% Calculating the voltage produced by cell 1_1:
    if I(j) <= Iph1_1 % If the cell operates in the direct bias
      f(j) = Iph1_1-Is1_1*(exp((V1_1(j)+I(j)*Rs1_1)/(Vth*n1_1))-1)-(V1_1(j)+I(j)*Rs1_1)/Rsh1_1-I(j);
      while (abs(f(j))>0.000000001)
        f(j) = Iph1_1-Is1_1*(exp((V1_1(j)+I(j)*Rs1_1)/(Vth*n1_1))-1)-(V1_1(j)+I(j)*Rs1_1)/Rsh1_1-I(j);
        dif_f(j) = - 1/Rsh1_1 - (Is1_1*exp((V1_1(j) + I(j)*Rs1_1)/(Vth*n1_1)))/(Vth*n1_1);
        Vc(j) = V1_1(j)-((f(j))/(dif_f(j)));
        V1_1(j) = Vc(j);
      end
    else % If the cell operates in the reverse bias
        V1_1(j) = (-(I(j)-Iph1_1)*Rsh1_1)-(I(j)*Rs1_1);
    end

 % Calculating the voltage produced by cell 1_2:
    if I(j) <= Iph1_2 % If the cell operates in the direct bias
      f(j) = Iph1_2-Is1_2*(exp((V1_2(j)+I(j)*Rs1_2)/(Vth*n1_2))-1)-(V1_2(j)+I(j)*Rs1_2)/Rsh1_2-I(j);
      while (abs(f(j))>0.000000001)
        f(j) = Iph1_2-Is1_2*(exp((V1_2(j)+I(j)*Rs1_2)/(Vth*n1_2))-1)-(V1_2(j)+I(j)*Rs1_2)/Rsh1_2-I(j);
        dif_f(j) = - 1/Rsh1_2 - (Is1_2*exp((V1_2(j) + I(j)*Rs1_2)/(Vth*n1_2)))/(Vth*n1_2);
        Vc(j) = V1_2(j)-((f(j))/(dif_f(j)));
        V1_2(j) = Vc(j);
      end
    else % If the cell operates in the reverse bias
        V1_2(j) = (-(I(j)-Iph1_2)*Rsh1_2)-(I(j)*Rs1_2);
    end

% Calculating the voltage produced by cell 1_3:
    if I(j) <= Iph1_3 % If the cell operates in the direct bias
      f(j) = Iph1_3-Is1_3*(exp((V1_3(j)+I(j)*Rs1_3)/(Vth*n1_3))-1)-(V1_3(j)+I(j)*Rs1_3)/Rsh1_3-I(j);
      while (abs(f(j))>0.000000001)
```

```
        f(j) = Iph1_3-Is1_3*(exp((V1_3(j)+I(j)*Rs1_3)/(Vth*n1_3))-1)-(V1_3(j)+I(j)*Rs1_3)/Rsh1_3-I(j);
        dif_f(j) = - 1/Rsh1_3 - (Is1_3*exp((V1_3(j) + I(j)*Rs1_3)/(Vth*n1_3)))/(Vth*n1_3);
        Vc(j) = V1_3(j)-((f(j))/(dif_f(j)));
        V1_3(j) = Vc(j);
      end
    else % If the cell operates in the reverse bias
        V1_3(j) = (-(I(j)-Iph1_3)*Rsh1_3)-(I(j)*Rs1_3);
    end

% Calculating the voltage produced by cell 1_4:
    if I(j) <= Iph1_4 % If the cell operates in the direct bias
      f(j) = Iph1_4-Is1_4*(exp((V1_4(j)+I(j)*Rs1_4)/(Vth*n1_4))-1)-(V1_4(j)+I(j)*Rs1_4)/Rsh1_4-I(j);
      while (abs(f(j))>0.000000001)
        f(j) = Iph1_4-Is1_4*(exp((V1_4(j)+I(j)*Rs1_4)/(Vth*n1_4))-1)-(V1_4(j)+I(j)*Rs1_4)/Rsh1_4-I(j);
        dif_f(j) = - 1/Rsh1_4 - (Is1_4*exp((V1_4(j) + I(j)*Rs1_4)/(Vth*n1_4)))/(Vth*n1_4);
        Vc(j) = V1_4(j)-((f(j))/(dif_f(j)));
        V1_4(j) = Vc(j);
      end
    else % If the cell operates in the reverse bias
        V1_4(j) = (-(I(j)-Iph1_4)*Rsh1_4)-(I(j)*Rs1_4);
    end

% Calculating the voltage produced by cell 1_5:
    if I(j) <= Iph1_5 % If the cell operates in the direct bias
      f(j) = Iph1_5-Is1_5*(exp((V1_5(j)+I(j)*Rs1_5)/(Vth*n1_5))-1)-(V1_5(j)+I(j)*Rs1_5)/Rsh1_5-I(j);
      while (abs(f(j))>0.000000001)
        f(j) = Iph1_5-Is1_5*(exp((V1_5(j)+I(j)*Rs1_5)/(Vth*n1_5))-1)-(V1_5(j)+I(j)*Rs1_5)/Rsh1_5-I(j);
        dif_f(j) = - 1/Rsh1_5 - (Is1_5*exp((V1_5(j) + I(j)*Rs1_5)/(Vth*n1_5)))/(Vth*n1_5);
        Vc(j) = V1_5(j)-((f(j))/(dif_f(j)));
        V1_5(j) = Vc(j);
      end
    else % If the cell operates in the reverse bias
        V1_5(j) = (-(I(j)-Iph1_5)*Rsh1_5)-(I(j)*Rs1_5);
    end

% Calculating the voltage produced by cell 1_6:
    if I(j) <= Iph1_6 % If the cell operates in the direct bias
      f(j) = Iph1_6-Is1_6*(exp((V1_6(j)+I(j)*Rs1_6)/(Vth*n1_6))-1)-(V1_6(j)+I(j)*Rs1_6)/Rsh1_6-I(j);
      while (abs(f(j))>0.000000001)
        f(j) = Iph1_6-Is1_6*(exp((V1_6(j)+I(j)*Rs1_6)/(Vth*n1_6))-1)-(V1_6(j)+I(j)*Rs1_6)/Rsh1_6-I(j);
        dif_f(j) = - 1/Rsh1_6 - (Is1_6*exp((V1_6(j) + I(j)*Rs1_6)/(Vth*n1_6)))/(Vth*n1_6);
        Vc(j) = V1_6(j)-((f(j))/(dif_f(j)));
        V1_6(j) = Vc(j);
      end
    else % If the cell operates in the reverse bias
        V1_6(j) = (-(I(j)-Iph1_6)*Rsh1_6)-(I(j)*Rs1_6);
    end

% Calculating the voltage produced by cell 1_7:
    if I(j) <= Iph1_7 % If the cell operates in the direct bias
      f(j) = Iph1_7-Is1_7*(exp((V1_7(j)+I(j)*Rs1_7)/(Vth*n1_7))-1)-(V1_7(j)+I(j)*Rs1_7)/Rsh1_7-I(j);
      while (abs(f(j))>0.000000001)
        f(j) = Iph1_7-Is1_7*(exp((V1_7(j)+I(j)*Rs1_7)/(Vth*n1_7))-1)-(V1_7(j)+I(j)*Rs1_7)/Rsh1_7-I(j);
        dif_f(j) = - 1/Rsh1_7 - (Is1_7*exp((V1_7(j) + I(j)*Rs1_7)/(Vth*n1_7)))/(Vth*n1_7);
        Vc(j) = V1_7(j)-((f(j))/(dif_f(j)));
        V1_7(j) = Vc(j);
      end
    else % If the cell operates in the reverse bias
        V1_7(j) = (-(I(j)-Iph1_7)*Rsh1_7)-(I(j)*Rs1_7);
    end
```

```
% Calculating the voltage produced by cell 1_8:
    if I(j) <= Iph1_8 % If the cell operates in the direct bias
      f(j) = Iph1_8-Is1_8*(exp((V1_8(j)+I(j)*Rs1_8)/(Vth*n1_8))-1)-(V1_8(j)+I(j)*Rs1_8)/Rsh1_8-I(j);
      while (abs(f(j))>0.000000001)
        f(j) = Iph1_8-Is1_8*(exp((V1_8(j)+I(j)*Rs1_8)/(Vth*n1_8))-1)-(V1_8(j)+I(j)*Rs1_8)/Rsh1_8-I(j);
        dif_f(j) = - 1/Rsh1_8 - (Is1_8*exp((V1_8(j) + I(j)*Rs1_8)/(Vth*n1_8)))/(Vth*n1_8);
        Vc(j) = V1_8(j)-((f(j))/(dif_f(j)));
        V1_8(j) = Vc(j);
      end
    else % If the cell operates in the reverse bias
        V1_8(j) = (-(I(j)-Iph1_8)*Rsh1_8)-(I(j)*Rs1_8);
    end

% Calculating the voltage produced by cell 1_9:
    if I(j) <= Iph1_9 % If the cell operates in the direct bias
      f(j) = Iph1_9-Is1_9*(exp((V1_9(j)+I(j)*Rs1_9)/(Vth*n1_9))-1)-(V1_9(j)+I(j)*Rs1_9)/Rsh1_9-I(j);
      while (abs(f(j))>0.000000001)
        f(j) = Iph1_9-Is1_9*(exp((V1_9(j)+I(j)*Rs1_9)/(Vth*n1_9))-1)-(V1_9(j)+I(j)*Rs1_9)/Rsh1_9-I(j);
        dif_f(j) = - 1/Rsh1_9 - (Is1_9*exp((V1_9(j) + I(j)*Rs1_9)/(Vth*n1_9)))/(Vth*n1_9);
        Vc(j) = V1_9(j)-((f(j))/(dif_f(j)));
        V1_9(j) = Vc(j);
      end
    else % If the cell operates in the reverse bias
        V1_9(j) = (-(I(j)-Iph1_9)*Rsh1_9)-(I(j)*Rs1_9);
    end

% Calculating the voltage produced by cell 1_10:
    if I(j) <= Iph1_10 % If the cell operates in the direct bias
      f(j) = Iph1_10-Is1_10*(exp((V1_10(j)+I(j)*Rs1_10)/(Vth*n1_10))-1)-
(V1_10(j)+I(j)*Rs1_10)/Rsh1_10-I(j);
      while (abs(f(j))>0.000000001)
        f(j) = Iph1_10-Is1_10*(exp((V1_10(j)+I(j)*Rs1_10)/(Vth*n1_10))-1)-
(V1_10(j)+I(j)*Rs1_10)/Rsh1_10-I(j);
        dif_f(j) = - 1/Rsh1_10 - (Is1_10*exp((V1_10(j) + I(j)*Rs1_10)/(Vth*n1_10)))/(Vth*n1_10);
        Vc(j) = V1_10(j)-((f(j))/(dif_f(j)));
        V1_10(j) = Vc(j);
      end
    else % If the cell operates in the reverse bias
      V1_10(j) = (-(I(j)-Iph1_10)*Rsh1_10)-(I(j)*Rs1_10);
    end

% Calculating the voltage produced by cell 1_11:
    if I(j) <= Iph1_11 % If the cell operates in the direct bias
      f(j) = Iph1_11-Is1_11*(exp((V1_11(j)+I(j)*Rs1_11)/(Vth*n1_11))-1)-
(V1_11(j)+I(j)*Rs1_11)/Rsh1_11-I(j);
      while (abs(f(j))>0.000000001)
        f(j) = Iph1_11-Is1_11*(exp((V1_11(j)+I(j)*Rs1_11)/(Vth*n1_11))-1)-
(V1_11(j)+I(j)*Rs1_11)/Rsh1_11-I(j);
        dif_f(j) = - 1/Rsh1_11 - (Is1_11*exp((V1_11(j) + I(j)*Rs1_11)/(Vth*n1_11)))/(Vth*n1_11);
        Vc(j) = V1_11(j)-((f(j))/(dif_f(j)));
        V1_11(j) = Vc(j);
      end
    else % If the cell operates in the reverse bias
      V1_11(j) = (-(I(j)-Iph1_11)*Rsh1_11)-(I(j)*Rs1_11);
    end

% Calculating the voltage produced by cell 1_12:
    if I(j) <= Iph1_12 % If the cell operates in the direct bias
```

```
      f(j) = Iph1_12-Is1_12*(exp((V1_12(j)+I(j)*Rs1_12)/(Vth*n1_12))-1)-
(V1_12(j)+I(j)*Rs1_12)/Rsh1_12-I(j);
      while (abs(f(j))>0.000000001)
         f(j) = Iph1_12-Is1_12*(exp((V1_12(j)+I(j)*Rs1_12)/(Vth*n1_12))-1)-
(V1_12(j)+I(j)*Rs1_12)/Rsh1_12-I(j);
         dif_f(j) = - 1/Rsh1_12 - (Is1_12*exp((V1_12(j) + I(j)*Rs1_12)/(Vth*n1_12)))/(Vth*n1_12);
         Vc(j) = V1_12(j)-((f(j))/(dif_f(j)));
         V1_12(j) = Vc(j);
      end
   else % If the cell operates in the reverse bias
      V1_12(j) = (-(I(j)-Iph1_12)*Rsh1_12)-(I(j)*Rs1_12);
   end

 % Calculating the voltage produced by cell 1_13:
   if I(j) <= Iph1_13 % If the cell operates in the direct bias
      f(j) = Iph1_13-Is1_13*(exp((V1_13(j)+I(j)*Rs1_13)/(Vth*n1_13))-1)-
(V1_13(j)+I(j)*Rs1_13)/Rsh1_13-I(j);
      while (abs(f(j))>0.000000001)
         f(j) = Iph1_13-Is1_13*(exp((V1_13(j)+I(j)*Rs1_13)/(Vth*n1_13))-1)-
(V1_13(j)+I(j)*Rs1_13)/Rsh1_13-I(j);
         dif_f(j) = - 1/Rsh1_13 - (Is1_13*exp((V1_13(j) + I(j)*Rs1_13)/(Vth*n1_13)))/(Vth*n1_13);
         Vc(j) = V1_13(j)-((f(j))/(dif_f(j)));
         V1_13(j) = Vc(j);
      end
   else % If the cell operates in the reverse bias
      V1_13(j) = (-(I(j)-Iph1_13)*Rsh1_13)-(I(j)*Rs1_13);
   end

% Calculating the voltage produced by cell 1_14:
   if I(j) <= Iph1_14 % If the cell operates in the direct bias
      f(j) = Iph1_14-Is1_14*(exp((V1_14(j)+I(j)*Rs1_14)/(Vth*n1_14))-1)-
(V1_14(j)+I(j)*Rs1_14)/Rsh1_14-I(j);
      while (abs(f(j))>0.000000001)
         f(j) = Iph1_14-Is1_14*(exp((V1_14(j)+I(j)*Rs1_14)/(Vth*n1_14))-1)-
(V1_14(j)+I(j)*Rs1_14)/Rsh1_14-I(j);
         dif_f(j) = - 1/Rsh1_14 - (Is1_14*exp((V1_14(j) + I(j)*Rs1_14)/(Vth*n1_14)))/(Vth*n1_14);
         Vc(j) = V1_14(j)-((f(j))/(dif_f(j)));
         V1_14(j) = Vc(j);
      end
   else % If the cell operates in the reverse bias
      V1_14(j) = (-(I(j)-Iph1_14)*Rsh1_14)-(I(j)*Rs1_14);
   end

% Calculating the voltage produced by cell 1_15:
   if I(j) <= Iph1_15 % If the cell operates in the direct bias
      f(j) = Iph1_15-Is1_15*(exp((V1_15(j)+I(j)*Rs1_15)/(Vth*n1_15))-1)-
(V1_15(j)+I(j)*Rs1_15)/Rsh1_15-I(j);
      while (abs(f(j))>0.000000001)
         f(j) = Iph1_15-Is1_15*(exp((V1_15(j)+I(j)*Rs1_15)/(Vth*n1_15))-1)-
(V1_15(j)+I(j)*Rs1_15)/Rsh1_15-I(j);
         dif_f(j) = - 1/Rsh1_15 - (Is1_15*exp((V1_15(j) + I(j)*Rs1_15)/(Vth*n1_15)))/(Vth*n1_15);
         Vc(j) = V1_15(j)-((f(j))/(dif_f(j)));
         V1_15(j) = Vc(j);
      end
   else % If the cell operates in the reverse bias
      V1_15(j) = (-(I(j)-Iph1_15)*Rsh1_15)-(I(j)*Rs1_15);
   end

% Calculating the voltage produced by cell 1_16:
   if I(j) <= Iph1_16 % If the cell operates in the direct bias
```

```
      f(j) = Iph1_16-Is1_16*(exp((V1_16(j)+I(j)*Rs1_16)/(Vth*n1_16))-1)-
(V1_16(j)+I(j)*Rs1_16)/Rsh1_16-I(j);
      while (abs(f(j))>0.000000001)
         f(j) = Iph1_16-Is1_16*(exp((V1_16(j)+I(j)*Rs1_16)/(Vth*n1_16))-1)-
(V1_16(j)+I(j)*Rs1_16)/Rsh1_16-I(j);
         dif_f(j) = - 1/Rsh1_16 - (Is1_16*exp((V1_16(j) + I(j)*Rs1_16)/(Vth*n1_16)))/(Vth*n1_16);
         Vc(j) = V1_16(j)-((f(j))/(dif_f(j)));
         V1_16(j) = Vc(j);
      end
   else % If the cell operates in the reverse bias
      V1_16(j) = (-(I(j)-Iph1_16)*Rsh1_16)-(I(j)*Rs1_16);
   end

% Calculating the voltage produced by cell 1_17:
   if I(j) <= Iph1_17 % If the cell operates in the direct bias
      f(j) = Iph1_17-Is1_17*(exp((V1_17(j)+I(j)*Rs1_17)/(Vth*n1_17))-1)-
(V1_17(j)+I(j)*Rs1_17)/Rsh1_17-I(j);
      while (abs(f(j))>0.000000001)
         f(j) = Iph1_17-Is1_17*(exp((V1_17(j)+I(j)*Rs1_17)/(Vth*n1_17))-1)-
(V1_17(j)+I(j)*Rs1_17)/Rsh1_17-I(j);
         dif_f(j) = - 1/Rsh1_17 - (Is1_17*exp((V1_17(j) + I(j)*Rs1_17)/(Vth*n1_17)))/(Vth*n1_17);
         Vc(j) = V1_17(j)-((f(j))/(dif_f(j)));
         V1_17(j) = Vc(j);
      end
   else % If the cell operates in the reverse bias
      V1_17(j) = (-(I(j)-Iph1_17)*Rsh1_17)-(I(j)*Rs1_17);
   end

% Calculating the voltage produced by cell 1_18:
   if I(j) <= Iph1_18 % If the cell operates in the direct bias
      f(j) = Iph1_18-Is1_18*(exp((V1_18(j)+I(j)*Rs1_18)/(Vth*n1_18))-1)-
(V1_18(j)+I(j)*Rs1_18)/Rsh1_18-I(j);
      while (abs(f(j))>0.000000001)
         f(j) = Iph1_18-Is1_18*(exp((V1_18(j)+I(j)*Rs1_18)/(Vth*n1_18))-1)-
(V1_18(j)+I(j)*Rs1_18)/Rsh1_18-I(j);
         dif_f(j) = - 1/Rsh1_18 - (Is1_18*exp((V1_18(j) + I(j)*Rs1_18)/(Vth*n1_18)))/(Vth*n1_18);
         Vc(j) = V1_18(j)-((f(j))/(dif_f(j)));
         V1_18(j) = Vc(j);
      end
   else % If the cell operates in the reverse bias
      V1_18(j) = (-(I(j)-Iph1_18)*Rsh1_18)-(I(j)*Rs1_18);
   end


% Calculating the voltage produced by cell 2_1:
   if I(j) <= Iph2_1 % If the cell operates in the direct bias
      f(j) = Iph2_1-Is2_1*(exp((V2_1(j)+I(j)*Rs2_1)/(Vth*n2_1))-1)-(V2_1(j)+I(j)*Rs2_1)/Rsh2_1-I(j);
      while (abs(f(j))>0.000000001)
         f(j) = Iph2_1-Is2_1*(exp((V2_1(j)+I(j)*Rs2_1)/(Vth*n2_1))-1)-(V2_1(j)+I(j)*Rs2_1)/Rsh2_1-I(j);
         dif_f(j) = - 1/Rsh2_1 - (Is2_1*exp((V2_1(j) + I(j)*Rs2_1)/(Vth*n2_1)))/(Vth*n2_1);
         Vc(j) = V2_1(j)-((f(j))/(dif_f(j)));
         V2_1(j) = Vc(j);
      end
   else % If the cell operates in the reverse bias
      V2_1(j) = (-(I(j)-Iph2_1)*Rsh2_1)-(I(j)*Rs2_1);
   end

% Calculating the voltage produced by cell 2_2:
   if I(j) <= Iph2_2 % If the cell operates in the direct bias
      f(j) = Iph2_2-Is2_2*(exp((V2_2(j)+I(j)*Rs2_2)/(Vth*n2_2))-1)-(V2_2(j)+I(j)*Rs2_2)/Rsh2_2-I(j);
```

```
    while (abs(f(j))>0.000000001)
      f(j) = Iph2_2-Is2_2*(exp((V2_2(j)+I(j)*Rs2_2)/(Vth*n2_2))-1)-(V2_2(j)+I(j)*Rs2_2)/Rsh2_2-I(j);
      dif_f(j) = - 1/Rsh2_2 - (Is2_2*exp((V2_2(j) + I(j)*Rs2_2)/(Vth*n2_2)))/(Vth*n2_2);
      Vc(j) = V2_2(j)-((f(j))/(dif_f(j)));
      V2_2(j) = Vc(j);
    end
  else % If the cell operates in the reverse bias
    V2_2(j) = (-(I(j)-Iph2_2)*Rsh2_2)-(I(j)*Rs2_2);
  end

% Calculating the voltage produced by cell 2_3:
  if I(j) <= Iph2_3 % If the cell operates in the direct bias
    f(j) = Iph2_3-Is2_3*(exp((V2_3(j)+I(j)*Rs2_3)/(Vth*n2_3))-1)-(V2_3(j)+I(j)*Rs2_3)/Rsh2_3-I(j);
    while (abs(f(j))>0.000000001)
      f(j) = Iph2_3-Is2_3*(exp((V2_3(j)+I(j)*Rs2_3)/(Vth*n2_3))-1)-(V2_3(j)+I(j)*Rs2_3)/Rsh2_3-I(j);
      dif_f(j) = - 1/Rsh2_3 - (Is2_3*exp((V2_3(j) + I(j)*Rs2_3)/(Vth*n2_3)))/(Vth*n2_3);
      Vc(j) = V2_3(j)-((f(j))/(dif_f(j)));
      V2_3(j) = Vc(j);
    end
  else % If the cell operates in the reverse bias
    V2_3(j) = (-(I(j)-Iph2_3)*Rsh2_3)-(I(j)*Rs2_3);
  end

% Calculating the voltage produced by cell 2_4:
  if I(j) <= Iph2_4 % If the cell operates in the direct bias
    f(j) = Iph2_4-Is2_4*(exp((V2_4(j)+I(j)*Rs2_4)/(Vth*n2_4))-1)-(V2_4(j)+I(j)*Rs2_4)/Rsh2_4-I(j);
    while (abs(f(j))>0.000000001)
      f(j) = Iph2_4-Is2_4*(exp((V2_4(j)+I(j)*Rs2_4)/(Vth*n2_4))-1)-(V2_4(j)+I(j)*Rs2_4)/Rsh2_4-I(j);
      dif_f(j) = - 1/Rsh2_4 - (Is2_4*exp((V2_4(j) + I(j)*Rs2_4)/(Vth*n2_4)))/(Vth*n2_4);
      Vc(j) = V2_4(j)-((f(j))/(dif_f(j)));
      V2_4(j) = Vc(j);
    end
  else % If the cell operates in the reverse bias
    V2_4(j) = (-(I(j)-Iph2_4)*Rsh2_4)-(I(j)*Rs2_4);
  end

% Calculating the voltage produced by cell 2_5:
  if I(j) <= Iph2_5 % If the cell operates in the direct bias
    f(j) = Iph2_5-Is2_5*(exp((V2_5(j)+I(j)*Rs2_5)/(Vth*n2_5))-1)-(V2_5(j)+I(j)*Rs2_5)/Rsh2_5-I(j);
    while (abs(f(j))>0.000000001)
      f(j) = Iph2_5-Is2_5*(exp((V2_5(j)+I(j)*Rs2_5)/(Vth*n2_5))-1)-(V2_5(j)+I(j)*Rs2_5)/Rsh2_5-I(j);
      dif_f(j) = - 1/Rsh2_5 - (Is2_5*exp((V2_5(j) + I(j)*Rs2_5)/(Vth*n2_5)))/(Vth*n2_5);
      Vc(j) = V2_5(j)-((f(j))/(dif_f(j)));
      V2_5(j) = Vc(j);
    end
  else % If the cell operates in the reverse bias
    V2_5(j) = (-(I(j)-Iph2_5)*Rsh2_5)-(I(j)*Rs2_5);
  end

% Calculating the voltage produced by cell 2_6:
  if I(j) <= Iph2_6 % If the cell operates in the direct bias
    f(j) = Iph2_6-Is2_6*(exp((V2_6(j)+I(j)*Rs2_6)/(Vth*n2_6))-1)-(V2_6(j)+I(j)*Rs2_6)/Rsh2_6-I(j);
    while (abs(f(j))>0.000000001)
      f(j) = Iph2_6-Is2_6*(exp((V2_6(j)+I(j)*Rs2_6)/(Vth*n2_6))-1)-(V2_6(j)+I(j)*Rs2_6)/Rsh2_6-I(j);
      dif_f(j) = - 1/Rsh2_6 - (Is2_6*exp((V2_6(j) + I(j)*Rs2_6)/(Vth*n2_6)))/(Vth*n2_6);
      Vc(j) = V2_6(j)-((f(j))/(dif_f(j)));
      V2_6(j) = Vc(j);
    end
  else % If the cell operates in the reverse bias
    V2_6(j) = (-(I(j)-Iph2_6)*Rsh2_6)-(I(j)*Rs2_6);
```

```
    end

% Calculating the voltage produced by cell 2_7:
    if I(j) <= Iph2_7 % If the cell operates in the direct bias
      f(j) = Iph2_7-Is2_7*(exp((V2_7(j)+I(j)*Rs2_7)/(Vth*n2_7))-1)-(V2_7(j)+I(j)*Rs2_7)/Rsh2_7-I(j);
      while (abs(f(j))>0.000000001)
        f(j) = Iph2_7-Is2_7*(exp((V2_7(j)+I(j)*Rs2_7)/(Vth*n2_7))-1)-(V2_7(j)+I(j)*Rs2_7)/Rsh2_7-I(j);
        dif_f(j) = - 1/Rsh2_7 - (Is2_7*exp((V2_7(j) + I(j)*Rs2_7)/(Vth*n2_7)))/(Vth*n2_7);
        Vc(j) = V2_7(j)-((f(j))/(dif_f(j)));
        V2_7(j) = Vc(j);
      end
    else % If the cell operates in the reverse bias
        V2_7(j) = (-(I(j)-Iph2_7)*Rsh2_7)-(I(j)*Rs2_7);
    end

% Calculating the voltage produced by cell 2_8:
    if I(j) <= Iph2_8 % If the cell operates in the direct bias
      f(j) = Iph2_8-Is2_8*(exp((V2_8(j)+I(j)*Rs2_8)/(Vth*n2_8))-1)-(V2_8(j)+I(j)*Rs2_8)/Rsh2_8-I(j);
      while (abs(f(j))>0.000000001)
        f(j) = Iph2_8-Is2_8*(exp((V2_8(j)+I(j)*Rs2_8)/(Vth*n2_8))-1)-(V2_8(j)+I(j)*Rs2_8)/Rsh2_8-I(j);
        dif_f(j) = - 1/Rsh2_8 - (Is2_8*exp((V2_8(j) + I(j)*Rs2_8)/(Vth*n2_8)))/(Vth*n2_8);
        Vc(j) = V2_8(j)-((f(j))/(dif_f(j)));
        V2_8(j) = Vc(j);
      end
    else % If the cell operates in the reverse bias
        V2_8(j) = (-(I(j)-Iph2_8)*Rsh2_8)-(I(j)*Rs2_8);
    end

% Calculating the voltage produced by cell 2_9:
    if I(j) <= Iph2_9 % If the cell operates in the direct bias
      f(j) = Iph2_9-Is2_9*(exp((V2_9(j)+I(j)*Rs2_9)/(Vth*n2_9))-1)-(V2_9(j)+I(j)*Rs2_9)/Rsh2_9-I(j);
      while (abs(f(j))>0.000000001)
        f(j) = Iph2_9-Is2_9*(exp((V2_9(j)+I(j)*Rs2_9)/(Vth*n2_9))-1)-(V2_9(j)+I(j)*Rs2_9)/Rsh2_9-I(j);
        dif_f(j) = - 1/Rsh2_9 - (Is2_9*exp((V2_9(j) + I(j)*Rs2_9)/(Vth*n2_9)))/(Vth*n2_9);
        Vc(j) = V2_9(j)-((f(j))/(dif_f(j)));
        V2_9(j) = Vc(j);
      end
    else % If the cell operates in the reverse bias
        V2_9(j) = (-(I(j)-Iph2_9)*Rsh2_9)-(I(j)*Rs2_9);
    end

% Calculating the voltage produced by cell 2_10:
    if I(j) <= Iph2_10 % If the cell operates in the direct bias
      f(j) = Iph2_10-Is2_10*(exp((V2_10(j)+I(j)*Rs2_10)/(Vth*n2_10))-1)-
(V2_10(j)+I(j)*Rs2_10)/Rsh2_10-I(j);
      while (abs(f(j))>0.000000001)
        f(j) = Iph2_10-Is2_10*(exp((V2_10(j)+I(j)*Rs2_10)/(Vth*n2_10))-1)-
(V2_10(j)+I(j)*Rs2_10)/Rsh2_10-I(j);
        dif_f(j) = - 1/Rsh2_10 - (Is2_10*exp((V2_10(j) + I(j)*Rs2_10)/(Vth*n2_10)))/(Vth*n2_10);
        Vc(j) = V2_10(j)-((f(j))/(dif_f(j)));
        V2_10(j) = Vc(j);
      end
    else % If the cell operates in the reverse bias
      V2_10(j) = (-(I(j)-Iph2_10)*Rsh2_10)-(I(j)*Rs2_10);
    end

% Calculating the voltage produced by cell 2_11:
    if I(j) <= Iph2_11 % If the cell operates in the direct bias
      f(j) = Iph2_11-Is2_11*(exp((V2_11(j)+I(j)*Rs2_11)/(Vth*n2_11))-1)-
(V2_11(j)+I(j)*Rs2_11)/Rsh2_11-I(j);
```

```
        while (abs(f(j))>0.000000001)
            f(j) = Iph2_11-Is2_11*(exp((V2_11(j)+I(j)*Rs2_11)/(Vth*n2_11))-1)-
(V2_11(j)+I(j)*Rs2_11)/Rsh2_11-I(j);
            dif_f(j) = - 1/Rsh2_11 - (Is2_11*exp((V2_11(j) + I(j)*Rs2_11)/(Vth*n2_11)))/(Vth*n2_11);
            Vc(j) = V2_11(j)-((f(j))/(dif_f(j)));
            V2_11(j) = Vc(j);
        end
    else % If the cell operates in the reverse bias
        V2_11(j) = (-(I(j)-Iph2_11)*Rsh2_11)-(I(j)*Rs2_11);
    end

% Calculating the voltage produced by cell 2_12:
    if I(j) <= Iph2_12 % If the cell operates in the direct bias
        f(j) = Iph2_12-Is2_12*(exp((V2_12(j)+I(j)*Rs2_12)/(Vth*n2_12))-1)-
(V2_12(j)+I(j)*Rs2_12)/Rsh2_12-I(j);
        while (abs(f(j))>0.000000001)
            f(j) = Iph2_12-Is2_12*(exp((V2_12(j)+I(j)*Rs2_12)/(Vth*n2_12))-1)-
(V2_12(j)+I(j)*Rs2_12)/Rsh2_12-I(j);
            dif_f(j) = - 1/Rsh2_12 - (Is2_12*exp((V2_12(j) + I(j)*Rs2_12)/(Vth*n2_12)))/(Vth*n2_12);
            Vc(j) = V2_12(j)-((f(j))/(dif_f(j)));
            V2_12(j) = Vc(j);
        end
    else % If the cell operates in the reverse bias
        V2_12(j) = (-(I(j)-Iph2_12)*Rsh2_12)-(I(j)*Rs2_12);
    end

% Calculating the voltage produced by cell 2_13:
    if I(j) <= Iph2_13 % If the cell operates in the direct bias
        f(j) = Iph2_13-Is2_13*(exp((V2_13(j)+I(j)*Rs2_13)/(Vth*n2_13))-1)-
(V2_13(j)+I(j)*Rs2_13)/Rsh2_13-I(j);
        while (abs(f(j))>0.000000001)
            f(j) = Iph2_13-Is2_13*(exp((V2_13(j)+I(j)*Rs2_13)/(Vth*n2_13))-1)-
(V2_13(j)+I(j)*Rs2_13)/Rsh2_13-I(j);
            dif_f(j) = - 1/Rsh2_13 - (Is2_13*exp((V2_13(j) + I(j)*Rs2_13)/(Vth*n2_13)))/(Vth*n2_13);
            Vc(j) = V2_13(j)-((f(j))/(dif_f(j)));
            V2_13(j) = Vc(j);
        end
    else % If the cell operates in the reverse bias
        V2_13(j) = (-(I(j)-Iph2_13)*Rsh2_13)-(I(j)*Rs2_13);
    end

% Calculating the voltage produced by cell 2_14:
    if I(j) <= Iph2_14 % If the cell operates in the direct bias
        f(j) = Iph2_14-Is2_14*(exp((V2_14(j)+I(j)*Rs2_14)/(Vth*n2_14))-1)-
(V2_14(j)+I(j)*Rs2_14)/Rsh2_14-I(j);
        while (abs(f(j))>0.000000001)
            f(j) = Iph2_14-Is2_14*(exp((V2_14(j)+I(j)*Rs2_14)/(Vth*n2_14))-1)-
(V2_14(j)+I(j)*Rs2_14)/Rsh2_14-I(j);
            dif_f(j) = - 1/Rsh2_14 - (Is2_14*exp((V2_14(j) + I(j)*Rs2_14)/(Vth*n2_14)))/(Vth*n2_14);
            Vc(j) = V2_14(j)-((f(j))/(dif_f(j)));
            V2_14(j) = Vc(j);
        end
    else % If the cell operates in the reverse bias
        V2_14(j) = (-(I(j)-Iph2_14)*Rsh2_14)-(I(j)*Rs2_14);
    end

% Calculating the voltage produced by cell 2_15:
    if I(j) <= Iph2_15 % If the cell operates in the direct bias
        f(j) = Iph2_15-Is2_15*(exp((V2_15(j)+I(j)*Rs2_15)/(Vth*n2_15))-1)-
(V2_15(j)+I(j)*Rs2_15)/Rsh2_15-I(j);
```

```
      while (abs(f(j))>0.000000001)
         f(j) = Iph2_15-Is2_15*(exp((V2_15(j)+I(j)*Rs2_15)/(Vth*n2_15))-1)-
(V2_15(j)+I(j)*Rs2_15)/Rsh2_15-I(j);
         dif_f(j) = - 1/Rsh2_15 - (Is2_15*exp((V2_15(j) + I(j)*Rs2_15)/(Vth*n2_15)))/(Vth*n2_15);
         Vc(j) = V2_15(j)-((f(j))/(dif_f(j)));
         V2_15(j) = Vc(j);
      end
    else % If the cell operates in the reverse bias
       V2_15(j) = (-(I(j)-Iph2_15)*Rsh2_15)-(I(j)*Rs2_15);
    end

% Calculating the voltage produced by cell 2_16:
    if I(j) <= Iph2_16 % If the cell operates in the direct bias
      f(j) = Iph2_16-Is2_16*(exp((V2_16(j)+I(j)*Rs2_16)/(Vth*n2_16))-1)-
(V2_16(j)+I(j)*Rs2_16)/Rsh2_16-I(j);
      while (abs(f(j))>0.000000001)
         f(j) = Iph2_16-Is2_16*(exp((V2_16(j)+I(j)*Rs2_16)/(Vth*n2_16))-1)-
(V2_16(j)+I(j)*Rs2_16)/Rsh2_16-I(j);
         dif_f(j) = - 1/Rsh2_16 - (Is2_16*exp((V2_16(j) + I(j)*Rs2_16)/(Vth*n2_16)))/(Vth*n2_16);
         Vc(j) = V2_16(j)-((f(j))/(dif_f(j)));
         V2_16(j) = Vc(j);
      end
    else % If the cell operates in the reverse bias
       V2_16(j) = (-(I(j)-Iph2_16)*Rsh2_16)-(I(j)*Rs2_16);
    end

% Calculating the voltage produced by cell 2_17:
    if I(j) <= Iph2_17 % If the cell operates in the direct bias
      f(j) = Iph2_17-Is2_17*(exp((V2_17(j)+I(j)*Rs2_17)/(Vth*n2_17))-1)-
(V2_17(j)+I(j)*Rs2_17)/Rsh2_17-I(j);
      while (abs(f(j))>0.000000001)
         f(j) = Iph2_17-Is2_17*(exp((V2_17(j)+I(j)*Rs2_17)/(Vth*n2_17))-1)-
(V2_17(j)+I(j)*Rs2_17)/Rsh2_17-I(j);
         dif_f(j) = - 1/Rsh2_17 - (Is2_17*exp((V2_17(j) + I(j)*Rs2_17)/(Vth*n2_17)))/(Vth*n2_17);
         Vc(j) = V2_17(j)-((f(j))/(dif_f(j)));
         V2_17(j) = Vc(j);
      end
    else % If the cell operates in the reverse bias
       V2_17(j) = (-(I(j)-Iph2_17)*Rsh2_17)-(I(j)*Rs2_17);
    end

% Calculating the voltage produced by cell 2_18:
    if I(j) <= Iph2_18 % If the cell operates in the direct bias
      f(j) = Iph2_18-Is2_18*(exp((V2_18(j)+I(j)*Rs2_18)/(Vth*n2_18))-1)-
(V2_18(j)+I(j)*Rs2_18)/Rsh2_18-I(j);
      while (abs(f(j))>0.000000001)
         f(j) = Iph2_18-Is2_18*(exp((V2_18(j)+I(j)*Rs2_18)/(Vth*n2_18))-1)-
(V2_18(j)+I(j)*Rs2_18)/Rsh2_18-I(j);
         dif_f(j) = - 1/Rsh2_18 - (Is2_18*exp((V2_18(j) + I(j)*Rs2_18)/(Vth*n2_18)))/(Vth*n2_18);
         Vc(j) = V2_18(j)-((f(j))/(dif_f(j)));
         V2_18(j) = Vc(j);
      end
    else % If the cell operates in the reverse bias
       V2_18(j) = (-(I(j)-Iph2_18)*Rsh2_18)-(I(j)*Rs2_18);
    end

end

%======== Calculate the voltages of cell-strings ========
```

```
Vst1 = V1_1 + V1_2 + V1_3 + V1_4 + V1_5 + V1_6 + V1_7 + V1_8 + V1_9 + V1_10 + V1_11 +
V1_12 + V1_13 + V1_14 + V1_15 + V1_16 + V1_17 + V1_18;
Vst2 = V2_1 + V2_2 + V2_3 + V2_4 + V2_5 + V2_6 + V2_7 + V2_8 + V2_9 + V2_10 + V2_11 +
V2_12 + V2_13 + V2_14 + V2_15 + V2_16 + V2_17 + V2_18;

%======== Calculate the PV module I-V curve ========

Vmo = ones(1,length(I)); % Initialise module total voltage

if (BP_Diodes == 0) || (Alfa1 == Alfa2) % If the module is not equipped with bypass diodes, if there is no
shading or if both cell-strings are equally shaded
   Vmo = Vst1 + Vst2;

else % If the module is equipped with bypass diodes and there is shading

  % Determine Iph of cell-strings:
Iph1_vec=[Iph1_1,Iph1_2,Iph1_3,Iph1_4,Iph1_5,Iph1_6,Iph1_7,Iph1_8,Iph1_9,Iph1_10,Iph1_11,Iph1_1
2,Iph1_13,Iph1_14,Iph1_15,Iph1_16,Iph1_17,Iph1_18];
Iph2_vec=[Iph2_1,Iph2_2,Iph2_3,Iph2_4,Iph2_5,Iph2_6,Iph2_7,Iph2_8,Iph2_9,Iph2_10,Iph2_11,Iph2_1
2,Iph2_13,Iph2_14,Iph2_15,Iph2_16,Iph2_17,Iph2_18];
  Iph1 = min(Iph1_vec);
  Iph2 = min(Iph2_vec);

  % Calculate module voltage considering partial shading and conduction of bypass diodes using a
piecewise approach:
  if  (Alfa1 > Alfa2) % If cell-string 1 is shaded
    I_inf = Iph1; % The inflection current, which is the minimum Iph
    for j = 1 : size(I,2)
      if (I(j) >= 0) && (I(j) <= I_inf)
        Vmo (j) = Vst1(j) + Vst2(j);
      elseif I(j) > I_inf
        if Vst1(j) >= -VD
          Vmo (j) = Vst1(j) + Vst2(j);
        else
          Vmo(j) = Vst2(j) + (-VD);
        end
      end
    end
  end
  if  (Alfa2 > Alfa1) % If cell-string 2 is shaded
    I_inf = Iph2; % The inflection current, which is the minimum Iph
    for j = 1 : size(I,2)
      if (I(j) >= 0) && (I(j) <= I_inf)
        Vmo (j) = Vst1(j) + Vst2(j);
      elseif I(j) > I_inf
        if Vst2(j) >= -VD
          Vmo(j) = Vst1(j) + Vst2(j);
        else
          Vmo(j) = Vst1(j) + (-VD);
        end
      end
    end
  end
end

%======== Plot experimental and modelled I-V and P-V curves ========

figure (1)
plot(V_exp,I_exp, 'o','LineWidth',2, 'color', 'K')
hold on
```

```
plot (Vmo, I, '-', 'LineWidth',2, 'color', 'R')
title ('Experimental vs modelled I-V curve');
xlabel('Voltage (V)');
ylabel('Current (A)');
grid on
legend ('Experimental data', 'Model')
Pe = V_exp.*I_exp; % Experimental power
Pc = Vmo.*I; % Calculated power
figure (2)
plot(V_exp,Pe, 'o','LineWidth',2, 'color', 'K')
hold on
plot (Vmo, Pc, '-', 'LineWidth',2, 'color', 'R')
title ('Experimental vs modelled P-V curve');
xlabel('Voltage (V)');
ylabel('Power (W)');
grid on
legend ('Experimental data', 'Model')
```

Appendix F: Assessment of the Influence of Measurement Error and Shading Object Placement Error on the PV Module Model

This appendix presents an assessment of the proposed PV module modelling approach accuracy considering the ±RSD of R_{sh} shown by the error bars in Figure 5.3 (b) and considering the error of R_{sh} due to placing the shading object within ±0.2 mm (refer to Section 5.5.3).

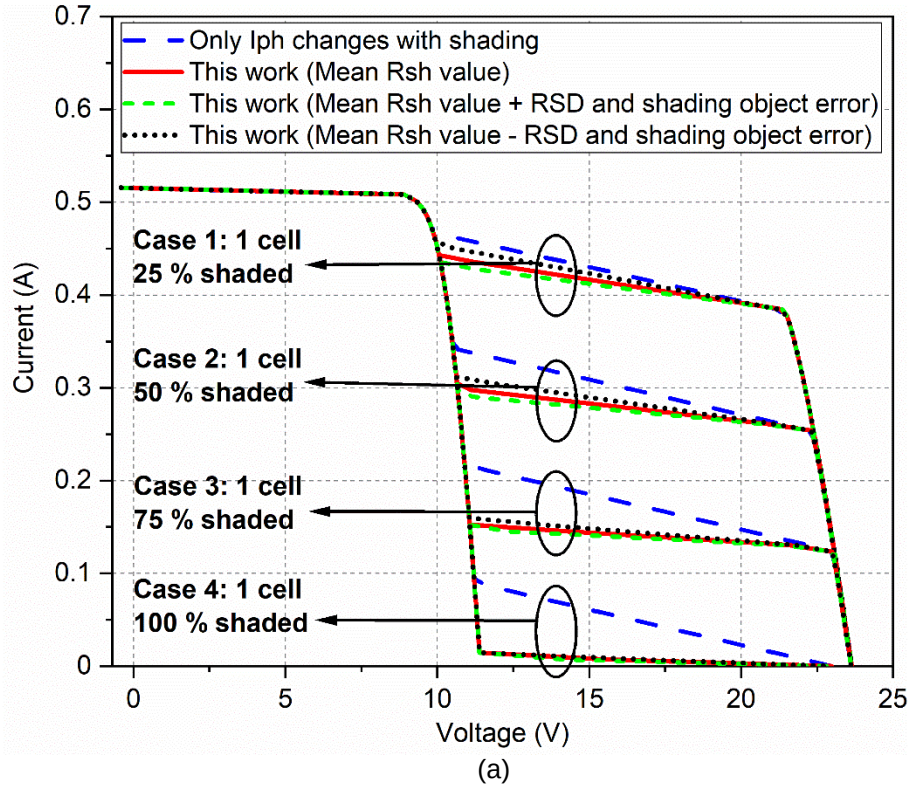

(a)

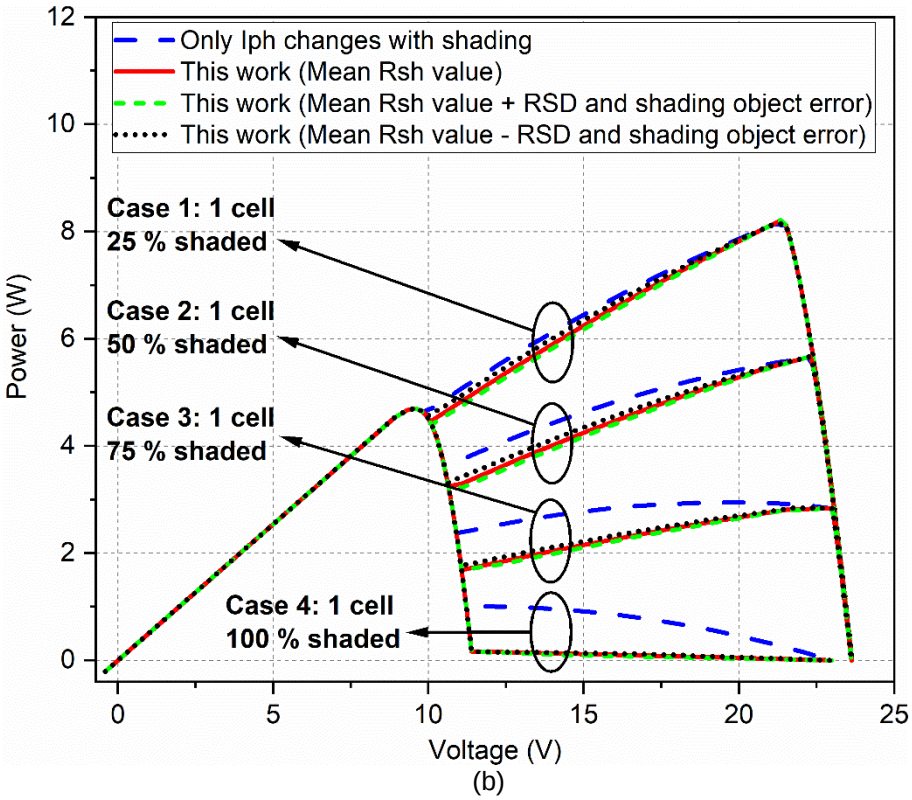

(b)

Appendix Figure F.1. Assessing the influence of shading object placement error (±0.2 mm) and relative standard deviation of the shunt resistance on the improvement in modelling accuracy of the 10 W PV module under shading of a single cell with different percentages (case 1 to 4): (a) I-V curves and (b) P-V curves. (The experimental data is not included here to avoid crowd of plots. The term "This work" is the proposed modelling approach that takes into account the variations of photo-generated current and shunt resistance with shading).

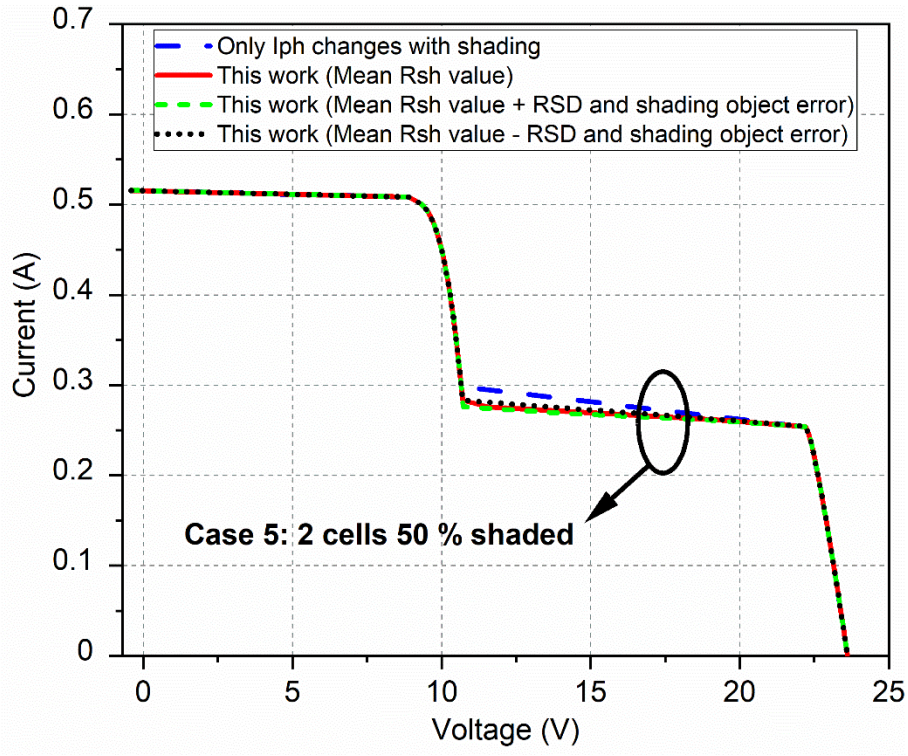

(a)

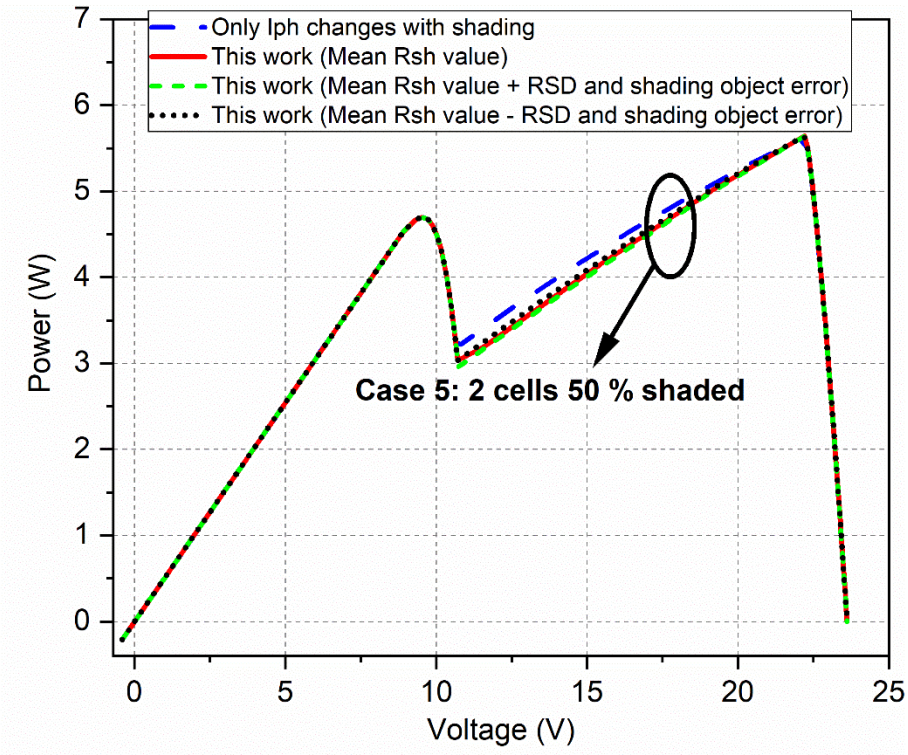

(b)

Appendix Figure F.2. Assessing the influence of shading object placement error (±0.2 mm) and relative standard deviation of the shunt resistance on the improvement in modelling accuracy of the 10 W PV module when shading two cells in string-2 (case 5): (a) I-V curves and (b) P-V curves. (The experimental data is not included here to avoid crowd of plots. The term "This work" is the proposed modelling approach that takes into account the variations of photo-generated current and shunt resistance with shading).

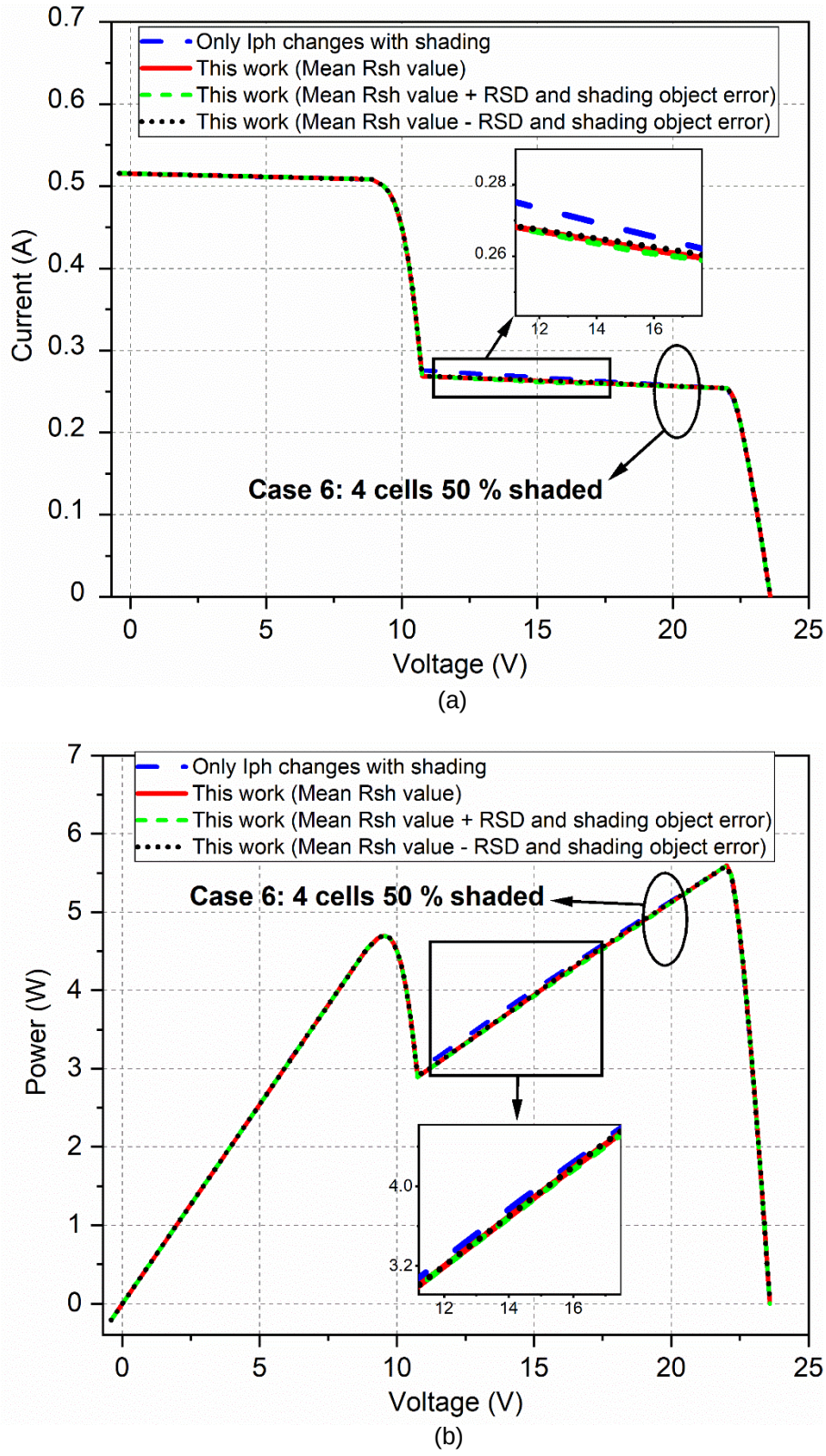

Appendix Figure F.3. Assessing the influence of shading object placement error (±0.2 mm) and relative standard deviation of the shunt resistance on the improvement in modelling accuracy of the 10 W PV module when shading four cells in string-2 (case 6): (a) I-V curves and (b) P-V curves. (The experimental data is not included here to avoid crowd of plots. The term "This work" is the proposed modelling approach that takes into account the variations of photo-generated current and shunt resistance with shading).